Small angle neutron scattering from superconductors

Allen, Peter James

Small Angle Neutron Scattering from Superconductors

by

Peter James Allen

A Thesis submitted in partial fulfilment of the requirements for the degree of Doctor of Philosophy

Department of Physics

The University of Durham
1991

Dedicated to my parents

Abstract

Small angle neutron scattering is a well known technique for studying the properties of solids at small but finite energies and momenta. In this work it has been applied to the study of the low energy properties of superconductors. The low transition temperature superconductors niobium and lead and the high transition temperature superconductor $Y_1Ba_2Cu_3O_7$ have been investigated. The results indicate a temperature dependent excess scattering of around 150 mbarn/sr/atom from $Y_1Ba_2Cu_3O_7$ at wavevectors q of around 0.03 $Å^{-1}$ and an energy of less than 30 μeV. No such effect was observable, even at much lower wavevectors (q around 0.004 $Å^{-1}$) in the low transition temperature superconductor niobium. However, a drop in transmission of a niobium sample at T_c indicates an increase in cross section of 71 $\pm$ 15 mbarn/atom. No simple explanation for these effects has been found.

Acknowledgements

This work was funded by a grant from the Science and Engineering Research Council.

I am grateful to Professors A.W.Wolfendale and A.D.Martin for allowing me use of the facilities of the Physics Department of Durham University.

My thanks to Dr D.Corner and Professor B.K.Tanner for their leadership of the Solid State group and their general enthusiasm for condensed matter physics, at least some of which I hope has rubbed off on me.

Also to my supervisor, the irrepressible Dr N.R.Bernhoeft, for his helpful encouragement of this project and for his invaluable help.

My thanks go to the various other members of the Solid State Group who have put up with me and helped greatly both by their help and their advice. Specific mention must go to M.Delap, S.Thompson, S.Cockerton, and P.Warren.

Also to Mr P.Foley and Mr J.Scott for their provision of technical support. The secretarial staff of the department also deserve praise for their efficient handling of so many administrative tasks.

In the Physics Department workshops, Mr D.Jobling, Mr P.Armstrong, Mr G.Teasdale and Mr M.Greener in the student workshop have been more than willing to help with design and construction of various components. Needless to say their work has been, as ever, of the highest standard. I am also grateful to Mr T.W.Hogg of the main workshop for expediting a job at short notice. Mr T.Jackson, Mr C.Mullaney, Mr D.Stockdale, Mr T.Adamson and Mr C.Moore in the Electronics workshop have been wellsprings of useful advice and components.

In the drawing office, Mrs P.Russell has been a great help in giving advice concerning graphics and in producing drawings for posters.

The time and effort spent by those in other universities, interested in these experiments, in discussions and in help finding useful data in the literature are gratefully acknowledged; in particular, Dr D.McK.Paul and Dr D.J.Godfrey.

I am very grateful to Dr A.Boothroyd and Mr T.Brown for the use of their crystals of niobium and lead respectively.

None of these experiments would have been possible without the help of the staff of the Institüt Laue-Langevin at Grenoble; Dr S.Hayden, Dr F.Rieutord, Dr L.Needham, Mr R.Baker, Mr S.Jenkins, and Mr D.Puschner were all involved at various stages and it is a pleasure to record here their willing cooperation and expertise. Thanks are also due to the University Liaison secretariat of RAL for their willing help.

Declaration

I declare that the work contained in this thesis has not been submitted for a degree at this University or any other. All the work presented herein was conducted by the author unless stated otherwise.

Publications

"Anomalous Neutron Scattering near the Superconducting Phase Transition"
N.R.Bernhoeft, P.J.Allen, D.McK.Paul, S.M.Hayden, P.A.Timmins and
G.G.Lonzarich, Nature **350** pp690-692

Contents

Chapter I

Superconductivity

1.1 Existence of Superconductors

In 1911 a Dutch Physicist, Onnes, observed an abrupt disappearance of the electrical resistance of a sample of mercury when he cooled it using liquid helium. This effect occured at a temperature of 4.15 K, its transition temperature (T_c). This phenomenon he named superconductivity (Onnes). The explanation of superconductivity was eagerly sought by theoreticians, as well as experimentalists who were prompted to investigate the physical properties of superconductors in great detail. Historical studies of this science can be found in many articles (e.g. Pippard).

To the present day, physicists have engaged in a hunt for further similar materials. In addition to investigating their properties, they have also sought the correct ways to parameterize these effects in order to understand this interesting new state. Since 1911 some several thousand superconducting materials, (including alloys), with more and more interesting properties have been discovered. Indeed, "superconductors now come in more flavors than Baskin-Robbins ice cream" (Cooper). Superconductors are now routinely used in technological applications, especially for the production of intense magnetic fields (Kunzler). Good sources of data on materials are Savitskii et al, Matthias et al (and references therein), and the appendices of Phillips (Savitskii, Matthias, Phillips).

This field of study is now so large as to preclude review except of individual areas of activity. Many books and articles have also been written about superconductivity, at various levels, e.g. the excellent text of Tinkham, and the relevant section in the introductory Solid State Physics text of Kittel.

1.2 Properties of Superconductors

All superconductors share a number of properties. These common features are :-

1. All superconductors yet discovered are found to be metallic in character.

2. Ferromagnetism and superconductivity are seen to be mutually exclusive, at a first glance. Of the transition elements, few do not exhibit either superconductivity or magnetic order at the lowest temperatures yet reached. The notable exceptions are the noble metals, which show no such phase transitions at the lowest temperatures yet reached.

3. Superconductors undergo a transition from the normal metallic state to a state of zero electrical resistance, the superconducting state, at a temperature T_c. This is a constant of the material, for pure specimens. The transition temperatures of so far discovered vary over several orders of magnitude. See table 1.1 for some examples.

4. The critical temperatures are very low compared to the typical energy of electronic processes in solids e.g. the Fermi energy.

5. The critical temperature measured in a sample is usually extremely sensitive to the levels of paramagnetic impurities. It is fortuitous that Onnes was using mercury because it is easy to purify.

6. Superconductors possess interesting magnetic properties below T_c. Principally, at low fields, they are perfect diamagnets, both excluding applied field and expelling field from the bulk of the material when cooled through T_c. Thus in the bulk of a superconductor, we have both $E = 0$ and $B = 0$. This latter effect is one of the few not discovered by Onnes in his pioneering experiments, being discovered later by Ochsenfeld and Meissner, and is generally known as the Meissner effect (Meissner). Note that the field is not discontinuous at the surface, but falls away exponentially with a characteristic length, known as the London penetration depth. This penetration depth is temperature dependent.

Table 1.1 — Table of superconducting elements and selected compounds

Elements			
Element	T_c (K)	Element	T_c (K)
Al	1.14	Re	1.40
Cd	0.56	Ru	0.51
Ga	1.09	Sn	3.72
Hf	0.12	Ta	4.48
Hg	4.15	Tc	7.77
In	3.40	Th	1.36
Ir	0.14	Ti	0.39
La	6.00	Tl	2.39
Lu	0.10	U	0.20
Mo	0.92	V	5.38
Nb	9.20	W	0.48
Os	0.66	Zn	0.88
Pa	1.40	Zr	0.54
Pb	7.49		

Compounds	
Formula	T_c (K)
Nb_3Ge	23.2
Nb_3Ga	21.0
Nb_3Sn	18.1
NbN	17.2
V_3Si	17.2
V_3Ga	16.8
Ta_3Pb	16.0
$Mo_6Pb_{0.9}S_{7.5}$	15.2
Mo_3Re	15.0
MoC	14.3
$LuRh_4B_4$	11.7
La_3In	10.4
ZrV_2	8.8
$LaSn_3$	6.55

Taken from Savitskii, Matthias, and Phillips.

7. The magnetic properties at higher fields are also interesting. There is a magnetic field at which superconductivity will be destroyed. This varies with temperature, increasing from zero at T_c to a maximum at zero temperature. See the following phase diagram (figure 1.1). There exist two types of superconductor, types I and II, which differ in their response to applied high magnetic fields. Type I superconductivity is immediately destroyed at a critical field strength B_c, whereas type II will still possess diamagnetism but not exclude flux perfectly in a certain range of larger fields, and then be destroyed by a further increase . Thus a type II has two critical fields, B_{c1} for flux penetration and B_{c2} for destruction of superconductivity. B_{c1} tends to be rather small, in the milliTesla range, but B_{c2} can be very large indeed, up to many tens of Tesla (see figure 1.1).

8. Although possessing zero resistance, a superconductor cannot carry an infinite current; superconductivity is destroyed at a certain critical current density. This varies with the temperature and applied magnetic field, and is related to the self field of the conductor destroying the superconductivity (Silsbee). This is an extremely important limitation to the practical application of superconductors in many environments.

9. The superconducting transition is visible in the thermal properties; there is a peak in the specific heat below T_c which is abruptly reduced on warming through the transition (Phillips). Using the effect of an applied magnetic field, the normal state can still be probed below the zero field T_c, and the difference in specific heat measured. The electronic specific heat appears to be exponentially small in a superconductor at temperatures well below T_c. In superconductors with a thermal conductivity dominated by electronic processes, there is also a large change in the behaviour of the thermal conductivity, with a marked decrease in thermal conductivity with decreasing temperature.

10. It is possible to describe many more properties which are changed by the superconductivity, involving phonon and photon absorption as functions of frequency, temperature etc. As this list is large, I refer the reader to the literature. For many properties the reduced temperature T/T_c is a useful

Figure 1.1 —

The magnetic field / temperature phase diagram
of types I and II superconductors

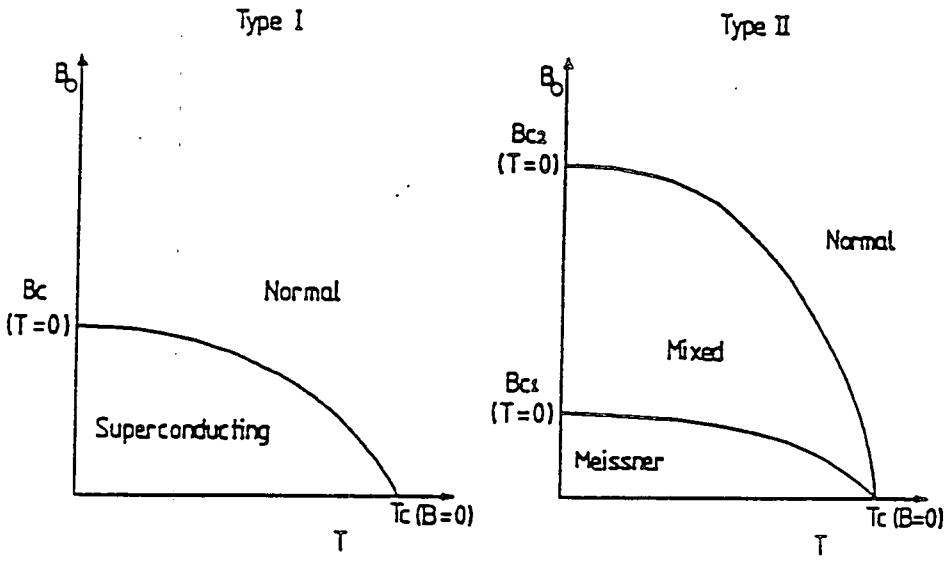

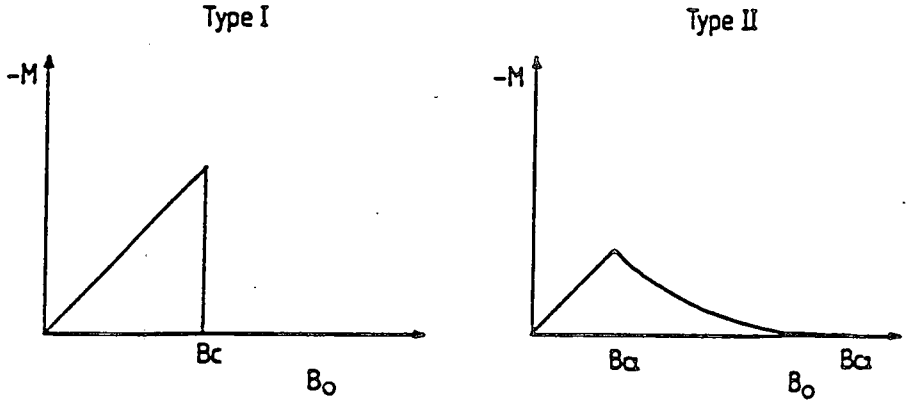

parameterisation, allowing the comparison of rather different T_c materials. In particular, many properties vary as (1- $(T/T_c)^4$).

11. Another idea found to be useful is that there exists below T_c some gap in the electronic excitation spectrum; this would presumably aid the zero resistance by removing scattering processes, and would give the observed behaviour of the specific heat some explanation. Nevertheless, the mechanism by which this gap can occur is not obvious.

1.3 Models of the Superconducting State

1.3.1 Macroscopic Theory

The first to arrive upon a means of reconciling Maxwell's equations and the Meissner-Ochsenfeld effect were the London brothers, using a "two - fluid" model similar to that used for superfluid helium 4 (London). This assumes that there are "normal" and "super" electrons and that the number of "super" electrons varies with temperature. Note that it is dangerous to talk of two different sorts of electrons, normal ones and superconducting ones, as we must reconcile this with the indistinguishability of electrons. Nevertheless, it does allow a classical discussion of the superconductor at finite temperatures. For the analagous discussion of superfluid ^{4}He, see the paper of Landau (Landau).

The Londons assumed a density of superconducting electrons n_s, zero above T_c and finite below T_c. These possess zero resistance and thus short out the normal electron contribution, (at least in a DC sense). They then postulated an equation as an extra condition to Maxwell's equations in a superconductor. This equation is :-

$$J_s = -\frac{n_s e^2}{m} A$$

if we choose the gauge such that $\nabla . A = 0$

and $A_\perp = 0$ on any surface through which no current is flowing

If added as a condition to Maxwell's equations, this implies that the screening currents causing the perfect diamagnetism flow such that the field falls exponentially with a length scale λ given by

$$\lambda = \sqrt{\epsilon_0 m c^2 / n_s e^2}$$

and thus that the field does not penetrate into the bulk of a superconductor, but falls away in a transition region at the surface. This has been confirmed by observation of the magnetic properties of small samples of superconductor (e.g. Laurmann). Thus we have an explanation of the superconducting diamagnetism, without radically altering Maxwell's equations. Such a two-fluid model can reproduce those effects with a $(1\text{-}(T/T_c)^4)$ dependence by using this form for the number density of "super" electrons.

1.3.2 Coherence Length

In addition to the above penetration depth, it was realised that there was at least 1 other characteristic length scale involved in the properties of the superconducting state (Pippard). Dubbed the "coherence length", ξ, it represents the length scale over which non-local effects become important. The electron mean free path effectively influences the coherence length, so that ξ can be sample dependent. A sample with an electronic mean free path much larger than the coherence length is said to be in the "clean limit". If vice versa, as in some alloys, then the sample is in the "dirty limit".

1.3.3 Summary of Characteristic Lengths

A consideration of the forms used to represent the two characteristic lengths used in this discussion leads to the diagram shown (figure 1.2), using reciprocal

Figure 1.2 —

Diagram showing the relevant characteristic wavevector scales of superconductivity and their relation to ω_g and ω_{ps}, where $\omega_{ps} = \sqrt{\frac{n_s e^2}{\epsilon_0 m}}$ and $\hbar\omega_g = 2\Delta$.

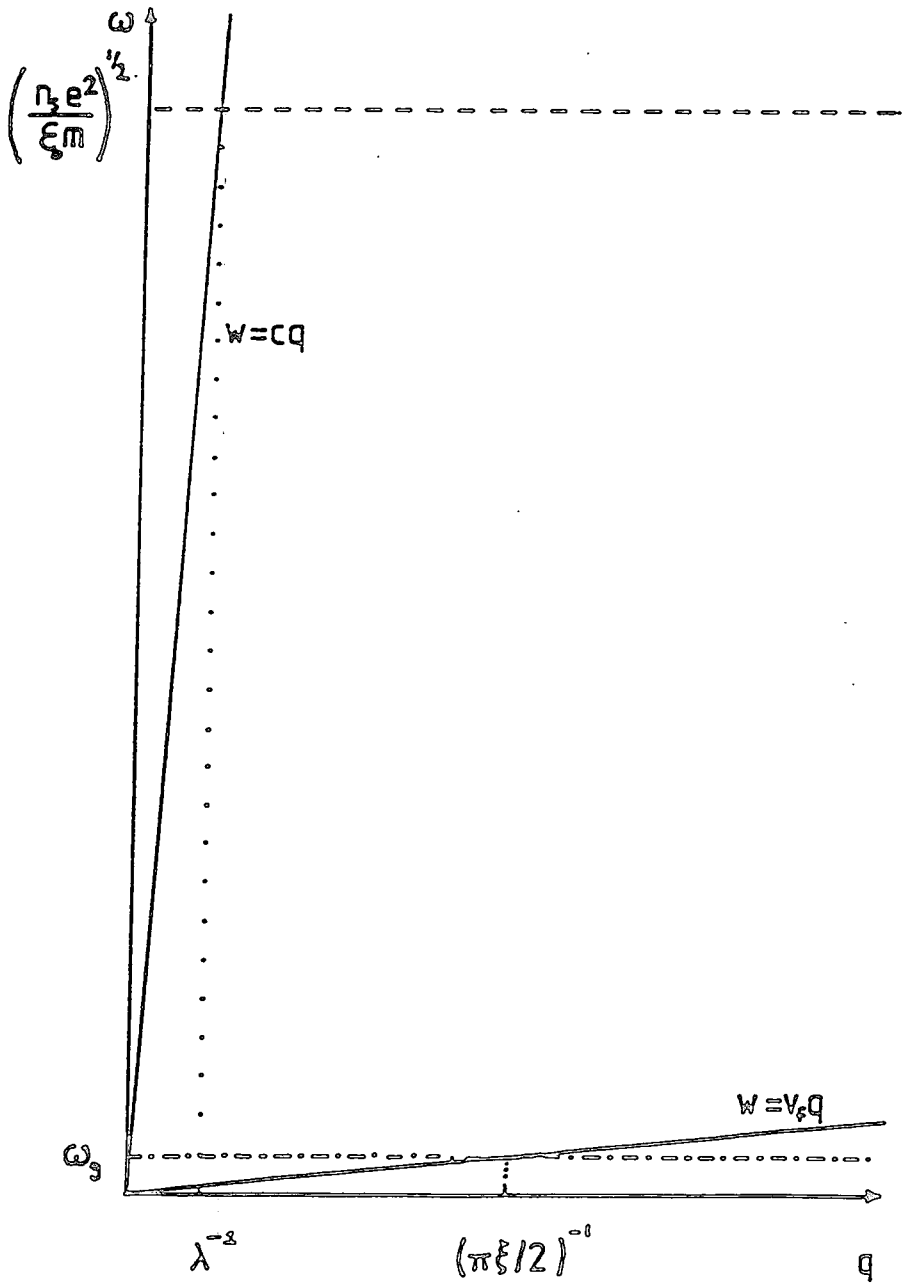

space as the best means of illustration. Here it is the "plasma frequency", (if written $\sqrt{\frac{n_s e^2}{\epsilon_0 m}}$), associated with the superconducting electrons that determines the screening length λ. This implies that low electron density materials will always have rather large λ's due to their low plasma frequency. This diagram also makes it clear that a material with a large gap in the electronic density of states, will inevitably posess a short coherence length, given that a Fermi velocity is rather similar from one solid to another. A large gap will be necessary for any system to have a high T_c - thus a high T_c superconductor will always have a low coherence length.

These characteristic wavevector q's are rather small, as a fraction of the available range of q. This is a consequence of the generally long range character of superconductivity.

1.4 Ginzburg - Landau (GL) Theory

Working from insight rather than rigorous methods, Ginzburg and Landau produced a form of the free energy for the superconducting state, based upon the idea of an order parameter for the superconducting state (Ginzburg , Landau). This order parameter, when squared, corresponds to the local density of superconducting electrons. This enables the discussion of nonuniform effects in the superconductor, such as the behaviour at the interface of a superconductor and a normal metal in a magnetic field, and enables the difference between type I and type II superconductors clearly to be seen. This theory has been shown to be derivable from current microscopic theories, at least close to T_c (Gorkov): this is important if the wider use of such a theory is contemplated. Essentially, GL postulate a free energy of the form:

$$f = f_n + \alpha|\Psi|^2 + \frac{\beta}{2}|\Psi|^4 + \frac{1}{2m^*}|(-i\hbar\nabla - e^*.A)\Psi|^2 + \frac{B^2}{2\mu_0}$$

which is based upon an order parameter Ψ , whose thermodynamic time average value rises from zero at T_c; this is rather like the order parameter (magnetisation) of a ferromagnet, but possessing a phase. This is thus a quantum or complex order parameter. GL then arrive at two equations for the order parameter which

govern its evolution in time and space. In this picture, the coherence length is the length scale required to vary the superconducting order parameter without an "undue" energy cost.

1.4.1 Type I and Type II

Given that screening of magnetic fields takes place over lengths of the order λ, and superconductivity can vary over a length ξ, the differences between Type I and II can be seen. Essentially the surface energy between a region of superconducting material and normal material can be either positive or negative, depending upon the dimensionless ratio λ/ξ, called κ. In the case where $\kappa > 1/\sqrt{2}$, type II, the minimum free energy above a certain applied field will be given by the superconductor posessing discrete regions in which the field occurs, as lines of flux or fluxons, where the superconducting order parameter falls to zero magnitude, surrounded by areas of superconducting material. In large fields, these fluxons tend to form a hexagonal lattice. See, for example, the beautiful images of this lattice in the paper of Traüble and Essmann (Traüble). This behaviour was first derived from the GL theory by Abrikosov, and is thus called the Abrikosov lattice (Abrikosov). The properties of this flux lattice are extremely important for the high field properties of type II superconductors.

1.4.2 Fluctuation Effects

It is also possible to consider fluctuations in the order parameter above T_c, having a non zero time average for the amplitude, i.e.$|\Psi|^2$. This enables the treatment of so called fluctuation effects. These occur above the transition, where the superconductivity can arise in small regions momentarily, before decaying, giving observable effects due to the extreme electrical and magnetic properties of the superconducting state. For example, a rounding of the resistivity versus temperature graph may be seen (Craven, Ferrell, Glover).

This concludes a very brief look at the "macroscopic" theory of superconductivity. In this we have seen how, given the GL equations, the problems of spatial inhomogeneity in a superconductor can be understood. However, we need to have this rather useful empirical theory backed up by a microscopic mechanism by which the rather dramatic changes in many properties may take place.

1.5 Microscopic Theory

1.5.1 Cooper's Theorem

In 1956 L.Cooper showed that in an electron gas in a "jellium"solid, (where the positive ions are ignored except in order to produce overall charge balance), an arbitrarily small attractive force between the electrons would cause a distinct lower energy ground state (Cooper). This state consists of electrons paired to form "Cooper pairs" of no net spin and zero total momentum. Thus the concept arises of a pairing interaction, giving rise to these pairs, which might be expected to possess some of the properties of bosons.

Now the pairing on its own would be insufficient if these pairs could be broken up easily; indeed the normal metal could easily be described as such pairs. However, the combination of the attractive potential, giving this paired state a distinct lower energy than the lowest "two - electron" state, and the Pauli principle, denying access to all the filled states of the system for any scattered or broken up pair, means that this pairing will give the state the radically different electrical, magnetic and thermal properties that we know to be a feature of superconductivity.

The crucial features of this approach are the necessity of considering the entire electron gas as being important through the Pauli principle, and the importance of the interactions between electrons at or near the Fermi surface. This idea was developed further by Bardeen Cooper and Schrieffer (BCS) to form the basis of the first plausible explanation of superconductivity.

1.6 BCS Theory

A mechanism to provide the necessary attractive interaction was proposed by BCS in 1957. This was then rapidly developed, particularly in its notation (Bogoliubov, Anderson), which helped to clarify many of the ideas involved. Subsequently it has withstood a great deal of experimental investigation. Essentially, the theory states that electrons within a small energy of the Fermi level, which are the only important electrons at low temperatures, are attracted by each other due to their mutual interaction with the crystal lattice. This is at first sight surprising; the Coulomb repulsion forces for electrons are quite severe. The reason for this lies in

the fact that this Coulomb force is screened by the other electrons and the lattice: this can in certain circumstances lead to an overscreening, due to the fact that the ion cores remain polarised in the wake of a conduction electron due to their large mass. The problem solved by BCS was essentially for a particular "reduced" Hamiltonian including these electron - phonon interactions as being the essential physics behind superconductivity.

Thus there can be a net attractive force between two electrons, via the exchange of energy and momentum by a phonon. This interaction is now accepted as being a plausible explanation for most of the elemental superconductors, mainly because using it, BCS were able to correctly predict various properties, such as the variation of T_c with isotopic mass, known as the isotope effect (see, for example the tabulation in Rickayzen). However, other interactions could give similar pairing effects, and many of the BCS predictions are now thought to be independent of the detailed pairing mechanism.

1.6.1 Coherence Effects

More importantly, the BCS theory correctly predicts the fact that various properties behave in similar ways. These are due to what are known as "coherence effects" . These arise because the electron states are no longer independent, being paired. In essence, any sum over electron states must consider whether the terms for a pair of electrons of opposite momentum k and spin σ will add (case 2), or cancel (case 1), in the final expression. Properties for which the relevant interaction processes have a certain symmetry with respect to the paired electrons have one coherence factor, and vice versa. This can be made particularly clear by considering the ratios of various quantities in the superconducting and (magnetic field induced) normal states, for two typical processes with cases 1 and 2 coherence factors. Only case 1 coherence factors show the near two-fluid type response, the other showing a pronounced peak below T_c, e.g.the "Hebel-Slichter" peak in the NMR linewidth (Hebel). This case 2 coherence factor would diverge at $\omega = 0$ in the BCS theory, which is obviously unphysical. These effects, once observed, give very strong support to the picture of pairing between electrons as the mechanism of superconductivity (see figure 1.3).

Figure 1.3 —

Diagram of the temperature dependences of ratios of absorption coefficients α in normal and superconducting states, typical of cases 1 and 2 coherence effects showing enhancement / supression below T_c, and frequency dependence of case 2. Redrawn from Bardeen and Schrieffer

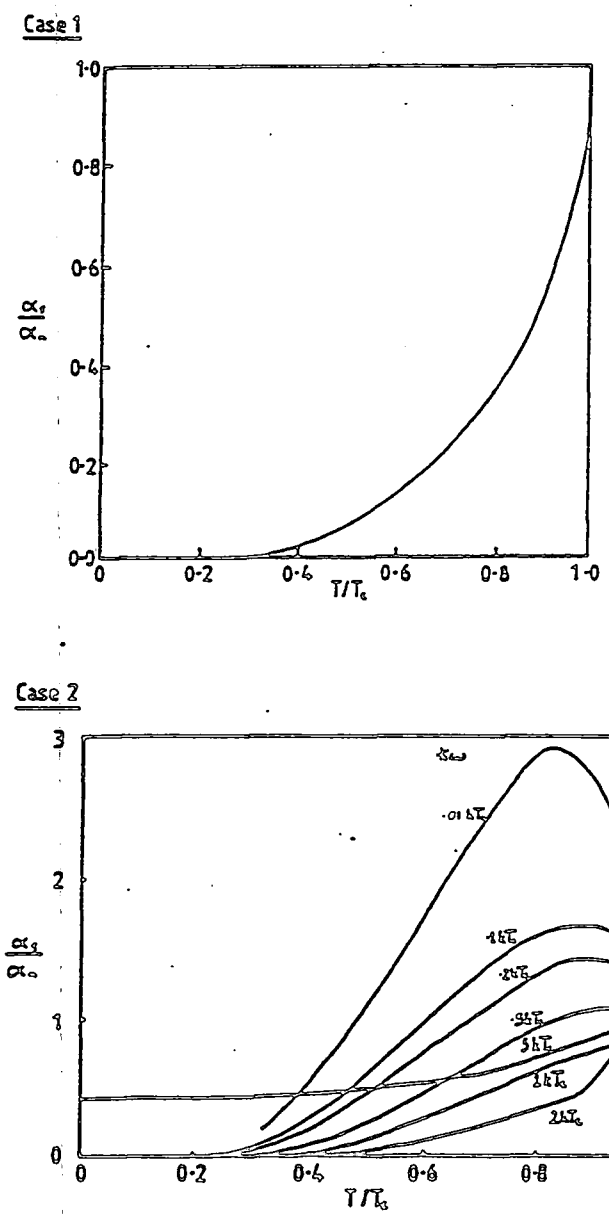

1.7 Effect of Gap

The gap in the electronic excitation spectrum is undoubtedly important to a simple discussion of superconductors. It is, nevertheless, not necessary for the occurence of superconductivity *per se* , as has been shown (e.g., Phillips) in the study of superconductors with paramagnetic impurities. The pair breaking effects of the impurities can lead to a system with no electronic gap, but which still possesses the necessary phase coherence for the electrons to be superconducting. This is surprising at first glance, to say the least. However, we know that superconductivity is surprisingly robust, maintaining phase coherence over long distances in real samples. It is at least likely that it can survive small quantities of impurities.

1.7.1 Other Collective Modes

There are collective excitations of the system with energies inside the gap, even in more conventional systems. These are the phonons! Though an unavoidable consequence of finite temperatures, they do not interfere with the superconductivity. They will however complicate various experimental measurements at relatively high temperatures.

The question of whether there exist any possible collective modes of the electronic system, with energies inside the gap, is an interesting and complicated one. This has been discussed at length by many authors. The main problem is that low lying excitations obviously affect the gap. In conjunction, early discussion also focussed upon the gauge invariance of the Meissner effect derivation within the BCS theory : as has been pointed out (e.g. by Martin) this is not really relevant.

Anderson concluded that in the case of charged quasiparticles, the phase fluctuation mode becomes modified by the Coulomb interaction into the plasmon (Anderson, Yosida). Thouless and Tilley found that the phase fluctuation mode can exist at finite temperatures but has a high velocity, (much greater than that of the phonons). They calculate that it thus makes little contribution to the specific heat (Thouless). All these modes are intimately connected with the nature of the the superconducting state. Leggett has investigated theoretically possible effects in superconductors with more than one band of superconducting electrons, finding a collective excitation due to the relative phase of the two "condensate" wave

functions, which will of course only exist in a two-band system (Leggett).

This field of study is made no easier by the fact that it may only have important consequences at finite temperatures where the theoretical work becomes rather difficult. The fact that gapless superconductivity does exist must indicate that there is no absolute requirement for no states to be available in the gap.

1.8 Conductivity

The opening of the gap and development of phase coherence has a profound effect on the conductivity, as shown by the startling DC properties. The question then arises, what happens to the full (q,ω) form of these functions? This might be though of as the ultimate task in a macroscopic picture of the superconducting state, as the nature of the conductivity ultimately determines the low field electromagnetic behaviour of the ideal superconductor. The mixed state is not considered in this picture. The early effort in this topic was concentrated upon the q = 0 case, in the BCS superconductor (Mattis).

Tinkham and Ferrell, and Nakajima, addressed the problem directly, and their papers (Tinkham, Nakajima) show the manner of the problem at zero temperature, deriving the free parameter in Pippard's form for the coherence length from the BCS theory in an elegant manner. They ask the question posed above, and obtain the zero temperature behaviour of σ' and σ'', the real and imaginary parts of the conductivity. σ' is affected by the gap and all the weight from the conductivity at finite frequencies which must be removed by the gap, (due to the lack of scattering processes), is taken into a delta function at $\omega = 0$ (see figure 1.4). This gives a corresponding $1/\omega$ component to the imaginary part, σ_2, via the Kramers-Kronig relations (see Kittel for a brief discussion).

At higher q, ($q\xi > 1$), essentially the point is that although the gap persists, the delta function pole at $\omega = 0$ in σ'(q,ω) is of reduced strength at these wavevectors. This is due to the availability of normal excitations giving weight to the lossy part of the conductivity (i.e. σ') at high frequencies.

Thus there is a direct physical way in which the coherence length affects the macroscopic quantities such as conductivity at small but finite q. Of course, if

Figure 1.4 —

Schematic diagram of $\sigma'(q,\omega)$ in clean and dirty superconductors in the normal and superconducting states, at high and low q. Notice the q dependence of the δ-function.

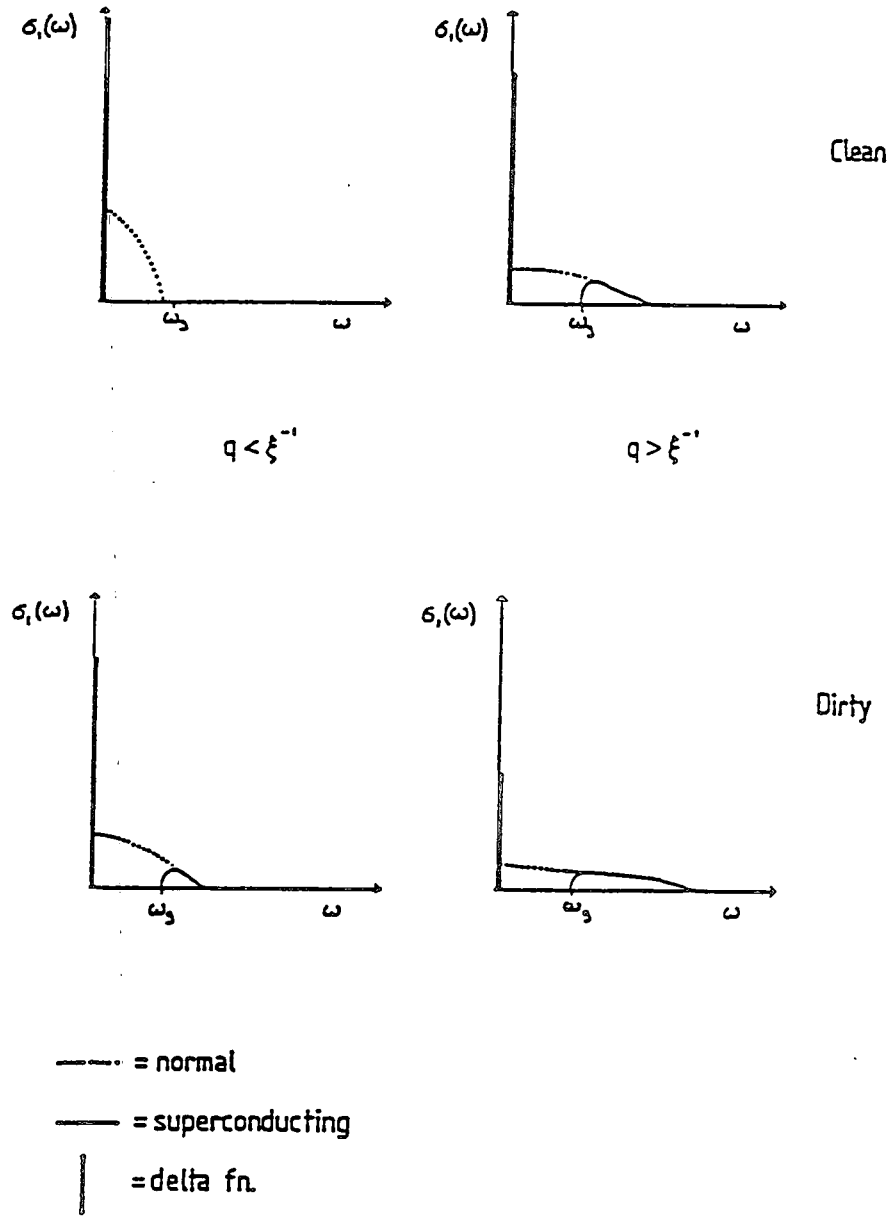

we are in the dirty limit, then there is a non-zero term in the conductivity at frequencies greater than the gap due to the large width in frequency of $\sigma'(q,\omega)$, due to the short mean free path, even at $q = 0$. In this case, not all the available conductivity weight will be in the delta function even at zero temperature and low q. The use of sum rules on integrals of $\sigma'(q,\omega)$ is of obvious importance in this subject, as it is this property that makes it very easy to see why the delta function will arise if there is a gap.

Now, if it is the temperature dependent energy gap that determines the relevant scale for these processes, then the coherence length in this argument will also be temperature dependent. An experiment that could measure at these scales of q would in principle be able to measure the coherence length directly in zero applied magnetic field, by looking for the length scale at which the strength of the delta function started to diminish. Finite temperatures will complicate the analysis due to the "normal" electron contribution to the conductivity.

Chapter II

High T_c Superconductors

P.B.Allen. "(Do you think that) ... the interplay between superconductivity and metal-insulator transitions in perovskite compounds deserves further study ?"

B.Matthias. "Yes."

Conference discussion in Ternary Superconductors, (Ed. Shenoy), 1980

2.1 History

Since the discovery of superconductivity, there have always been systems where the T_c was higher than others, e.g, niobium which has the highest T_c for an element, 9.2 K. These systems were generally regarded as just the highest members of the series of lower T_c materials. However, when more and more compounds were tested for superconductivity, (in particular by Matthias and coworkers, (Matthias)), many intermetallic compounds were found to have higher T_c's than any element, with T_c's eventually reaching of the order of 20 K in compounds similar to V_3Ga and Nb_3Ge. A selection is given in Table 1.1 in chapter I. As there was much interest in these particular materials for technological applications, they were generically called High T_c materials.

Other compounds with higher than elemental T_c's were also known as High T_c, in particular the $Ba_{1-x}Pb_xBiO_3$ perovskite (Sleight). This was all the more strange because it would need an anomalously large electron-phonon coupling, if a BCS model were to be used, or a non - BCS mechanism. Many efforts had been made to understand the nature of superconductivity in this compound, none entirely successful. This is what led to the rather prophetic quote heading this chapter.

Table 2.1 — Table of superconducting oxides

Low T_c Oxides	
Formula	Tc (K)
NbO	1.25
SnO	3.81
TiO	0.68
TiReO	5.74
$Pd_{.285}Zr_{.61}O_{.105}$	2.09
$Ti_{.573}Rh_{.287}O_{.14}$	3.37
$Zr_{.611}Rh_{.285}O_{.105}$	11.8
Zr_3V_3O	7.5
$Mo_2PbS_6O_2$	11.7
$Mo_2Cu_2S_6O_2$	9.0
$Tl_{.3}WO_3$	2.14
$K_{.33}WO_3$	6.3
$Na_{.33}WO_3$	3.0
$Ba_{.13}WO_3$	1.9
$SrTiO_3$	0.39
$Sr_{.7}Ca_{.3}TiO_3$	0.6
$(Ba_{.1}Sr_{.9})TiO_3$	0.6
$(Ca_{.31}Sr_{.69})TiO_3$	0.6
$Li_{2-x}Ti_{1+x}O_4$	13.7
$BaPb_{1-x}Bi_xO_{3-y}$	12.0

High T_c Oxides	
Formula	T_c (K)
$(Ba_{1-x}K_x)BiO_3$	30
$La_{2-x}Ba_xCuO_4$	35
$La_{2-x}Sr_xCuO_4$	38.5
$La_{2-x}Ca_xCuO_4$	18
$Y_1Ba_2Cu_3O_{7-x}$	93
$Y_1Ba_2Cu_4O_{8-x}$	80
$Y_2Ba_4Cu_7O_{15-x}$	40
$Bi_2(Sr_{2-x}Bi_x)CuO_6$	6
$Bi_2Sr_2CaCu_2O_8$	90
$(Bi,Pb)_2(Sr,Ca)_4Cu_3O_8$	110
$Tl_2Ba_2CuO_6$	80
$Tl_2Ba_2CaCu_2O_8$	110
$Tl_2Ba_2Ca_2Cu_3O_{10}$	125

The report of Mo_3O_5 in Savitskii is thought to be in error, a misreading of Mo_3Os. Data is from (Savitskii, Yvon).

2.1.1 Discovery of $La_{2-x}Sr_xCuO$

The greatest development in this field to date was the discovery of Bednorz and Müller of superconductivity in the LaSrCuO system, in a compound now known to be $La_{2-x}Sr_xCuO_4$ (Bednorz +Müller). A history of this discovery is contained in (Bednorz +Müller). This compound has a T_c of 38K at the optimum Sr content. This discovery has moved the standard for High T_c; as a result the term now generally refers to this family of compounds and its successors and relatives. As the LaSrCuO system shares many features with subsequent High T_c materials, I shall not go into its properties, but go straight on to the system studied in this thesis.

2.1.2 Development of Higher T_c's

A very high pressure dependence of T_c of LaSrCuO, showing a dT_c/dP of > 1 K /kbar, compared with other superconductors at around .01 K /kbar (Brandt), was discovered by Chu et al (Chu). Wu et al tried to increase T_c in these systems by the use of chemical pressure, i.e. using smaller cations to decrease the bond lengths (Wu). This led to the accidental discovery of another family of High T_c compounds, now known to be based on the chemical formula $Y_1Ba_2Cu_3O_7$, (e.g. Hinks) whose T_c is 93K. The properties of $Y_1Ba_2Cu_3O_7$ are summarised below.

2.1.3 Further Series of Compounds

Following the work of Chu and Wu at al., many other High T_c superconducting oxide compounds have been discovered. The most important are based on the compounds $Bi_2Sr_2CaCu_2O_8$ and $Tl_2Ba_2CaCu_2O_8$ (Maeda, Sheng) and their related compounds. Although showing some marked differences to $Y_1Ba_2Cu_3O_7$, sample preparation difficulties are seriously hampering experiments on bulk material, and I will not discuss them further here.

A table of High T_c oxides is shown (table 2.1), compared with the low T_c oxide superconductors.

Figure 2.1 —

Diagram of crystal structure of $Y_1Ba_2Cu_3O_{7-\delta}$,
showing planes and chains of CuO.
Redrawn from Calestani

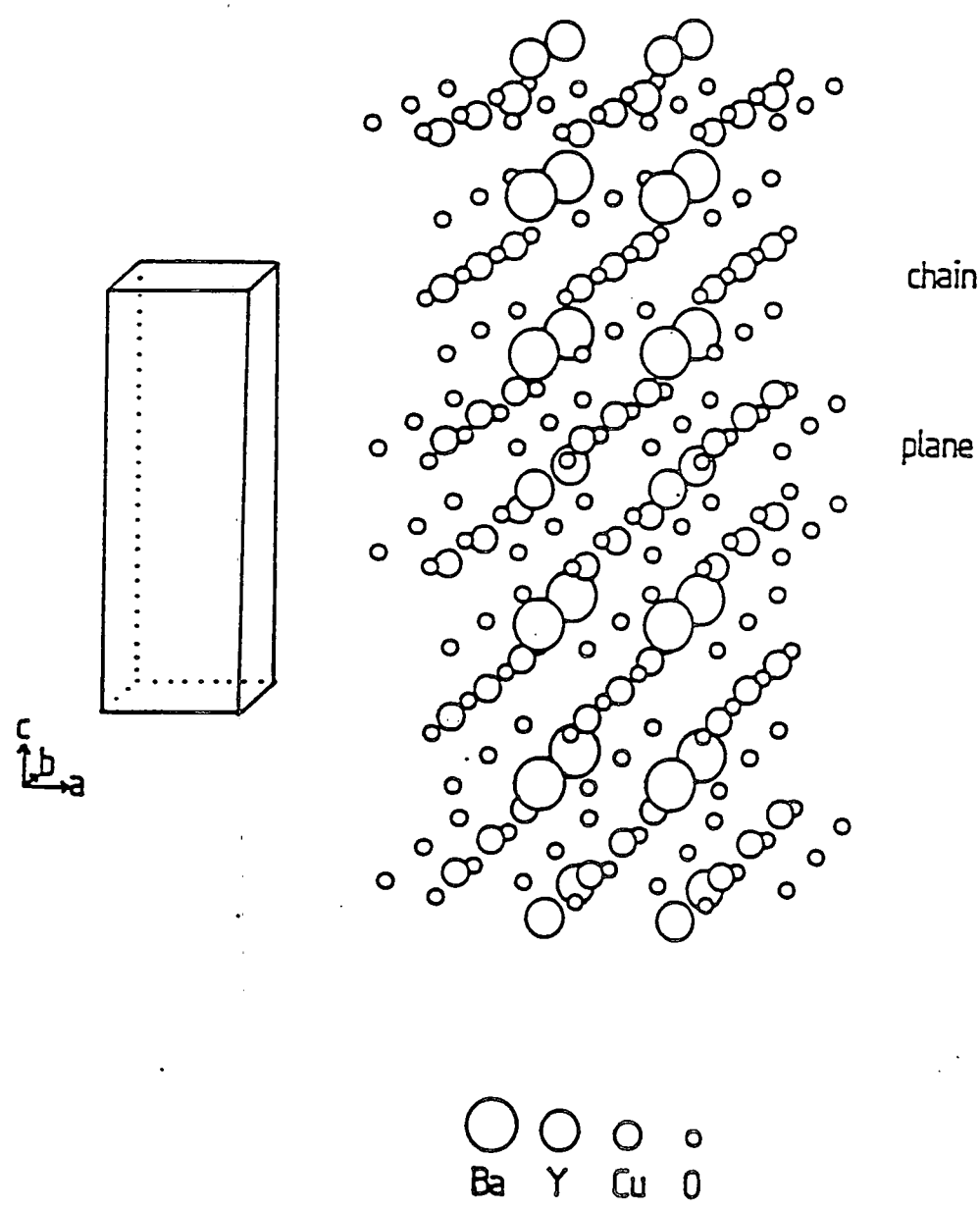

2.2 Properties of $Y_1Ba_2Cu_3O_7$

$Y_1Ba_2Cu_3O_7$ is the most studied High T_c system, mainly because it was the first to break through the important commercial barrier of $T_c = 77$ K, the boiling point of liquid nitrogen at atmospheric pressure. It is the most studied member of a whole family of related compounds with members of the rare earths taking the place of yttrium in the structure. All but Ce, Pr and Nd give superconductivity at very similar T_c's (e.g. Maple). There are other compounds in this quaternary system which are superconducting, e.g. $Y_1Ba_2Cu_4O_y$ and $Y_2Ba_4Cu_7O_z$, and their rare earth analogues, but they are more difficult to produce reliably (e.g. Cava, Miyatake). Their T_c's are not very different, but they do vary in their properties from $Y_1Ba_2Cu_3O_7$, (e.g. Morris). They are however much less studied than $Y_1Ba_2Cu_3O_7$ as yet.

Just about every technique of solid state physics has been brought to bear on both doped and undoped $Y_1Ba_2Cu_3O_7$. There exists a massive amount of data in the published literature. See, for example the review article of Tinkham and Lobb (Tinkham), the MRS proceedings on High T_c Superconductivity (Ed. Brodsky), the Los Alamos symposium proceedings (Ed. Bedell) and the book "Physical properties of High Tc Superconductors" (Ed. Ginsberg). It is an unfortunate fact that the rather awkward sample production, and the extreme popularity of the study of this material conspire against easy analysis. However, this special attention also means that there is a wealth of data with which to compare and test new experimental results. Different techniques appear to give different values for the same quantities; different sample production just confuses the issue. The fact that these materials can easily be inhomogenous and are certainly anisotropic means that various techniques do genuinely measure different quantities which would presumably agree if the inhomogeneity were removed. Priority in discovery of results is also a very difficult area; references gived here are purely for their utility, and do not imply priority.

2.2.1 Antiferromagnetism

The "parent" compound of this family is $Y_1Ba_2Cu_3O_6$, an insulating compound showing antiferromagnetic order of the copper sites, with a Néel temperature of around 420K. Its structure is essentially a tetragonal unit cell very similar

Figure 2.2 —

Phase diagram showing Neel temperature T_N and Superconducting T_c
vs. oxygen content δ in $Y_1Ba_2Cu_3O_{7-\delta}$,
showing competition between antiferromagnetism and superconductivity.
Redrawn from Birgeneau

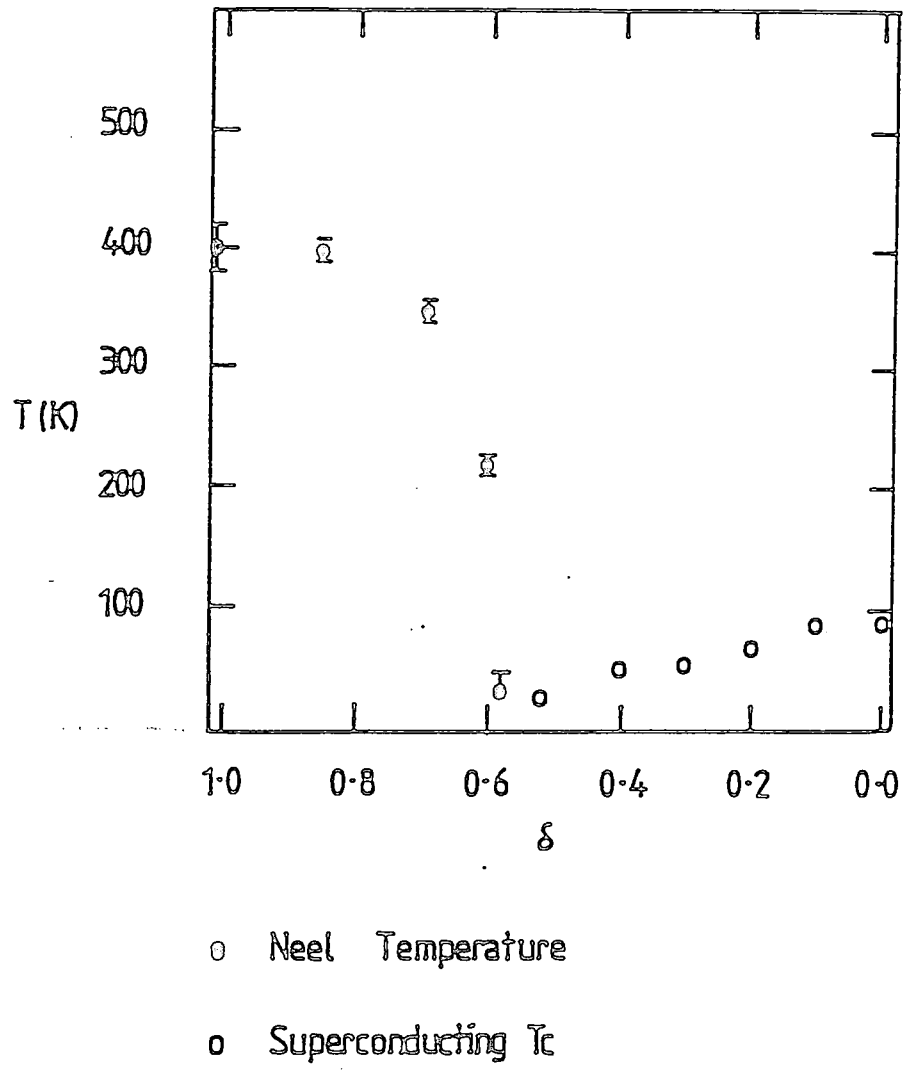

to that of $Y_1Ba_2Cu_3O_7$, which is shown in figure 2.1. It contains planes of copper and oxygen atoms separated by the yttrium and barium atoms. CuO itself might be considered the parent of this compound, but possessing three dimensional Cu-O order rather than the planar two dimensional order of Cu-O in $Y_1Ba_2Cu_3O_6$. CuO posesses antiferromagnetic order below around 240 K, and is not metallic or superconducting. CuO also possesses unusually stiff antiferromagnetic excitations, in common with various of the "parent" compounds of several high T_c systems (Aïn).

2.2.2 Occurence of Superconductivity

Superconductivity can be introduced by doping $Y_1Ba_2Cu_3O_6$ with extra oxygen. This gradually destroys the antiferromagnetism, shown by a decrease in the Neel temperature, and eventually makes the material metallic, with T_c increasing with oxygen content. T_c is optimised for a particular concentration, $Y_1Ba_2Cu_3O_7$ (See figure 2.2, Birgeneau). The crossover region between the insulating antiferromagnetism and metallic superconductivity is complex, and studies are hindered by metallurgical decomposition effects, leading to the possibility of domains of both phases separately in the same microstructure.

2.2.3 Structure

The properties of the crystal structure of this family and its modifications are extremely important in order to explain the physical properties of this material. (For a more full review, see Yvon, Schuller).

The superconducting phase is an orthorhombic distortion of a tripled perovskite structure. In this structure $a \simeq b \simeq c/3$, as shown in figure 2.1 (Calestani). The orthorhombic distortion is not visible in this diagram. This distorted phase is stable, as regards the cations, only below a transition temperature some way below the melting point . Above this orthorhombic / tetragonal (O-T) transition temperature, the tetragonal undistorted structure with a = b is the stable structure. This (O-T) transition temperature and the melting point vary considerably with the partial pressure of oxygen over the solid, and with the yttrium site cation (see figure 2.3, Specht, Kubo). This compound melts incongruently: the solid par-

tially melts to liquid and solid of different chemical composition. This is a major obstacle to the growth of crystals in a controlled manner.

2.2.4 Twinning

The orthorhombic distortion arising spontaneously at the (O-T) transition leads to crystallographic twinning, on a very small scale. Briefly, twinning is caused by the loss of $a = b$ symmetry; some regions choose to relax such that a is in one direction and some in the other. The energy cost at the walls of these domains is low, because the change in lattice parameter is small. These twins are a great nuisance. They could easily act as miniature "weak links", which break up the long range phase coherence of the superconductor. For our experiments, they also provide structures at the sort of real space scale that will contribute to the background in a small angle neutron scattering experiment. This is undesirable, especially with very small signals to distinguish.

Several groups have managed to reduce the numbers of twins in single crystals by applying compressional stress to single crystal plates and annealing them (Welp). This is however as yet a difficult way of making samples, as it risks fracture of the extremely thin crystals. Annealing samples just below the O-T transition temperature may also be a possible way to produce such crystals. No such techniques have yet been developed for polycrystalline materials.

2.2.5 Variation of Oxygen Content

This distorted phase can absorb oxygen reversibly over an extended temperature range, taking up oxygen at relatively low temperatures (of order 400 °C), and losing it at higher temperatures (Gallagher). Samples are remarkably sensitive to the atmosphere in which they are placed, particularly its O_2 partial pressure, as mentioned prevously (Karpinski,Specht). In addition, they continuously absorb or emit O_2 to reach thermodynamic equilibrium with their surroundings, but the diffusion rates of O_2 in these materials are low (Tu). Thus metastable O_2 contents are easily reached, whether this is desirable or not. This is probably the single greatest problem of sample preparation of $Y_1Ba_2Cu_3O_7$ based high T_c systems.

Figure 2.3 —

Diagram of oxygen content variation with partial pressure of O_2 $P(O_2)$ and temperature T for $Y_1Ba_2Cu_3O_{7-\delta}$, (Specht) showing the strong dependence of δ on $P(O_2)$ and T, and also the orthorhombic / tetragonal phase boundary line.

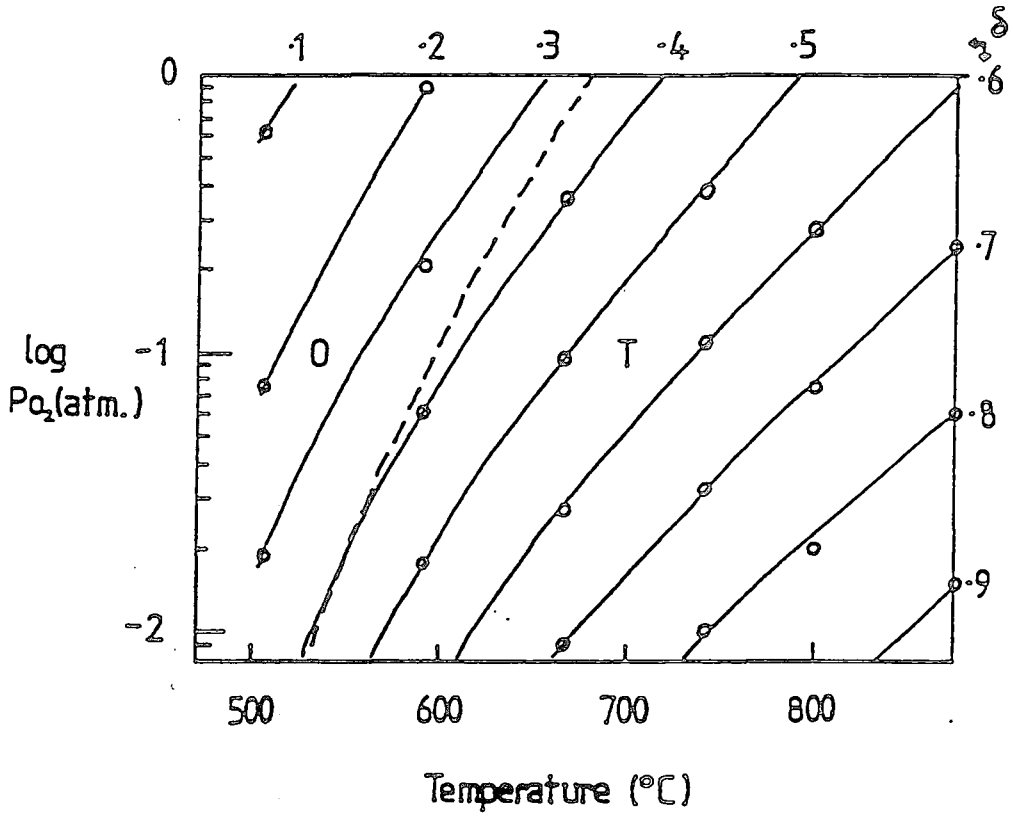

2.2.6 Effect of Oxygen Doping on Properties

All electronic properties including conductivity, the accessible regions of the extremely complicated phase diagram (Lee, Maeda), and the crystal structure, vary markedly with the oxygen content of the lattice (See figure 2.4, Beyers, Jorgensen).

Hence we see that the thermal history of samples is crucial to producing and reproducing meaningful results. Considerable care is needed to make sure that the properties of the sample are not misrepresented by electrical or magnetic testing, as a fraction of the system may mask the behaviour of the rest, due to "shells" of material with differing properties at the surface.[1]

2.2.7 Measurement of Oxygen Content

X-ray powder diffraction patterns give very little information on the oxygen content directly, due to the presence of much more massive atoms in the structure. Indirectly, the bulk average lattice parameters can be used if a suitably trusted data set can be found, for example, from a neutron scattering study which is inherently more suited to this problem. Neutron powder diffraction is sensitive, but expensive and needs bulk samples with which to work. The superconducting transition temperature would be a good tool in this case other than for the fact that it is of little or no use if there is any inhomogeneity. Testing the local oxygen content is also extremely hard as oxygen analysis is close to state-of-the-art elemental microprobe analysis, due to the long wavelength X rays that must be detected. Titrimetric analysis is a destructive technique but can give accurate bulk averaged results.

2.2.8 Normal State Conductivity

The metallic properties are extremely anisotropic, with orders of magnitude difference between the conductivity in one crystallographic plane ($a-b$) and in the c-direction. This is presumably due to the layered nature of the structure, with the high conductivity in the (doped) Cu-O planes (see figure 2.5, Penney, Tozer).

[1] As little as 30% of the superconducting phase in a random network shows superconductivity by electrical resistivity tests (Delap) - and an ordered distribution can make this a lot worse !

Figure 2.4 —

Diagram showing the variation in lattice parameters and T_c with δ in $Y_1Ba_2Cu_3O_{7-\delta}$, showing the orthorhombic distortion. Redrawn from Jorgensen

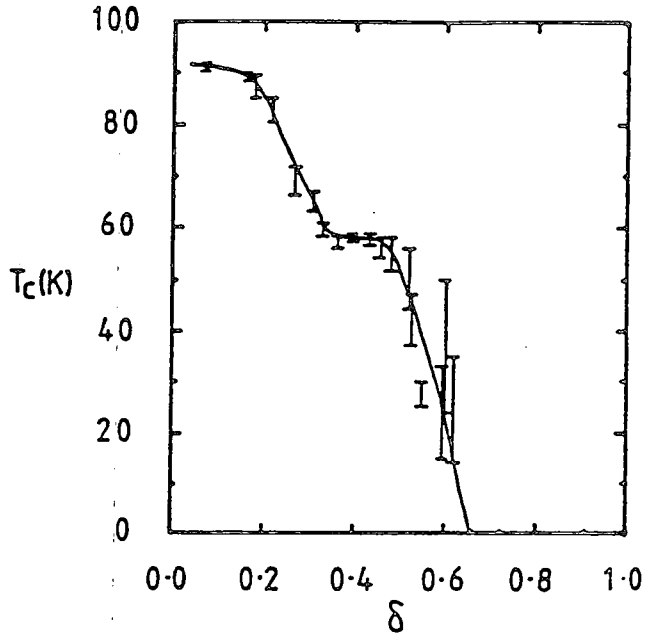

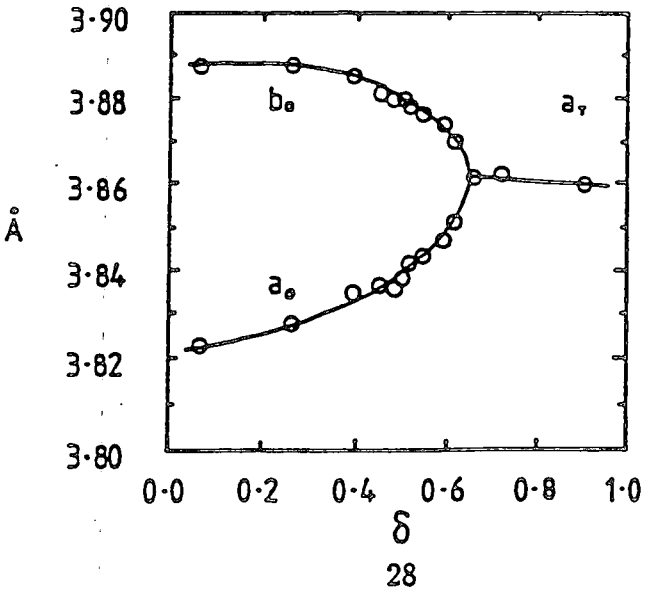

(Though the dopant sites are not themselves in the planes, being on the "chains" in the lattice).

The normal state anisotropy implies that the superconductivity is also likely to be strongly anisotropic. This is a major complication for many measurements. The resistivity above T_c is also closely linear with temperature to high temperatures. This in itself is also a fascinating property for a high T_c superconductor, as it implies that if electron - phonon effects are strong in this system, (as would be required for BCS mechanism superconductor), then the conductivity shows no effects due to the characteristic energy scale of phonons, e.g. the Debye temperature. The true behaviour of this quantity at low temperatures is of course masked by the superconductivity; however, measurements on other related systems such as $Bi_{2+x}Sr_{2-x}CuO_y$ ($T_c \simeq 6K$) indicate linearity over a very large range (Martin). It is perhaps worth noting that this is only strange because the T_c's are high and we expect strong electron-phonon interactions. It is arguable that the problem of the normal state of this material is worthy of considerable effort to understand; without this, obtaining insight into the more exotic superconducting state is likely to be difficult.

2.3 Superconducting Properties

Now that I have discussed $Y_1Ba_2Cu_3O_{7-\delta}$ and its crystal structure and the existence of superconductivity in this compound, I shall briefly outline the known facts about the superconducting properties of the highest T_c phase, $Y_1Ba_2Cu_3O_7$.

The superconductivity is extremely type II, with a large penetration depth and short coherence length. This is not very surprising, and can be seen to follow from the discussion of characteristic lengths in chapter I. Any high T_c system must have a large gap; Fermi velocities do not change very greatly from one metal to another. Thus a short coherence length is inevitable. The low electron density of this compound gives a large penetration depth directly.

As very many techniques have been used by myriad groups, not all of them can be summarised here. Instead a selection of the approximate values of certain properties is included. For a more complete review, see the references cited above.

Figure 2.5 —

Graph showing the anisotropic resistivity in the *ab* plane
and in the *c* direction above T_c in twinned single crystal $Y_1Ba_2Cu_3O_7$
Redrawn from Penney . *ab* plane data is for two different samples.

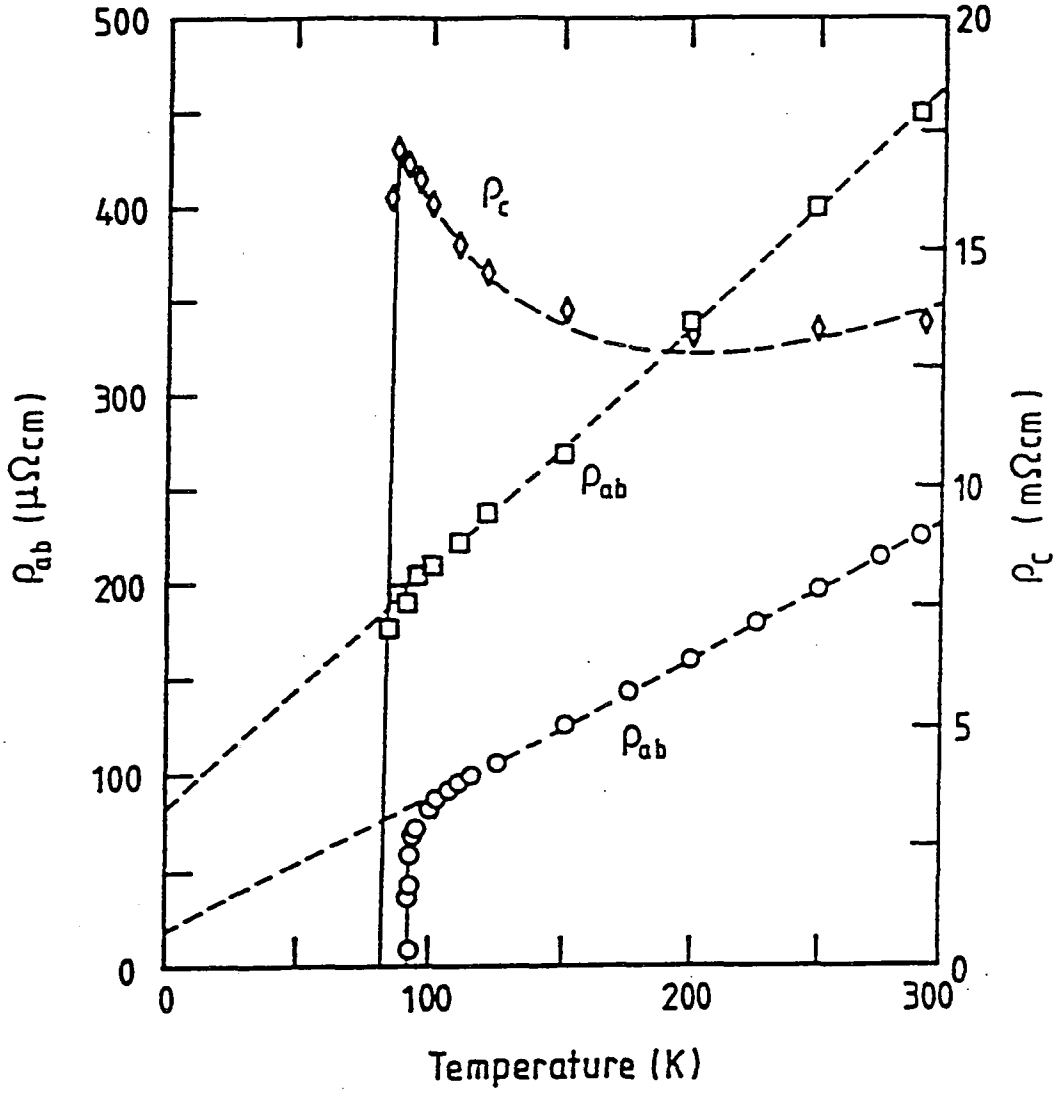

The anisotropy mentioned above means that all these quantities vary with direction; subscripts are used to indicate the direction concerned. All these properties are to some extent interdependent, but no attempt has been made here to force these chosen representative experimental values to be self-consistent.

Table 2.2 — Superconducting properties

Quantity	Value	Reference	Technique
$\lambda_{ab}(0)$	18000 Å	Forgan	μSR
$\lambda_c(0)$	1400 Å	Forgan	μSR
ξ_{ab}	12-15 Å	Hikita	Fluctuation σ
ξ_c	1.5-3 Å	Hikita	Fluctuation σ
$B_{c1}(0)_{ab}$	24mT	Fruchter	Torque magnetometry
$B_{c1}(0)_c$	110mT	Fruchter	Torque magnetometry
$B_{c2}(0)_{ab}$	34T	Gallagher	Magnetisation
$B_{c2}(0)_c$	240T	Gallagher	Magnetisation
$\Delta(0)_{ab}$	6.7 $k_B T_c$	Tsai	Tunneling
$\Delta(0)_c$	3.4 $k_B T_c$	Tsai	Tunneling

In addition, the following three techniques are particularly complementary to neutron scattering studies; they are thus useful to bear in mind for our purposes.

2.3.1 Nuclear Magnetic Resonance

NMR is a sensitive probe of excitations and internal magnetic fields of many systems. Basically, the absorption of radio frequency energy at a fixed frequency is measured whilst applying an increasing B field, tracing out a plot of the absorption resonances obtained. The positions and widths of the resonances obtained contain information upon the local B fields at the site of the atom chosen. This technique can be applied by choosing suitable isotopes and frequency / field ranges. The

linewidths characterise the excitations available to the system. As they measure the relaxation at a point in real space, an integral over all q at the resonance frequency is obtained. These frequencies are quite low, of order MHz. However, in the superconducting state it does suffer from needing an applied magnetic field in order to measure the resonances, which is repelled by the Meissner-London diamagnetism of the sample. At high frequencies skin depth effects in all metals mean that NMR samples should be thin. The subject of NMR in superconductors has been reviewed by MacLaughlin (MacLaughlin).

Interpretation of the results obtained on $Y_1Ba_2Cu_3O_7$ is difficult as the BCS prediction for NMR relaxation rate possesses a "Hebel-Slichter" peak in the relaxation rate due to the coherence factor for this process but $Y_1Ba_2Cu_3O_7$ ^{17}O NMR appears not to show such a peak. The reason for this is not clear (e.g. Barrett).

2.3.2 Muon Spin Resonance (μSR)

Muon spin resonance provides a means of measurement of the B fields at the sites occupied by muons when they are implanted within the sample. Thus this technique has been used to determine the penetration depth , by performing the experiments in the mixed state and looking at the B field distribution, which is an average over the flux line lattice (e.g. the Forgan paper referenced above).

This technique has also been used to examine the question of whether a DC B field can exist in the bulk of a superconductor, as required by various new theories such as those postulating particles with fractional statistics (Anyons) as a means of obtaining the rather odd properties of these materials. Kiefl and co-workers find evidence for some random magnetic field of magnitude 0.2 mT at the muon stopping site in $Y_1Ba_2Cu_3O_7$, but estimate that the nuclear dipole moment of the copper nuclei can cause such effects and estimate 0.08 mT as the upper limit for anomalous magnetic fields within the sample (Kiefl). The sensitivity claimed in the latter experiment is very high; these techniques are in fact somewhat complementary to neutron techniques which measure B field gradients in space and time, as they measure the magnitude of the B fields at the muon stopping sites. Thus μSR is a local probe technique rather like NMR but there is no requirement for an applied magnetic field. This is obviously a great advantage when working

with superconductors ! Fields of approximately .01 mT can be measured by this technique.

2.3.3 IR Reflectivity

The electronic properties of metals can be probed by their reflectivity of electromagnetic radiation. This is directly related to the conductivity; both have real and imaginary parts related by Kramers-Kronig relations. Measurements over wide ranges of frequency, together with suitable approximations for the behaviour away from this region, are needed to allow continuation to the whole of frequency space needed for the Kramers-Kronig inversion. The conductivity of superconductors is strongly modified below T_c, at frequencies below the gap, i.e. when there is insufficient energy to break up a Cooper pair. This is a good way to examine the low energy electromagnetic properties. The fact that high T_c materials are strongly two dimensional may also complicate matters due to residual states outside the Cu-O planes, giving apparent states in the gap. Typical results do indicate the opening of a gap, but of only some 80% of the weight in the gap being removed (e.g. Batlogg, Timusk and Tanner).

2.4 Sample Preparation

2.4.1 Powder Technique

Because of the rather difficult properties of this material, the best superconducting properties in bulk samples, large enough for our purposes, (i.e. mm in all dimensions), have been produced by a powder processing solid state reaction technique. This technique is very useful for making new compounds, mainly because it relies only on solid state processes and can be carried out at below the melting temperature to avoid undesired decompositions or incongruent melting. It is also extremely simple. In other fields, however, the disadvantage of the large surface area of powders permitting absorptions of unwanted chemicals into the exposed surface, especially atmospheric gases, outweighs these advantages.

The raw materials can be chosen from a range of suitable compounds available commercially, but if the oxides and carbonates are used, they are all insulators with relatively high melting points, and are prone to react with practical crucible

materials (Wolf, Scheel). The oxides and carbonates are however commercially available at extremely high purities, up to 6N (1ppm cation impurities).

2.4.2 Technique used

Our method consists of mixing suitable oxide or carbonate reagents, i.e. Specpure Y_2O_3, CuO, $BaCO_3$, 10 ppm total metal impurity (Johnson Matthey), in the correct cation ratios. These are then placed in a crucible of Al_2O_3 (Degussa, AL23) and heated in a resistive oven, to approximately 990 - 1000 °C, the uncertainty being due to thermometry; this is close to the incongruent melting point, so there is a need for care to avoid overheating. As an aside, this is due to the need for high temperatures to decompose the barium salt, but avoiding very high temperatures because this causes one of the incongruent melt products to wick out of the slightly porous alumina crucible, causing a stoichiometry variation. Too high a temperature also causes an extremely strong sintering of the grains, probably due to a wetting of the grain boundaries by the lower melting BaCuO/CuO eutectic, which is undesirable at this stage. This heat treatment causes them to decompose first into an intimate mixture of oxides, and then allows a solid state reaction to take place turning the mixture into a compound, or mixture of compounds. This initial mixing / reacting process may be repeated with grinding periodically in order to ensure good mixing, as this is essential for good stoichiometry material to be able to form.

The powder is then weighed out and pressed into pellets of the form required for the experiment, in a die at approx 10kbar. The die used is a modified Specac 3mm IR pellet die (Specac), having a shortened push rod to allow the quantity of material to be pressed to be increased. A second push rod is very useful to force the main push rod back through the die once the pellet is pressed, as the small amount of material trapped between the push rod and the die body can cause it to jam in the die.

This produces a density of 77 % of the theoretical density with typical particles, depending on the grinding process used, of tens to hundreds of microns. These pellets are then heated to a high temperature, allowing the grains to sinter together at typically 900-950 °C . The pellets are finally cooled in a flowing oxygen atmosphere, cooling slowly through the orthorhombic / tetragonal transition,

to minimise strain, and leaving at around 400 °C for a long time - typically one week, to maximise oxygen uptake. This leads to material with good electrical and magnetic properties.

2.4.3 Disadvantages

Major problems which arise are mainly due to the multitude of phases available to this quaternary system; common problems include inadequate initial reaction producing unreacted barium carbonate, and various other compounds such as the green phase $Y_2Ba_1Cu_1O_x$, and others. These can lead to a paramagnetism due to undesirable Cu^{2+} ions. This is obviously a complication for any bulk magnetic measurements at low temperatures. Further, if the oxygen content is not exactly correct, the T_c will be lower (as shown above). The solids thus produced are also extremely sensitive to their local environment and decay in wet air by losing barium from the compound, forming other salts. Samples for experiments, when in this sintered powder form, are best re-oxygenated prior to any experiment. Any crystals grown by other means, however, do not suffer as badly in this way, due again to the extremely slow diffusion of the oxygen from the bulk.

2.4.4 Sample Characterisation and Results

The major primary characterisation tool for this work was the resistive transition of the samples; a low absolute magnitude of resistivity is not strictly necessary for our experiments as these are probing the superconductivity at length scales of the order of 100 Å, i.e. well within the grains. Thus grain boundaries, which are the main limiting factor in the resistivity measurement, are not the dominant regions in the experiments described in chapters IV and V. More important for our purposes is the total homogeneity; however, this is very difficult to measure. Too high a density can reduce the homogeneity of oxygen site occupancy throughout the sample, leading to resistance behaviour dominated by well oxygenated surface sheaths. This is because the oxygen diffusion is slow and we thus need a good pore structure to enable the oxygen to penetrate deep into the sample. A high T_c is obviously desirable to show that we have good material of the correct phase and stoichiometry.

Figure 2.6 —

Graph showing the processing temperature vs. time
for preparation of the $Y_1Ba_2Cu_3O_7$ used in this work.

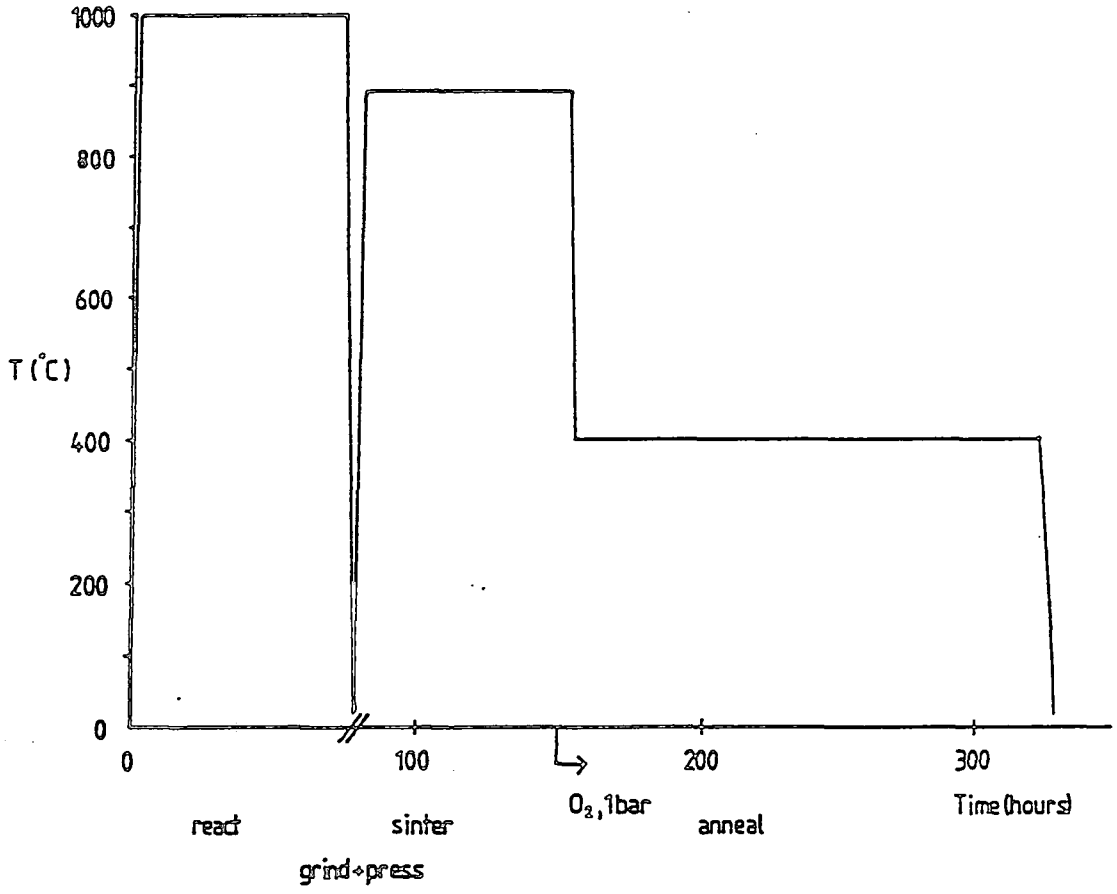

The use of a "long thin bar" sample geometry in these resistivity measurements was precluded by the size of the samples and the technique used for making contacts to the sample with conducting silver DAG paint (Acheson 915 DAG, (Agar Scientific), thinned with heptan-2-one), which leads inevitably to contacts of the order of 0.2-0.3 mm in size. Accordingly the "corner - corner" technique of Montgomery (Montgomery) was used to obtain the resistivity graphs shown, on a filed sample of dimensions 1.92 × 1.82 × 1.45 mm (all ± .02mm). Fields of 0.2 (± 0.1) mT and 3.0 (± 0.1) mT were applied using an iron-cored electromagnet and measured using a Bell 640 Gaussmeter and Hall probe. The thermometer was a copper/constantan thermocouple referenced to 77 K. The absolute magnitude of these resistivity measurements is probably only good at the 15% level, due principally to the finite contact size interfering with the calculation of the correction factors needed in this geometry. As the contacts used were along the edges of the "cube", no thickness corrections were used.

The absolute magnitude of the resistivity of these samples is rather high compared to that of the the best samples reported in the literature, which have a resistivity at 100K below 1 mΩcm. This is probably due to the fact that my samples were calcined at rather high temperatures (990°C) but only sintered at 900°C. Thus we probably have some second phase segregation or disorder at the grain boundaries, which raises the resistance and may be responsible for the tail to the R vs. T plot due to weak link effects.

X-ray powder diffraction performed with the Philips diffractometer in the Geology Department at Durham [1] indicated that the material was the expected phase (i.e. $Y_1Ba_2Cu_3O_{7-\delta}$) and structure with lattice parameters a = 3.82(±.02) Å b = 3.89(±.02) Å c = 11.63(±.01) Å. Very small peaks attributable to BaCuO at the 1 % level were seen. This was confirmed by 100 K bulk magnetisation measurements which indictated about 1-2 % Cu^{2+} paramagnetism.

[1] I am grateful to Mr. Ron Hardy for the use of this equipment.

Figure 2.7 —

Graph showing the resistivity vs. temperature
for sintered $Y_1Ba_2Cu_3O_{7-\delta}$
in .2 and 3 mT applied magnetic field.
Notice the high T_c and the resistive "tail".

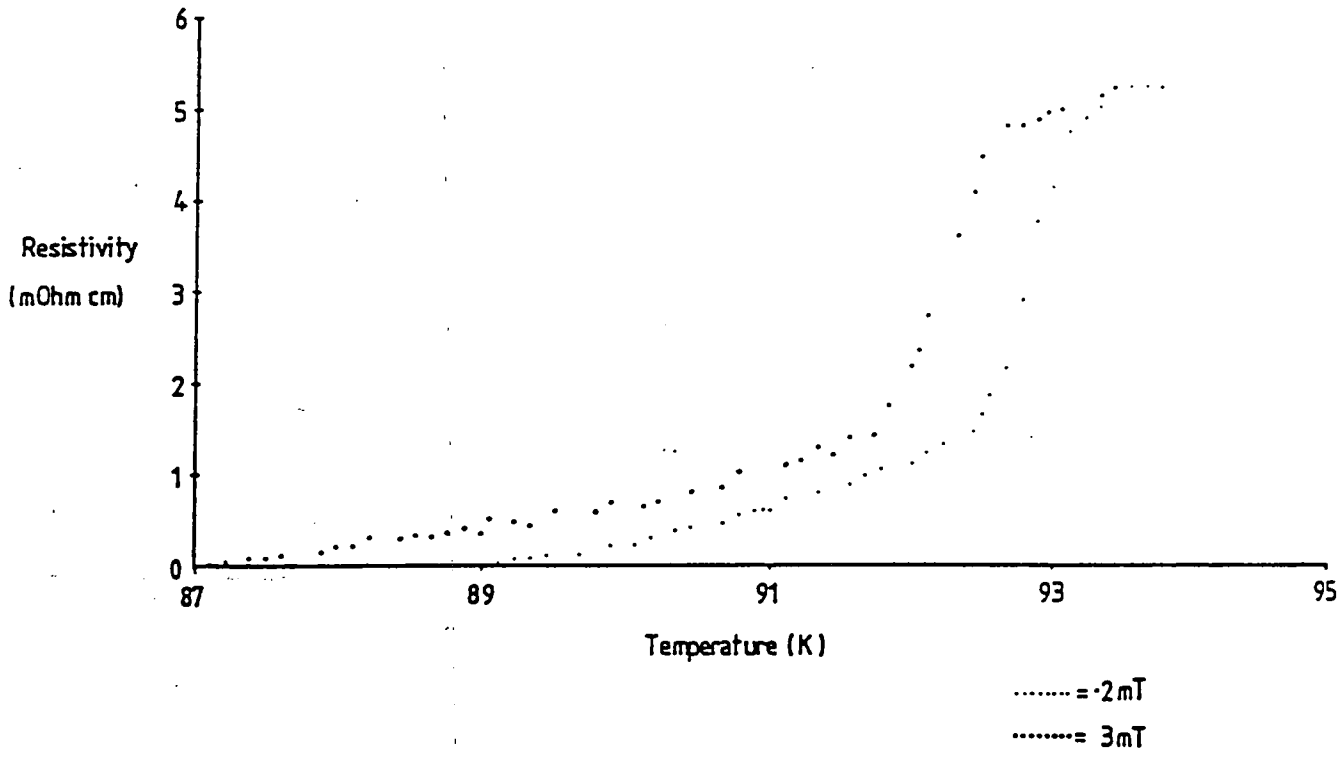

Chapter III

Neutron Scattering from Superconductors

Many of the subtleties we shall discuss are unlikely to concern the experimentalist. However, this paper contains some problems which may interest him.

Paul C. Martin, Phys. Rev. **161**, pp143-155 (1967)

3.1 Previous Work

Neutron techniques have not an obvious application to the study of superconductivity *per se*. This is in direct contrast to the field of the study of magnetism where the neutron can couple directly to the order parameter involved, that is to say microscopic magnetic (B) fields. I here ignore all structural studies of superconductors where neutron scattering obtains similar, but complementary, information to X-ray diffraction.

Those experiments which have been done are essentially involved with the changes of scattering due to the interaction of that scattering mechanism with superconductivity. In this way the effects on static magnetic order, (in terms of competition), the effect on antiferromagnetic excitations and the effects of the superconductivity upon the phonons have been examined. In addition, the spatial arrangement of the flux lines of the Abrikosov lattice has been examined by magnetic diffraction, and reflectometry has been used to measure the penetration of magnetic field into the surface of the superconductor.

These papers are concerned with many aspects of neutron scattering, that is to say magnetic diffraction from ordered atomic moments, magnetic inelastic scattering, nuclear inelastic scattering, and magnetic diffraction from modulated B fields. All of these could potentially complicate the results of our experiments, so I will discuss them briefly here.

3.1.1 Competing Ferromagnetic Order

The first, which is of interest only in very specific systems, involves magnetic elastic scattering from magnetic order in a phase in competition for existence with the superconducting phase (e.g. Burlet). This superconducting phase can exist in a temperature interval between the magnetically ordered phases. This is interesting in its own right as being a case where superconductivity is not the ground state of a system in which it occurs. Put another way, this is one of the few cases where superconductivity can be approached from below in temperature ! Neutron scattering has been used to examine the magnetic ordering via the intensity and position of the diffraction peaks.

This does not occur in High T_c systems; a search for magnetic fluctuations in $Y_1Ba_2Cu_3O_7$ performed using D7 at the ILL has given a stringent lower bound upon any possible magnetic excitations over a wide range of (q,ω) space (Schärpf, Brückel).

3.1.2 Other Magnetic Effects and Superconductivity

With the discovery of superconductivity in so called heavy fermion systems, e.g. UPt_3 (e.g. Franse), the relationship between the unusual magnetic properties of these systems and superconductivity is currently a subject of much interest. This is partly because these systems may be examples of non s-wave superconductivity, where the Cooper pairs have a net orbital angular momentum. In such systems, neutron scattering may give vital information - see for example (Joynt). However, low energy inelastic scattering experiments from these systems are difficult, due partly to the low temperatures at which superconductivity occurs in these systems, below 1K. This can lead to considerable experimental difficulties. Few modes are thermally excited at these temperatures, and cold neutrons have a very low incident energy, so we can only reach a limited part of phase space.

In High T_c systems, antiferromagnetic order on the Cu sites is in competition with superconductivity: we know this because it occurs in the non-superconducting tetragonal oxygen deficient $Y_1Ba_2Cu_3O_{<6.4}$, as I have mentioned in chapter II. Studies of possible coexistence of copper site antiferromagnetism and superconductivity are complicated by phase segregation effects, as mentioned previously.

The studies of antiferromagnetic excitations by experiments in single crystals near this region of composition may yet resolve this point. (See the reviews of Birgeneau and Tranquada). Although some of the rare earth $RE_1Ba_2Cu_3O_7$ compounds do show antiferromagnetic order on the rare earth site at very low temperatures, ($\simeq$ 2K), this does not affect their superconductivity. Yttrium, as in many other cases, behaves as a non-magnetic rare earth in these systems.

3.1.3 Flux Line Lattice Studies

In this case, the modulated magnetic field of the Abrikosov flux lattice is examined by neutron diffraction. Information from the various Bragg reflections and their intensities can be combined to give the field distribution across one flux line and the spatial arrangement of these lines. In some sense this measurement is complementary to DC magnetisation measurements; what is measured is the field contrast, as there is no scattering from a spatially uniform field. This is a very useful technique, and has been applied to several materials, including $Y_1Ba_2Cu_3O_7$ (Schelten, Christen, Forgan).

High T_c systems are particularly difficult ones for this sort of measurement, mainly due to the extremely low wavevector q of the reflections at experimentally reasonable B fields, and the need for a single crystal. The experimental geometry is also somewhat awkward, due to the need for sizeable B fields parallel to the neutron beam, whilst of necessity maintaining a small volume of apparatus in the beam. This low contrast and the high fields required mean that it is rather unlikely that our experiment can observe any scattering from a flux line lattice, especially as we are only in the earth's magnetic field.

3.1.4 Reflectometry

At the superconductor surface, in an applied small magnetic field (below B_{c1}), the field distribution is given simply by the geometry and the penetration depth. Neutron reflectometry is a powerful tool for the study of surface magnetic field distributions and has been used to measure this penetration depth (Mansour). Values obtained for High T_c materials vary and are rather different depending upon the sample, but can give results that are at least consistent with other means of measuring the penetration depth. Note that the anisotropic nature of the solid

may have to be taken into account in a polycrystalline sample. This effect is of little consequence for our purposes as we have a bulk sample in a weak magnetic field (the earth's). In addition, it would be expected to be strongly affected by any change in the applied magnetic field.

3.1.5 Phonons

The phonons at low energy in superconductors are affected by the strongly modified low energy properties of the electron gas. Longitudinal phonons, with their associated (screened) charge fluctuations might be expected to be affected by the dramatic change in response of the superconductivity (Allen). However, it appears that transverse phonons are affected in similar ways (Shirane). This is perhaps not so surprising in that phonon frequencies are only weakly dependent on such low energy properties of the electron sea. The damping, however, can be dramatically reduced. The energy resolution required to measure these low dampings is a difficult constraint for current experiments. The most odd feature of these experiments is that whilst low energy phonons soften and lose damping, at phonon energies just above the gap the damping can increase ! This shows that the phonon-electron system is not a simple one to analyse. Nevertheless, the measurements are at least broadly in agreement with the theory. Not many experiments have been done on this effect, it seems, as even in elemental superconductors these are not easy experiments, as very high resolution is required. For more information see (Youngblood, Axe). There is no published data on the effects on specific phonons of varying temperature in $Y_1Ba_2Cu_3O_7$ at finite wavevector q.

Incoherent one phonon neutron scattering can also be used to measure the total density of states of the phonons weighted by various factors relating to the neutron cross-section. Its temperature dependence can also be measured. This can show up the broad trends in the phonons, giving an idea of where the softening occurs in terms of the phonon energies (e.g. Reichardt).

3.2 Directly Probing the Superconducting State with Neutrons

3.2.1 Analogy

It may be worthwhile here to show that there is a weak analogy between High T_c superconductors and weak itinerant ferromagnets, which are metallic systems which develop ferromagnetic order at temperatures of order 30 K. Notice that the critical temperatures, and hence energy scales of the phenomena are of the same order. Here in both cases, there are strong magnetic correlations; one produces perfect diamagnetism whereas the other has a non-vanishing magnetisation in zero applied field. In weak ferromagnets, these correlations can be observed both above and below the Curie temperature T_C by small angle neutron scattering experiments.

Drawing upon this example, it may be useful to ask whether there are any low energy excitations of the superconductor which could be measured with neutrons in a similar way. The neutron has a great advantage over other probes in this regard as it has its own magnetic moment, and can thus probe the response to an applied field even in the bulk of a superconductor. Naturally, the neutron moment will be screened by currents flowing in the superconductor around it, but these screening currents after all correspond to the magnetic response of the system to the perturbation, that is to say the neutron!

It may be wise to treat this analogy with a degree of suspicion. One reason for this is that although we have examples of incipient ferromagnetism, (e.g. Ni_3Ga), where strong ferromagnetic correlations exist but ferromagnetism does not actually occur, no such system has ever been found that demonstrates incipient superconductivity.

3.2.2 Suitable Regions of (q,ω) Space

Now if this is a sensible idea, we have to estimate at what scales of (q,ω) we are likely to see any effects at all. In chapter I, it was pointed out that all the relevant q-scales for superconductivity are rather small. This is especially true by comparison with the weak ferromagnets, where there can be appreciable effects out to a sizeable fraction of the zone boundary. The response of the superconducting

state is only of full strength, (even at zero temperature), at $q < \xi^{-1}$. This expresses the fact that the coherence length represents that distance scale over which we can vary the order parameter. We know also, that in tending towards truly macroscopic length scales (i.e. small wavevectors), the magnetic response will be dominated by screening effects. This may be expressed in wavevector terms by saying that, to a first approximation, only effects at $q > \lambda^{-1}$ will be unaffected.

Thus the q-range that seems to be likely to be interesting is $\lambda^{-1} < q < \xi^{-1}$. An extreme type II superconductor with a short coherence length seems to be the ideal object for study in this case. Unfortunately, no element seems to be an obvious low T_c test case to investigate - the most type II element (niobium) is not extremely type II. Thankfully, High T_c systems provide just such a case. These q-ranges, in High T_c systems, are right at the lower limit for feasible neutron scattering experiments, using the small angle scattering technique. It is important to note that these q scales are temperature dependent and that there is no way that we could reach ξ^{-1} at T_c as it approaches bulk (i.e. very small) wavevectors.

3.3 Theoretical Calculations of the Neutron Cross-Section

This question is closely related to the problem of the scattering of neutrons from the normal electron gas in a metal treated by Sasaki and Obata (Sasaki). At extremely low q, they showed that the screening effects of the motion of the electrons are important, even in the normal metal. This can be thought of as the effect of eddy currents, which respond to damp any changing magnetic field. This low q screening has never been experimentally observed, as in the normal metal the experimental q's required are truly daunting (of order 4×10^{-5} Å^{-1}).

The only published direct attempts to deal with this whole problem in a superconductor and specifically in a High T_c system are the various of papers of Rajagopal, Mahanti and Jin (Rajagopal,Jin). † Both these papers, and that mentioned above, address the problem by formulating the neutron scattering cross-section in terms of the current-current correlation function of the system.

It is possible that the low q screening may well be much stronger in the superconductor if we take account of the Meissner-London diamagnetic response at

† The paper of Joynt mentioned above treats only the spin part of the susceptibility

wavevector scales of order q < λ^{-1}, giving a greatly increased screening effect - in addition, as the superconductor currents are persistent, they screen even DC fields (unlike eddy currents).

Rajagopal et al focus attention upon the orbital part of the susceptibility at low q as the best place to see effects from the superconducting transition. They predict a decrease in orbital scattering in the superconductor compared with a non-superconductor at T = 0. However, they give the relevant expression for the cross-section leaving out various constant factors; this leaves the question of intensity open ! They also expressly ignore the effects of the screening at low q.

Appendix A contains a derivation of the quantity we are measuring here in as short a form as possible. The main result is (in c.g.s):-

$$\frac{d^2\sigma}{d\Omega d\omega} = \frac{\gamma^2 e^2 k'}{48\pi^3\hbar^2 c^2 nk} \langle\ |\mathbf{B}(\mathbf{q},\omega)|^2\rangle$$

$$\text{where } \langle\ |\mathbf{B}(\mathbf{q},\omega)|^2\rangle = 6(4\pi)^2\hbar\omega n(\omega)\left[K^\dagger \frac{\sigma'_{reg}(\mathbf{q},\omega)}{c^2q^2}\right]$$

$$\text{where } K^\dagger = \mu^2[(1-\mu\omega^2/c^2q^2+4\pi\mu\omega\sigma''_{reg}(q,\omega)/c^2q^2)^2+(4\pi\mu\omega\sigma'_{reg}(q,\omega)/c^2q^2)^2]^{-1}$$

where γ is the neutron gyromagnetic ratio, n the number of atoms per unit volume, and k' and k the final and initial neutron wavevectors respectively. μ is $\mu(q)$ in all the above equations.

This result demonstrates the sensitivity of neutrons to the effects of the conductivity fluctuations in a solid, and contains the relevant small q screening as discussed above, but with a slightly different result which expressly includes the Meissner-London diamagnetism in μ.

Ignored in this formulation are the nuclear scattering terms, and spin susceptibility scattering (spin waves, paramagnons etc.). Other measurements such as those of the bulk paramagnetic susceptibility of $Y_1Ba_2Cu_3O_7$ (e.g. Junod) do not indicate strong enhancement of susceptibility in bulk material, so this can safely be ignored in this system at low q.

The discussion of chapter I leads us to expect that the regular part of the conductivity will in fact lose weight at low energies as the gap develops and the weight in the delta function increases: this expression is therefore in at least broad agreement with that of Rajagopal mentioned above. Thus the theory predicts firstly a loss of scattering below T_c, caused by the opening of the gap, and perhaps a slight enhancement of scattering above T_c due to fluctuation effects.

We must not though forget the "normal" electron contribution at around T_c. This is especially true given that the coherence efects mentioned in chapter I may also be important here, as the NMR relaxation rate shows; such coherence effects can enhance such relaxation / scattering processes, but only by numerical factors of order 2 in real systems. In any case, such enhancements have not yet been observed in High T_c systems such as $Y_1Ba_2Cu_3O_7$ and may not actually occur in these sorts of system.

3.3.1 Sum Rules

Sum rules on the quantities used to derive the cross-section (i.e. σ'_{reg}) must give an upper limit to the cross-section that can be measured. These are also illustrated in appendix A. The total cross-section if integrated over all the conductivity, for reasonable choices of parameters for $Y_1Ba_2Cu_3O_7$, gives a total cross-section even at low q (q = 0.04 $Å^{-1}$) of order 10 mbarn/sr/atom (Bernhoeft).

Now we can only use this result as the maximum cross-section possible just for orbital scattering, if all the scattering lies within the window for neutron scattering allowed by momentum and energy conservation. This means that all the conductivity has to be at low energies. This implies in turn we will need to be in the clean limit, with a long mean free path, and a low Fermi velocity even to see this much scattering at low q. Nevertheless, it gives a feel for the orders of magnitude involved. These effects are, in this formalism, rather weak and do not

seem to be enhanced: this is in direct contrast to the paramagnetic term near the ferromagnetic transition.

Experiments to try to measure these effects are discussed in the next 2 chapters.

Chapter IV

SANS Studies of $Y_1Ba_2Cu_3O_{7-\delta}$ – Background

"I saw the flying atom-streams, and torrents of her myriad universe. "

Lord Tennyson, Lucretius

4.1 The Small Angle Neutron Scattering Technique (SANS)

4.1.1 General Introduction

SANS is, as its name suggests, the investigation of the small angle scattering of neutrons. Small angle scattering is interesting because it probes the long wavelength (low wavevector q) properties of the sample, at typical q's of 0.004 to 0.2 $Å^{-1}$. The technique is sensitive to any property of a sample that gives rise to elastic or low energy inelastic scattering phenomena at these scales of distance or momentum. It is thus used across large ranges of modern science. Examples of the elastic scattering investigated include diffuse scattering due to macroscopic changes in scattering length in polymers and diffraction studies of large scale crystal structures. It is also of great interest for probing the collective excitations of many solids, especially close to phase transitions. See (Windsor, Bernhoeft). Low angle scattering is inherently a good place to look for magnetic scattering due to the lack of phonon creation scattering, as $v_n < v_{ph}$ (e.g. Lovesey).

The separation of the dynamical from static effects is usually done by varying the temperature and observing changes in the scattering of neutrons. To first order only the difference in populations of the various collective modes, (phonons, magnons, paramagnons), of the sample will then contribute. This subtraction technique can get rid of the small angle scattering from the inhomogeneity of the sample, diffuse scattering, which is not of interest in these experiments.

Energy analysis of the outgoing beam may also be employed. Obviously, energy analysis gives a more complete picture of the nature of the scattering, which may

permit a more detailed model to be constructed. However, there is a corresponding cost in the time required for the experiment, due to the need to monochromate and analyse the beam. The advantage of such inelastic experiments is their ability to choose to work at finite energy transfer to minimise potential sources of error due to other scattering mechanisms.

4.2 Discussion of Other Published Work on $Y_1Ba_2Cu_3O_7$

To date, there have been various studies of high T_c materials by SANS, all of which have given published results which are not quantified in terms of the absolute cross-sections. They are briefly discussed below. All are by total scattering techniques, with no energy analysis.

4.2.1 Search for Suppression of Paramagnetic Scattering

In this paper (Lynn) magnetic fluctuations in the rare-earth substituted High T_c system $Er_1Ba_2Cu_3O_7$ are considered. The experiment seeks to show the effects on the paramagnetic scattering, (from the Er ions), due to the screening effects of the superconducting state. In order to do this they use high temperature data as the standard to remove the "metallurgical" defect scattering and seek a decrease in the overall scattering. Their results do show that at temperatures below T_c there is less scattering at q's below around 0.045 $Å^{-1}$. See figure 4.1. They use this to obtain a London penetration depth of around 20 Å even close to T_c, which is not consistent with other measurements by possibly two orders of magnitude: see chapter II.

Other questions remain too; no absolute magnitude is given for the observed scattering, so comparison with our data is impossible. The error bars used are also of uncertain origin and size, with apparently very small size at some points. Using a system with a rare-earth in it leads to the possibility of scattering from "crystal field" levels at finite energies. These can be thermally populated and give temperature dependent changes. No account is taken of the possible incoherent phonon scattering or multiple scattering effects changing the subtracted "metallurgical" background level at high temperatures, leading to an error by overestimating the subtracted background. On the other hand, it would be possible to look at this data and to say that there was excess scatter at low q close to T_c, using the

Figure 4.1 —

The SANS results of Lynn et al.
The first graph shows the temperature dependence of the scattering intensity I summed over a range of low q's, using a high temperature subtraction.
The second shows the q dependence at two particular temperatures, using the same high temperature subtraction.

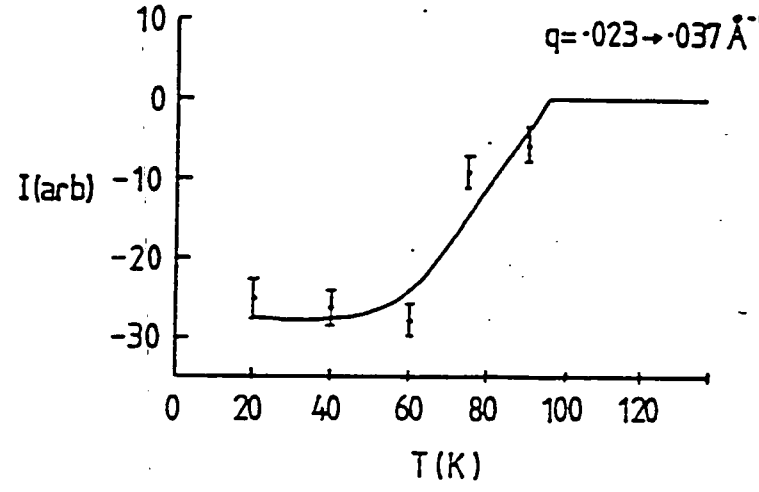

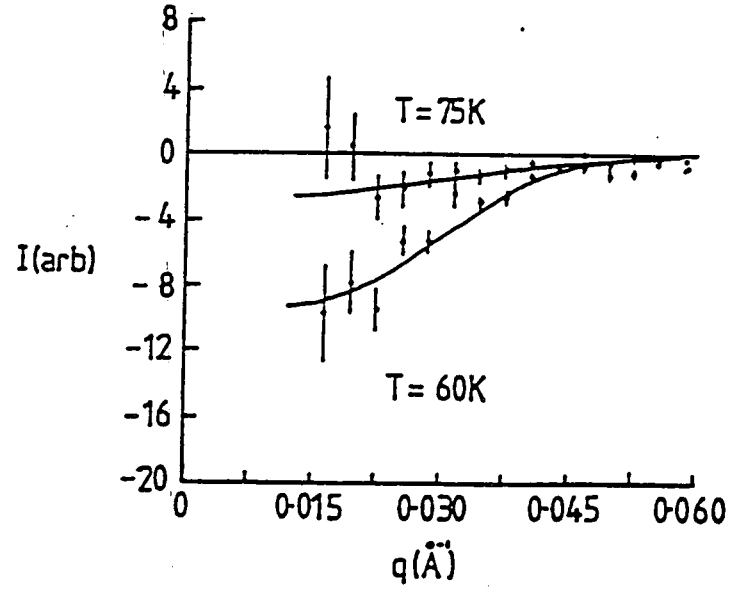

60 K data as the baseline for the subtraction. Without the absolute calibration, however, this is about all that can be said.

4.2.2 Search for Suppression of Spin Susceptibility

This paper (Bulaevskii) uses the experimental data of Lynn discussed above. However, it comes to the conclusion that as superconductors are known to possess a vanishing conduction electron spin susceptibility, due to the opposite spin pairing, then the superconducting state will supress the spin fluctuations due to the atomic Er moments on the length scale of ξ^{-1}. However, there are two objections to this: the atomic moments are not due to the same electrons as those that pair, (which are in the Cu-O planes), and there is still little enough screening that antiferromagnetic ordering of the Er moments eventually arises at roughly 0.5 K. It is difficult to see how the model can be claimed to work without an absolute value for the expected scattering and its supression. In other words, whilst arriving at a reasonable length scale, this is still a "handwaving argument", and suffers from the same experimental defects, as it uses the same data.

4.2.3 Polarized Neutron Experiment

This paper (Axelrod) uses the transmitted beam and very low angle scatter from a sample of $Y_1Ba_2Cu_3O_7$, and appears to show distinct changes in scatter and polarisation at temperatures between 60 and 90 K. In this temperature range, the beam is depolarised by $\simeq 2\%$, small angle scatter is supressed, and transmitted beam measurement is enhanced (see figure 4.2). This is a very difficult combination of results to explain, if genuinely intrinsic to the samples.

The authors attempt to do this by proposing that liquid oxygen forms in the pores of the sample. This effectively increases its homogeneity in scattering amplitude and thus decreases low angle scatter, but introducing magnetic scattering from this oxygen which depolarises the beam. They suppose that this oxygen must come from the sample or the air in the pores in the sample when sealed into its ampoule for the experiment. However, the amount of oxygen required must be quite large, to fill a substantial number of the pores with liquid oxygen. A further point to consider is the difficulty of performing truly polarised beam experiments with a superconducting sample; the Meissner diamagnetism makes it impossible

Figure 4.2 —

The SANS results of Axelrod et al.
The top two graphs are at very low q; the bottom two are transmitted beam measurements. Here I is the measured intensity, and P/P_i is the fractional polarisation of the beam.

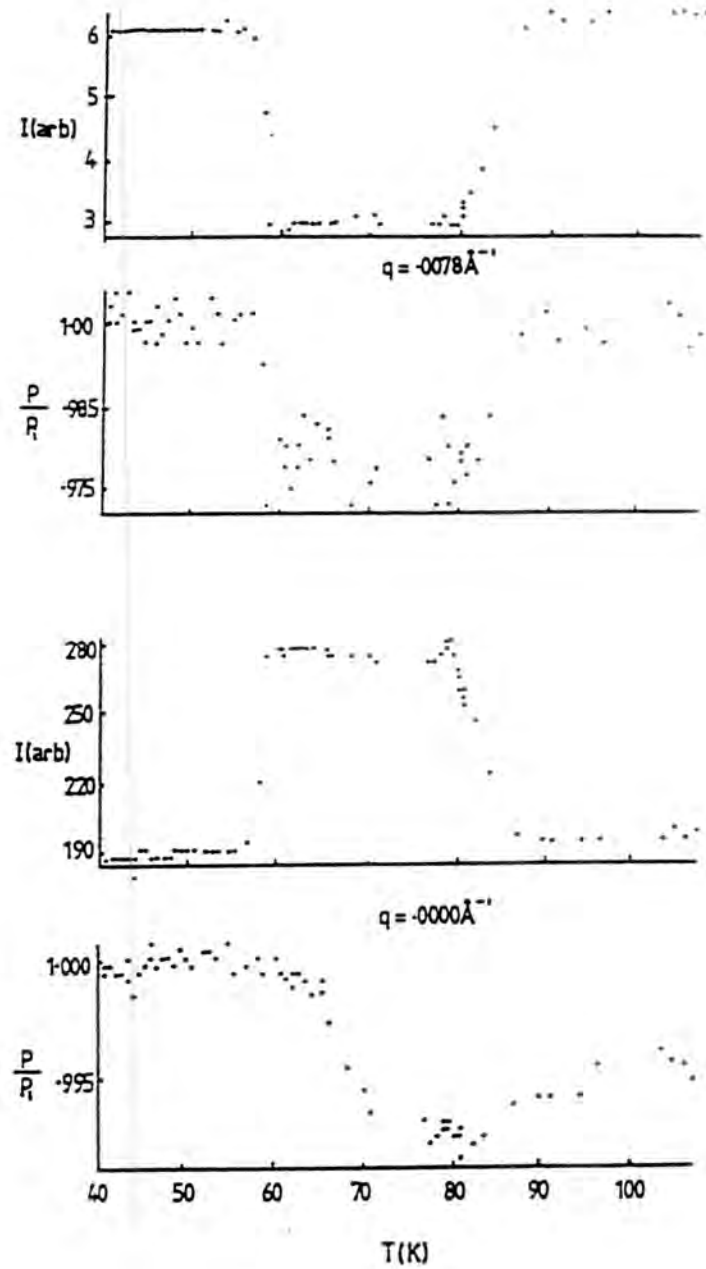

to have the necessary small magnetic "guide" field to maintain polarization inside the sample. This problem may not be too severe if the sample is thin.

This possible oxygen condensation mechanism is avoided explicitly in our experiments by using an evacuated sample space containing the minimum amount of helium gas for the required temperature stability.

4.2.4 Search for Possible Large Scale Structure

This paper (Kahn), is concerned with scattering at small angles at room temperature, of small single crystals of $Y_1Ba_2Cu_3O_6$ and $Y_1Ba_2Cu_3O_7$. The small angle diffraction is analysed in terms of the dimensions of the misaligned platelets making up the sample; 100 Å is the size deduced in the c direction. Also, a peak at extremely low q is ascribed to a possible ordered structure of period 560 ± 50 Å in the superconducting sample ($Y_1Ba_2Cu_3O_7$). This might be a long-range oxygen ordering in the lattice forming a superstructure.

4.2.5 Conclusion from Previous Experiments

There appears to be no consensus at all upon the low temperature small-angle scattering results or even the interpretation of that data which has been published. At high temperatures there is a possibility of an ordered phase with an extremely large period. This would be at an unobservably small q in our experiments, so I will not mention it further.

4.3 Experimental Design

4.3.1 Introduction

The typical SANS experiment consists of:-

1. a source of sufficiently monochromatic neutrons,
2. collimators to define the beam,
3. a sample, in some environment (e.g. cryostat),
4. a long sample to detector flight path to allow the detection of small angles of scatter with reasonable sizes of detector,
5. a beamstop in order to remove unscattered neutrons,
6. a large detector in order to make efficient use of the whole solid angle of scatter available.

Small angle scattering can be particularly efficient in this last area as all the relevant scattered intensity can be contained on one multielement detector. At the ILL in Grenoble, the three instruments that we have used are called D11, IN5, and IN3, which are briefly described in the sections referring to the individual experiments below. Further details of these instruments are contained in the "Yellow book" produced by the ILL.

4.3.2 Background Scattering

Now, a brief discussion of the possible background scattering, which needs to be eliminated from the signal as measured on the instruments in order to reasonably interpret the data.

4.3.2.1 Bragg Scattering

In all such experiments it is at least desirable that the total number of background scattering processes available should be minimised. Thus, if possible, the so-called Bragg cutoff wavelength should be exceeded. This corresponds to a wavelength of incoming neutrons such that the smallest scattering reciprocal lattice vec-

tor would need to scatter the neutron at a physically impossible angle. Exceeding this value would eliminate all Bragg scattering events in the sample, and perhaps also in the cryostat walls and windows, depending on the relevant materials and wavelengths. With a finite spread of wavelengths coming from the monochromator, one must exceed this wavelength by a safety margin to allow for this spread in incoming wavelength.

With all High T_c ceramic systems, the unit cells are large i.e. c axes are of order 12 Å, so it is impracticable to reach the Bragg cutoff wavelength of $2c$ with a reasonable flux from a cold neutron source at this time. Nevertheless, this might be considered as a way to make the experiment "cleaner". Thus Bragg scattering from the sample will be observable in the collected signal, especially at the rather high angles available on IN5. See figure 4.3. Single Bragg events are however unimportant as they appear at a well defined angle for a monochromatic incident beam, and are thus easy to reject during the analysis.

4.3.2.2 Phonons

Coherent or incoherent single phonon annihilation or creation is also a possibility; however, the phonons disperse rather rapidly. Thus at the relevant q scale they have rather large energies, and hence small (thermal) populations for neutron energy gain. They are unavailable for neutron energy loss events, due to the low incident neutron energy.

Phonons are also much more visible at higher q, as can be seen from the following expression for the cross-section for scattering from a phonon (e.g. Squires):-

$$\frac{d^2\sigma}{d\Omega d\omega} = \frac{k_f}{k_i}\frac{(2\pi)^3}{2v_0}\sum_s\sum_\tau \frac{1}{\omega_s}\left|\sum_d \frac{\overline{b_d}}{\sqrt{M_d}} e^{-W_d} e^{i\mathbf{q}.\mathbf{d}}(\mathbf{q}.\mathbf{e}_{ds})\right|^2$$
$$\times \langle n_s\rangle \delta(\omega-\omega_s)\delta(\mathbf{q}-\mathbf{k}-\tau)$$

where d is the nuclear species, s the phonon branch index, v_0 the unit cell volume, M_d the nuclear mass, $\overline{b_d}$ the coherent scattering length, $\mathbf{d}$ the equilibrium position of atom d, q is the wavevector transfer, k_f the final neutron wavevector, k_i the initial neutron wavevector, k is the phonon wavevector, τ is a reciprocal lattice

Figure 4.3 —

Total scattering on IN5, showing the first Bragg peak

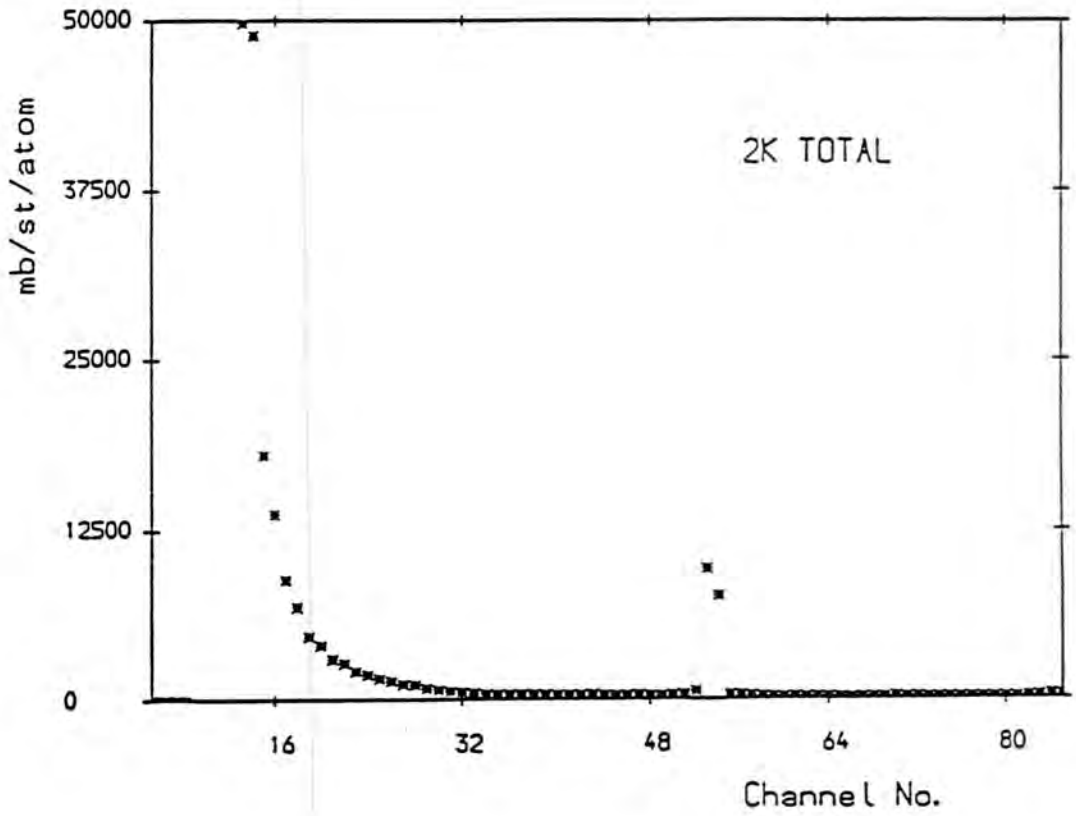

vector, ω is the energy transfer, ω_s is the phonon energy, $\langle n_s \rangle$ the Bose factor, and e^{-W_d} the Debye-Waller factor.

As can be seen, the phonon cross-section increases as q^2, and its importance at low q can thus be estimated from the high angle results on IN5.

4.3.2.3 Multiple Bragg Scattering

A more pernicious problem is multiple scattering in the sample by a combination of Bragg reflections and phonons. This combination can allow small net changes in energy and wavevector, giving a signal apparently in the desired range of (q,ω). In addition, it can have a temperature dependence due to the change in population factors of the relevant phonons. Multiple phonon + Bragg scattering should however be at least broad in its energy range due to the extreme averaging over angles and energies involved.

4.3.2.4 Structural Changes

Thankfully, there are no major structural changes in $Y_1Ba_2Cu_3O_7$, at or around T_c (David); such changes would introduce extra Bragg reflections and invalidate the subtraction technique.

4.3.2.5 Other Sources of Scatter

Other sources of noise at low angles include the extreme wings of the direct beam hitting the detector rather than the beamstop, cryostat scattering, incoherent scattering from the sample and cryostat, electronic noise in the detector system (these last two being present at all angles), and the diffuse scatter from the variations in the bulk structure of the sample due to inclusions, defects, etc.

These show no temperature dependence except possibly due to the change in transmission of the sample and can be subtracted away using the lowest temperature run as a calibration. Any thermally populated collective modes will be virtually empty if their energy scales are much higher than that of the lowest temperature available. This use of a low temperature subtraction is, however, not without problems; the error due to statistics alone is from the total counts, not just

those counts remaining after subtraction. The effect of a variation in the sample transmission on this subtraction must also be considered.

4.3.3 Summary

The experimental solutions to these problems are :-

1. The experiments are best performed at low temperatures, in order to have as few phonons excited as possible.

2. Suitable designs of sample and shielding mask are used, to give the minimum free path for neutrons scattered at high angles, in order to minimise the amount of multiple scatter back into the low angle detectors.

3. The incident wavelength used is kept as long as possible in order to keep to a minimum the number of available Bragg reflections.

4. A further safeguard is to keep the total scattering to a small fraction of the incident beam, typically less than 5%.

4.4 Calibrations

As an absolute calibration, we can use the incoherent scatter from suitable samples such as vanadium and plexiglas (PMMA). Plexiglas is also used to calibrate the relative detector efficiency and solid angle viewed by each group of detectors. These two standards are used because vanadium has a well known absolute cross-section, dominated by its large incoherent (angle-independent) scattering (4.97 barns/atom). However, vanadium also gives a peak in scattering at low angles, of uncertain origin. Plexiglas, being amorphous, has no structure at these wavevectors and can thus be used for the relative solid angle and efficiency calculation for all detector angles. Once calibrated against vanadium it can also be used as a secondary standard, useful because it has a much larger cross-section. This is helpful in extremely low q work, allowing rapid calibration runs and thus maximising the available time for the weakly scattering experiment. Care must be taken however, as plexiglas can absorb water, which is also a strong incoherent scatterer, thus leading to an error in the scattering as it will change over a long time period.

Figure 4.4 —

Total inelastic scattering on IN5, showing noisy channels

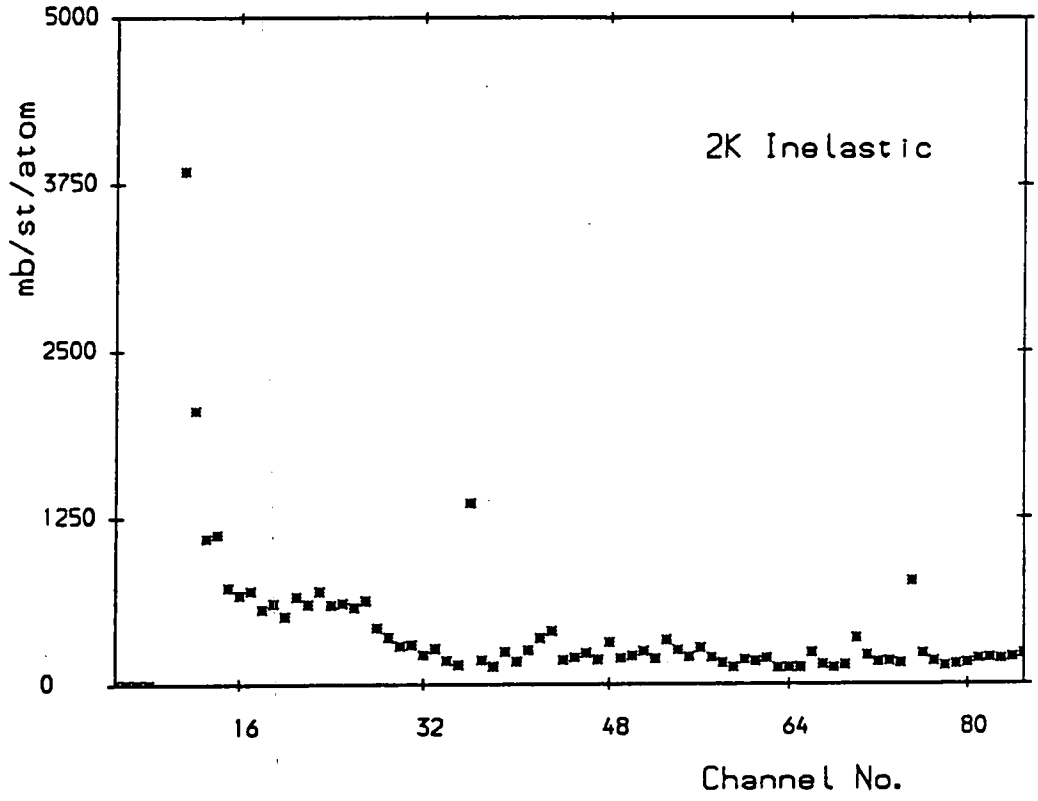

Electronic noise can be removed from the signal and calibration data by a run with no beam transmitted through the sample; this is most easily achieved by the use of an absorbing piece of cadmium in front of the sample, and is only important when measuring very weak signals as the detectors are well shielded. On IN5, noisy angles to be rejected in the analysis can be detected by their high numbers of counts for apparently inelastic scattering (see figure 4.4). On D11, a direct calibration of the absolute sample transmission is made by removing the sample and measuring the direct beam counts passing through a hole in the beamstop. This beamstop is also used during the experiment as a check that the machine is still operating in a reasonable fashion, by directly monitoring the transmitted beam, which allows continuous measurement of the sample transmission.

4.5 Temperature Control

Temperature control in these experiments is from an ILL precision temperature controller, using diode and resistance temperature sensors. A minimal amount of He exchange gas must be used in the sample space in order to ensure good thermal contact between the sample and the heat exchanger, whilst not risking giving an appreciable amount of scattering from the helium. The corresponding problem of lack of thermal response means that the experiments are usually done with exchange gas present to cool to 10 K and pumped out below this temperature. This seems to be an acceptable compromise of use of beam time and risk to the experiment.

4.6 Sample and Holder Design

For these experiments it is important to minimise unwanted scattering of neutrons at low angles. The usual procedure involves making all structural elements of the sample holder either from the minimum of aluminium, or from cadmium, or a combination of these two. Aluminium is a very weak scatterer and hardly absorbs neutrons. Cadmium is on the other hand a very efficient absorber of neutrons, and is soft and malleable. However it is toxic, awkward to machine, and is not very strong for its weight. Thermal mass considerations are important here, as we wish to be able to get away with the minimum exchange gas. Similar sample holders were used for all these experiments.

Figure 4.5 —

The IN5 sample holder used for these experiments

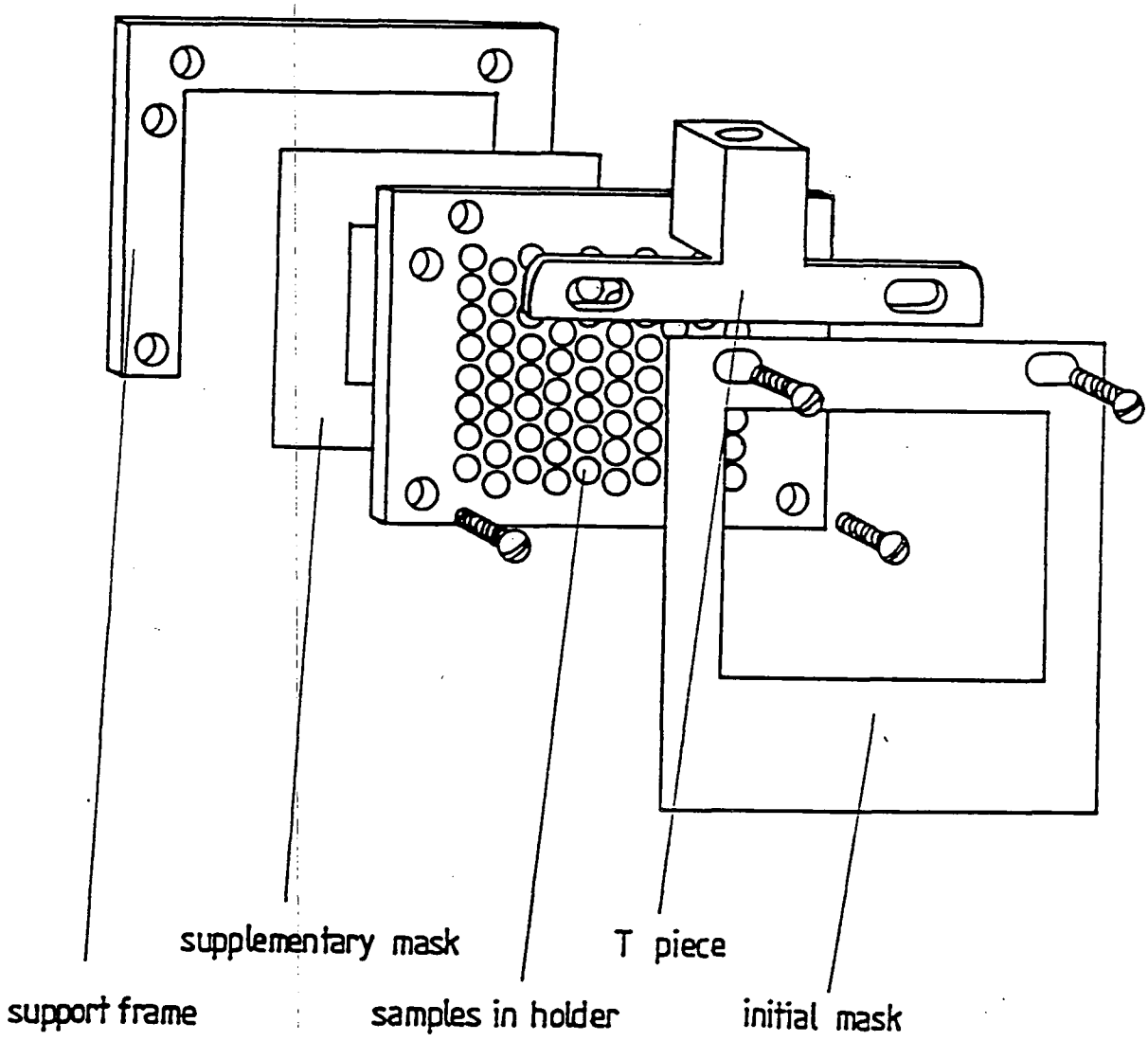

The sample discs, as described in chapter II, are held in a cadmium sheet of equal thickness, in holes just big enough to allow them to slip in. These holes are pre-drilled using a drill of nominally the pellet size, then enlarged by the use of a tapering brass punch to allow the pellets to fit. It is fortunate that cadmium is so malleable as to allow this rapid adjustment, as the pellets are not really exactly sized, due to the nature of the production technique. Space around the sides of the pellets is only really important in that it is a waste of neutrons, as the sample transmission is designed to be greater than 95%. However, the samples are only held in by the pressure from the cadmium walls and thin aluminium foil at the front and back of the holder. If held too loosely they might fall out, especially when being loaded into the cryostat with inevitable shaking of the sample stick. This would mean that there was less sample in the beam; again a waste of neutrons, and a small error in the experimental calibration would result.

The samples themselves were 3mm diameter pellets, 2mm in thickness, arranged in a hexagonal array with around 1mm of cadmium wall between each neighbouring pair, (as shown in figure 4.5). This arrangement is to minimise the path length available for a second scattering event, to neutrons scattered at high angles. These events are the most troubling for the multiple scatter into low angles, principally due to the large volumes of phase space available at high q. In a slab geometry, near 90° scatter can be a real problem, principally due to the long path length available in which a second scattering event can occur.

There is no real advantage in going to much smaller pellet diameters, as the available path at high angles other than those around 90° will not be much diminished, and there is a considerable amount of trouble in dealing with the production of large quantities of small pellets. A further consideration is the supply of suitable dies; 3mm is as small as our supplier can do, and even here there can be problems due to the abrasive nature of the powder being pressed. Pellets longer than their diameter will be extremely likely to fracture when removed from the die; if such shapes are desired, a section cut from a rod formed by other means is probably the best solution.

This slab of cadmium containing the $Y_1Ba_2Cu_3O_7$ is then held on the sample stick of the cryostat either simply by a bolt through a hole in the top of the

cadmium, or in a dedicated adjustable aluminium frame. The latter can permit a limited amount of movement of the sample, if required. The sample holder shown above was designed for the 70mm diameter sample space on IN5, to enable position adjustments of the sample to be made without moving the cryostat or lengthening the sample stick. Extra pieces of cadmium to suitably mask the vanadium and plexiglas calibration samples are made for each sample holder, as these are not always the same size as the array of holes for the samples.

Chapter V

SANS Studies of $Y_1Ba_2Cu_3O_{7-\delta}$ – Experiments

5.1 Experiment 1 – D11

5.1.1 Motivation

The primary motivation for this experiment was to see if any of the effects discussed up to this point in this thesis were visible in real systems. D11 is the instrument of choice for such screening measurements to see what effects can be seen at low q, due to its high flux at long wavelengths and excellent collimation.

5.1.2 Description of D11

D11 is a standard design of small angle scattering instrument. It uses a single circular multidetector, of nominally 64 × 64 cells, to detect the scattered neutrons. D11's great strength is the large flux of cold neutrons available, permitting delicate and difficult experiments. The incoming neutron wavelength is chosen using a helical slit velocity selector, at a fixed resolution (10 % for our experiments). The fact that there are no other moving parts in the experiment is a great advantage, as this means that there is no worry about the reproducibility of each run. A schematic diagram of D11 is shown in figure 5.1. The detector can be moved in its vacuum pipe up to 40 metres from the sample position, to allow a variable coverage of q space and adjustable q resolution. The incoming collimation can also both be varied, with the end of the neutron guide tube positioned 2.5m, 5m, 10m, 20m, or 40m from the sample space, though it is usually matched to the detector distance used. Note that this is not necessarily the best way to use the instrument.

Rings of multidetector elements are summed together for data analysis purposes. Each of these rings receives neutrons scattered by a constant angle, which can be scattered elastically or inelastically. Thus, as there is no energy resolution, each angle of D11 integrates over parabolic "constant scattering angle" curves through (q,ω) space. Figure 5.2 shows such paths for the configuration

Figure 5.1 —

The D11 small angle spectrometer at ILL.
Notice the immense size of this instrument.
My thanks to Mr R.Baker for this diagram.

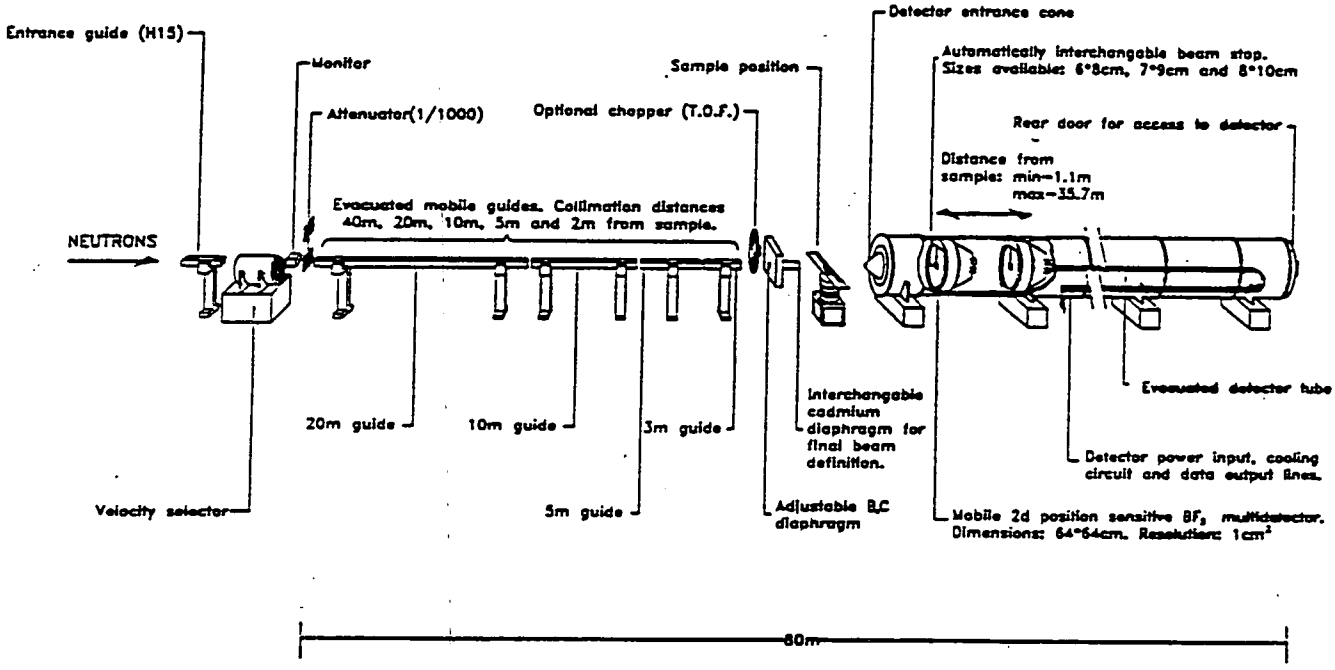

Figure 5.2 —

The D11 integration paths for the configuration used
for this experiment, (2.5m / 2.5m, 6.5 Å).
The lines represent segments of the integration paths for channels 8 to 25.

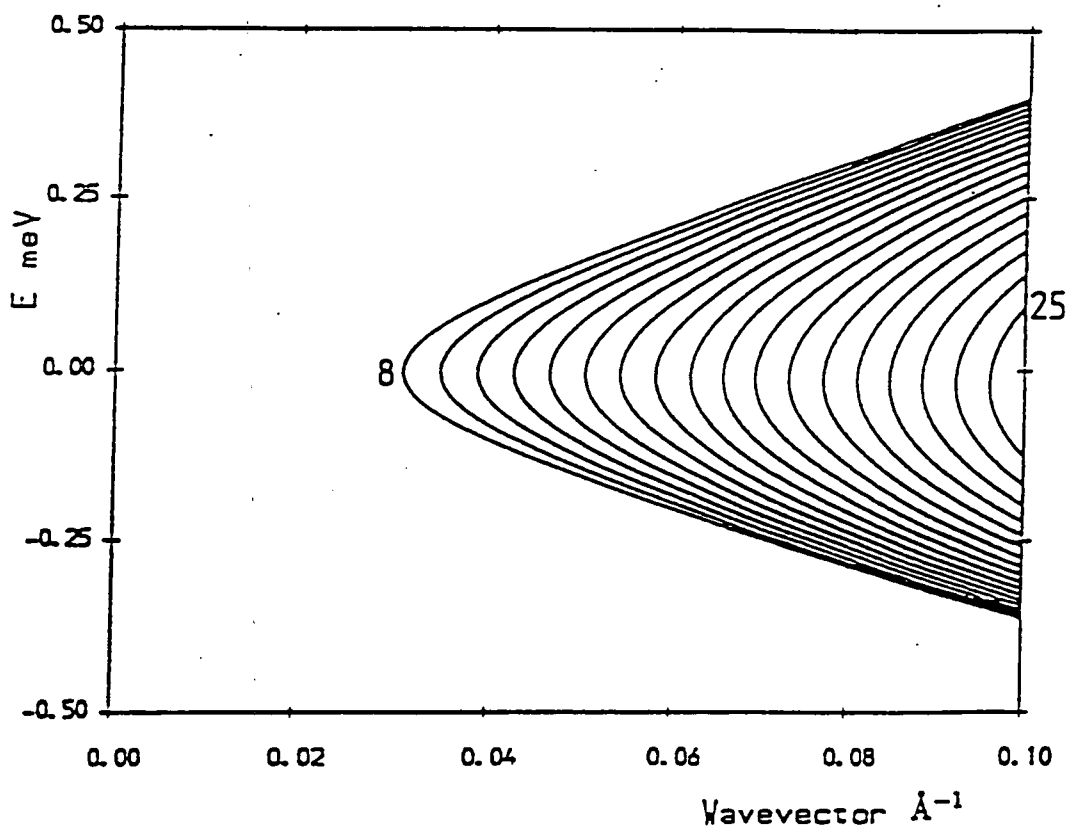

used. These paths are usually labelled by their elastic q, q_0, that is the q at zero energy transfer. Effectively, the scattered neutrons are not collimated; the flight path alone separates out the neutrons scattered by different angles. This means that there is a minimum size of sample that it is efficient to use, approximately given by the cell size of the multidetector; the maximum sample size is set by the cryostat, for low temperature work. A typical experimental configuration is shown below.

Table 5.1 — Typical Configuration of D11

variable	value
beam pipe-sample	2.5 m
sample-detector	2.5 m
wavelength	6.5 Å
flux	6×10^6 (n/cm^2/sec)
monochromation	10 %
q_0 range	0.03 - 0.3 Å^{-1}
sample diameter	1 cm
sample transmission	95 %

5.1.3 Cryostat

A unique ILL "orange" cryostat exists for the two small angle spectrometers D11 and D17. This has a specially designed tail having sapphire windows, to give beam access into the sample space with very low amounts of small angle scattering from the cryostat. These also facilitate visual checks upon the sample. The beam pipe and detector pipe windows can be brought up very close to the cryostat windows ($\simeq$ 2mm), in order to minimise any scattering in air between the beam pipe and the windows.

5.1.4 Experimental Details

D11 was used with 2.5m / 2.5m collimation and the special D11 cryostat as described above. Seven 3mm diameter pellets of $Y_1Ba_2Cu_3O_7$ in an array of holes giving an effective sample diameter of 1cm were used, in a cadmium slab sample holder very similar to that described in chapter IV. An incident wavelength of 6.5 Å was chosen as a balance between the highest flux available, and the need to limit the number of available Bragg scattering processes to cut down the sample background. Calibration was performed against vanadium and plexiglas standard scatterers. The results are shown at various elastic wavevectors q_0 as a function of temperature. As usual, the 2 K values have been subtracted to remove the low angle "metallurgical" scattering.

5.2 Results

5.2.1 Comment

The data show two main features. Both are substantially stronger at the lowest q's. The first and most obvious feature is excess scattering at and in the immediate vicinity of T_c, of around 150 mb/sr/atom at q = 0.03 $Å^{-1}$. This appears to be arising just above T_c. This strongly suggests that it is connected with the superconducting transition. In addition, effects that are not connected to the superconducting transition can be ruled out by the fact that higher temperatures appear closely to self-subtract. This self subtraction is best at the lowest q where phonon effects are expected to be small, and this is also where the strongest effects at T_c appear. This means that simple phonon scattering effects cannot be invoked to explain the increase at the higher temperatures over the low temperature scattering; only rather complex changes in the phonon spectrum could give such effects.

Figure 5.3 —

Sample scattering, showing sharp increase at low q

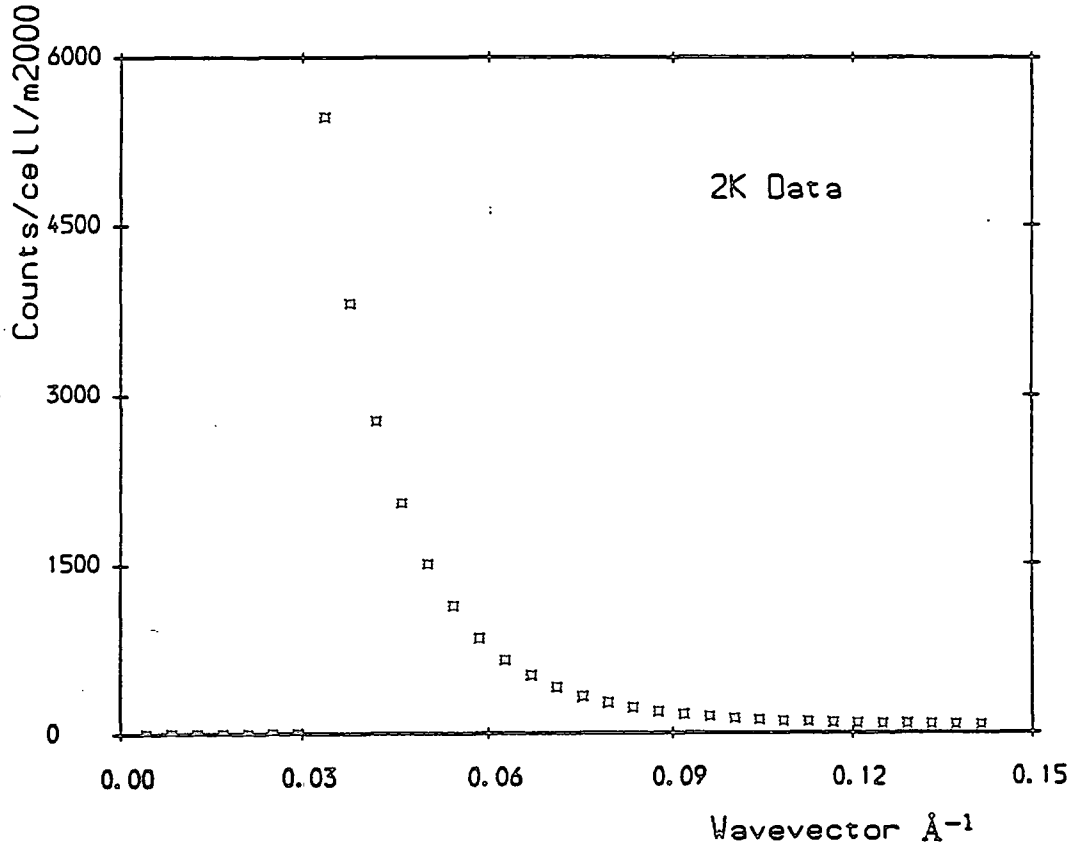

Figure 5.4 —

Difference in scattering vs. Temperature
$q_0 = .031$ Å^{-1}, $.035$ Å^{-1}

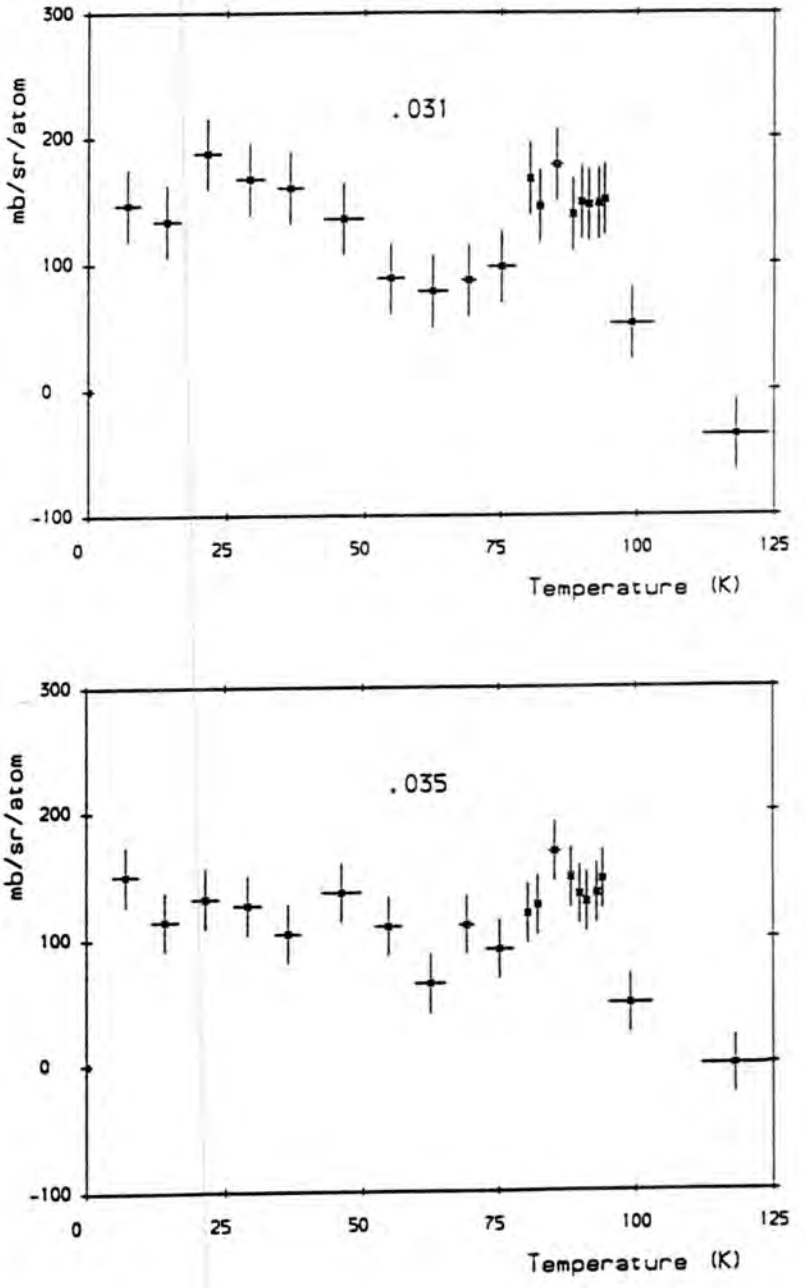

Figure 5.5 —

Difference in scattering vs. Temperature
$q_0 = .04$ Å^{-1}, $.0425$ Å^{-1}

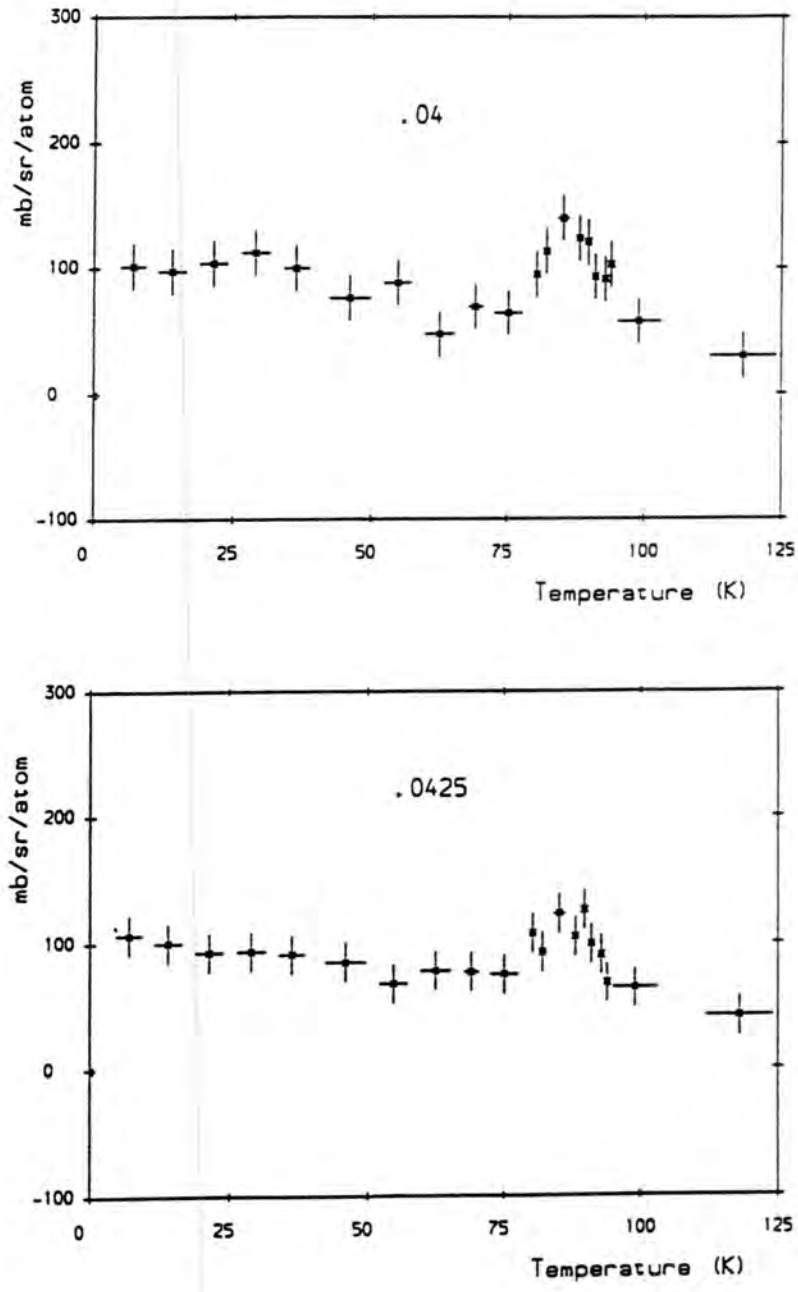

Figure 5.6 —

Difference in scattering vs. Temperature
$q_0 = .046$ Å^{-1}, $.050$ Å^{-1}

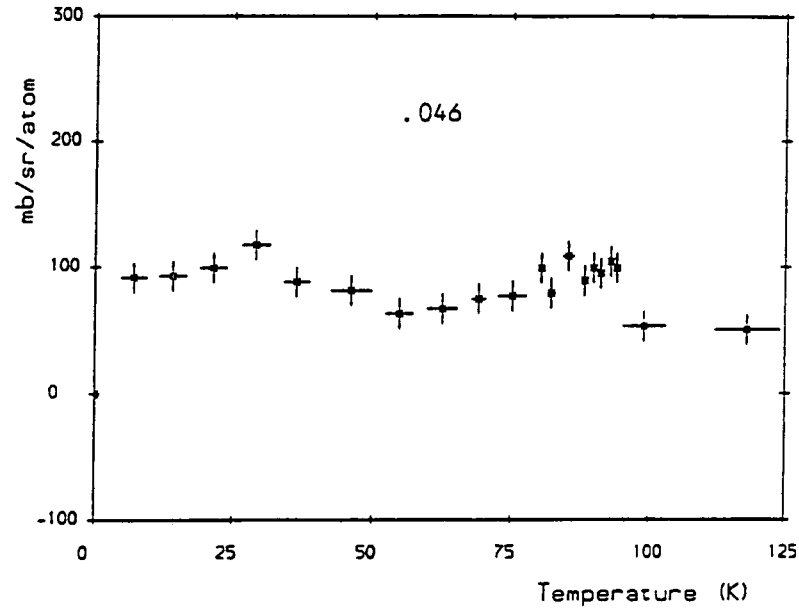

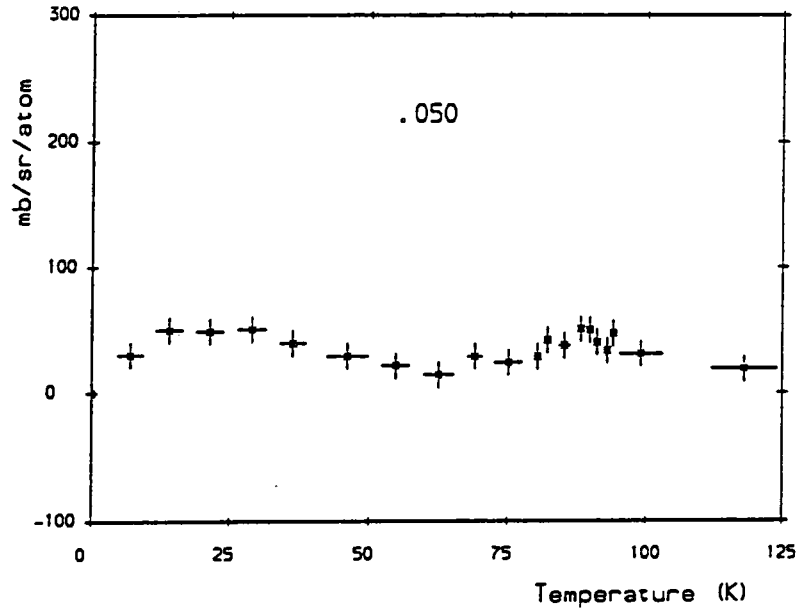

Figure 5.7 —

Difference in scattering vs. Temperature
$q_0 = .054$ Å^{-1}, $.062$ Å^{-1}

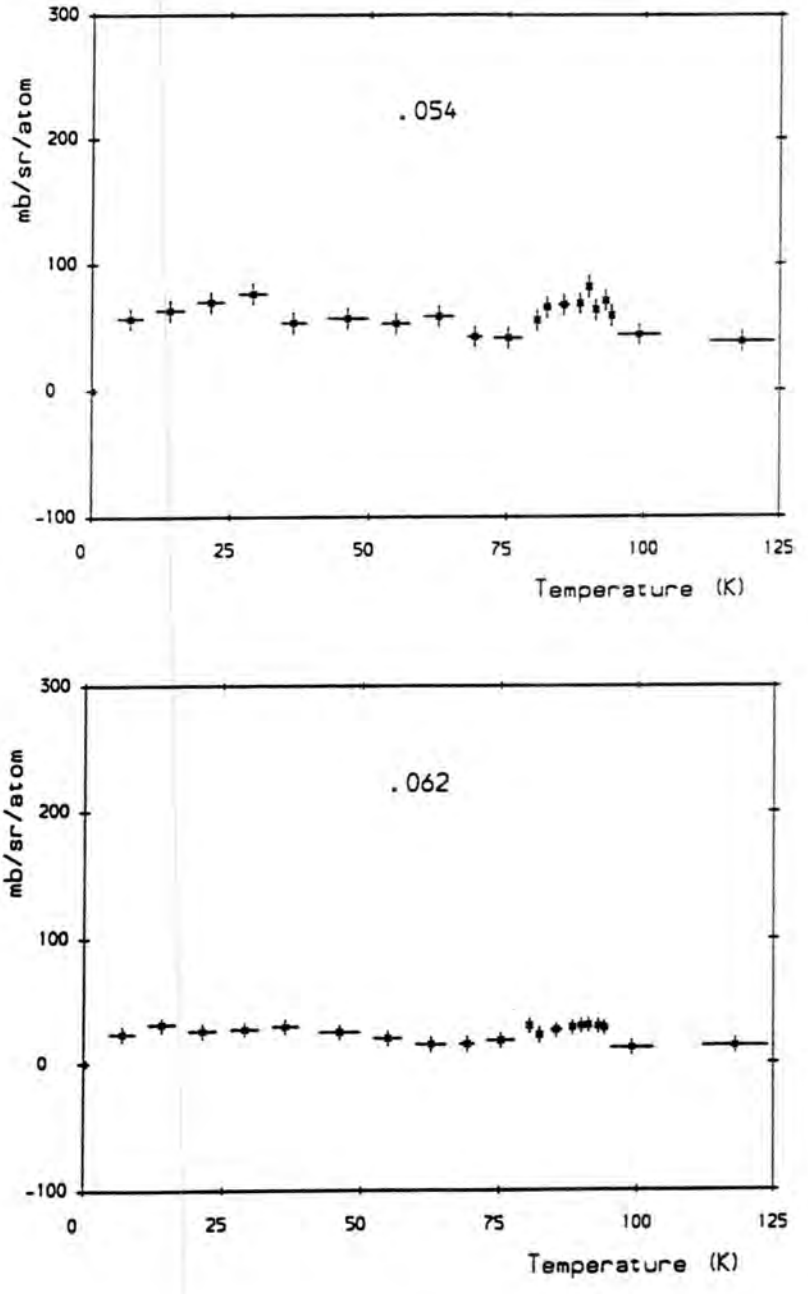

5.3 Experiment 2 – IN3

5.3.1 Motivation

In order to see whether we could confirm and extend this result, IN3 was used to measure in the same region of q but confining the signal detected to a single energy transfer, at the elastic position. This experiment also set out to see whether a small magnetic field, (1.5 mT), would significantly change the result. The result remaining unchanged would rule out explanations involving scattering from flux lines introduced into the sample, as this would be expected to be radically increased.

5.3.2 Description of IN3

This instrument is a standard triple axis spectrometer (TAS). See figure 5.8. The great strength of such machines is their ability to examine a single well defined portion of (q,ω) space with a relatively high flux and resolution. This enables them to perform experimental scans along straight lines in (q,ω) space, making interpretation of the results more tractable. IN3 is situated on a thermal neutron beam, and loses greatly in flux at 5.5 Å, compared to a cold neutron beam instrument such as IN12. IN3 was used solely because it is much easier to obtain experimental time on this instrument.

5.3.3 Cryostat

A standard ILL "orange" cryostat with a large diameter sample tail was used, as in order to gain as much signal as possible it is necessary to use the whole size of the beam, (of order of 6 × 3 cm). This ruled out using the D11 cryostat for this experiment, as its sapphire windows are only 25mm in diameter. Standard TAS Helmholtz coils fit onto the supports of these cryostats in order to provide a magnetic field of 0 - 1.5 mT at the sample position. These coils are normally used for experiments using polarisation analysis.

5.3.4 Principle of Operation of a Triple Axis Spectrometer

A triple axis spectrometer works by controlling the neutron beam by Bragg reflection from suitable high quality crystals of controlled mosaic spread. The

Figure 5.8 —

A Schematic Diagram of IN3 at ILL,
in the configuration used in this experiment.

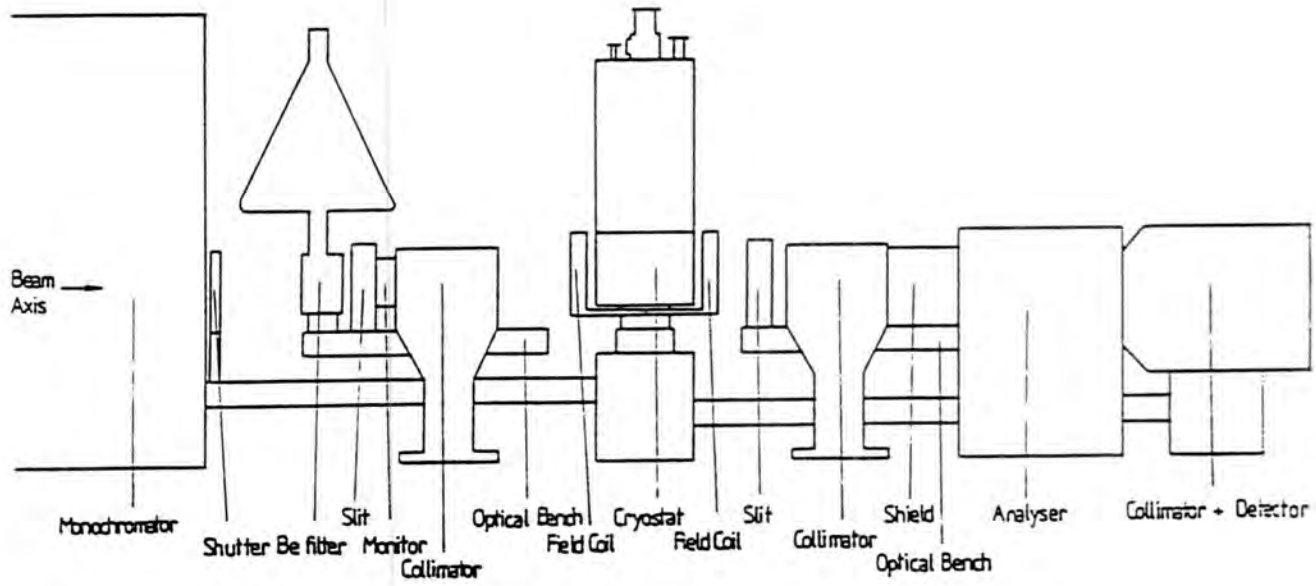

monochromator crystal, in the beam tube, provides a beam of nearly monochromatic neutrons. This beam is then collimated to decrease the divergence, if desired, from around 1°. The beam then hits the sample. The scattered beam at a selected angle then passes through a further collimator and is reflected from the analyser crystal if it meets the Bragg condition. A further collimator is in front of a large detector that thus detects the neutrons. The combination of these collimators and Bragg angles determines (q,ω), the energy and momentum resolution and the flux available. All the motions of the instrument are computer controlled.

5.3.5 Comparison with D11

A crude comparison between IN3 and D11 can be made, in order to show the sorts of times will be needed for a given experiment of IN3 if the total scattering has been measured on D11. This is done by a simple comparison of the fluxes of neutrons, the sample sizes available and the solid angle of detector used. A complication is that the effectiveness depends upon the experiment, because a small signal will be easier to measure if it is inelastic, due to the reduced inelastic "background" coming from the sample. For our purposes, however, this simple analysis will suffice.

The solid angle viewed by the detector at the relevant angle is fairly simple to calculate. On IN3 the detector area is 24 cm^2, at a distance of 2m, whereas on D11, at q = 0.03 $Å^{-1}$, it is 50cm^2, at a distance of 2.5m. Thus D11 gains by a factor of 2 here. IN3 has a maximum useable sample size of 6 × 2.5 cm^2, against 1cm^2 for D11 in its usual configuration. Thus IN3 gains by a factor of $\simeq$ 10 here. IN3 has a factor of $\simeq$ 180 less flux at 5.5 Å, if using 20′ incident collimation on IN3. Here we use a Be filter to cut out shorter wavelength harmonics which costs perhaps an extra factor of 2 in intensity. Thus in total, IN3 at 20′ with a Be filter needs roughly 60 times as long counting time to D11 per point of the scan through (q,ω) space, for comparable error bars.

Any further analysis must bear in mind that the relative efficiency depends upon where in (q,ω) space the scattering is taking place. D11 gives the response at many q's simultaneously - this is a marvellous way to screen many systems and temperatures for the strongest effects; IN3 enables tests of the response at finite energy uncomplicated by any elastic scattering, if this is what is desired. A

comparison of IN3 with a cold neutron beam instrument such as IN12 along similar lines implies that IN12 is better than IN3 by roughly a factor of 20 for this sort of experiment.

5.3.6 Experimental Details

IN3 was set up with k_i =1.2 $Å^{-1}$, (i.e. λ = 5.23 Å), a cooled Be filter, and 30′-30′-60′ collimation, by no means a standard configuration. This gives a FWHM resolution of 60 μeV. The experiment was performed at a fixed q of 0.04 $Å^{-1}$, and at a fixed energy transfer of 0μeV, i.e. at the elastic position. This use of a single spectrometer position for the whole experiment, rather than the more conventional "constant wavevector" scans, is forced on us here by the low flux; nevertheless, at low angles it may well be the best way to perform any TAS experiment if the sample background is large. This is because small and unrepeatable position errors in the machine alignments from one scan to the next increase the error on the background signal, as it can vary really very strongly with q ($\simeq q^{-4}$). This unrepeatability means that the background subtraction technique we rely upon becomes difficult if scans are used.

A Helmholtz pair of coils was attached to a standard ILL orange cryostat (with a wide base), to allow a 1.5 mT magnetic field to be applied to the sample parallel to the neutron beam direction. The sample was an array of 152 2mm thick 3mm diameter polycrystalline sintered pellets of the same batch as those used on D11, held in a mask of 2mm thick cadmium as described in chapter IV.

Counting times for this experiment were long due to the low flux at this wavelength on a thermal beam and due to the need to acquire large numbers of counts. This was necessary to allow the accurate subtraction of the low temperature value in order be able to remove the low-angle background scattering. A total of 17 hours counting time per temperature / field was necessary; accordingly the experiment was performed at four temperatures with no applied field and two in 1.5 mT.

The signal was calibrated by using plexiglas as a standard scatterer, as the vanadium signal was very small. This was due to the vanadium sample not being large enough to make use of the full beam size. The previously obtained calibration of the same piece of plexiglas against vanadium, (from D11), was used to obtain an

Figure 5.9 —

IN3 Signal vs. Temperature, q = .04 $Å^{-1}$
The filled line represents the D11 result.
Notice the pleasing agreement to within the relative errors.
This implies that the scattering measured on D11 is all at low energies.

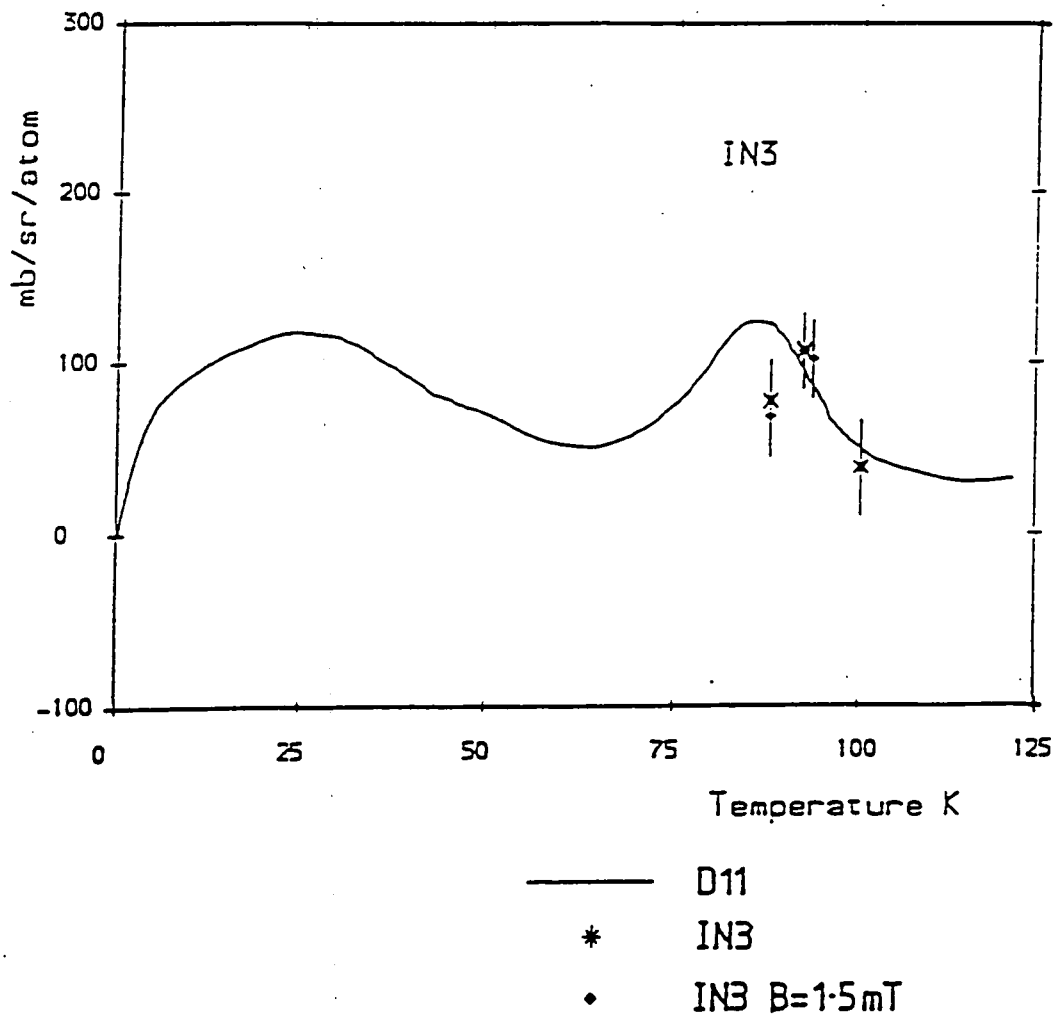

absolute calibration. In addition it would be difficult to calibrate with vanadium well at this low q, given that we can only do this at rather higher q and this means that the spectrometer is then in a different configuration from that used during the experiment.

5.3.7 Results

The results are shown in figure 5.9 and may be simply compared with the D11 data, with the D11 data shown as a filled line. The pleasing agreement with D11 both in shape and to within the relative calibration error implies that all the scattering on D11 is elastic, i.e. within 30 μeV of zero. This is a good confirmation of the D11 data as it involves a different type of spectrometer and cryostat, implying that the signal must be from the only common element, the samples.

In addition the failure of an applied field of 1.5 mT significantly to change the scattering implies that the scattering is unlikely to be from flux lines within the sample.

5.4 Experiment 3 - IN5

5.4.1 Description of IN5

IN5 is a time of flight inelastic scattering spectrometer with an exceptional variety of uses, due to its ability to be adjusted to suit the experiment at hand. It measures the times of arrival of scattered neutrons at many fixed angles simultaneously; the time of flight of the neutrons reveals their energy, and the combination of time and angle their wavevector. Each detector angle behaves rather like D11, giving a constant scattering angle "scan" through (q,ω) space (figures 5.11 and 5.12). Each segment of time of the time of flight, or bin, represents a small element of this path. The flight path of the neutrons after the cryostat is 3.997 metres, through a box filled with argon to reduce the scatter inside the box. Detectors are grouped in rings and arcs for the purposes of data collection, each at a constant angle, and are available from 1.7° to 128.7°. See figure 5.10.

The strength of the machine is its multiple chopper monochromator, consisting of four rotating discs, with neutron windows allowing the beam to pass through at certain angles. The velocity and relative phases of the choppers determine the energy resolution and the wavelength of the incident beam. A high velocity gives a high resolution at no direct cost in flux as the pulses of neutrons, though narrower, arrive more often. The reduced time between pulses, falling with increasing chopper speed, means that events which scatter by large energies can arrive either with the previous or next pulse's scattered neutrons. This problem is called frame overlap. To allow the user to choose what range of energy to examine, and in order to minimise this problem, one of the choppers may run at an integer fraction of the speed of the others, cutting out all but this fraction of the pulses. This does cost in flux, obviously, so the apparent higher resolution for no cost in flux is at least in part illusory.

Another advantage of this collimation / monochromation system as opposed to other systems is that it allows study at relatively low q. The q range available depends on the wavelength chosen, but is at least comparable with D11 at 2.5 metres collimation, for similar incident wavelengths. This is reasonable, given that larger samples are a necessity on IN5 due to the cost in flux of the high degree of monochromation and the pulsing of the beam required.

Figure 5.10 —

The cold neutron multichopper TOF spectrometer IN5 at ILL

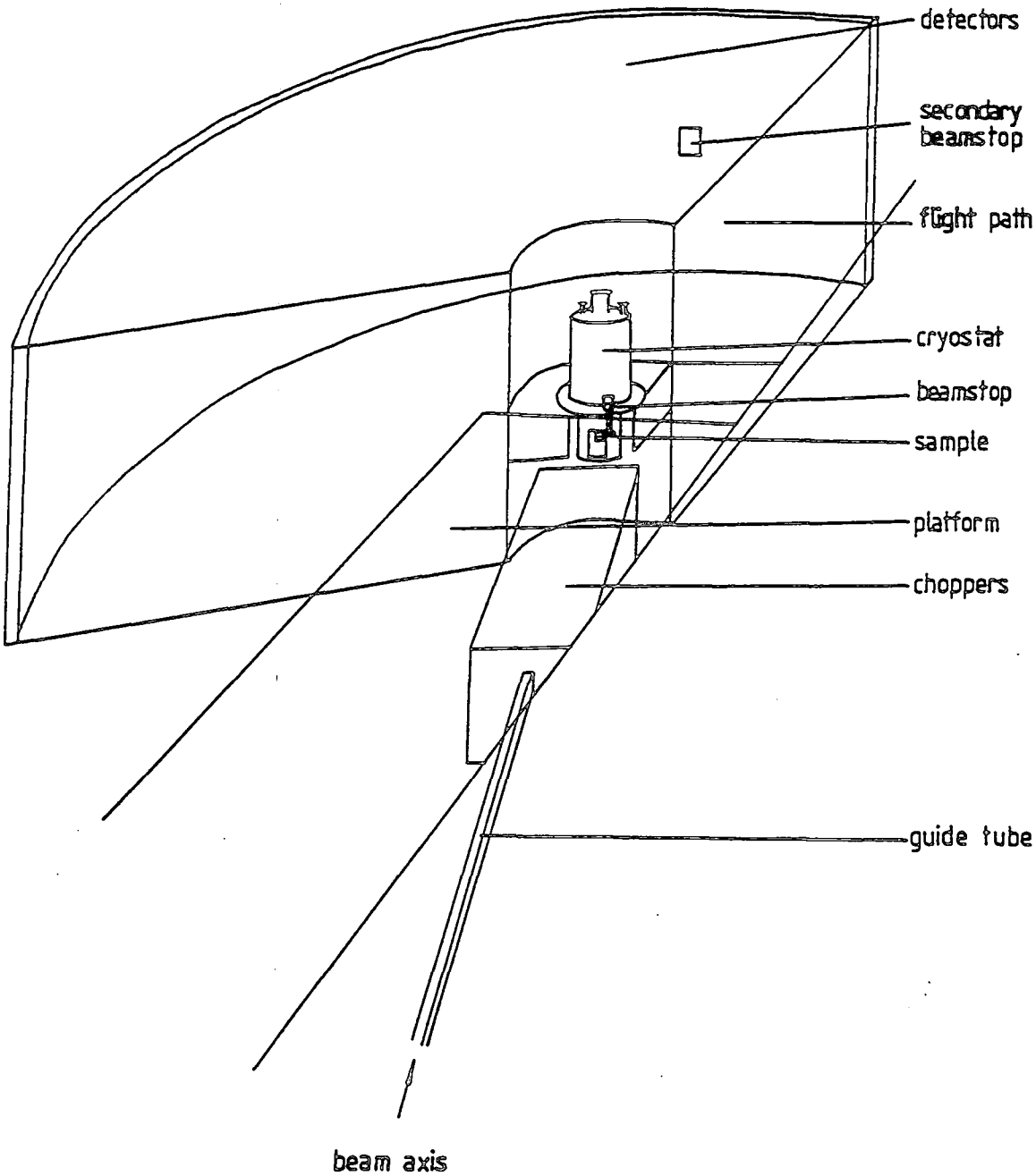

Figure 5.11 —

The IN5 constant angle paths, at low energy transfer, 7.1 Å
A to G represent the angles summed together.
Expressed as elastic wavevector transfer q_0,
A = 0.035 - 0.049 $Å^{-1}$, B = 0.049 - 0.069 $Å^{-1}$, C = 0.069 - 0.081 $Å^{-1}$,
D = 0.081 - 0.095 $Å^{-1}$, E = 0.095 - 0.114 $Å^{-1}$, F = 0.114 - 0.133 $Å^{-1}$,
G = 0.133 - 0.177 $Å^{-1}$

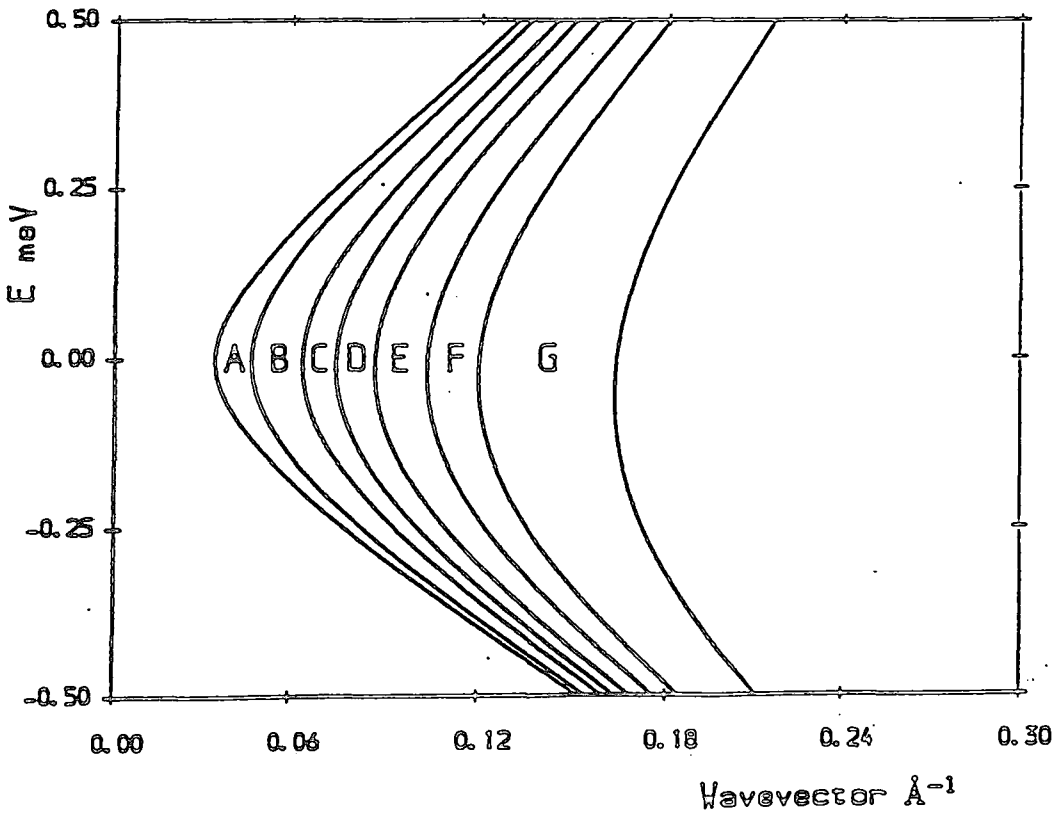

Figure 5.12 —

The IN5 constant angle paths, at higher energy transfer, 7.1 Å
The same ranges of elastic q are summed as on the previous diagram

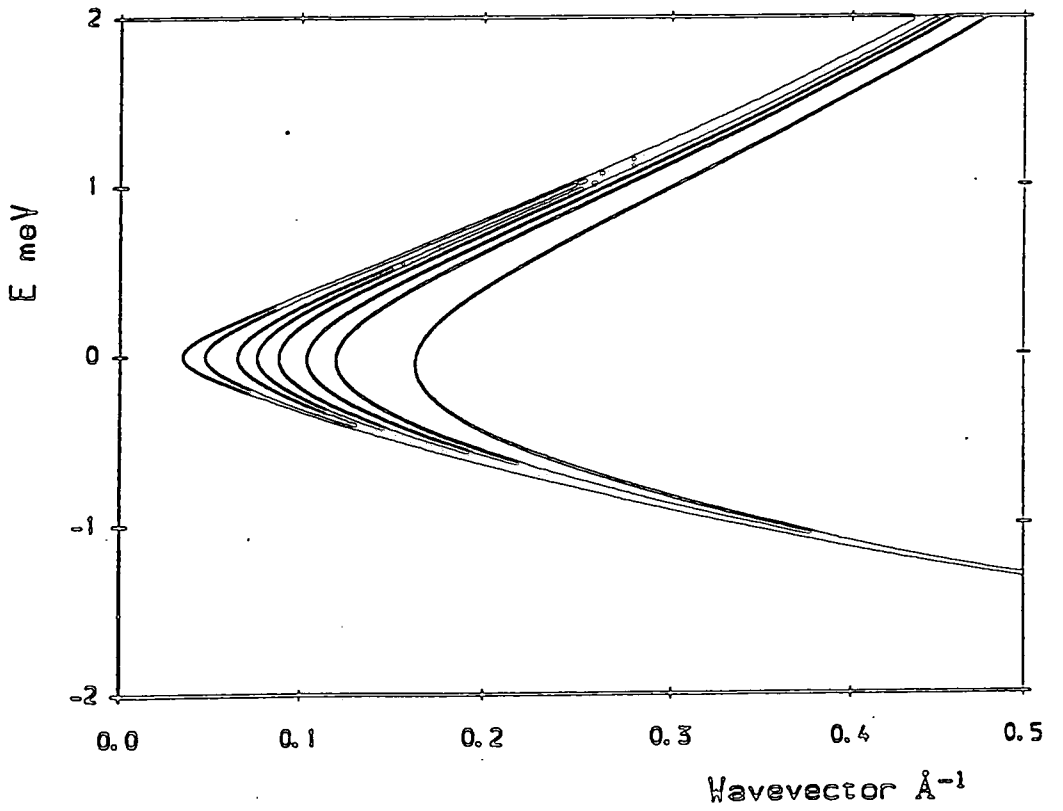

5.4.2 Cryostat

There are two cryostats dedicated to the instruments IN5 and IN6. Whilst maintaining the method of operation of the ILL orange cryostat, each has an especially large sample space in order to make Bragg reflections from the cryostat walls arrive at the detectors with suitably large times of flight, due to their extra path length. Multiple reflections will of course arrive even later at the detectors. This is especially important for measuring small cross-sections at low angles, due to the possibility of multiple scattering apparently being single low (q,ω) events, as discused in chapter IV. These effects should be substantially independent of the sample temperature. Also, as previously discussed, the He exchange gas must be kept to a minimum - however, as each individual counting time on IN5 is relatively large, the loss in thermal response speed of the cryostat is less important. Stability of temperature is still important, of course.

5.4.3 Experimental Details

In order to examine large volumes of (q,ω) space at these low values of q, a time-of-flight experiment was performed on IN5. This used 101 pellets of the same batch of sample as D11 in a sample holder as described above. Principally this experiment was to enable an accurate measure of any scattering at low energies with an energy resolution of roughly 100 μeV. The main configuration conditions of IN5 are summarised below.

5.4.4 Data Reduction

IN5 poses a series of problems concerned with data reduction and analysis, as the amount of raw data produced is very large. Each run produces approximately 0.5 Mbyte of data. The range of q usefully probed by our experiment does not however cover the whole detector bank due to the heavy shielding of the sample in its holder, which acts as a crude collimator system and removes much of the high angle scatter.

Table 5.2 — IN5 Experimental Parameters

parameter	value
runs at each T	3 × 4 hours
incident wavelength	7.1 Å
overlap	1
chopper speed	10 000 rpm
elastic channel no.	330
neutron energy gain	- 0.5 to 2.0 meV
time per channel	7.5 μs

However, the range of q left uncovered by other work can be reached, as this is only at up to 30° (q= 0.035 - 0.200 $Å^{-1}$). Nevertheless, certain choices have to be made as regards the optimum binning together of angles and time channels. Here we have binned together in constant time bins of 15 channels each of 7.5 μs and have chosen to group q's in roughly 30% of q intervals.

5.5 Results – IN5

One typical set of results for one temperature is given here. The remainder are presented in Appendix B.

Figure 5.13 —

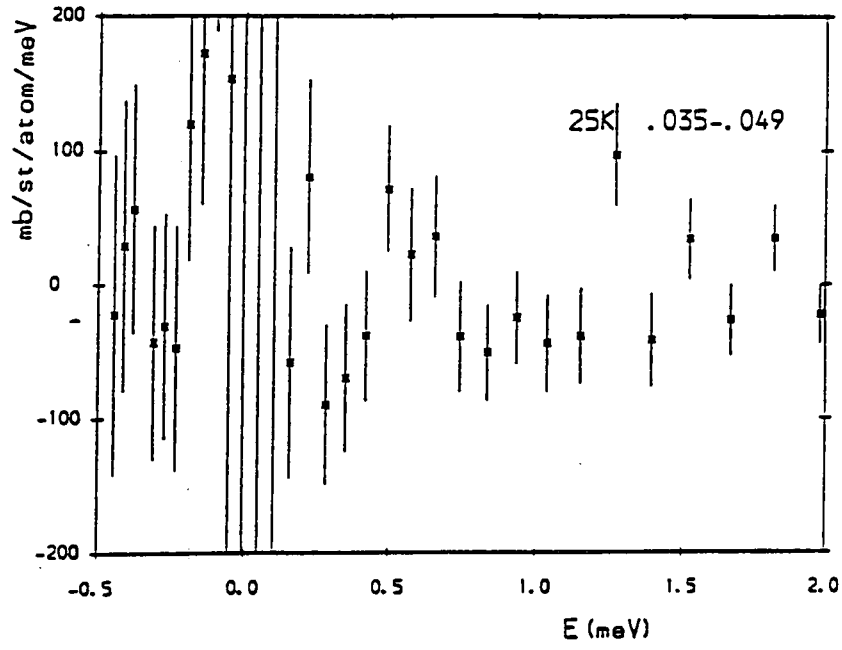
25K .035-.049
mb/st/atom/meV
200
100
0
-100
-200
-0.5
0.0
0.5
1.0
1.5
2.0
E (meV)

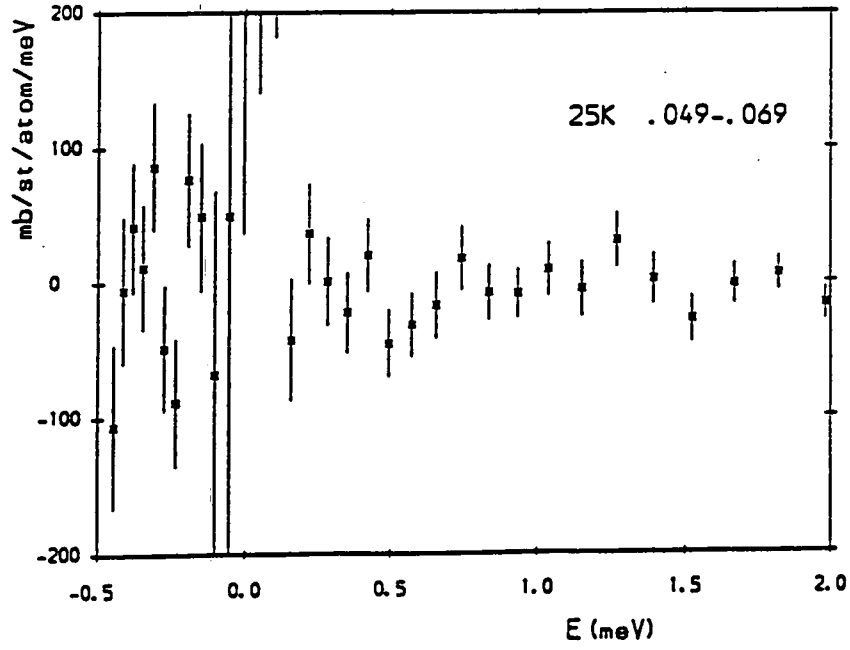
25K .049-.069
mb/st/atom/meV
200
100
0
-100
-200
-0.5
0.0
0.5
1.0
1.5
2.0
E (meV)

Figure 5.14 —

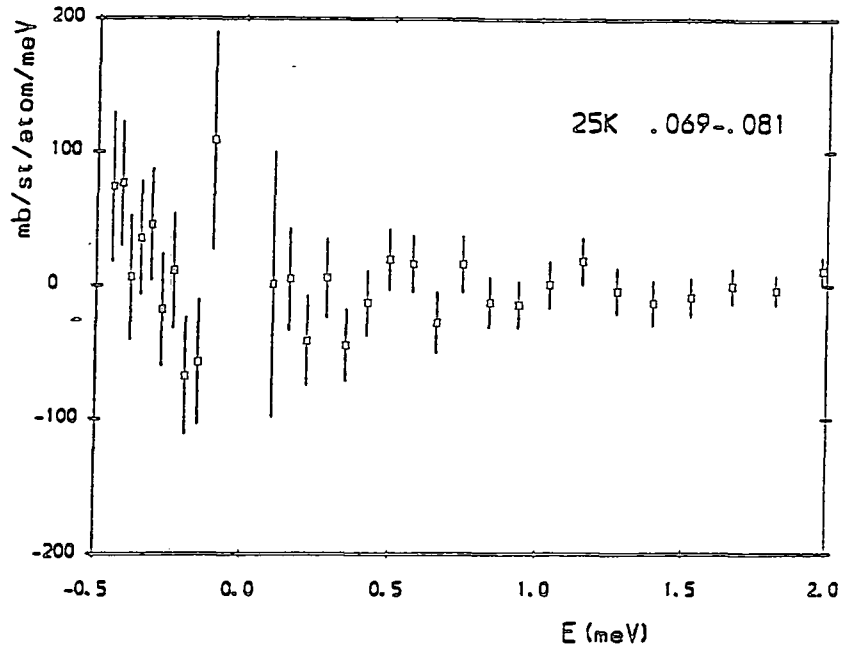
200
100
0
-100
-200
mb/st/atom/meV
25K .069-.081
-0.5
0.0
0.5
1.0
1.5
2.0
E (meV)

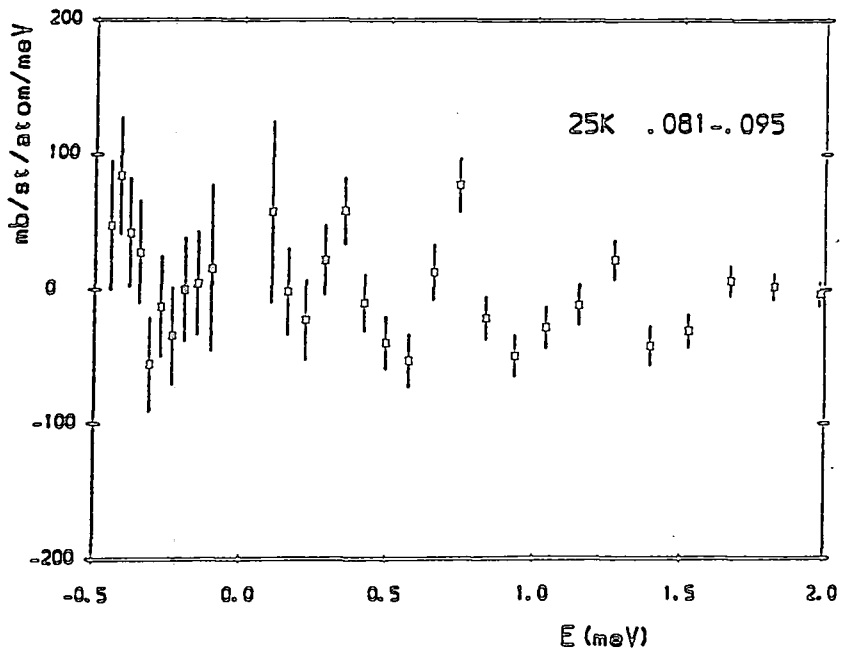
200
100
0
-100
-200
mb/st/atom/meV
25K .081-.095
-0.5
0.0
0.5
1.0
1.5
2.0
E (meV)

Figure 5.15 —

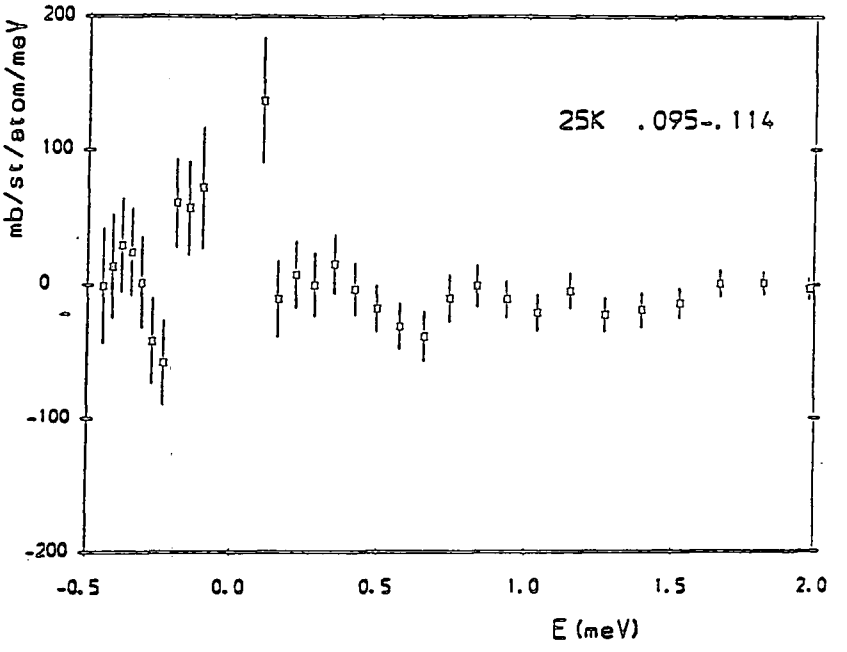
200
100
0
-100
-200
mb/st/atom/meV
25K .095-.114
-0.5
0.0
0.5
1.0
1.5
2.0
E (meV)

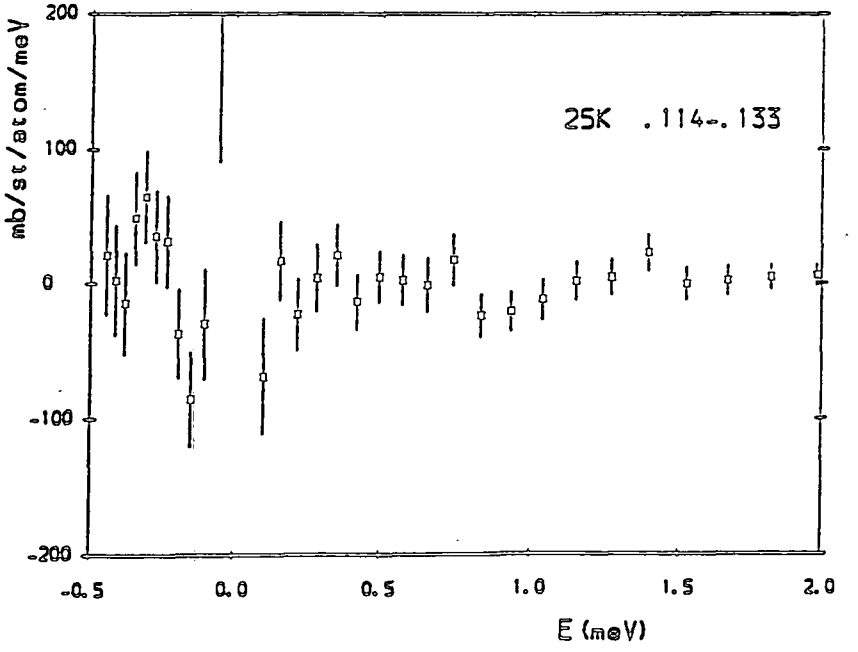
200
100
0
-100
-200
mb/st/atom/meV
25K .114-.133
-0.5
0.0
0.5
1.0
1.5
2.0
E (meV)

Figure 5.16 —

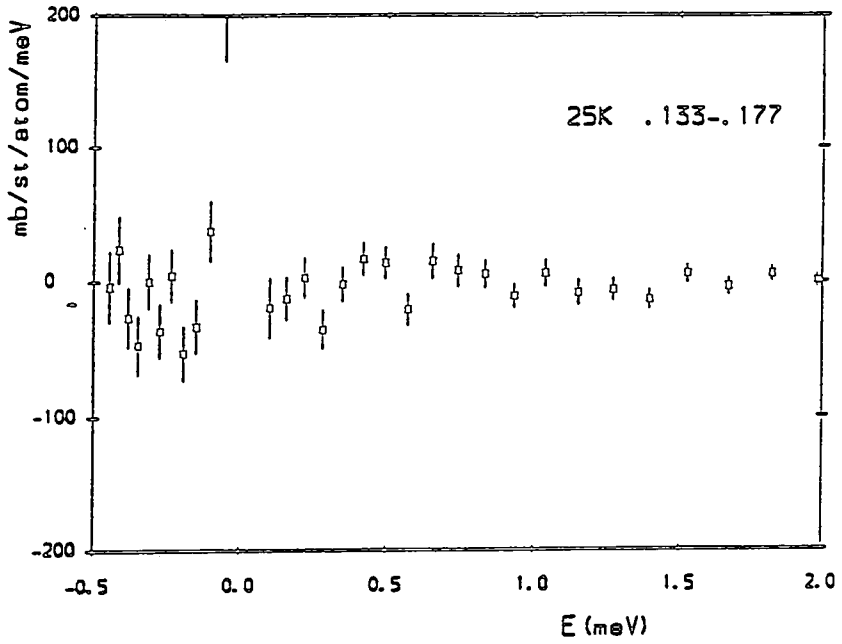

5.5.1 Total Inelastic Scattering

The total inelastic scattering differences can be investigated over a wide q-range and with a reduced error bar by summing all neutron energy gain events from the edge of the elastic peak (+50 μeV) out to 2meV. The q-range is eventually limited by the fact that the absolute calibration is not so good at high q, due to the standard scatterers not being of exactly the same geometry as the sample i.e., not in 3mm diameter pellets ! This leads to a difference in the mask shielding of high angle scattering events and thus an underestimate of the true sample scattering.

5.5.2 Comment

The immediate feature of this data is that there is very little or no scattering outside the elastic peak. The exception is that there may well be some scattering over a broad range of energy at high temperature, especially at the highest q's, which may be incoherent one-phonon scattering.

This data may be used to extend the result of Brückel (Brückel) that there is no measurable magnetic scattering (.75 mbarn/sr/atom $\pm$ 1.54 mbarn/sr/atom) integrated over the energy range -25 to 25 meV at q's of 0.18 to 2.45 Å^{-1}. A brief summary of the total inelastic scattering (energy gain) up to 2 meV and its error is given in the table below for all the temperatures measured. All q's from 0.04 to 0.187 Å^{-1} are here summed together for improved statistics. The errors given are from the spread of values and from the counting statistics. Using the counting statistics gives a lower error bound because it disregards structure in the range summed over; using this error, a confidence limit of 3σ is 13 mb/sr/atom which appears to be reasonable given the small spread of the averages about zero. This is a larger error than obtained by Brückel et al., which is probably reasonable given that we are working at lower q.

Likewise a test for consistency with D11 could be done by integrating all energies, (or just the elastic peak), and obtaining an absolute calibration. However, we do not have the ability to measure the transmission of the sample during the experiment, and thus cannot correct for any such variation.

Figure 5.17 —

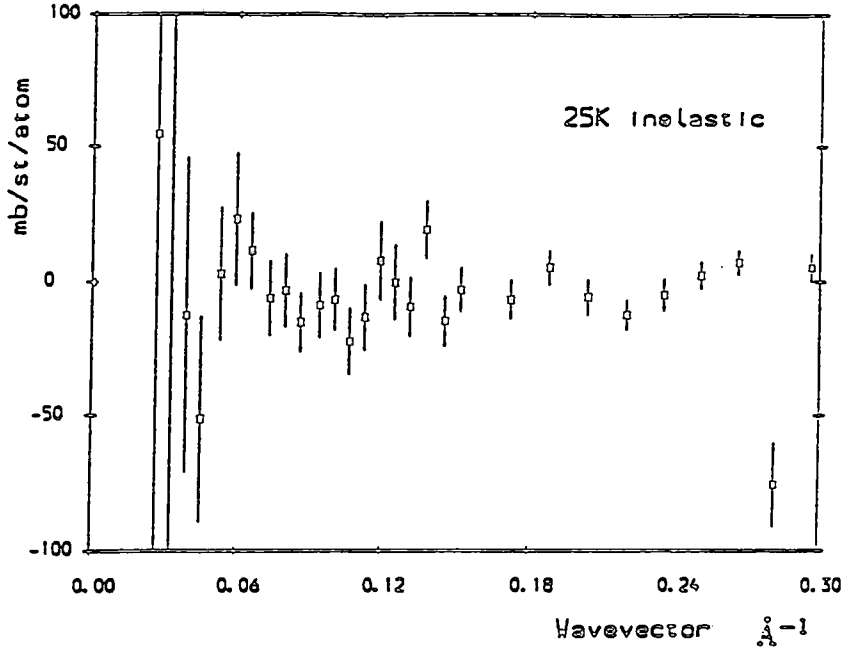
100
50
0
-50
-100
mb/st/atom
25K Inelastic
0.00
0.06
0.12
0.18
0.24
0.30
Wavevector Å-1

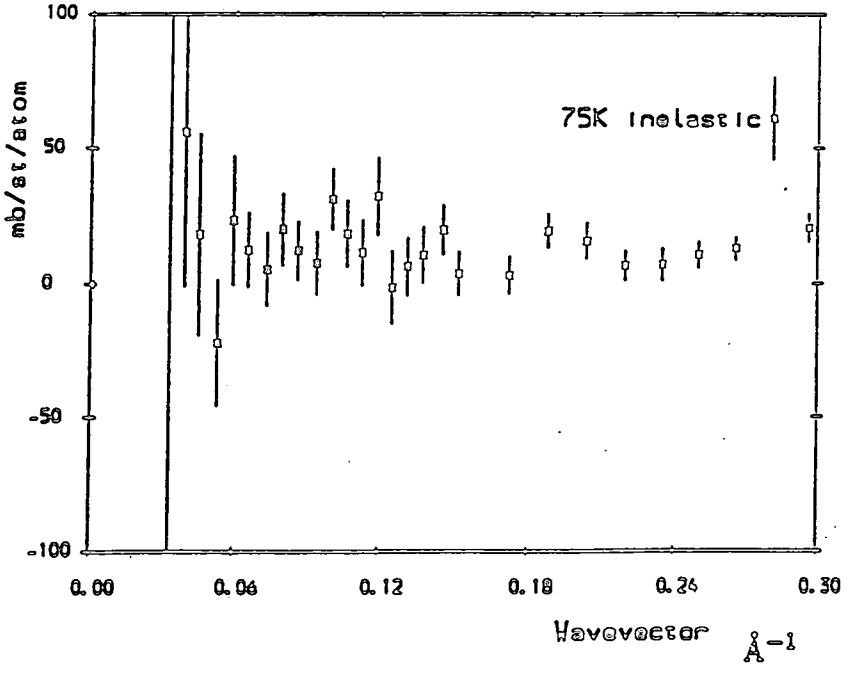
100
50
0
-50
-100
mb/st/atom
75K Inelastic
0.00
0.06
0.12
0.18
0.24
0.30
Wavevector Å-1

Figure 5.18 —

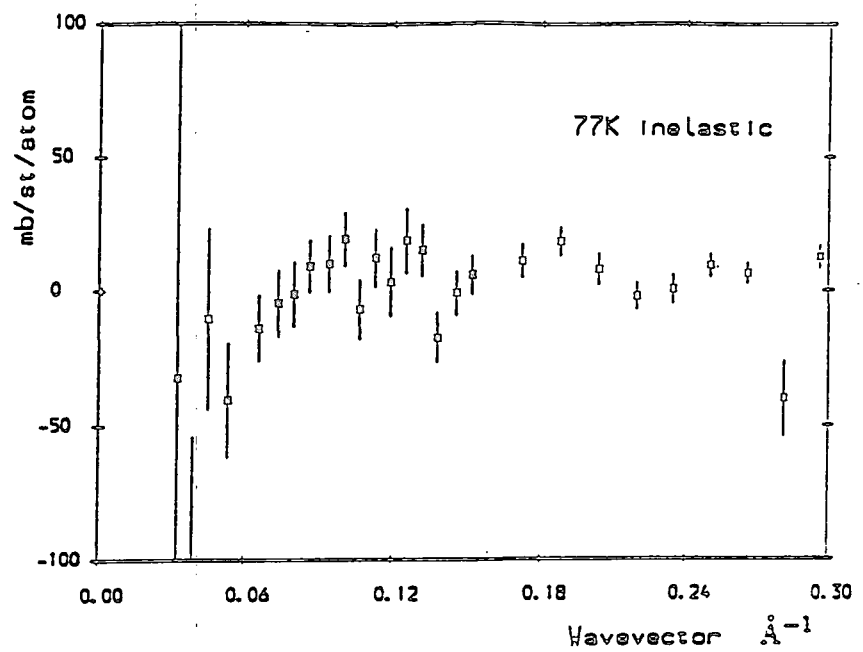
100
50
0
-50
-100
mb/st/atom
77K Inelastic
0.00
0.06
0.12
0.18
0.24
0.30
Wavevector Å-1

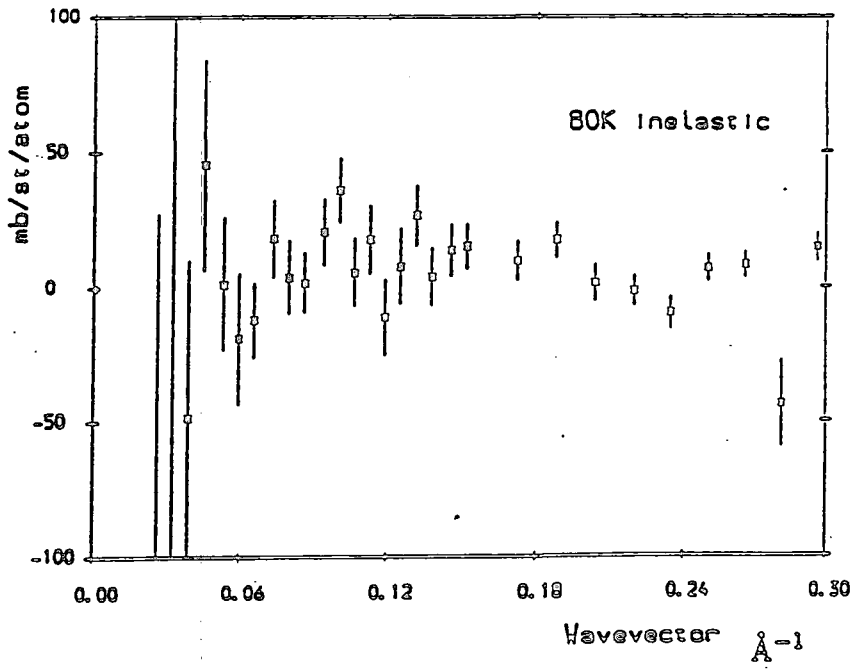
100
50
0
-50
-100
mb/st/atom
80K Inelastic
0.00
0.06
0.12
0.18
0.24
0.30
Wavevector Å-1

Figure 5.19 —

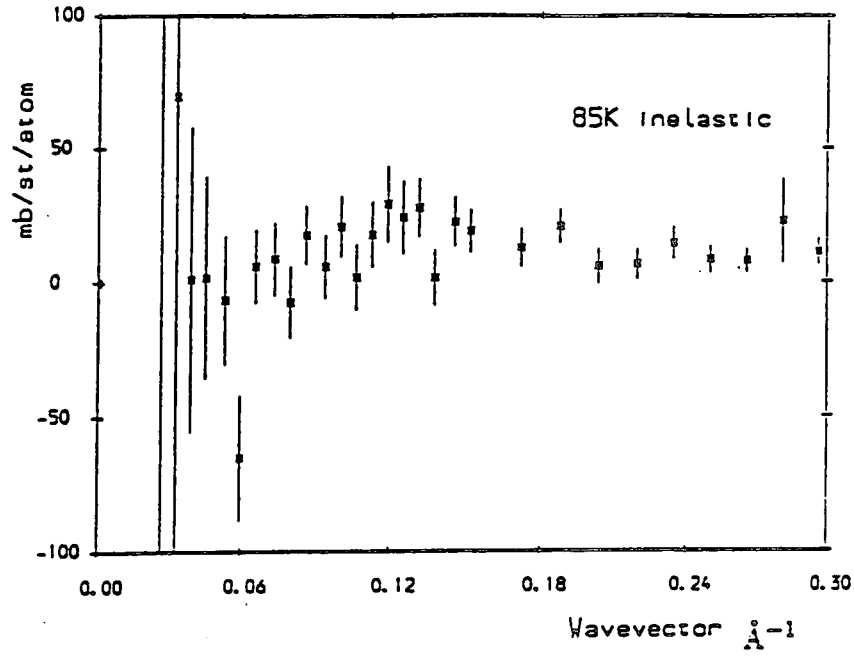
85K Inelastic
mb/st/atom
100
50
0
-50
-100
0.00
0.06
0.12
0.18
0.24
0.30
Wavevector Å-1

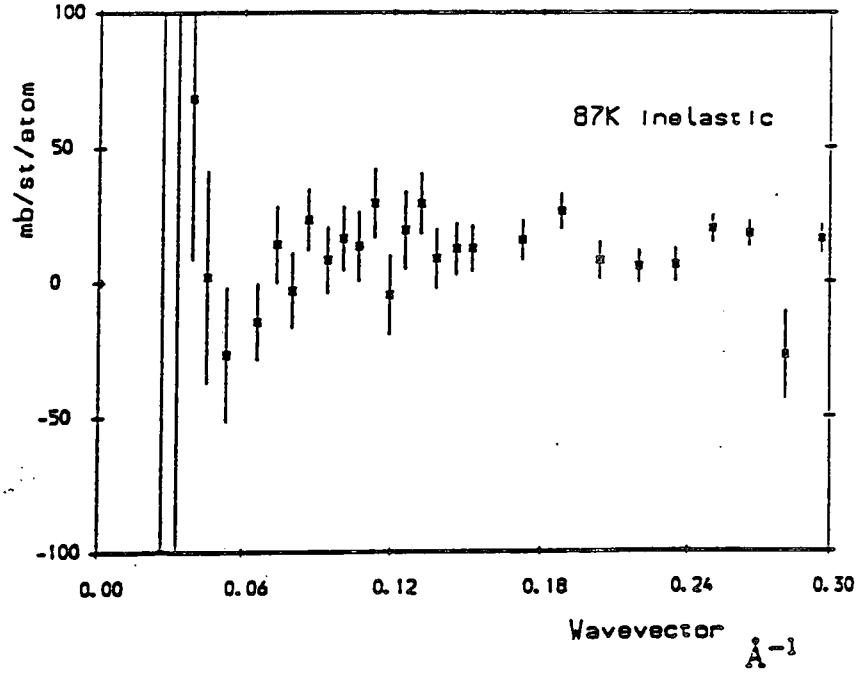
87K Inelastic
mb/st/atom
100
50
0
-50
-100
0.00
0.06
0.12
0.18
0.24
0.30
Wavevector Å-1

Figure 5.20 —

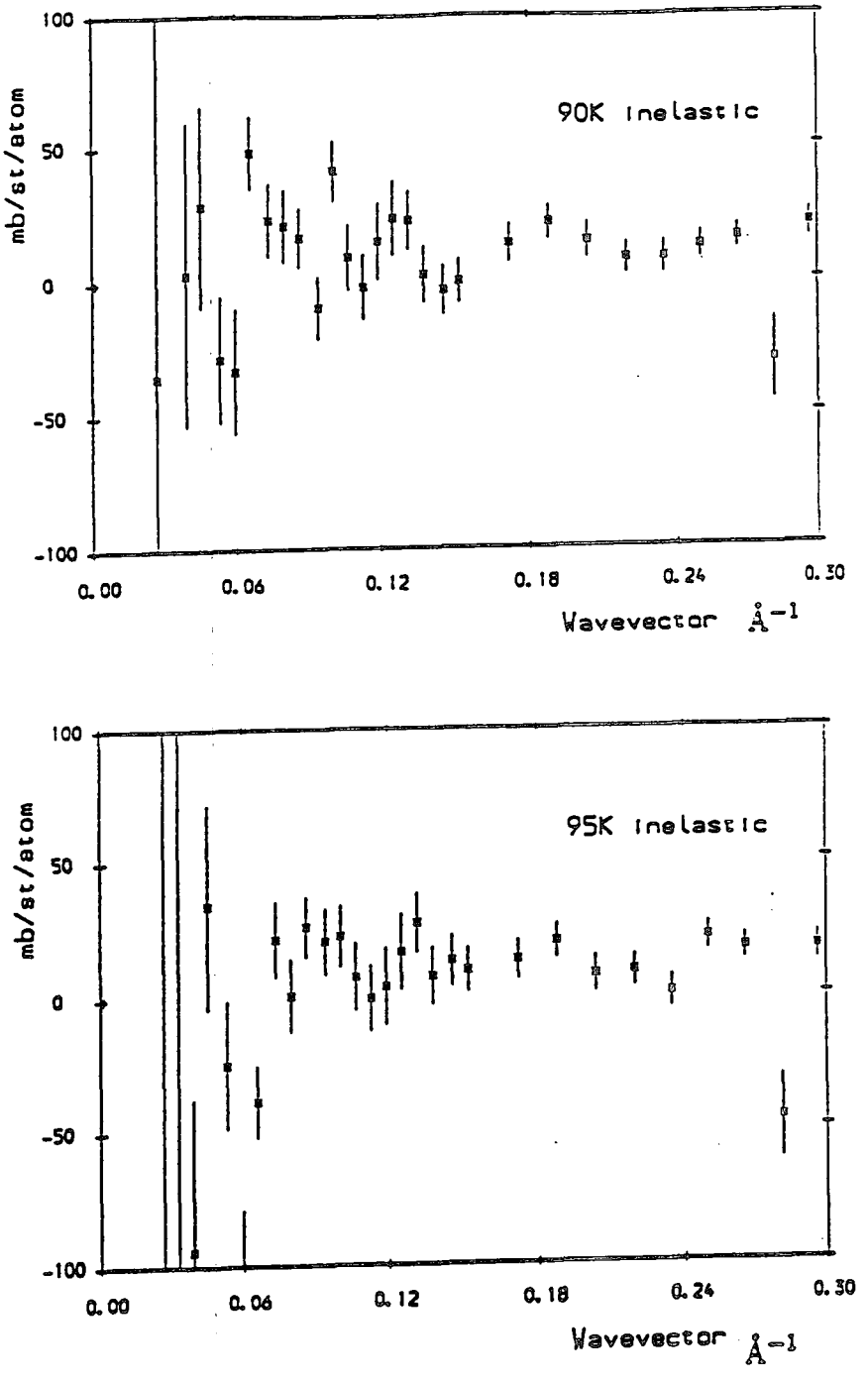
90K Inelastic
95K Inelastic
mb/st/atom
100
50
0
-50
-100
0.00
0.06
0.12
0.18
0.24
0.30
Wavevector Å⁻¹

Figure 5.21 —

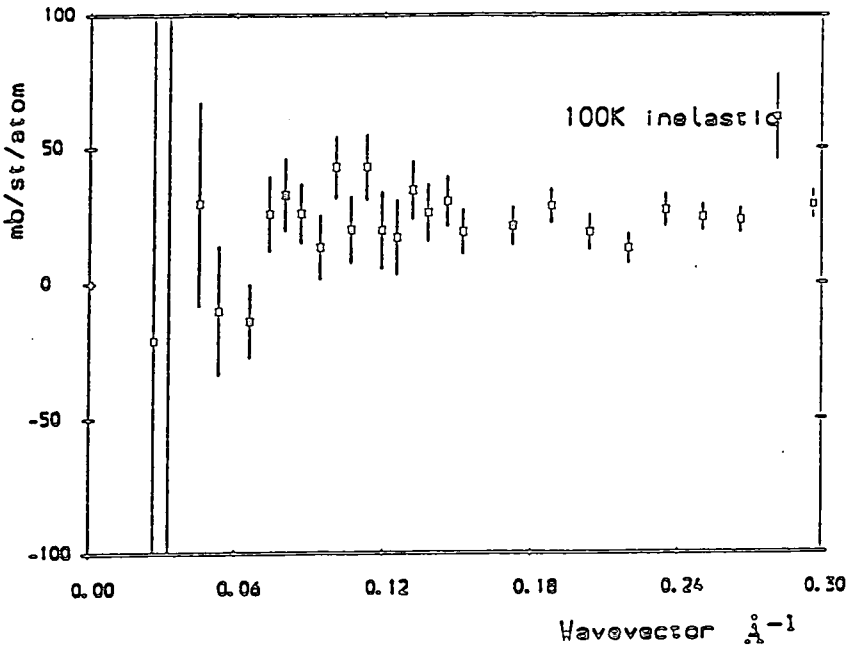
100
50
0
-50
-100
mb/st/atom
100K inelastic
0.00
0.06
0.12
0.18
0.24
0.30
Wavevector Å^{-1}

Table 5.3 — Table of Integrated Difference Scattering at Low q
$0.05 < \hbar\omega < 2$ meV, $q_0 = 0.04$ - 0.187 Å^{-1}

Temperature	Total Scattering	Error 1σ	Error 1σ
		(spread of values)	(counting stats.)
(K)	mb/sr/atom	mb/sr/atom	mb/sr/atom
25	-5.1	15.5	4.6
75	14.2	15.1	4.5
77	-11.9	43.4	4.0
80	7.7	19.8	4.6
85	7.9	19.9	4.4
87	4.7	40.3	4.7
90	10.6	19.8	4.4
95	0.9	36.5	4.5
100	5.0	54.2	4.4

5.6 Summary of Experimental Results

Small angle scattering from $Y_1Ba_2Cu_3O_{7-\delta}$ has been investigated over a wide range of temperature, using several complementary spectrometers. An excess of scattering has been found of around 150 mb/sr/atom at q's of around 0.03 Å^{-1} at temperatures at and slightly above T_c, with a second peak at lower temperatures. Different spectrometers give pleasing agreement both in form and magnitude of scattering around T_c. A small magnetic field does not affect this scattering measurably, thus ruling out flux line scattering as a possible mechanism. The simple model in chapter III gives the wrong temperature dependence and predicts only 10% of the intensity observed. A search for inelastic scattering at slightly higher q gives an upper bound of 13 mb/sr/atom for the difference in scattering between 2 K and higher temperatures at q's summed from 0.04 to 0.187 Å^{-1}.

Chapter VI

SANS Studies of Niobium and Lead

6.1 Introduction

To complement the results of the previous chapter, experiments were undertaken to check to see whether there was any observable signal from the two most suitable systems for neutron work amongst the elemental superconductors, these being niobium (Nb) and lead (Pb). These both posess cubic crystal structures, with amongst the highest T_c's for elements. Various of their properties are outlined below. The major points to notice are that lead is type I and niobium type II, and that the q-scales important in these elements are much more difficult to reach, as ξ is in both cases much greater than in $Y_1Ba_2Cu_3O_7$. The screening effects due to the London penetration depth are also to be expected to be much more important as here λ and ξ are of similar orders of magnitude.

Table 6.1 — Relevant Properties of Niobium and Lead

Property	Units	Niobium	Lead
λ	Å	390	370
ξ	Å	380	830
T_c	K	9.2	7.2
Gap $2\Delta(0)$	meV	3.05	2.73
structure		bcc	fcc
lattice parameter a	Å	3.3	4.95
incoherent cross-section	barns	0.0063	0.0013
absorbtion cross-section	barns	1.15	0.17

Data taken from Kittel, Phillips, and Kostorz and Lovesey

6.2 Details of Samples

The major advantage of these elements is that large single crystals can be both obtained and used in the experiment, due to the favourable absorption cross-sections. This use of good single crystals means that the low angle background can be very low indeed, as will be seen in the data obtained. This means that extremely hard experiments are possible: more importantly, as will be seen, D11 itself is capable of operating at these q ranges with an intrinsically low background.

Single crystals of these materials, as rods of length around 3 cm and diameter 1 cm were obtained from Dr A.Boothroyd and Mr T.Brown respectively. These were held in a specially made aluminium sample holder, the crystals being wrapped in very thin rolled cadmium sheet and the rest of the holder being screened at the front by a cadmium mask. This sample holder is shown in figure 6.1.

This was then mounted onto the D11 sample stick in the normal way; additionally a coil could be wrapped around the crystal in order to monitor T_c using the same temperature sensor as that for the experiment, but this was not done during the actual run, to avoid the possibility of scattering from the coil material.

6.3 Experiment 1 – Total Scattering Measurement

The first experiment used D11 with 2.5m collimation and 2.5m sample to detector distance. D11 is described in chapter IV. The experiment measured the signal through the central pinhole in the beamstop to monitor the total transmission through the sample as a function of temperature. This hole could perhaps be enlarged for this purpose, but the problem of saturation of the detector behind the hole would then have to be addressed. Both niobium and lead samples were investigated.

This experiment measures changes in the total cross-section (absorption + scattering) of the sample as a function of temperature. Essentially this is an integral over all (q,ω) available for neutron scattering, (the "neutron window"), except for a rather delicate region around q = 0 which will now be discussed. The point is that the detector is now effectively very small in this geometry, the pinhole being much smaller than the sample. Thus the neutrons detected have

Figure 6.1 —

The single crystal sample holder

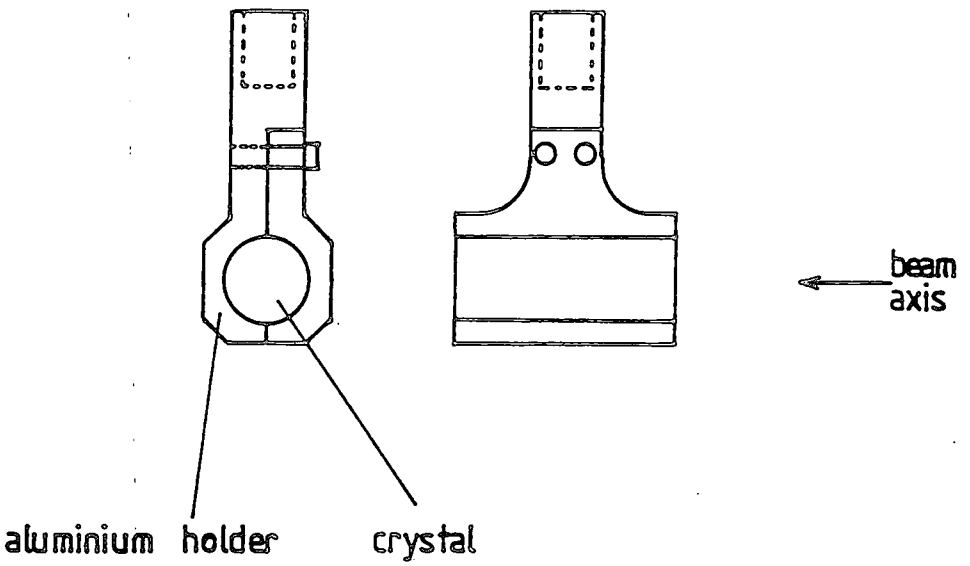

Figure 6.2 —

The scattering out / scattering in problem.
Scattering in compensates for the scattering out as shown,
for sufficiently small angles of scatter.

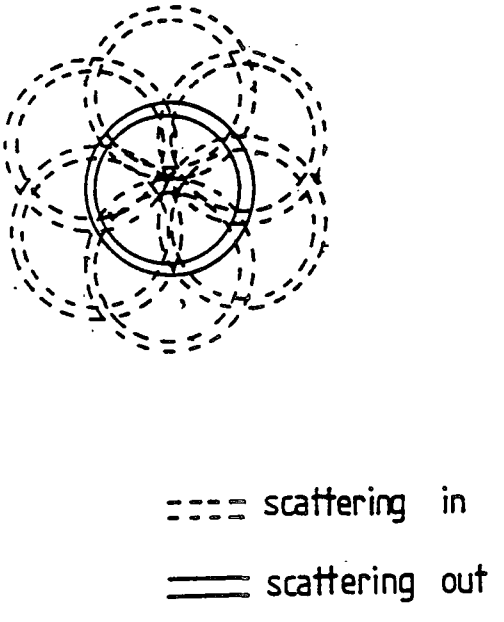

passed through an (imaginary) pinhole diameter tube through the sample. Now if some of these neutrons are scattered out of the beam at very small angles, (defined here as those angles which when projected onto the detector are less than the sample radius), then an equal number of neutrons will be scattered back into the detector by the other regions of the sample. This is schematically shown in figure 6.2, for six example regions scattering back into the central pinhole. Those neutrons scattered at higher angles are not compensated for in this manner, and we thus measure a decrease in the transmission. Figure 6.3 shows the total neutron window and that part which we can measure by this technique.

This is true as long as the pinhole was centred on the sample axis, but if this is not true, then at sufficiently large angles there will be insufficient weight from the scattering back into the "straight through" beam to get complete cancellation. Thus the lower cutoff for the wavevector integral detected may be rather difficult to define without a much better measure of the exact position of the pinhole. Beam divergence effects do not qualitatively change this fact, but will again change the effective cutoff wavevector in detail, as the situation is more complicated for a now off-sample-axis neutron.

A small angle scattering instrument is good for such extensive total scattering measurements, mainly because the collimation can be suitably matched to the sample dimensions and the flux is high on such machines due to their rather relaxed requirements in monochromation. Notice that there is for this experiment no strict restriction upon the incident wavelength – but in practice we would ideally carry out such experiments beyond the Bragg cutoff to remove all Bragg scattering effects.

A direct test of the temperature sensor was performed separately, using the inductively measured T_c of the niobium sample in the same cryostat to check that the temperature indicated was sufficiently accurate. The T_c of niobium is 9.2 K, and the result (figure 6.4) shows that this was obtained successfully.

Figure 6.3 —

The neutron window and the part of this measured by the transmission with a 1cm diameter sample, pinhole at 2.5m, 6.5 Å.

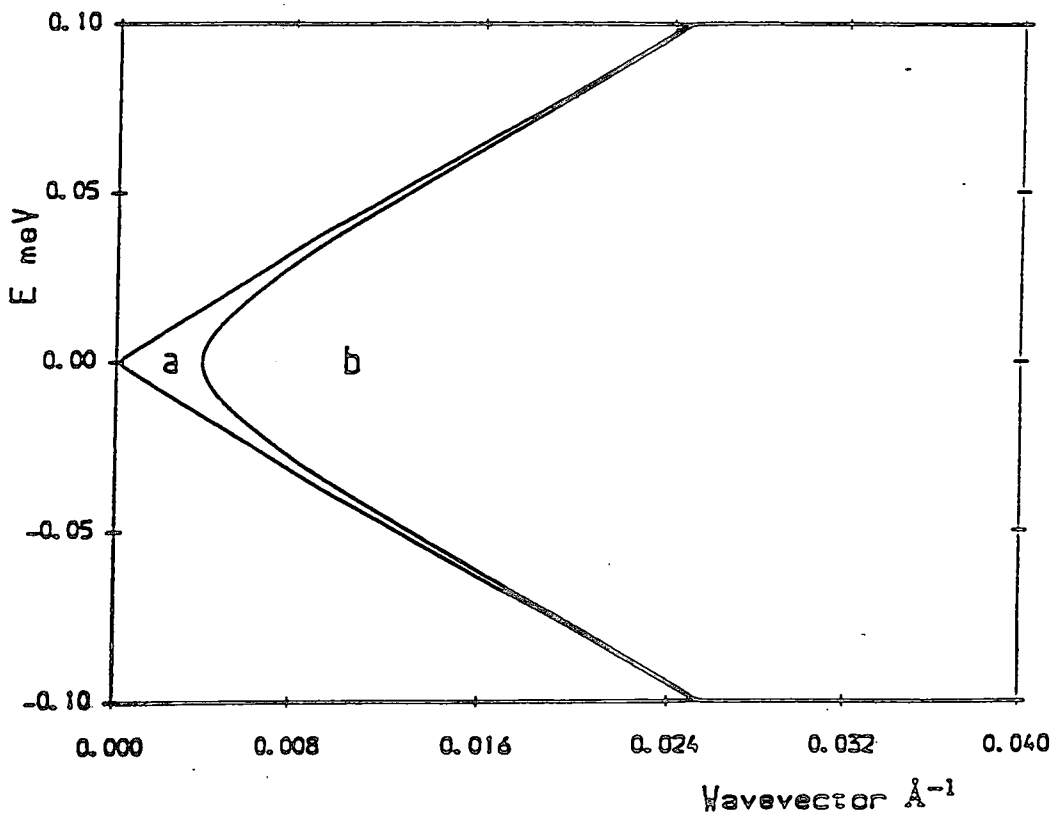

a+b = neutron "window"

b = transmission

6.4 Results

6.4.1 Comment

Both of these transmission graphs show some apparent feature at T_c, though the signal in lead is very weak if at all justifiable against the statistical noise and will not be treated further here. The niobium sample in particular shows a noticable "dip" in transmission centred upon T_c, and with a distinct width, of at least 0.5 K. If we average over a 0.2 K range around T_c, and compare this with the average value excepting points within 1 K of T_c, this dip is 39 ($\pm$ 8.5) counts/cell in these units. Changes in transmission can easily be converted into changes in total cross-section by the relation $\Delta I/I = 1 - e^{-nt\Delta\sigma}$, where n is the nuclear number density, t the thickness, and $\Delta\sigma$ the change in cross-section. These calibration factors convert, for the scales used here, into 18.1 mbarn/atom per 10 counts/cell change. To obtain the measured dip in transmission, we need 71 $\pm$ 15 mbarn/atom of excess scatter at and close to T_c.

Figure 6.4 —

Inductive T_c measurement showing the superconducting transition of the niobium sample at 9.2 K, thus confirming the temperature calibration.

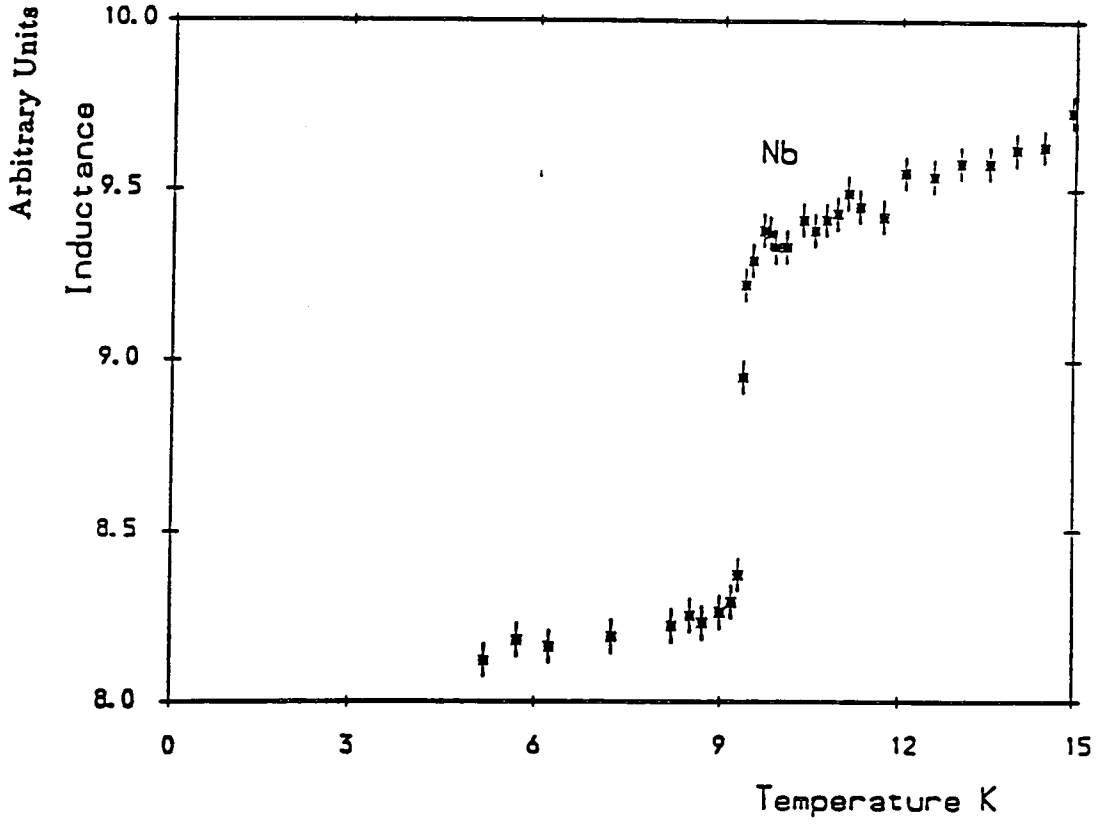

Figure 6.5 —

Transmission vs. temperature for niobium,
showing a dip in the signal at and around T_c.

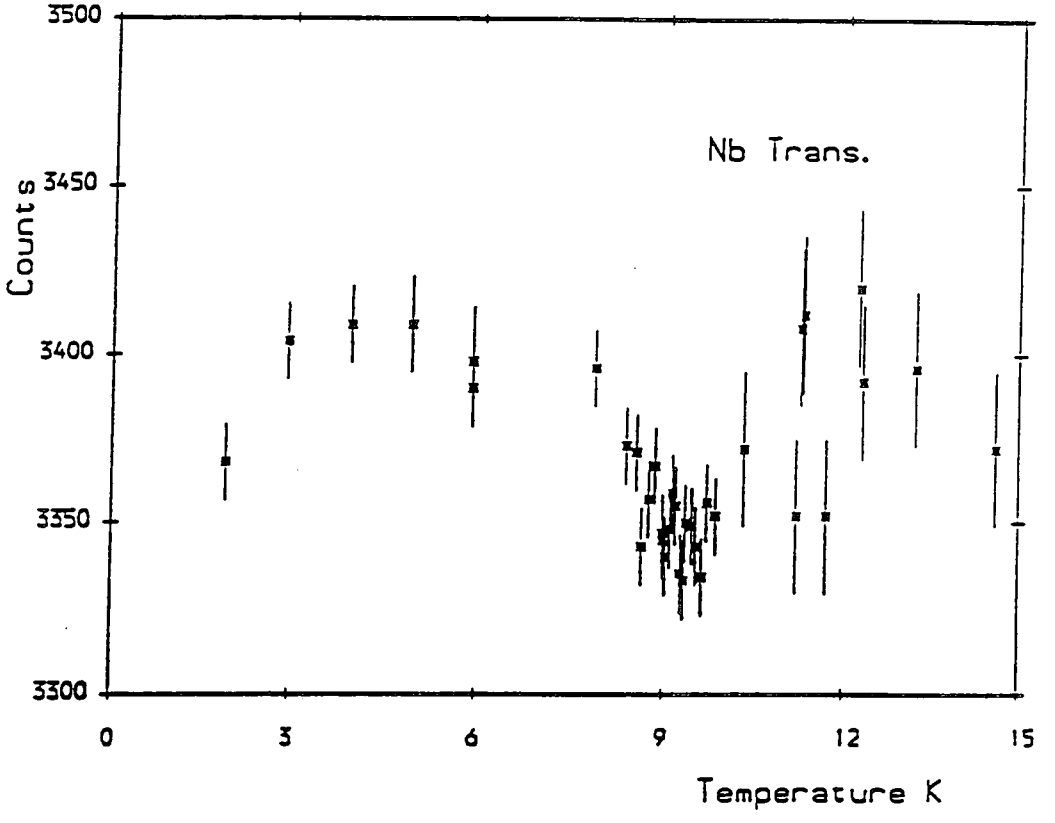

Figure 6.6 —

Transmission vs. temperature for lead,
showing no change at T_c.

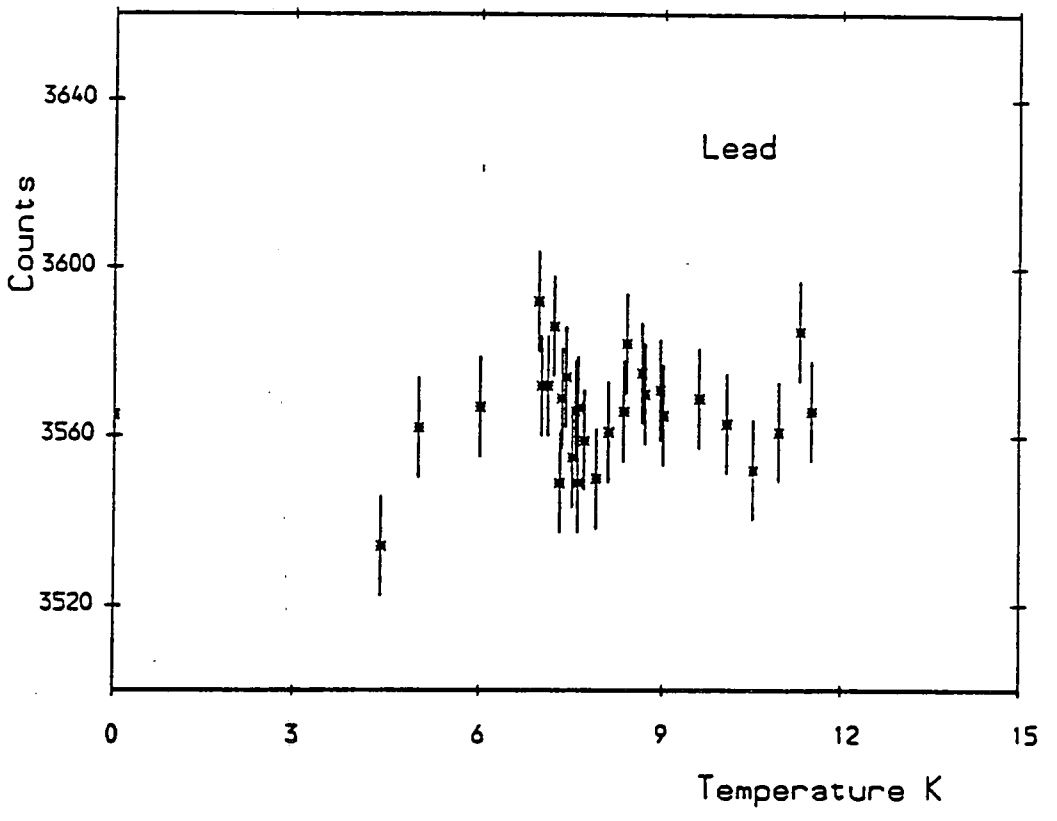

6.5 Second Experiment - Direct Scattering Measurement

6.5.1 Experimental Details

This experiment set out to measure whether this excess scatter at T_c in niobium was at small angles. For this, the smallest practicable q (of order $\xi(0)^{-1}$, i.e. around .003 $Å^{-1}$) was sought; D11 at 20m collimation and 20m sample-detector distance was used with a λ of 6.5 Å giving a q-range of 0.004 - 0.015 $Å^{-1}$. This collimation gives a loss in flux at the sample compared to 2.5 m collimation of a factor of 64 in theory, and a correspondingly smaller total solid angle viewed by the multidetector. In fact the flux loss is not quite as bad as this, as the 17.5m of guide tube now removed from the 2.5m setup is not perfectly efficient and we are removing this loss mechanism. In fact we can estimate the loss from the measured sample transmission at 20m / 20m, which gives a measured value of a factor of 38 (i.e. the guide is only 38/64 efficient).

This low flux causes real problems; centring the beamstop, which is usually a simple matter with a strong scatterer such as a piece of plexiglas, becomes more difficult. A better solution is to use a stronger scatterer giving a large amount of scatter into the very small angles most useful for centring purposes. On D11 biologists use PTFE for this purpose, and this idea we have successfully borrowed. Notice that gravity starts to become important in the centring of the beamstop at these collimator and sample-detector distances.

6.5.2 Calibration

The problem mentioned above causes difficulties for our calibration procedure i.e. using vanadium as the standard scatterer. This becomes unfeasible due to the now low flux and low solid angle viewed. We have here reverted to using plexiglas as a secondary standard, calibrated separately against vanadium at 2.5m / 2.5m. In addition, the standard programs used on D11 to average the counts in the annular constant scattering angle rings of the multidetector only work to the nearest 0.1 counts per cell. At noise limited count rates, this can be a serious problem as the rounding error can be significant, and should be addressed in future by recording all the data for the individual detector elements for such experiments. This aside, plexiglas calibration at 20m / 20m was feasible.

6.6 Results

Only two temperatures were investigated, 2.0 and 9.2 K, allocating 12 hours to each run, and changing only the temperature in between runs. This was to give the maximum possible chance to measure any scattering. Again the Bragg cutoff wavelength was exceeded by a suitable margin. The difference in scattering in absolute units is shown in figure 6.7.

It is apparent that there is no signal above the noise, always being within 1 standard deviation of zero. Angles which gave very low count rates for perspex at 2.5m / 2.5m have been rejected.

6.6.1 Background

The background seems to be mostly the wings of the direct beam, if allowance for the sample transmission is made ($\simeq$ 1/3). See figures 6.9 and 6.10. This background is still rather angle dependent and implies that with our sample size, a cross-section of around 50 mb/sr/atom at typical q's of 0.006 - 0.015 Å^{-1} would be visible given 12 hours counting time at each temperature. This is about the limit of performance of D11, as we are rapidly approaching both the electronic noise limit and the length of time available for any one experiment.

6.7 Comment on Both Results

It is perhaps not surprising that there is no transmission anomaly in lead; it is a type I superconductor, and would not be expected to show the electromagnetic effects discussed in chapter III, as any magnetic field fluctuations will be extremely efficiently screened even at q's approaching ξ^{-1}. This argument is strongest below T_c; in theory, fluctuation effects above T_c might be visible even in a type I superconductor due to the lack of screening effects. On the other hand there is evidence for a transmission anomaly in Nb which implies that there is extra scattering at and near T_c, with an integrated cross-section of 71 $\pm$ 15 mbarn/atom.

However, direct attempts to measure this scattering have failed even at q's as low as 0.004 Å^{-1}. This would be the wavevector scale expected if this were to be similar in form to the scattering from $Y_1Ba_2Cu_3O_7$. Further, to be at even smaller q, it would have to be concentrated in such a small volume of q space that the

Figure 6.7 —

The difference scattering between 9.2 K and 2 K.
Notice the lack of any scattering to within the error bars.

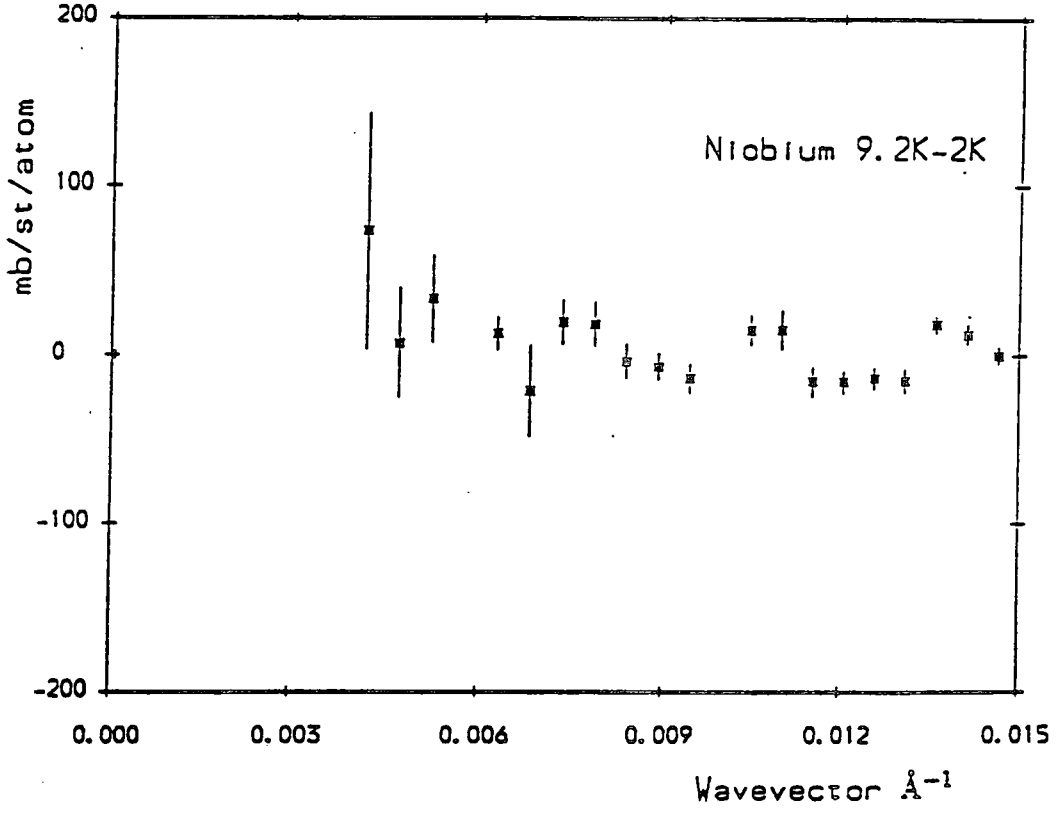

Figure 6.8 —

The D11 integration paths for the configuration used
in this experiment (20m / 20m , 6.5 Å).
Lines represent the integration paths for channels 8 to 30.

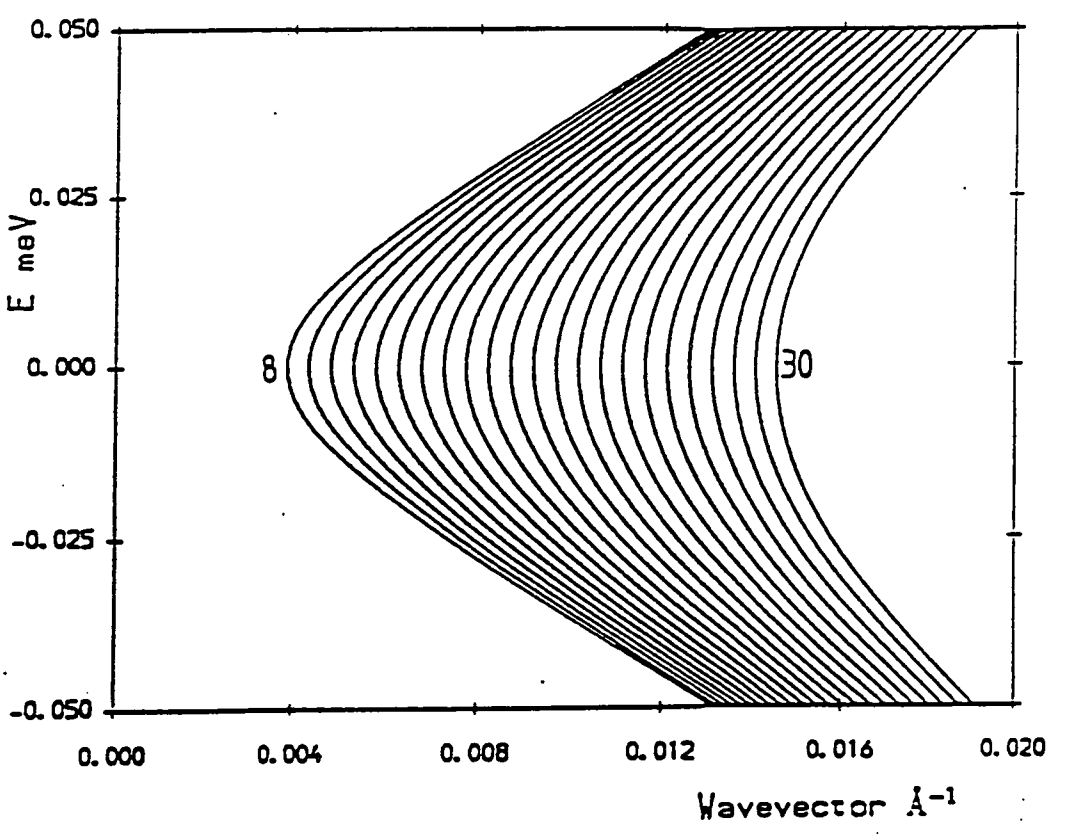

Figure 6.9 —

The background scatter without the sample on D11
(20m / 20m , 6.5 Å). This is the fundamental limit to D11 performance.

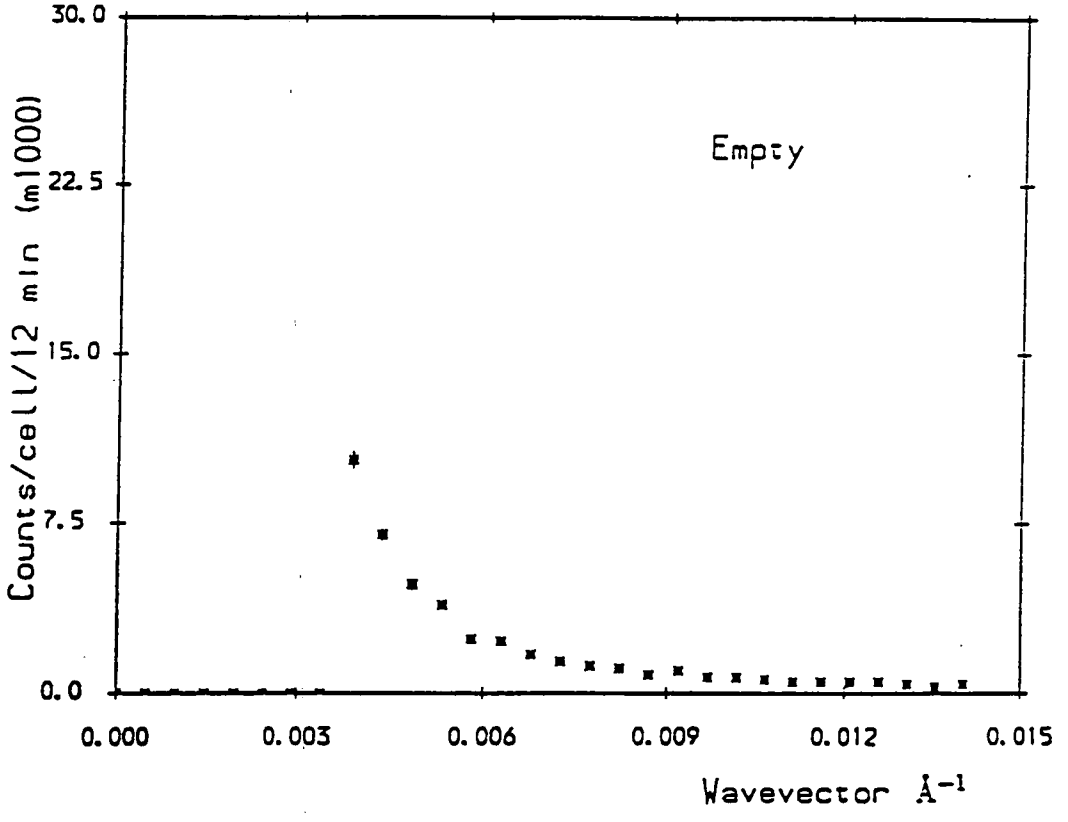

Figure 6.10 —

The background scatter with the niobium crystal
(20m / 20m, 6.5 Å). This shows how little extra
scatter is introduced by the sample, allowing for absorbtion.

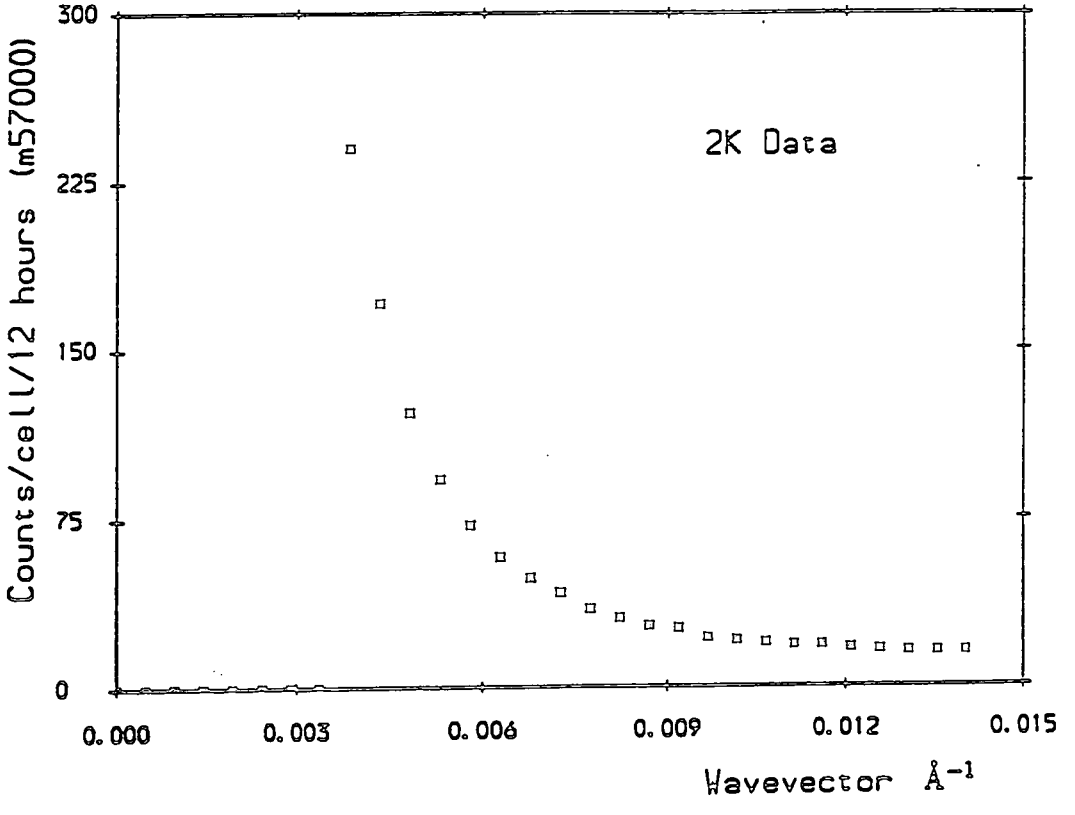

cross-section per steradian would be very large indeed. Also, there can be placed stringent limits on where this scattering could be, as after all channel 8 (8-9 cm) at 20m ($q = 0.004$ Å^{-1}) corresponds to channel 1 (1cm) at 2.5m. The low q limit on the integration performed by the transmission measurement, if the pinhole in the beamstop was perfectly centred with respect to the sample (the best case), is at half this at around 5mm at 2.5m, as the sample is 10mm in diameter.

Thus the only consistent explanation seems to be either that the scattering is at $0.0015 < q < 0.003$ Å^{-1} or it is at a much higher q and by a different mechanism, e.g. a phonon. It may also be appropriate to note that there are no neutron visible phonon anomalies at the superconducting transition in lead, but there are in niobium as mentioned in chapter III (see Youngblood, Shirane).

6.7.1 Phonon Scattering Interpretation

There are two points to consider, if we think that a phonon might be responsible. This effect must cause extra scattering only in the region immediately around T_c. Thus the phonon mode concerned must in all probability be near to the edge of the volume of phase space available and enter it and then leave it again below T_c.

This is rather difficult to visualise as the phonons are usually affected in the following way. They decrease in width (which takes weight spread out in ω and concentrates it) and may also decrease in energy, (soften), when below the gap in energy. If close to the gap in energy, they are increased in width. Both the phonon linewidth and frequency effects vary quite smoothly with temperature, with no obvious way in which they can combine to give the required temperature dependence.

At least in niobium, we are well away from the first Bragg reflection, as 100 is forbidden in a bcc structure – the first allowed reflection is 110 (2.692 Å^{-1}). Thus the only phonons that cut the integration paths at low energies even for scattering at 180° (if we put the velocity of the first phonon as 10 meV Å(Nakagawa)) are at energies of > 2.6 meV. See figure 6.11. This is inside the zero temperature gap for niobium ($2\Delta(0) = 3.05$ meV), but if we use the "two-fluid" model for the gap, it will not reach this energy until $T/T_c < 0.62$, i.e. not until $T < 5.7$ K. Thus the

Figure 6.11 —

Diagram showing the intersection of
the first phonon from the 110 Bragg peak
with the 6.5 Å, 180° integration path.
This shows that this scattering process only occurs at
energies of greater than 2.6 meV.

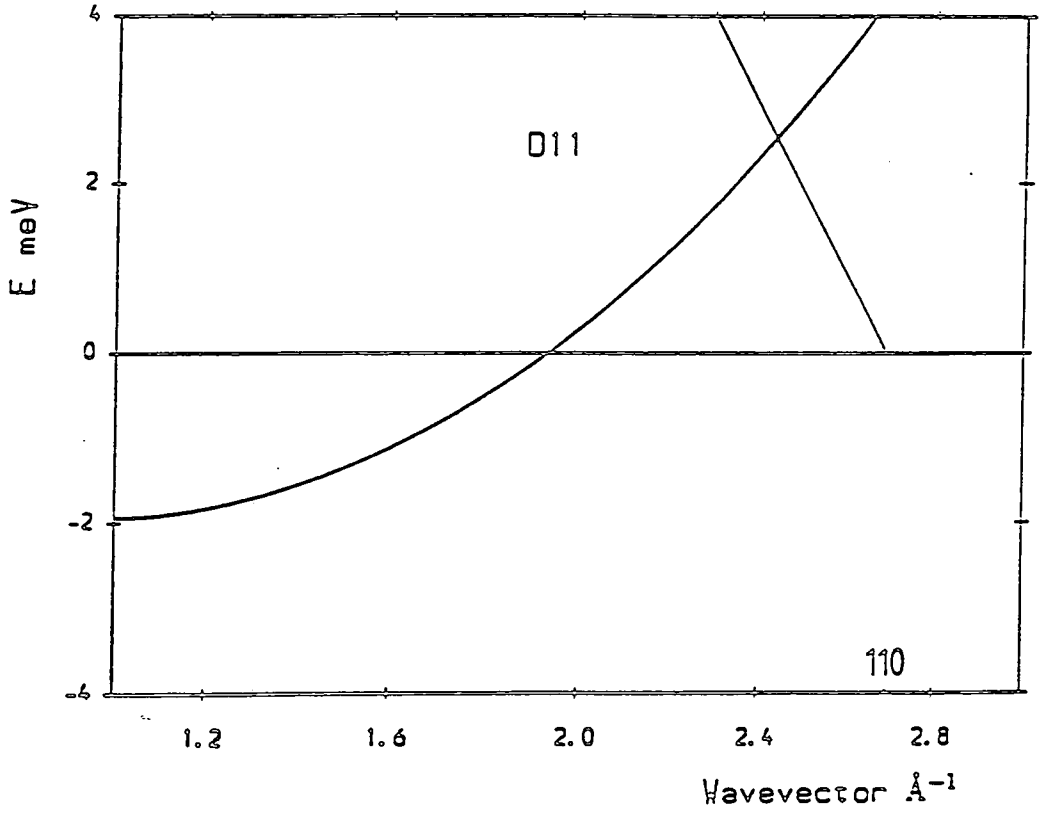

strongest effects on this phonon at these energies will not occur at T_c itself, as we would need if this were to provide our extra scattering.

A simple test of whether this effect is due to some subtle phonon anomaly would be to repeat the experiment with energy analysis, as a single phonon mechanism involves energy transfer. Another instrument, such as IN11, might be more suitable than D11 for this experiment.

Chapter VII

Conclusions and Suggestions for Further Work

"When at the first I took my pen in hand,
Thus for to write, I did not understand ..."

J.Bunyan, The Pilgrims Progress, Author's apology, initial lines (1678)

7.1 Results

The small-angle scattering technique especially in its quantitative form has been shown to be useful in principle for measurements upon the superconducting state. Extreme type II superconductors with high T_c's appear to be the best candidates for observing such effects, due to the small coherence lengths involved and the long penetration depth. These allow magnetic effects at q values of order the coherence length to be measured. The increased population of low energy modes due to the population factor also helps make experiments on current neutron spectrometers a practical proposition.

7.1.1 High T_c Superconductors

Experimental results on $Y_1Ba_2Cu_3O_7$ indicate a peak in the scattering at small angles at wavevectors of order .03 $Å^{-1}$ at and just above T_c and a further peak at lower temperature. Experiments on IN3 and IN5 restrict the energies for this scattering to be within -30 to +30 μ eV and -50 to +50 μeV respectively. That is to say this scattering is indistinguishable, due to the finite experimental resolution, from elastic scattering. There is no simple extrinsic explanation for this magnitude of scattering.

7.1.2 Interpretation

There is no obvious way to explain the magnitude of this peak within the framework of current theories if sensible parameters are to be used. In particular, the theory of scattering from the orbital effects of the conductivity changes in a

superconductor predicts a decrease in scattering at T_c not an increase. This is the opposite of what is observed here ! Even in the simpler case above T_c, the amount of scattering seen is very difficult to obtain from fluctuation conductivity models.

If these events are very low energy or elastic, we must be careful about the use of the population factors; truly elastic ($\omega = 0$) events should be genuinely temperature independent unless the mechanism which is causing scattering is changing. If the energy of these excitations is truly very low, then the assumption made that the mode is unpopulated at low temperatures (2 K) may not be good. Any collective modes of the system at finite energy will, however, be required to be seen in various other measurements which integrate over all available states of the system, specifically NMR, μSR and specific heat measurements. Although comprehensive results for all these have not yet been obtained, initial results do not indicate extreme behaviour in any of these. This does not however mean that these are yet well understood.

The upper bound on inelastic scattering energies obtained using IN5, of 13 mb/sr/atom at $0.05 < \hbar\omega < 2$ meV and q's of 0.04 to 0.187 Å^{-1}, puts the final nail in the coffin of theories invoking superconducting pairing by low energy ferromagnetic correlations in this system. Any theories involving B-fields in the bulk of the superconductor sample (e.g. Anyon theories) will also be restricted by this result, as it measures and places a limit on the (B,B) correlation function of the system at "macroscopic" wavevectors at finite energies. They might however take some comfort from the very low energy or elastic effects seen here.

7.1.3 Conventional Superconductors

Measurements on single crystal niobium have shown no directly measurable additional scatter at wavevectors of .004 to .015 Å^{-1} at T_c, at the 50 mbarn/sr/atom level. This cross section upper bound is a very restrictive limit upon the scattering at such values of q and is unlikely to be improved without a radical improvement upon current neutron sources. This experiment takes D11 to the electronic noise limited regime at 20m / 20m incident and outgoing collimation and demonstrates the possibility of using D11 in this q range for hard experiments. Given that niobium is a much less type II system than $Y_1Ba_2Cu_3O_7$ with a κ of 1.02, this is maybe not surprising even within the picture used above. Nevertheless, a dip in

the measured transmission of 6.5 Å neutrons through a niobium single crystal of around 1% at T_c has been measured. This pair of results is difficult to understand simply. A similar experiment with a lead crystal gave no such result. Lead is type I and would not be expected to show any magnetic effects, with the screening effects dominating at all ranges of q below T_c.

7.2 Suggestions for Further Work

Further work in this field should involve the continuation of the experiments on $Y_1Ba_2Cu_3O_7$, possibly using an oriented array of flux-grown crystals. Progress on the manufacture of such crystals of sufficient size is enough to allow the D11 experiment to be repeated although sufficient sample for IN5 probably remains out of reach at the moment. Such work will be able to exploit the lower background from superior samples to investigate the temperature and wavevector dependence more fully. In addition, it may be possible to investigate the effects above T_c, especially at the larger wavevectors (say .045 $Å^{-1}$ and above) where precursor effects might be more obvious, given that fluctuation effects may well be stronger at finite q. Other High T_c systems are also worth considering, if they can be made as homogenous bulk samples with a single T_c. As yet, none are obvious candidates, although samples of such systems may eventually overtake $Y_1Ba_2Cu_3O_7$ in their quality.

In conjunction with this, it is worthwhile considering looking at low T_c intermetallic compounds such as the cubic compound $LaSn_3$. The study of superconductivity possesses a great advantage over magnetism in this respect as there are many more intermetallic superconductors than ferromagnets; thus a compound with especially favourable properties for neutron work can be chosen, rather than being the only candidate system ! A low incoherent scattering cross section and a low absorbtion are the most important of these, and a cubic crystal structure helps to make the Bragg cutoff wavelength small. Systems with low temperature structural anomalies, (such as the structural transitions in Nb_3Sn and its related compounds), are however best avoided due to the possibility of small angle scattering arising from these effects swamping the signal.

A more adventurous experiment still would examine systems with other phase transitions that radically change the conductivity, such as metal-insulator tran-

sitions. However, for these experiments we need homogenous systems with no structural changes at the phase transition and with good neutron properties.

7.3 Final Remarks

Small angle scattering from superconductors is, as a field of study, restricted by two major problems. Firstly, these experiments are long and hard to perform by comparison with many other SANS experiments. The principal reason for this is that the interesting range of wavevector is extremely low , and this means small angles and long wavelengths must be used. The building of the new small angle instrument D22 at the ILL, which is optimised for longer wavelengths than D11, may make some of these experiments more feasible.

Secondly, the interesting region of (q,ω) space is the region where $q \leq \xi^{-1}$. This is a taxing theoretical problem , especially at finite temperatures. The question of what the superconductor looks like at these length scales is obviously an interesting and fundamental one. No other probe can unambiguously reach these wavevectors and energies; thus there is unfortunately little possibility of direct ancillary confirmation of these effects.

Neither of these two problems is in my view insurmountable. I hope that this thesis will provoke future effort into this interesting field.

Bibliography

1 References for Chapter I

H.Kamerlingh Onnes, Akad. von Wetenschappen (Amsterdam) 14, 113, 818 (1911)

A.B.Pippard, IEEE Trans. Mag. MAG-23, pp371-375 (1987) and other papers in the same volume

L.N. Cooper, IEEE Trans. Mag. MAG-23, pp376-379 (1987)

J.E.Kunzler, IEEE Trans. Mag. MAG-23, pp396-402 (1987)

E.M.Savitskii, V.V.Baron, Y.V.Efimov, M.I.Bychkova, and L.F.Myzenkova , "Superconducting Materials " , Plenum (1981) (trans. from Russian)

J.C.Phillips, "Physics of High T_c Superconductors" , Academic Press, (1989) ISBN 0-12-553990-8

B.T.Matthias, T.H.Geballe and V.B.Compton, Rev. Mod. Phys. 35, pp1-22 (1963)

M.Tinkham, "Introduction to Superconductivity", McGraw-Hill, New York, (1975) Reprint 1980, R.E.Krieger Publishing, ISBN 0-89874-049-5

C.Kittel, "Introduction to Solid State Physics", John Wiley and Sons, (1953), ISBN 0-471-49024-5

W.Meissner and R.Ochsenfeld, Naturwissenschaften 21, p787 (1933) (In German).

F.B.Silsbee, J. Wash. Acad. Sci. 6, pp597-602 (1916)

N.E.Phillips, Physical Review 114, pp676-685 (1959)

F. and H. London, Proc. Roy. Soc. (London) A149, p72 (1935)

L.Landau, Phys. Rev. 60, pp356-358 (1941)

E.Laurmann and D.Schoenberg, Proc. Roy. Soc. (London) A198, pp560-581 (1949)

A.B. Pippard, Proc. Roy. Soc. (London) **A216**, p547 (1953)

V.L.Ginzburg, Il Nuovo Cimento Serie 10 **2**, pp1234-1250 (1955)

L.D.Landau and V.L Ginzburg, JETP (USSR) **20**, p1064 (1950)
translation in: "Men of Physics, L.D.Landau v1 , Selected readings in Physics", ed. D. ter Haar, Pergamon (1965)

L.P.Gor'kov and T.K.Melik-Barkhydarov, Soviet Physics JETP **18**, p1031 (1964)

H.Traüble and U.Essmann, Phys. Stat. Sol. **25**, pp373-393 (1968) (in German)

A.A.Abrikosov, Soviet Physics JETP **5**, pp1174-1182 (1957)

R.A.Craven, G.A.Thomas, and R.D.Parks, Phys. Rev. B **7**, pp157-165 (1973)

R.A.Ferrell and H.Schmidt, Physics Letters **25A**, p544 (1967)

R.G.Glover, Physics Letters **25A**, pp542-544 (1967)

L.N.Cooper, Phys. Rev. **104**, p1189-90 (1956)

J.Bardeen, L.N.Cooper, and J.R.Schrieffer, Phys. Rev. **108**, pp1175-1204 (1957)

N.N.Bogoliubov, Il Nuovo Cimento **VII**, pp794-805 (1958)

P.W.Anderson, Phys. Rev. **110**, pp985-986 (1958)

G.Rickayzen, table on p73 in Chapter 2 of "Superconductivity" Ed. Parks, Marcel Dekker Inc. (1969)

L.C.Hebel and C.P.Slichter, Phys. Rev. **113**, pp1504-1519 (1959)

J.Bardeen and J.R.Schrieffer, Chapter 6 in Prog. in Low. Temp. Phys vol. III, (Ed. Gorter), North Holland, Amsterdam, (1961)

J.C.Phillips, Phys. Rev. Lett. **10**, pp96-98 (1963)

P.C.Martin, p374 in Chapter 7 of "Superconductivity" Ed. Parks, Marcel Dekker Inc. (1969)

P.W.Anderson, Phys. Rev. **110**, pp827-835 (1958)

P.W.Anderson, Phys. Rev. **112**, pp1900-1906 (1958)

K.Yosida, Prog. Theor. Phys. **21**, pp731-744 (1959)

D.J.Thouless and D.R.Tilley, Proc. Phys. Soc. **77**, pp1175-1181 (1961)

A.J.Leggett, Prog. Theor. Phys. **36**, pp901-930 (1966)

D.C.Mattis and J.Bardeen, Phys. Rev. **111**, pp412-417 (1958)

M.Tinkham and R.A.Ferrell, Phys. Rev. Lett. **2**, pp331-333 (1959)

S.Nakajima, Prog. Theor. Phys. **22**, pp430-436 (1959)

C.Kittel, "Introduction to Solid State Physics", John Wiley and Sons, (1953), ISBN 0-471-49024-5

2 References for Chapter II

"Ternary Superconductors ", Ed. Shenoy, Dunlap, Fradin, North Holland, (1980)

B.T.Matthias, T.H.Geballe and V.B.Compton, Rev. Mod. Phys. **35**, pp1-22 and references therein.

A.W.Sleight, J.L.Gillson and P.E.Bierstedt, Solid State Comms. **17**, pp27-28 (1975)

E.M.Savitskii, V.V.Baron, Y.V.Efimov, M.I.Bychkova, and L.F.Myzenkova , "Superconducting Materials " , Plenum (1981) (trans. from Russian)

J.G.Bednorz and K.A.Müller, Z. Phys **B64**, p189 (1986)

J.G.Bednorz and K.A.Müller, Rev. Mod. Phys. **60**, pp585-600 (1988)

N.B.Brandt and N.I.Ginzburg, Contemp. Phys. **10**, pp355-384 (1969)

C.W.Chu, P.H.Hor, R.L.Meng, L.Gao, Z.J.Huang, and Y.Q.Wang, Phys. Rev. Lett. **58**, pp405-407 (1987)

M.K.Wu, J.R.Ashburn, C.J.Torng, P.H.Hor, R.L.Meng, L.Gao, Z.J.Huang, Y.Q.Wang and C.W.Chu, Phys. Rev. Lett. **58**, pp908-910 (1987)

D.G.Hinks, L.Soderholm, D.W.Capone II, J.D.Jorgensen, Ivan K.Schuller, C.U.Segre, K.Zhang, and J.D.Grace, Appl. Phys. Lett. **50**, pp1688-1690 (1987)

H.Maeda, Y.Tanaka, M.Fukutomi, and T.Asano, Jap. J. App. Physics **27**, pp209-210

Z.Z.Sheng and A.M.Hermann, Nature **332**, pp55-58 (1988)

M.B.Maple, Y.Dalichaouch, J.M.Ferreira, R.R.Hake, B.W.Lee, J.J.Neumeier, M.S.Torikachvili, K.N.Yang, H.Zhou, R.P.Guertin and M.V.Kuric, Physica **148B**, pp155-162 (1987)

R.J.Cava. J.J.Krajewski, W.F.Peck Jr., B.Batlogg, and L.W.Rupp Jr., Physica C **159**, pp372-374 (1989)

T.Miyatake, K.Yamaguchi, T.Takata, S.Gotoh, N.Koshizuka and S.Tanaka, Physica C **160**, pp541-544 (1989)

D.E.Morris, J.H.Nickel, J.Y.T.Wei, N.G.Asmar, J.S.Scott, U.M.Scheven, C.T.Hultgren, A.G.Markelz, J.E.Post, P.J.Heaney, D.R.Veblen and R.M.Hazen, Phys. Rev. B **39**, pp7347-7350 (1989)

M.Tinkham and C.J.Lobb, Solid State Physics **42**, pp91-134

MRS Symposium proceedings v99, Ed. M.B.Brodsky, R.C.Dynes, K.Kitazawa, and H.L.Tuller, (1988)

"High Temperature Superconductivity, proceedings of the Los Alamos Symposium 1989" Ed. K.S.Bedell, D.Coffey, D.E.Meltzer, D.Pines and J.R.Schrieffer, Addison-Wesley (1990) ISBN 0-201-51249-1

D.M.Ginsberg (Ed.), "Physical properties of High T_c superconductors vol 1", World Scientific, Singapore (1989) ISBN 9971-50-683-1

M.Aïn, W.Reichardt, B.Hennion, G.Pepy, and B.M.Wanklyn, Physica C **162-164**, pp1279-1280 (1989)

R.J.Birgeneau and G.Shirane, Chapter 4 in "Physical properties of High T_c superconductors vol 1 ",(Ed.) D.M.Ginsberg , World Scientific, Singapore (1989) ISBN

9971-50-683-1

K.Yvon and M.François, Z.Phys B **76**, pp413-444 (1989)

I.K.Schuller and J.D.Jorgensen, MRS Bulletin, Jan 1989

G.Calestani and C.Rizzoli, Nature **328**, pp606-607 (1987)

E.D.Specht, C.J.Sparks, A.G.Dhere, J.Brynestad, O.B.Cavin, D.M.Kroeger, and H.A.Oye, Phys. Rev. B **37**, pp7426-7434 (1988)

Y.Kubo, Y.Nakabayashi, J.Tabuchi, T.Yoshitake, T.Manako, A.Ochi, K.Utsumi, H.Igarashi, and M.Yonezawa, Mat. Res. Soc. Symp. Proc. v99, pp89-100

U.Welp, M.Grimsditch, H.You, W.K.Kwok, M.M.Fang, G.W.Crabtree, and J.Z.Liu, Physica C **161**, pp1-5 (1989)

P.K.Gallagher, Advanced Ceramic Materials **2**, No. 3B, Special Issue, pp632-648 (1987)

J.Karpinski, C.Beeli, E.Kaldis, A.Wisard, E.Jilek, Physica C **153-155**, pp830-831 (1988)

J.Karpinski, K.Conder and E.Kaldis, Physica C **153-155**, pp401-402 (1988)

K.N.Tu, N.C.Yeh, S.I.Park, and C.C.Tsuei, Phys. Rev. B **39**, pp304-314 (1989)

B-J. Lee and D.N.Lee, J. Amer. Ceram. Soc. **72**, pp314-319 (1989)

M.Maeda, M.Kadoi, and T.Ikeda, Jap. J. App. Phys. **28**, pp1417-1420 (1989)

R.Beyers, B.T.Ahn, G.Gorman, V.Y.Lee, S.S.P.Parkin, M.L.Ramirez, K.P.Roche, J.E.Vazquez, T.M.Gur and R.A.Higgins, Nature **340**, pp619-621 (1989)

J.D.Jorgensen, B.W.Veal, A.P.Paulikas, L.J.Nowicki, G.W.Crabtree, H.Claus, and W.K.Kwok, Phys. Rev. B **41**, pp1863-1877 (1990)

M.R.Delap, Private Communication.

T.Penney, S.von Molnar, D.Kaiser, F.Holtzberg, and A.W.Kleinsasser, Phys. Rev. B **38**, pp2918-2921

H.E.Fischer, S.K.Watson and D.G.Cahill, Comments on Condensed Matter Physics 14, pp65-127 (1988)

S.W.Tozer, A.W.Kleinsasser, T.Penney, D.Kaiser, and F.Holtzberg, Phys. Rev. Lett. 59, pp1768-1771 (1987)

S.Martin, A.T.Fiory, R.M.Fleming, L.F.Schneemeyer, and J.V.Waszczak, Phys. Rev. B 41, pp846-849 (1990)

E.M.Forgan, S.L.Lee, S.Sutton, F.Wellhofer, J.S.Abell, C.E.Gough, S.F.J.Cox, and C.A.Scott, Supercond. Sci. Technol. 3, pp217-221 (1990)

M.Hikita and M.Suzuki, Phys Rev. B. 41, pp834-837 (1990)

L.Fruchter, C.Giovannella, G.Collin, and I.A.Campbell, Physica C 156, pp69-72 (1988)

W.J.Gallagher, T.K Worthington, T.R.Dinger, F.Holtzberg, D.L.Kaiser, and R.L.Sandstrom, Physica 148B, pp228-232 (1987)

J.S.Tsai, I.Takeuchi, J.Fujita, T.Yoshitake, S.Miura, S.Tanaka, T.Terashima, Y.Bando, K.Iijima and K.Yamamoto, Physica C 153-155, pp1385-1386 (1988)

D.E.MacLaughlin, Solid State Physics 31, pp1-69 (1976)

S.E.Barrett, J.A.Martindale, D.J.Durand, C.H.Pennington, C.P.Slichter, T.A.Friedmann, J.P.Rice, and D.M.Ginsberg, Phys. Rev. Lett. 66, pp108-111 (1991)

R.F.Kiefl, J.H.Brewer, I.Affleck, J.F.Carolan, P.Dosanjh, W.N.Hardy, T.Hsu, R.Kadono, J.R.Kempton, S.R.Kreitzman, Q.Li, A.H.O'Reilly, T.M.Riseman, P.Schleger, P.C.E.Stamp, H.Zhou, L.P.Le, G.M.Luke, B.Sternlieb, Y.J.Uemura, H.R.Hart, and K.W.Lay, Phys. Rev. Lett. 64, pp2082-2085 (1990)

B.Batlogg, pp37-93 in "High Temperature Superconductivity", proceedings of the Los Alamos Symposium 1989 Ed. K.S.Bedell, D.Coffey, D.E.Meltzer, D.Pines and J.R.Schrieffer, Addison-Wesley (1990) ISBN 0-201-51249-1

T.Timusk and D.B.Tanner, Chapter 7 in "Physical properties of High T_c superconductors" vol 1, Ed. D.M.Ginsberg , World Scientific, Singapore (1989) ISBN 9971-50-683-1

T.Wolf, W.Goldacker, B.Obst, G.Roth, and R.Flükiger, J. Crystal Growth **96**, pp1010-1018 (1989)

H.J.Scheel, J. of the Less Common Metals **150**, p219 (1989)

Matthey Catalogue Sales, Orchard Rd., Royston, Hertfordshire SG8 5H8

Degussa Ltd., Paul Ungerer House, Earl Rd., Stanley Green, Handforth, Wilmslow, Cheshire SK9 3RL

Specac Ltd., Cambridge Electronic Industries plc, River House, Lagoon Rd., St. Mary Cray, Orpington BR5 3QX

Agar Scientific Ltd., 66a Cambridge Rd., Stansted, Essex CM24 8DA

H.C.Montgomery, Jour. Appl. Phys. **42**, pp2971-2975 (1971)

3 References for Chapter III

P.C.Martin, Physical Review **161**, pp143-155 (1967)

P.Burlet, A.Dinia, S.Quezel, W.A.C.Erkelens, J.Rossat-Mignod, R.Horyn, O.Peña, C.Geantet, M.Sergent, and J.L.Genicon, Physica **148B**, pp99-105 (1987)

O.Schärpf, H.Capellmann, T.Brückel, A.Comberg, and H.Passing, Z. Phys. B **78**, pp345-359 (1990)

T.Brückel, H.Capellmann, W.Just, O.Schärpf, S.Kemmler-Sack, R.Kiemel, and W.Schaefer, Europhys. Lett. **4**, pp1189-1194 (1987)

J.J.M.Franse, A.Menovsky, A.de Visser, C.D.Bredl, U.Gottwick, W.Lieke, H.M.Mayer, U.Rauchschwalbe, G.Sparn, and F.Steglich, Z. Phys B **59**, pp15-19 (1985)

R.Joynt and T.M.Rice, Phys. Rev. B **38**, pp2345-2353 (1988)

J.M.Tranquada and G.Shirane, Physica C **162-164**, pp849-852 (1989)

R.J. Birgenau and G. Shirane, Chapter 4 in "Physical Properties of High T_c Superconductors v1", Ed. D.M.Ginsberg, World Scientific (1989)

J.Schelten, H.Ullmaier, and W.Schmatz, Phys. Stat. Sol. B **48**, pp619-628 (1971)

D.K.Christen, H.R.Kerchner, S.T.Sekula, and P.Thorel, Phys. Rev B **21**, pp102-117

E.M.Forgan, D.McK.Paul, H.A.Mook, P.A.Timmins, H.Keller, S.Sutton and J.S.Abell , Nature **343**, pp735-737 (1990)

A.Mansour, R.O.Hilleke, G.P.Felcher, R.B.Laibowitz, P.Chaudhari and S.S.P.Parkin , Physica B **156-157**, pp867-890 (1989)

P.B.Allen, Physical Review **B6**, pp2577-2579 (1972)

G.Shirane, J.D.Axe, and S.M.Shapiro, Solid State Comms. **13**, pp1893-1895 (1973)

R.Youngblood, Y.Noda, and G.Shirane, Solid State Comms. **27**, pp1433-1435 (1978)

J.D.Axe and G.Shirane, Phys. Rev. B **8**, pp1965-1977 (1973)

W.Reichardt, D.Ewert, E.Gering, F.Gompf, L.Pintschovius, B.Renker, G.Collin, A.J.Dianoux, and H.Mutka, Physica B **156 + 157**, pp897-901 (1989)

K.Sasaki and Y.Obata, Supp. Prog. Theor. Phys. **69**, pp406-419 (1980)

A.K.Rajagopal, S.D.Mahanti, and W.Jin, Solid State Comms. **69**, pp847-849 (1989)

A.K.Rajagopal, W.Jin, and S.D.Mahanti, Physica C **162-164**, pp247-248 (1989)

W.Jin, S.D.Mahanti, and A.K.Rajagopal, Solid State Comms. **71**, pp967-971 (1989)

A.Junod, A.Bezinge, T.Graf, J.L.Jorda, J.Muller, L.Antognazza, D.Cattani, J.Cors, M.Decroux, Ø .Fischer, M.Banovski, P.Genoud, L.Hoffmann, A.A.Manuel, M.Peter, E.Walker, M.François, and K.Yvon, Europhys. Lett. 4, pp247-252 (1987)

N.R.Bernhoeft, Private Communication

4 References for Chapter IV

C.G.Windsor, J.Appl. Cryst. **21**, pp582-588 (1988)

N.R.Bernhoeft, Ph.D. Thesis, University of Cambridge (1982)

S.W.Lovesey, p120 in "Theory of Neutron Scattering from Condensed Matter v1", Clarendon Press, Oxford, (1984) ISBN 0-19-852015-8

J.W.Lynn, W-H.Li, Q.Li, H.C.Ku, H.D.Yang, and R.N.Shelton, Phys Rev B, **36** pp2374-2377

L.N.Bulaevskii and A.I.Buzdin, Physica C **153-155**, pp1651-1652 (1988)

L.A.Axelrod, G.P.Gordeev, I.M.Lazebnik, V.T.Lebedev, S.V.Maleyev, A.I.Okorokov, V.V.Runov, V.N.Slyusar, B.P.Toperverg, A.D.Tretyakov, and R.Z.Yagud, Materials Science Forum **27-28**, pp273-278 (1988)

R.Kahn, A.Brulet, G.Collin, and B.Farnoux, Physica C **159**, pp323-328 (1989)

G.L.Squires, "Introduction to the Theory of Thermal Neutron Scattering ", Cambridge Univ. Press, Cambridge, (1978) ISBN 0-521-21884-5

W.I.F.David, P.P.Edwards, M.R.Harrison, R.Jones, and C.C.Wilson, Nature **331**, pp245-247 (1988)

5 References for Chapter V

T.Brückel, H.Capellmann, W.Just, O.Schärpf, S.Kemmler-Sack, R.Kiemel, and W.Schaefer, Europhys. Lett. **4**, pp1189-1194 (1987)

6 References for Chapter VI

C.Kittel, Introduction to Solid State Physics (5th edition), John Wiley and sons (1976) ISBN 0-471-49024-5

J.C.Phillips, Physics of High T_c Superconductors, Academic Press, (1989) ISBN 0-12-553990-8

G.Kostorz and S.W.Lovesey, Chapter 1 in Treatise on materials science and technology v15, Neutron scattering, G.Kostorz (Ed.), Academic Press (1979) ISBN 0-12-341815-1

S.W.Lovesey, Theory of Neutron Scattering from Condensed Matter, OUP (1984) ISBN 0-19-852028-X

R.Youngblood, Y.Noda, and G.Shirane, Solid State Comms. **27**, pp1433-1435 (1978)

G.Shirane, J.D.Axe, and S.M.Shapiro, Solid State Comms. **13**, pp1893-1895 (1973)

Y.Nakagawa and A.D.B.Woods, Phys. Rev. Lett. **11**, pp271-274 (1963)

Appendix A

Neutron Cross-Section Derivation

A.1 Introduction

The purpose of this appendix is to give as straightforward as possible a presentation of the steps leading to the cross-section formula for neutron scattering quoted in chapter III. This subject is fraught with subtleties and these will be studiously avoided if at all possible: c.g.s units are used to enable comparison with the references.

A.2 Neutron cross-section from conductivity fluctuations

The quantity we wish to calculate is the magnetic neutron scattering cross-section for an unpolarized beam given by (e.g. Sasaki) :-

$$\frac{d^2\sigma}{d\Omega d\omega} = \frac{\gamma^2 e^2 k'}{48\pi^3 \hbar^2 c^2 n k} \langle\ |\mathbf{B}(\mathbf{q},\omega)|^2 \rangle$$

where γ is the neutron gyromagnetic ratio , n the number of atoms per unit volume, and k and k' are the moduli of the incident and outgoing neutron wavevectors.

$\langle\ |\mathbf{B}(\mathbf{q},\omega)|^2 \rangle$ is the Fourier transform of the unsymmetrised magnetic field autocorrelation function, averaged over a long time and a large volume. (see e.g. Lovesey)

A.2.1 The Martin results

Here the paper of Martin becomes useful (Martin), as he calculates χ_{BB} for an isotropic system in terms of the transverse conductivity [1] .

The imaginary part of χ_{BB} can be readily related to the magnetic field - magnetic field (BB) correlation function seen above to be essentially the neutron

[1] The transverse conductivity is the conductivity that enters into discussions of propagating EM waves in a medium, giving damping and a phase shift.

cross-section with a few universal constants as prefactors.

A slight additional problem is that the neutron probes the BB correlation function, but it is sometimes easier to calculate the current-current (JJ) response functions when using linear response theory on the electron gas. Now the JJ correlation function and BB correlation functions are obviously intimately connected by Maxwell's equations, but care is needed here.

In addition, for these definitions it is best to work with an extension of the formalism to complex frequency, ($z = \omega + i\epsilon$), and to take the relevant limit of real frequency after the calculation. This is essentially to enable the treatment of the delta-functions that arise here without having to consider them explicitly (e.g. the delta functions considered in the discussion in chapter 1). Also, we write all functions in the form $X = X' + iX''$. Martin gives:-

$$\chi_{BB} = c^2q^2[c^2q^2 - z^2 - iz\sigma^T(q,z)]^{-1} \quad \text{(eq. 3.8 in Martin)}$$

$$\text{Thus } \chi''_{BB} = (c^2q^2)z\sigma^{T\prime}(q,z) \times K$$

$$\text{Where } K = [(c^2q^2 - z^2 + z\sigma^{T\prime\prime}(q,z))^2 + (z\sigma^{T\prime}(q,z))^2]^{-1}$$

and rearranging from (Martin) in terms of χ_{JJ},

$$\chi_{BB} = \frac{c^2q^2}{(c^2q^2 - z^2)^2}\chi_{JJ} + \frac{c^2q^2(c^2q^2 - z^2 - {\omega_p}^2)}{(c^2q^2 - z^2)^2}$$

$$\text{Also } \langle\ |\mathbf{B}(\mathbf{q},\omega)|^2\rangle = 2\hbar\omega n(\omega)\chi''_{BB}/\omega \qquad \text{(White)}$$

Where $n(\omega)$ is for neutron energy gain and must be replaced with $(1 + n(\omega))$ for neutron energy loss.

A certain amount of care is needed here as he is working in rationalised Gaussian units - these have no 4 π 's which we will have to substitute in at the end of the calculation, i.e. $\epsilon_0 = 1$ not $1/4\pi$.

Martin discusses how magnetism, but not magnetic order, can be included within this formalism (i.e. para- or diamagnetism only). This is achieved by the use of a delta function at $\omega = 0$ in σ^T (i.e. an anomalous part to σ^T). Superconductivity is treated in the same way in his paper.

So if we follow this approach and put in an anomalous term, and write:-

$$\sigma^T(q,z) = iA(q)/z + \sigma^T_{reg}(q,z) \qquad \text{(A(q) is real)}$$

$$\text{where as } \epsilon \to 0 \text{ , } i/z \text{ is } \pi\delta(\omega) + i/\omega$$

$$\text{and } \; A(q) = c^2q^2[1/\mu(q) - 1]$$

then following through as above,

$$\chi''_{BB} = (c^2q^2)\omega\sigma^{T\prime}_{reg}(q,\omega) \times K$$

$$\text{Where now } K = [(c^2q^2 - \omega^2 + A + \omega\sigma^{T\prime\prime}_{reg}(q,\omega))^2 + (\omega\sigma^{T\prime}_{reg}(q,\omega))^2]^{-1}$$

$$\text{or, } \; K \times (c^2q^2)^2 = [(1/\mu(q) - \omega^2/c^2q^2 + \omega\sigma^{T\prime\prime}_{reg}(q,\omega)/c^2q^2)^2 + (\omega\sigma^{T\prime}_{reg}(q,\omega)/c^2q^2)^2]^{-1}$$

Now there are no delta functions lurking unseen in σ as they are all expressed in μ (or equivalently A), which represents the flow of persistent currents whether in diamagnets, paramagnets or superconductors.

This use of anomalous parts for the effects of magnetism is undoubtedly convenient and indeed necessary to describe the superconductor adequately. However it is also rather different to the usual way of treating such magnetic effects using the generalised (q,ω) dependent complex spin susceptibility. The conventional spin susceptibility treatment could be added to this description, but we would then have explicitly split the problem into that of spin and charged current (orbital) parts. It would be simpler if everything could be treated in terms of σ^T alone. This may be difficult because a spin and an "equivalent" current loop are not the same at all distance scales.

Now in an isotropic system, there are three components of σ that contribute, in $x, y,$ and z directions. (The Sasaki definition above hasn't taken this into account).

$$\langle\ |\mathbf{B}(\mathbf{q},\omega)|^2\rangle = 3 \times 2\hbar\omega n(\omega)\left[K^\dagger \frac{\sigma'_{reg}(\mathbf{q},\omega)}{c^2q^2}\right]$$

Which upon converting to true c.g.s leads us to the desired result :-

$$\langle\ |\mathbf{B}(\mathbf{q},\omega)|^2\rangle = 6(4\pi)^2\hbar\omega n(\omega)\left[K^\dagger\frac{\sigma'_{reg}(\mathbf{q},\omega)}{c^2q^2}\right]$$

Where $K^\dagger = \mu^2[(1-\mu\omega^2/c^2q^2 + 4\pi\mu\omega\sigma''_{reg}/c^2q^2)^2 + (4\pi\mu\omega\sigma'_{reg}/c^2q^2)^2]^{-1}$

This orbital term resulting from the conductivity must indeed be affected by the superconducting transition. Notice the electromagnetic screening factor K which removes the divergences at (0,0). Notice also that it is not quite the same as the screening function found by Sasaki, in that here we have the ω dependence of the conductivity included. Also, the superconducting screening is naturally included in this formalism in $\mu(q)$.

A.2.2 Sum rules

Martin also gives the relevant sum rules for the conductivity, important because they enable at least an upper limit to the available cross-section to be evaluated within the approximations used. Although the transverse conductivity sum rule holds in general, it is only true for the regular part of σ^T if $\mu = 1$ i.e. if there are no magnetic effects. Thus the integral of the regular part has a diminished weight if $\mu \neq 1$, the rest of which is in the delta function. The sum rule can thus be written, again in true c.g.s :-

$$\int_{-\infty}^{+\infty} 4\sigma'^T(q,\omega)d\omega = {\omega_p}^2$$

$$\text{and } \int_{-\infty}^{+\infty} 4\sigma'^{reg\ T}(q,\omega)d\omega = {\omega_p}^2 - c^2q^2[\mu^{-1}(q)-1]$$

Now in a superconductor, we have $\mu(q) = q^2/(q^2 + \frac{1}{\lambda_L}^2)$, at least at q $\rightarrow$ 0. A reasonable first approximation to this quantity at low q must be to use this form, at least for q< ξ^{-1}.

A.3 References for this Appendix

K.Sasaki and Y.Obata, Supp. Prog. Theor. Phys. **69**, pp406-419 (1980)

S.W.Lovesey, Theory of Neutron Scattering from Condensed Matter, OUP (1984) ISBN 0-19-852028-X

P.C.Martin, Physical Review **161**, pp143-155 (1967)

R.M.White, Quantum Theory of Magnetism, McGraw-Hill, New York, (1970)

Appendix B

IN5 Experimental Data

B.1 Introduction

The purpose of this appendix is to present the full results of the IN5 experiment detailed in chapter V. Each set of data is labelled with the temperature and the range of angles summed together, expressed as the elastic wavevector transfer in Å^{-1}. The data is presented for the full energy range measured with this experiment. This data may be of use in this format if at a later date there are any concrete predictions of effects to which neutrons are sensitive in this range of wavevector and energy.

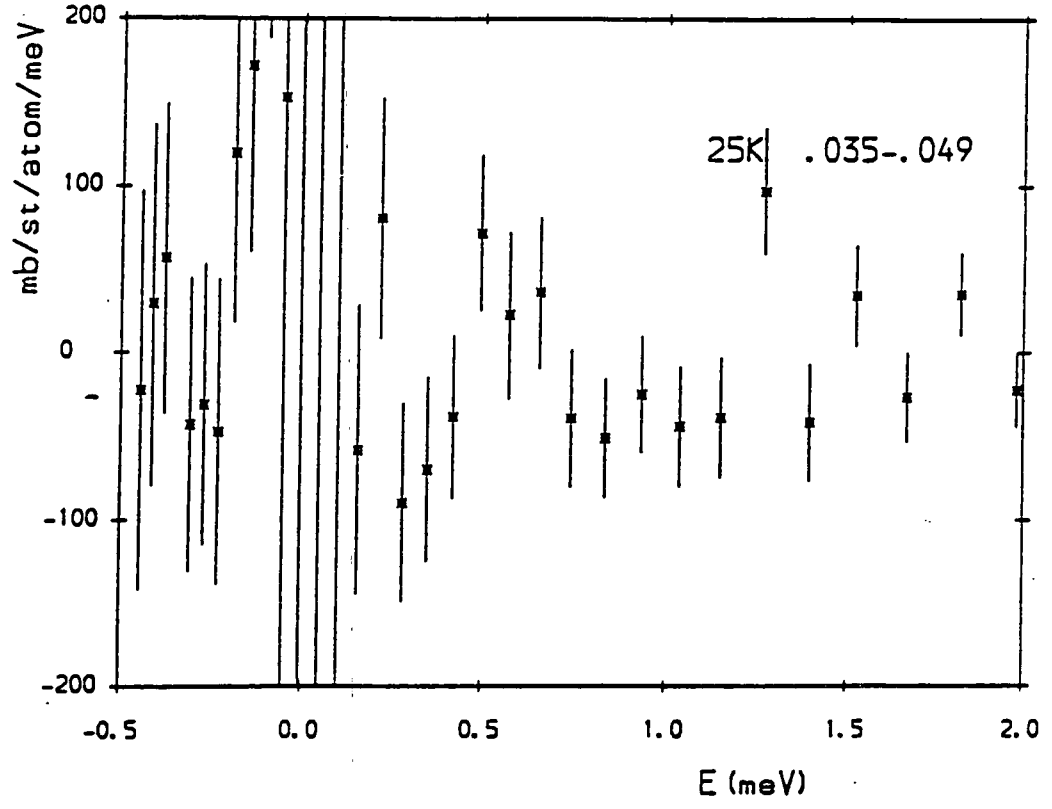
25K .035-.049
mb/st/atom/meV
E (meV)
200
100
0
-100
-200
-0.5
0.0
0.5
1.0
1.5
2.0

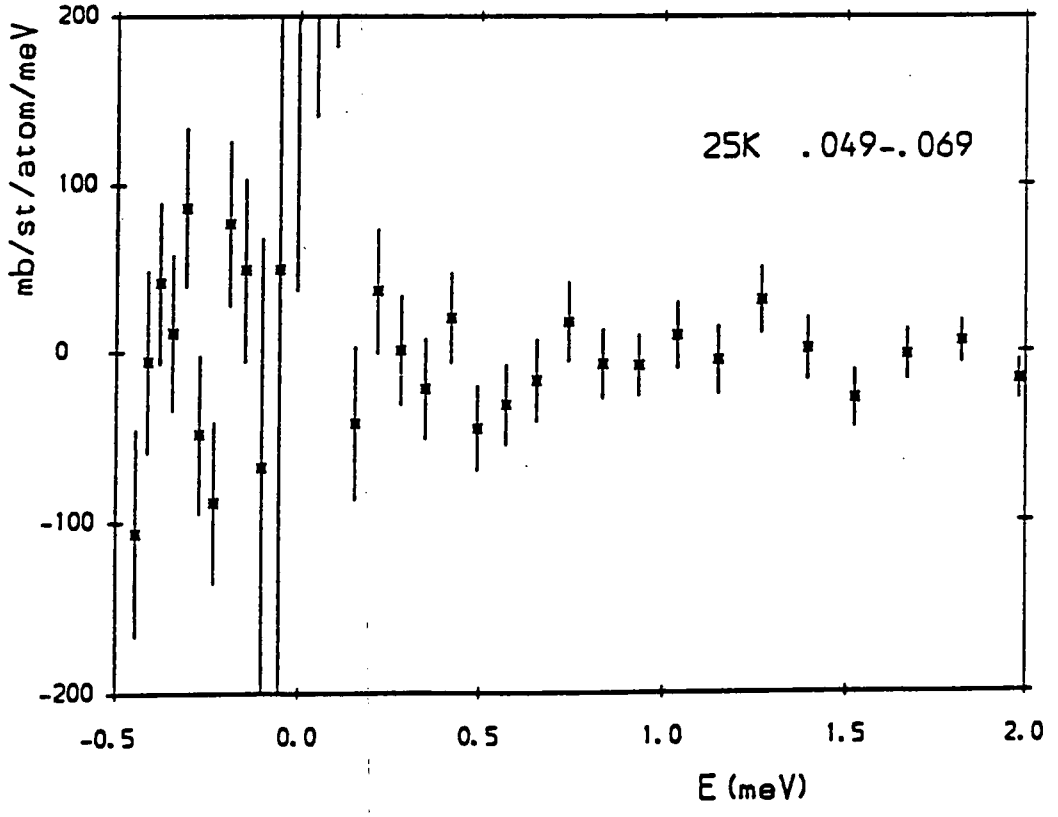
25K .049-.069
mb/st/atom/meV
E (meV)
200
100
0
-100
-200
-0.5
0.0
0.5
1.0
1.5
2.0

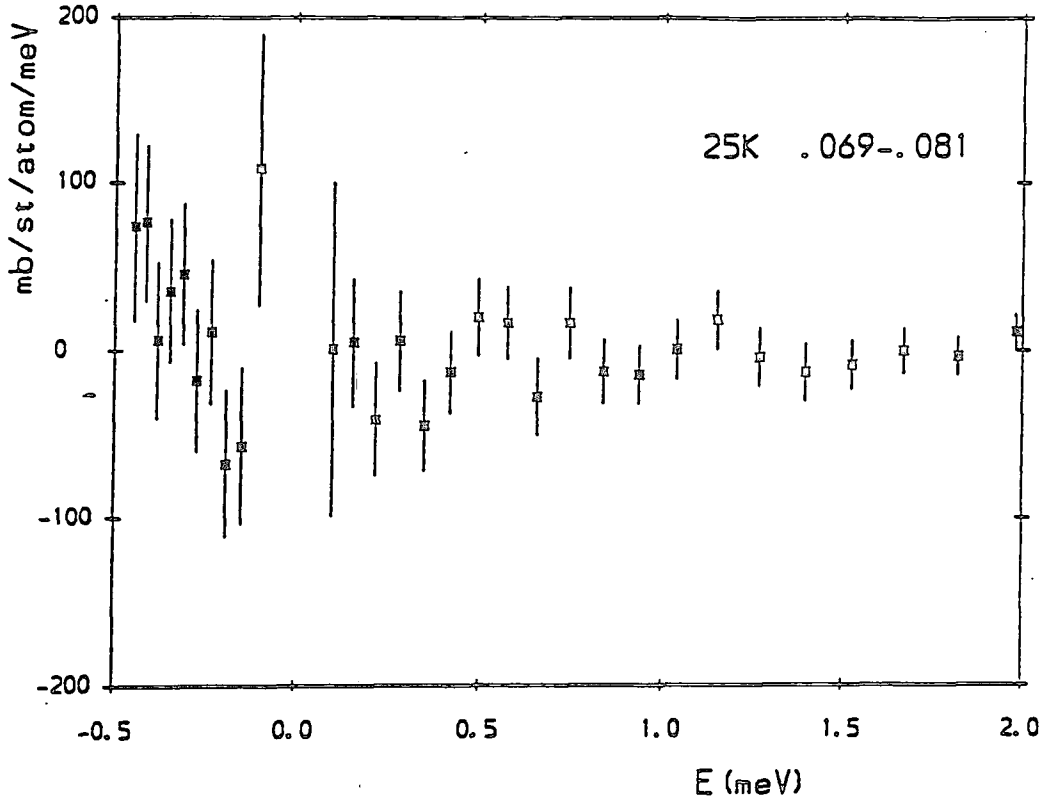
200
100
0
-100
-200
mb/st/atom/meV
25K .069-.081
-0.5
0.0
0.5
1.0
1.5
2.0
E (meV)

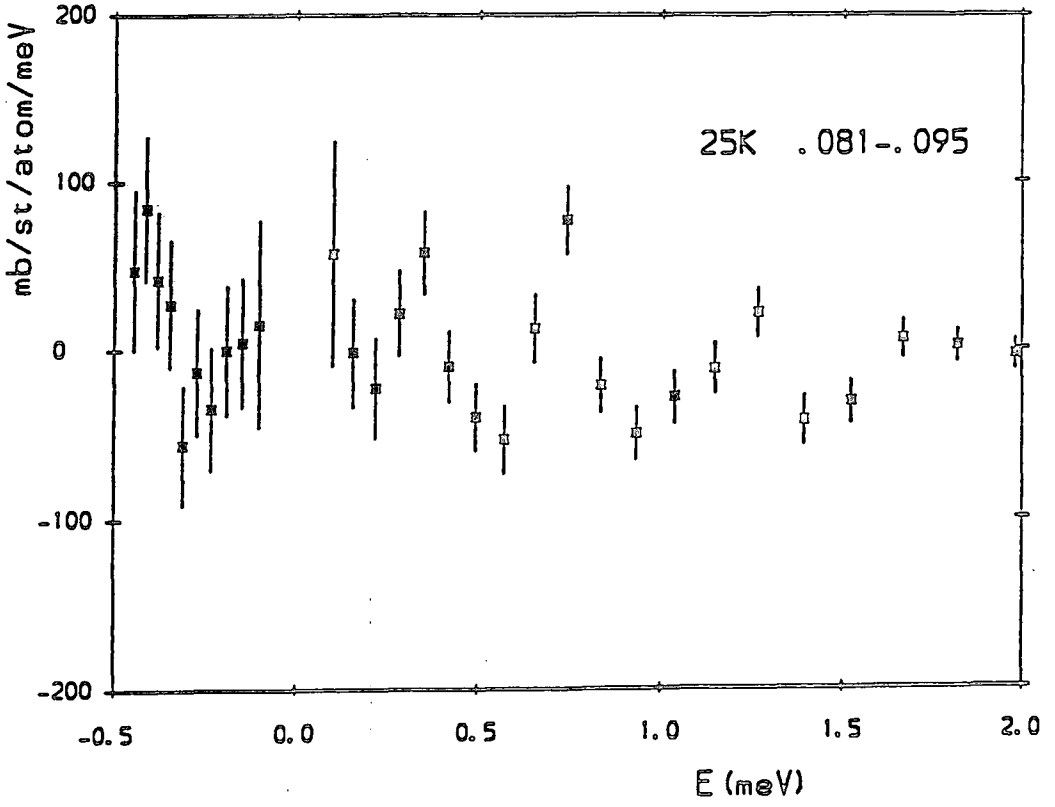
200
100
0
-100
-200
mb/st/atom/meV
25K .081-.095
-0.5
0.0
0.5
1.0
1.5
2.0
E (meV)

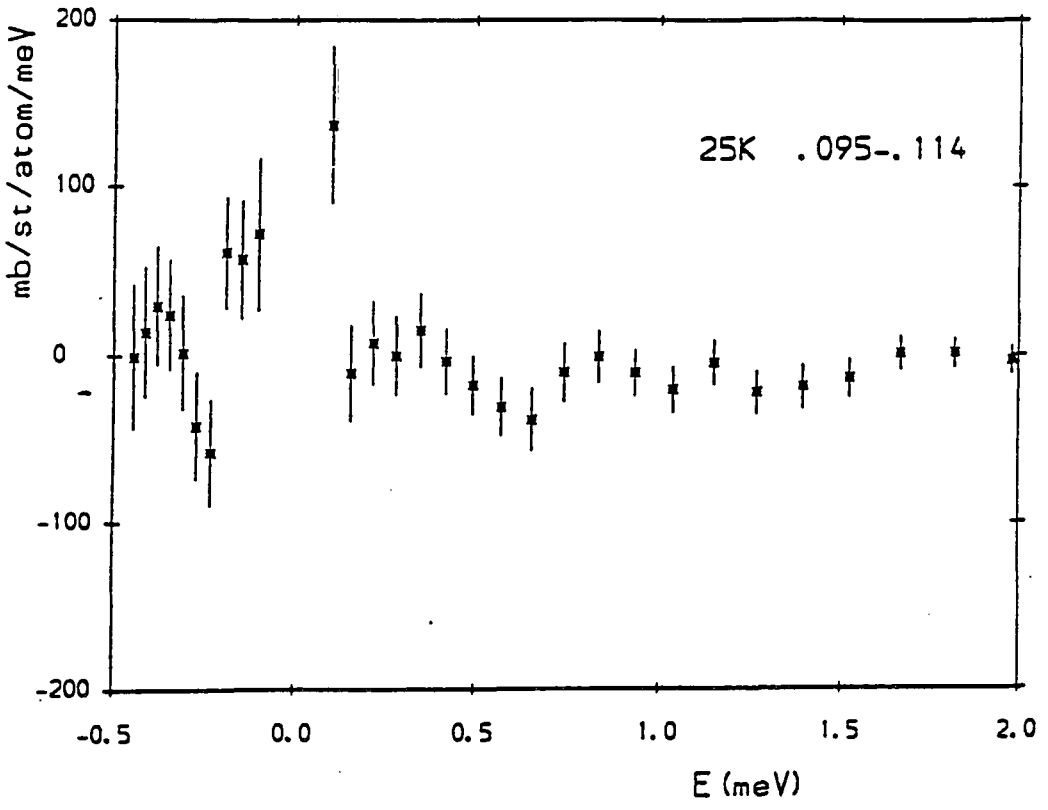
25K .095-.114
mb/st/atom/meV
200
100
0
-100
-200
-0.5
0.0
0.5
1.0
1.5
2.0
E (meV)

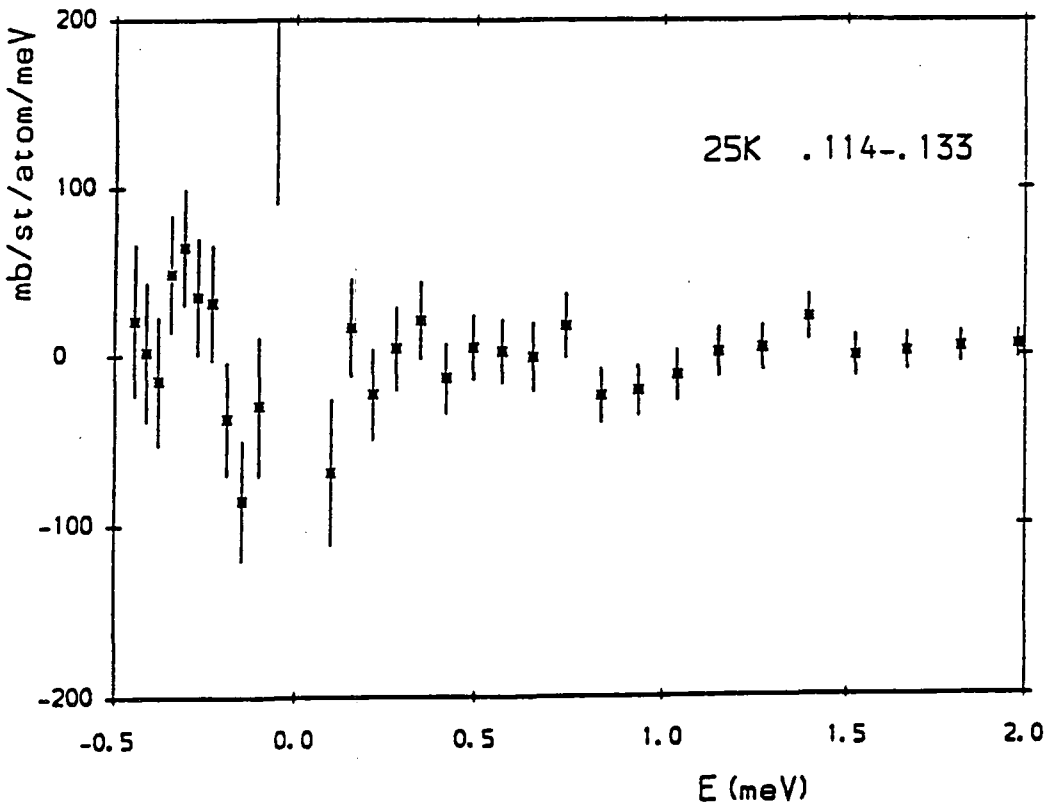
25K .114-.133
mb/st/atom/meV
200
100
0
-100
-200
-0.5
0.0
0.5
1.0
1.5
2.0
E (meV)

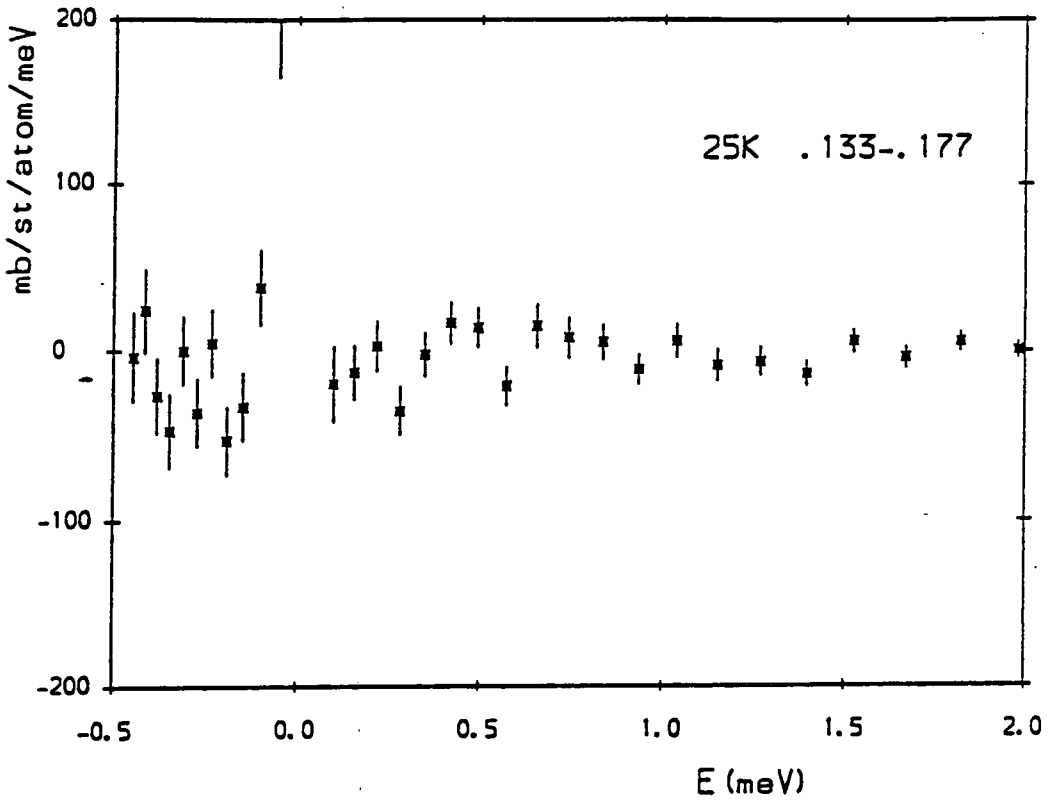
200
100
0
-100
-200
mb/st/atom/meV
25K .133-.177
-0.5
0.0
0.5
1.0
1.5
2.0
E (meV)

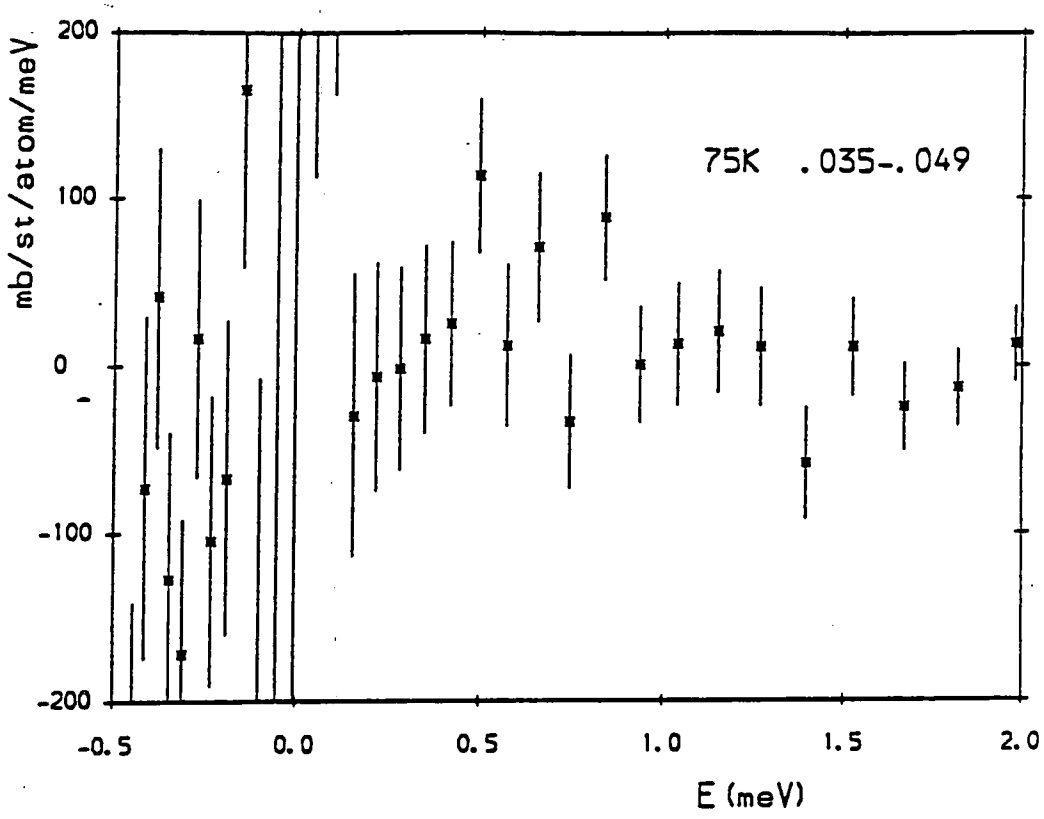
75K .035-.049
mb/st/atom/meV
200
100
0
-100
-200
-0.5
0.0
0.5
1.0
1.5
2.0
E (meV)

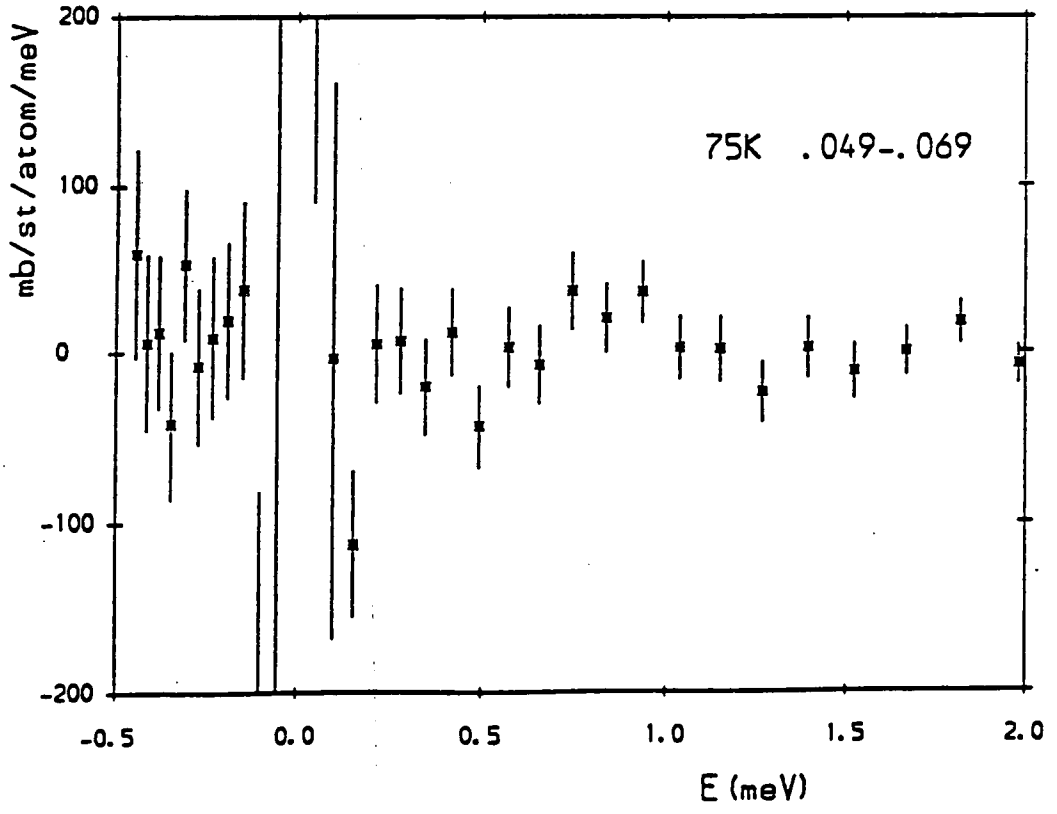
75K .049-.069
mb/st/atom/meV
200
100
0
-100
-200
-0.5
0.0
0.5
1.0
1.5
2.0
E (meV)

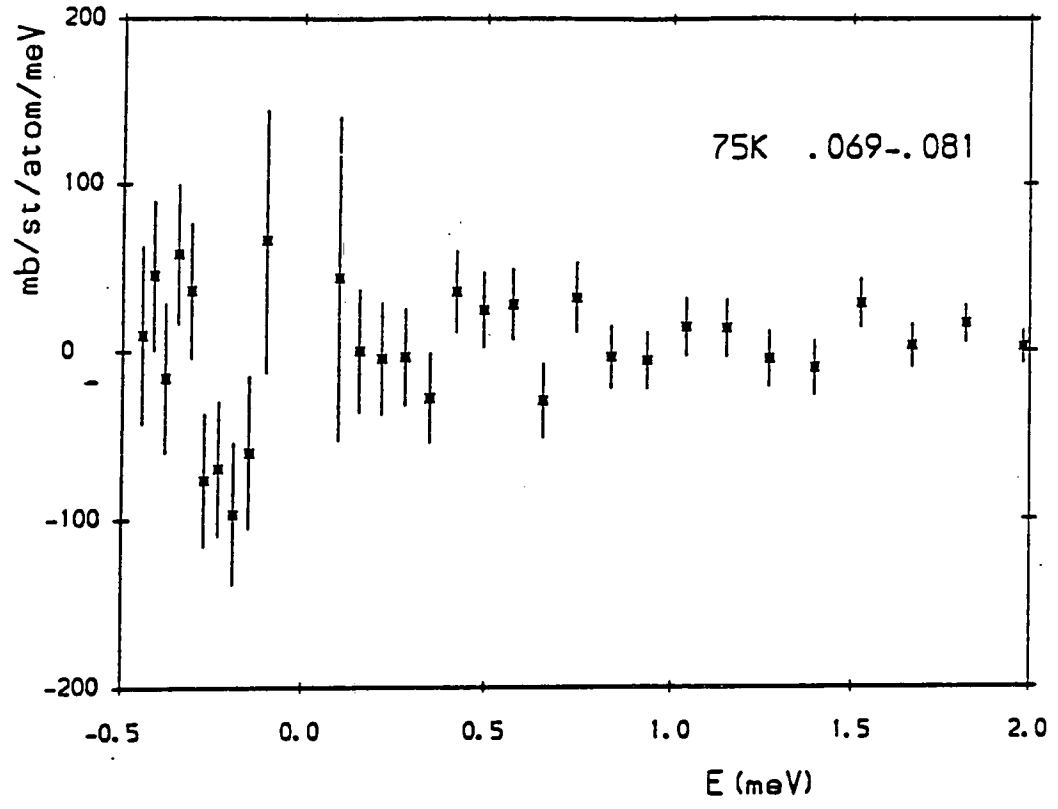
75K .069-.081
mb/st/atom/meV
200
100
0
-100
-200
-0.5
0.0
0.5
1.0
1.5
2.0
E (meV)

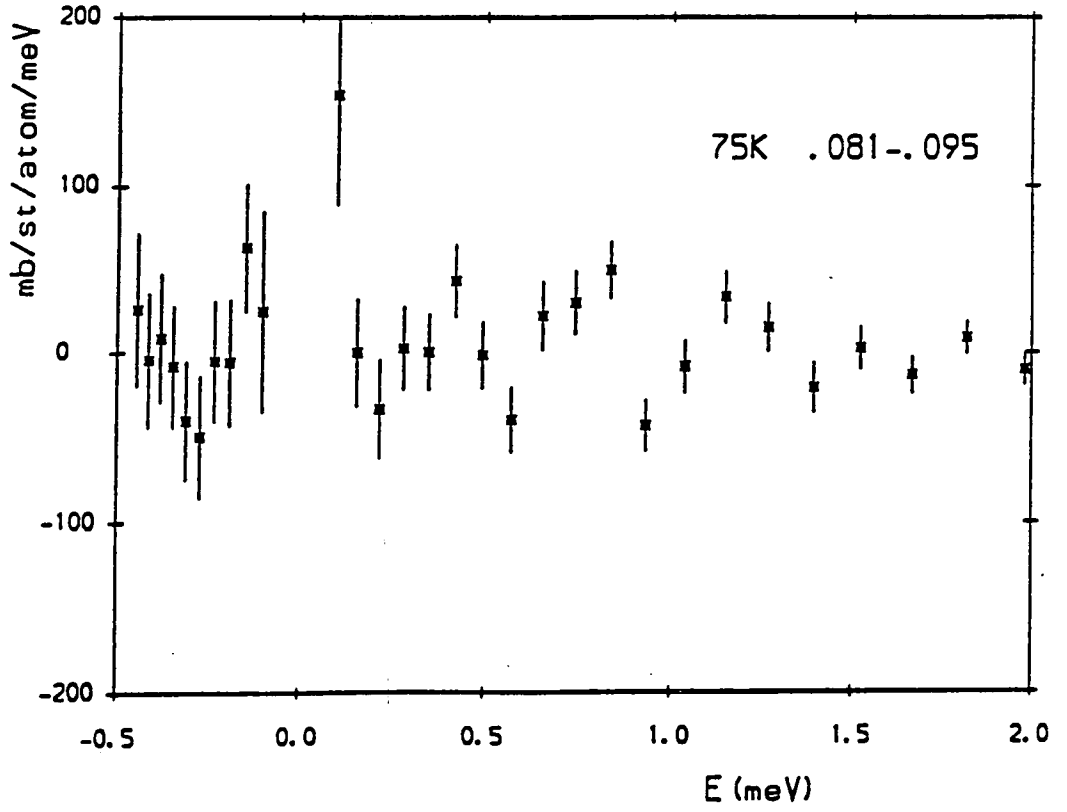
75K .081-.095
mb/st/atom/meV
200
100
0
-100
-200
-0.5
0.0
0.5
1.0
1.5
2.0
E (meV)

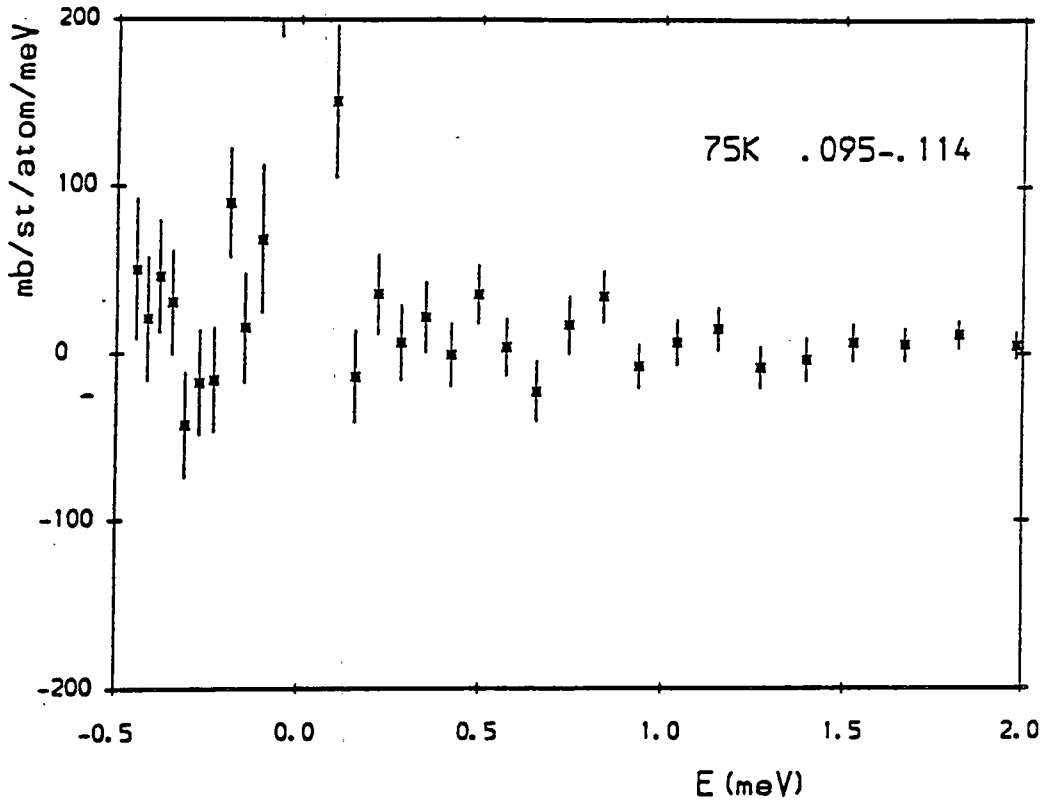
75K .095-.114
mb/st/atom/meV
200
100
0
-100
-200
-0.5
0.0
0.5
1.0
1.5
2.0
E (meV)

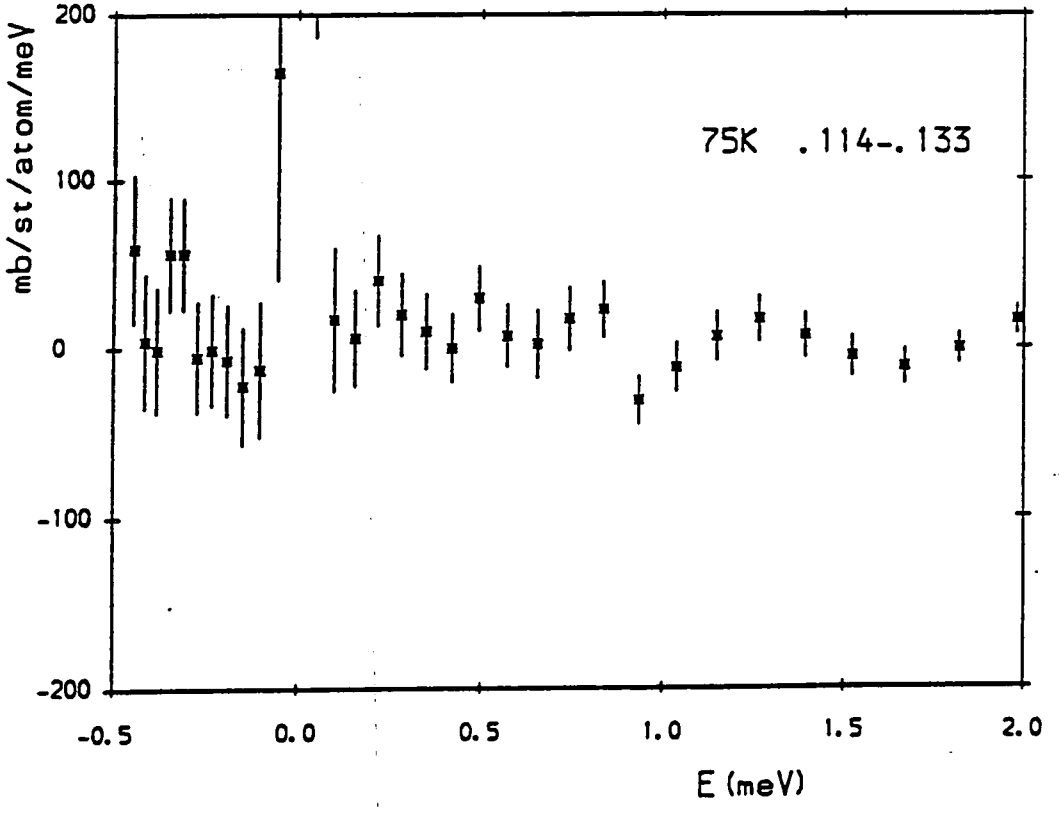
75K .114-.133
mb/st/atom/meV
200
100
0
-100
-200
-0.5
0.0
0.5
1.0
1.5
2.0
E (meV)

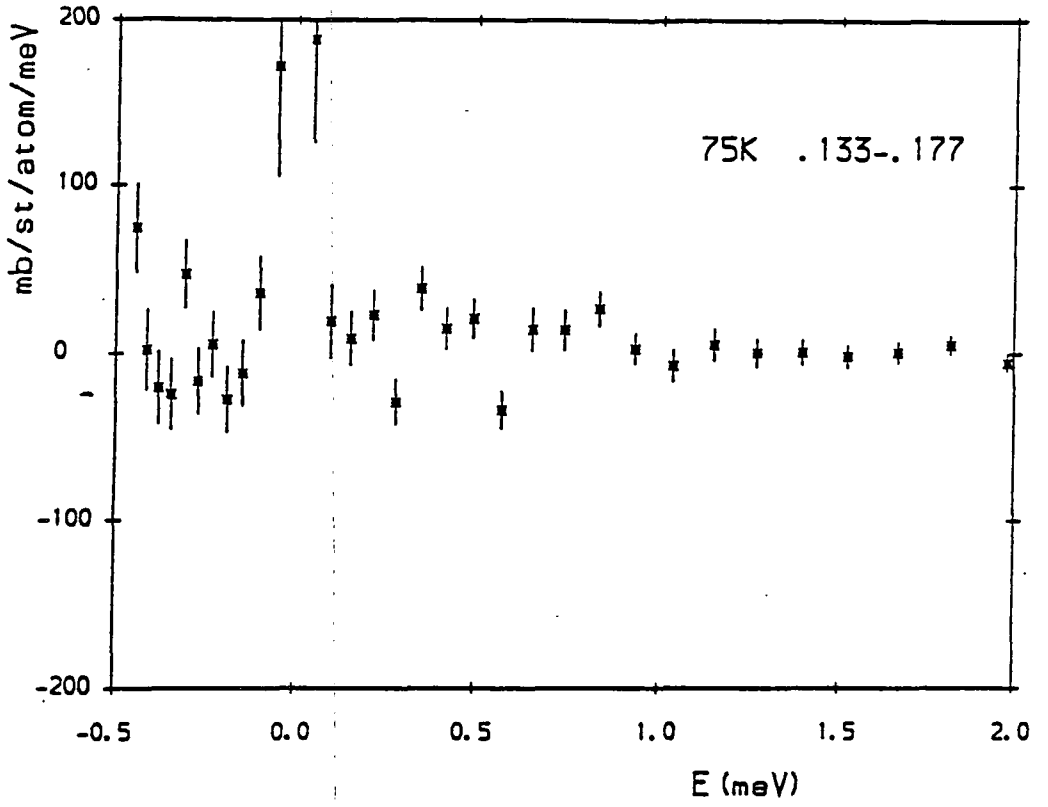
75K .133-.177
mb/st/atom/meV
200
100
0
-100
-200
-0.5
0.0
0.5
1.0
1.5
2.0
E (meV)

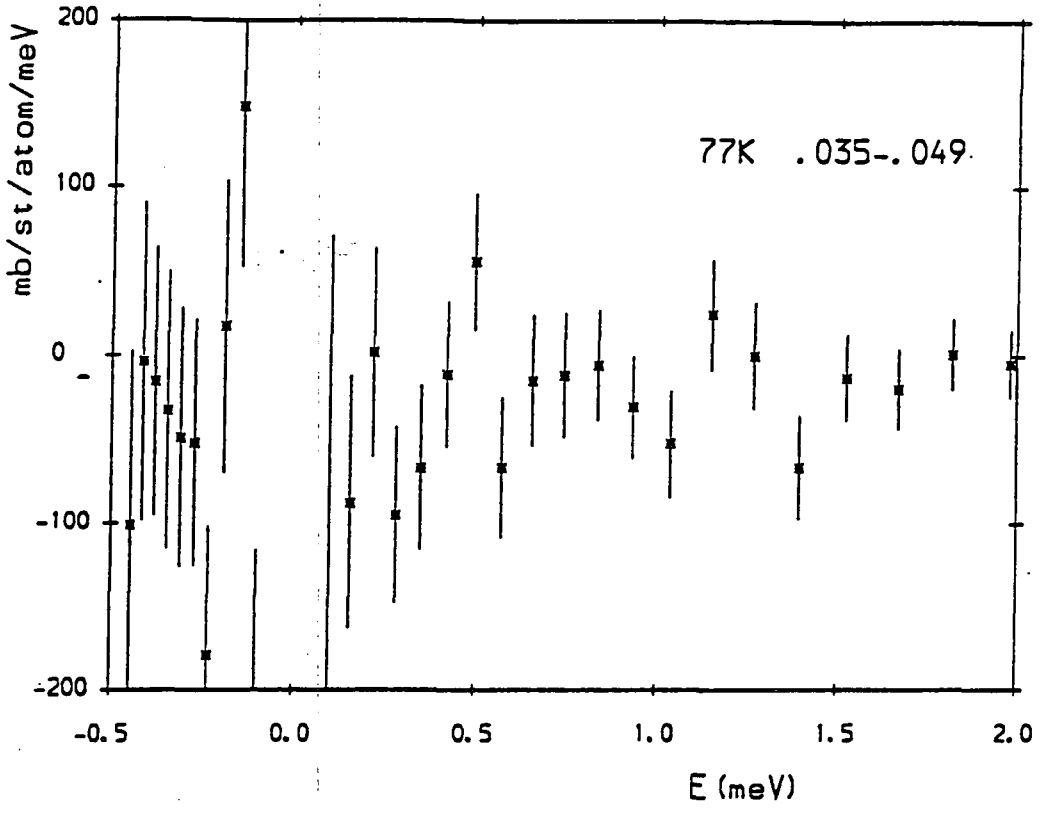
77K .035-.049
mb/st/atom/meV
200
100
0
-100
-200
-0.5
0.0
0.5
1.0
1.5
2.0
E (meV)

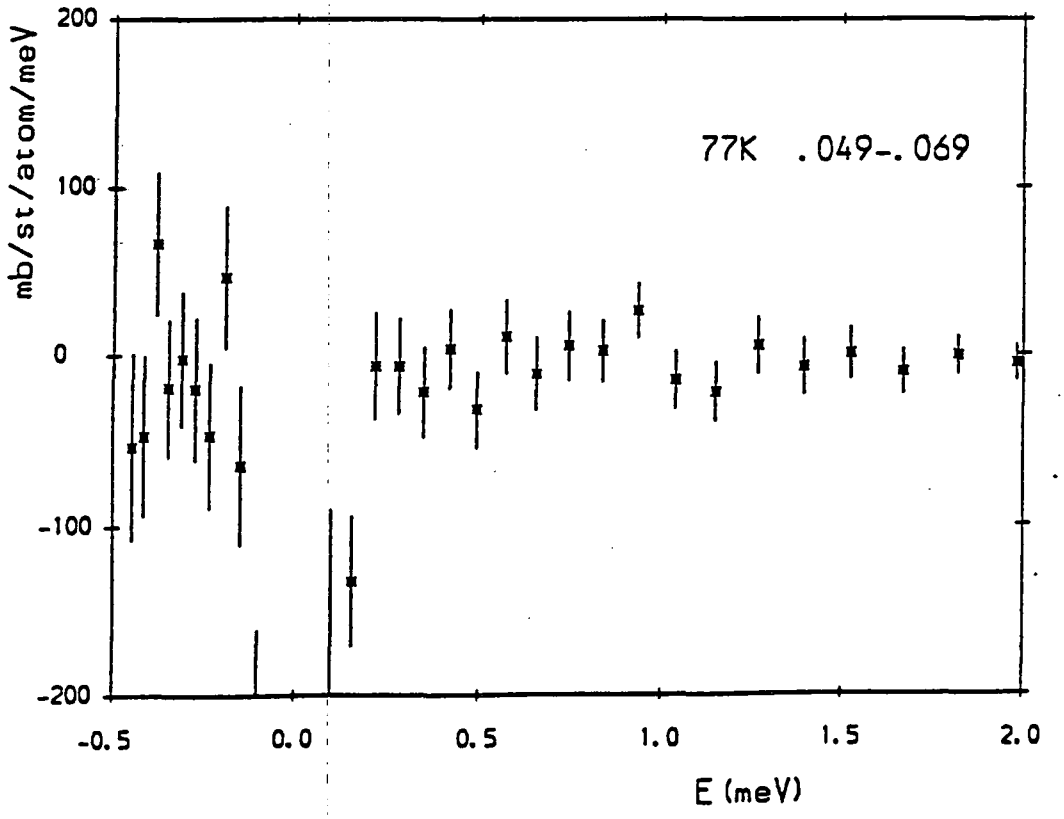
77K .049-.069
mb/st/atom/meV
200
100
0
-100
-200
-0.5
0.0
0.5
1.0
1.5
2.0
E (meV)

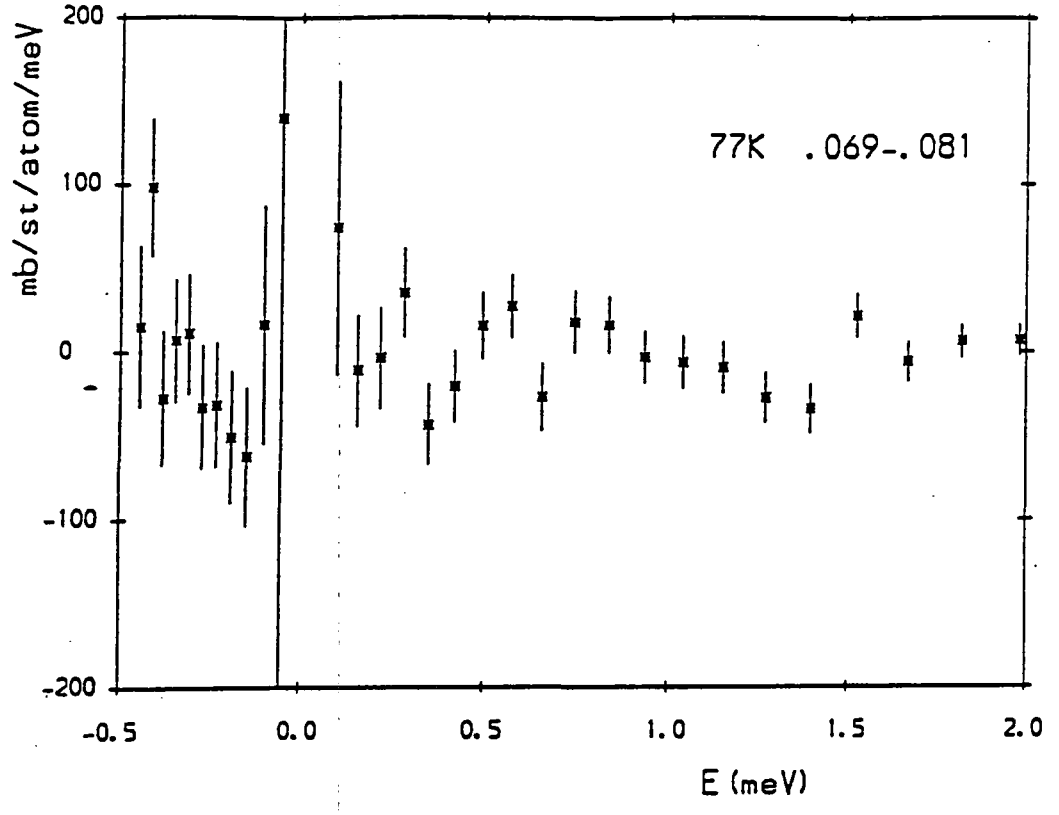
77K .069-.081
mb/st/atom/meV
200
100
0
-100
-200
-0.5
0.0
0.5
1.0
1.5
2.0
E (meV)

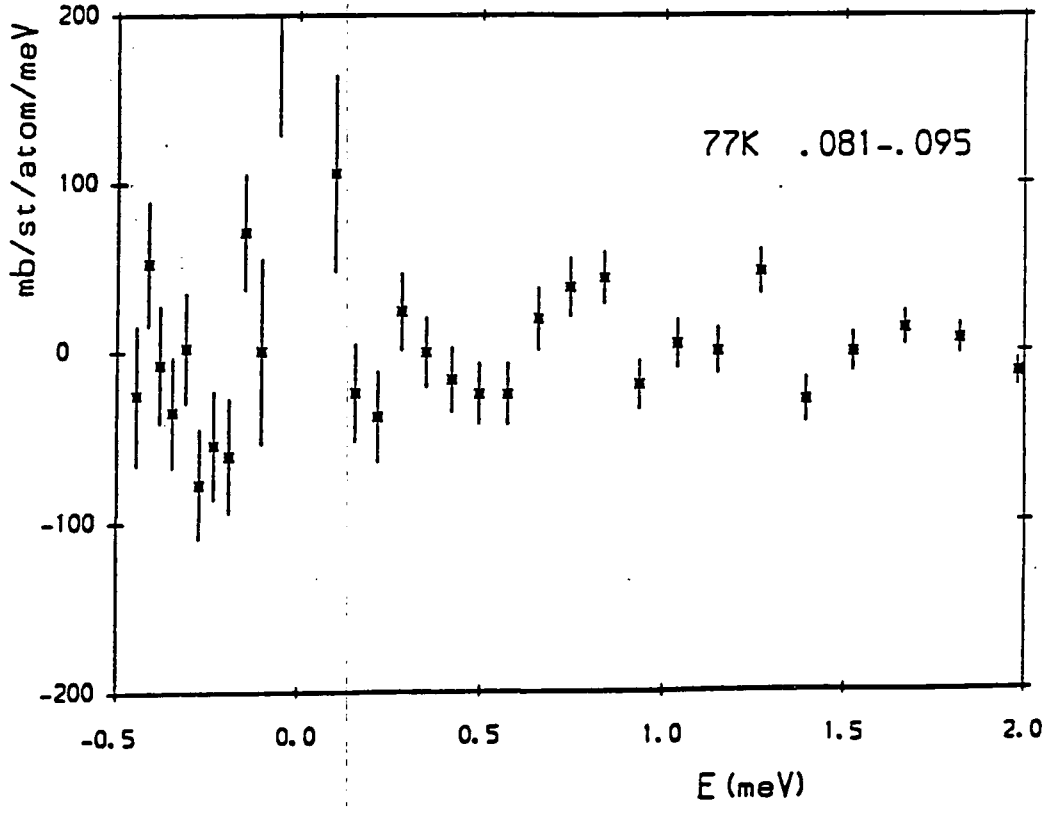
77K .081-.095
mb/st/atom/meV
200
100
0
-100
-200
-0.5
0.0
0.5
1.0
1.5
2.0
E (meV)

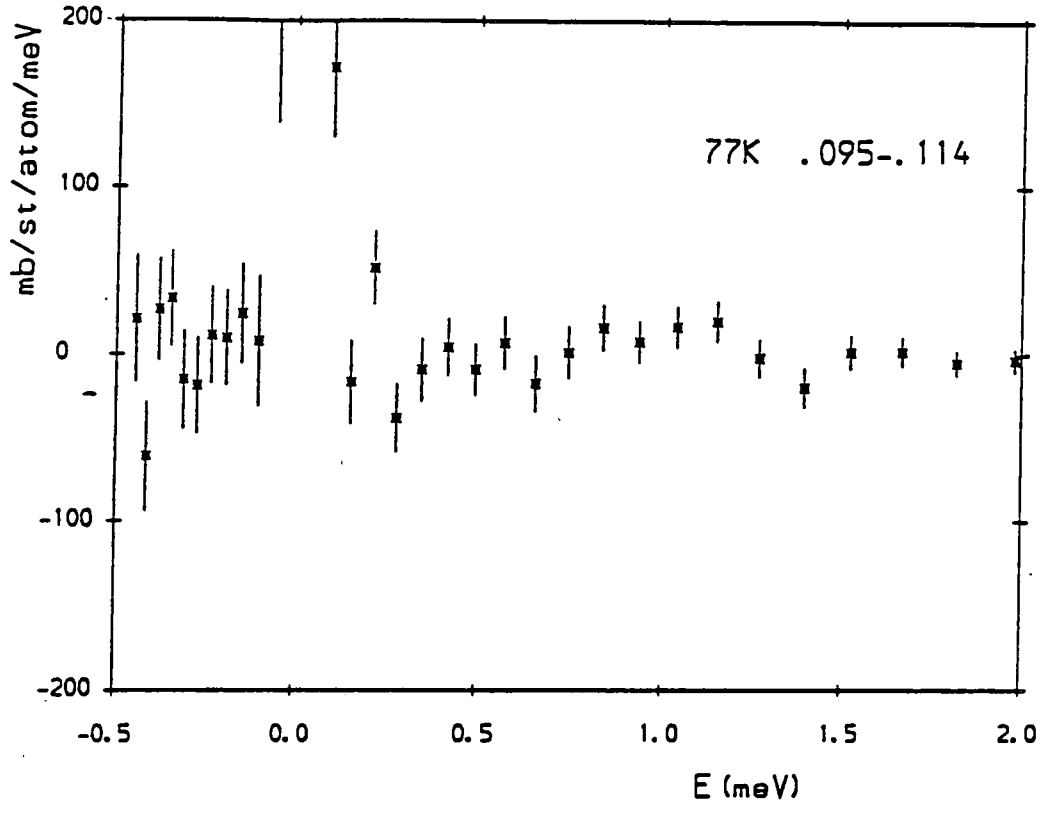
77K .095-.114
mb/st/atom/meV
200
100
0
-100
-200
-0.5
0.0
0.5
1.0
1.5
2.0
E (meV)

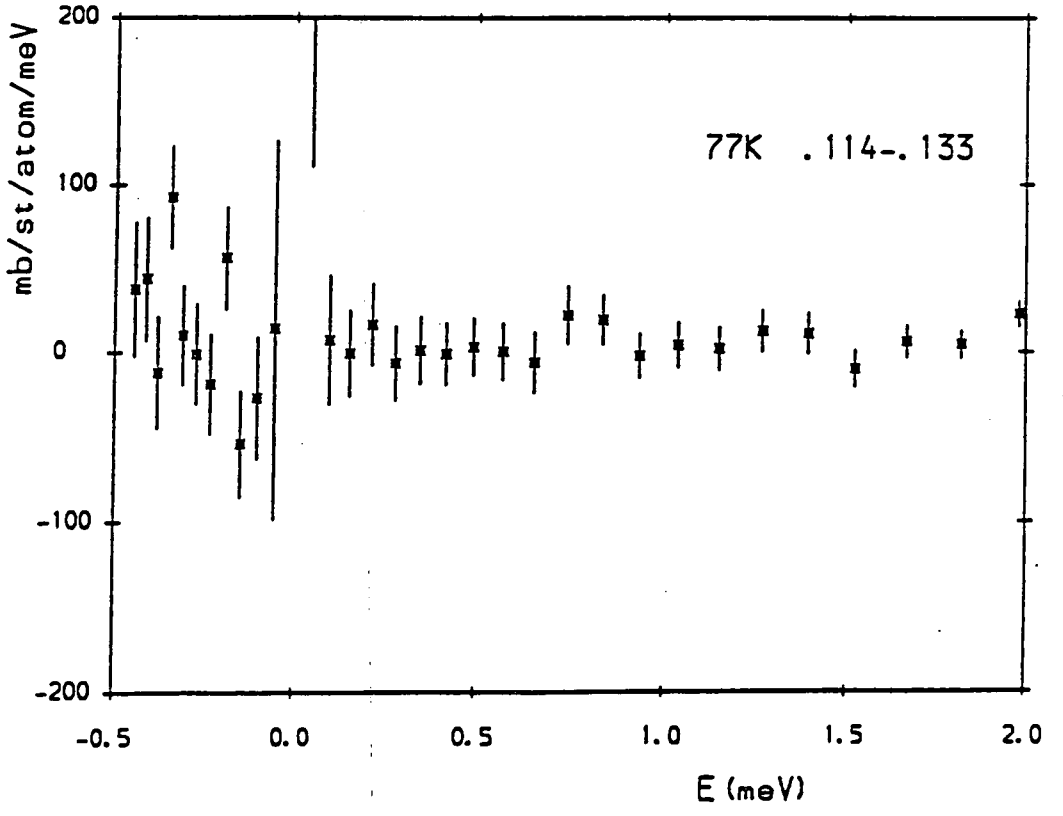
77K .114-.133
mb/st/atom/meV
200
100
0
-100
-200
-0.5
0.0
0.5
1.0
1.5
2.0
E (meV)

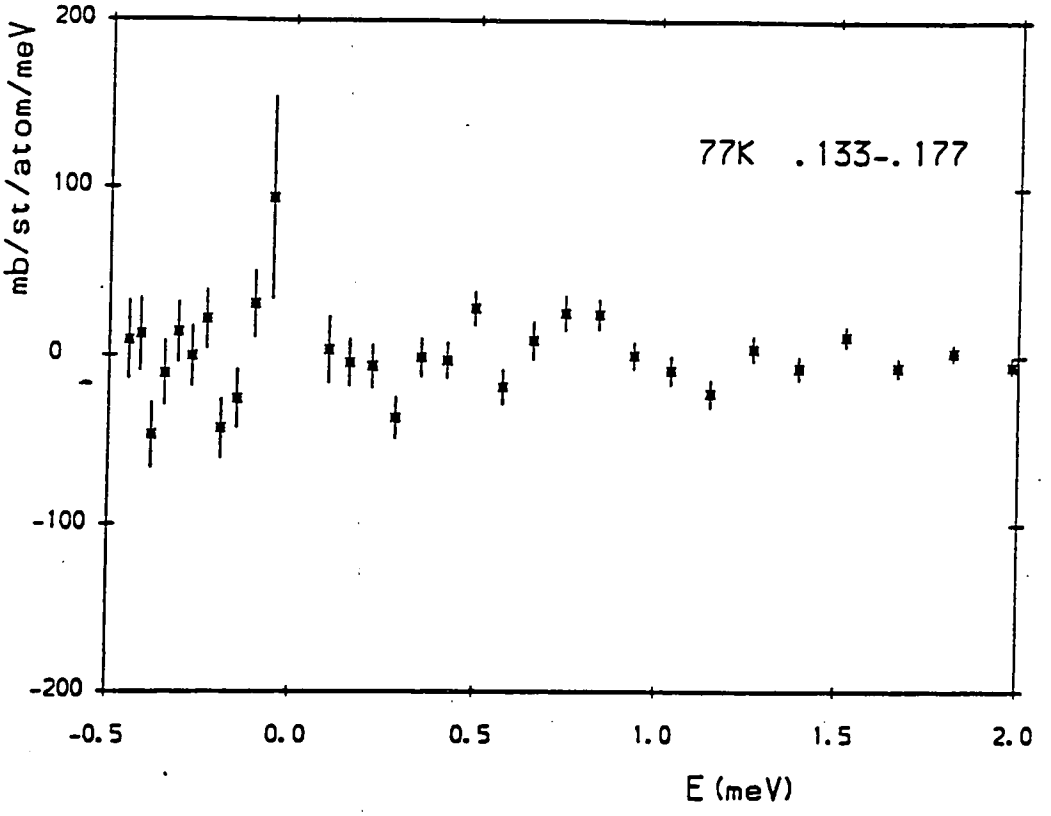
77K .133-.177
mb/st/atom/meV
200
100
0
-100
-200
-0.5
0.0
0.5
1.0
1.5
2.0
E (meV)

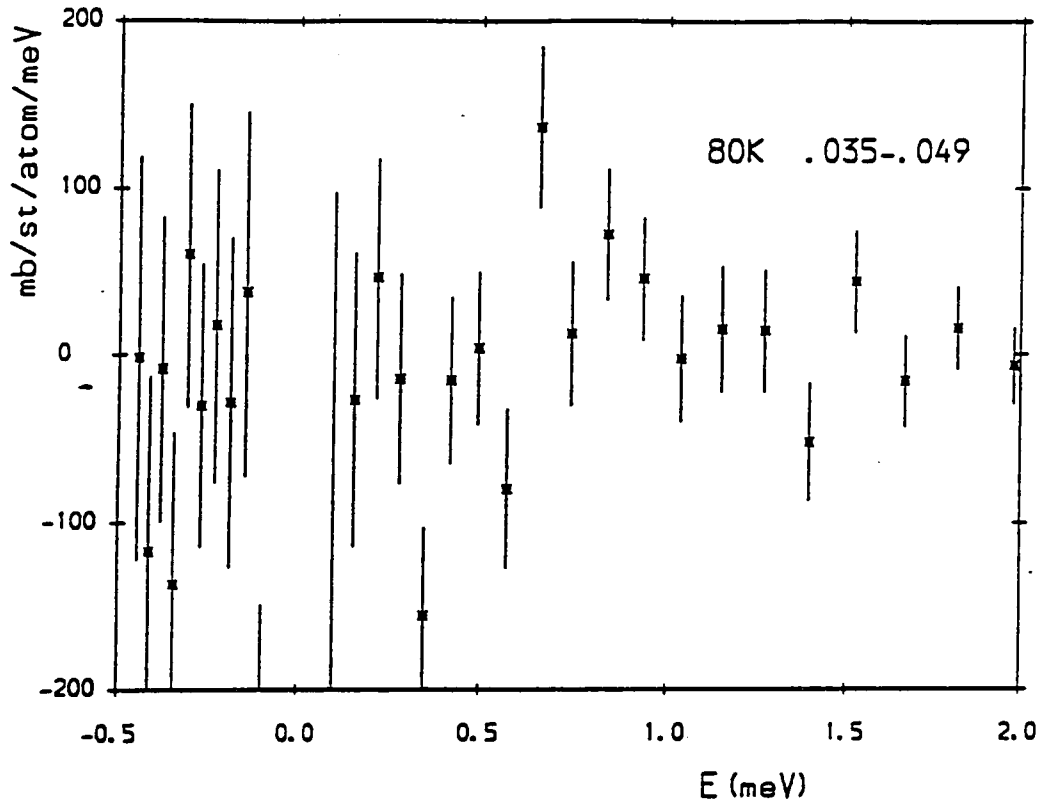
200
100
0
-100
-200
mb/st/atom/meV
80K .035-.049
-0.5
0.0
0.5
1.0
1.5
2.0
E (meV)

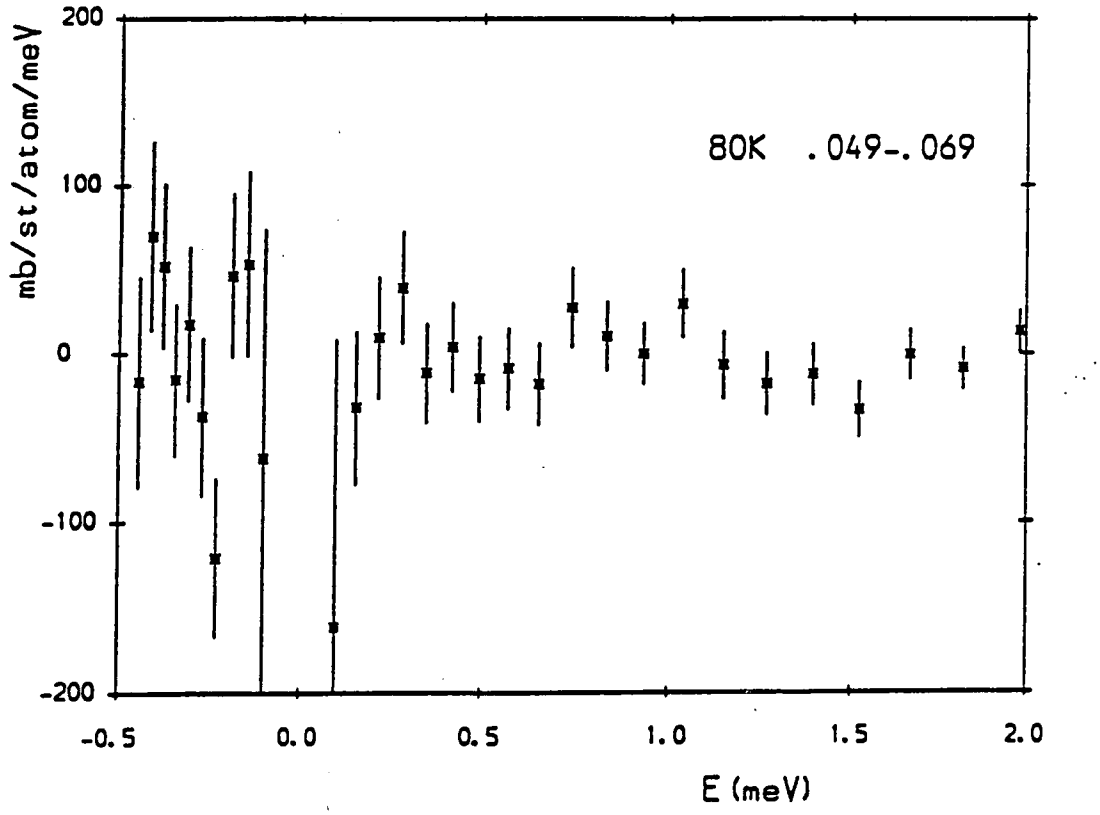
200
100
0
-100
-200
mb/st/atom/meV
80K .049-.069
-0.5
0.0
0.5
1.0
1.5
2.0
E (meV)

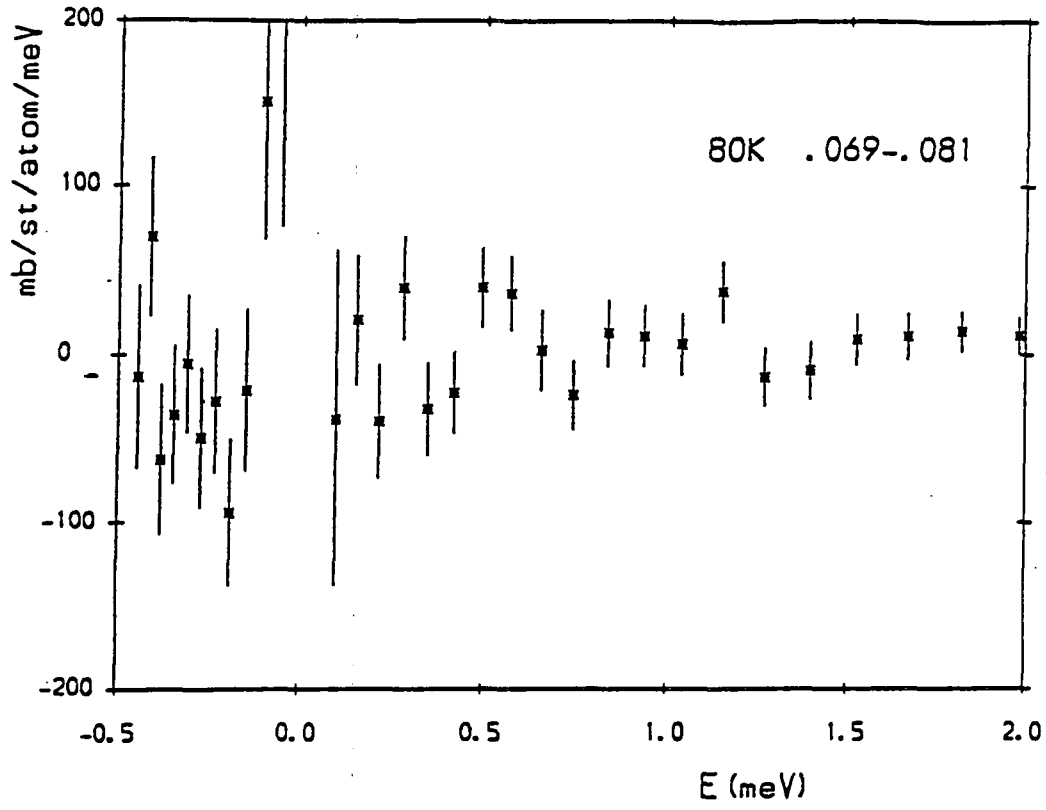
80K .069-.081
mb/st/atom/meV
200
100
0
-100
-200
-0.5
0.0
0.5
1.0
1.5
2.0
E (meV)

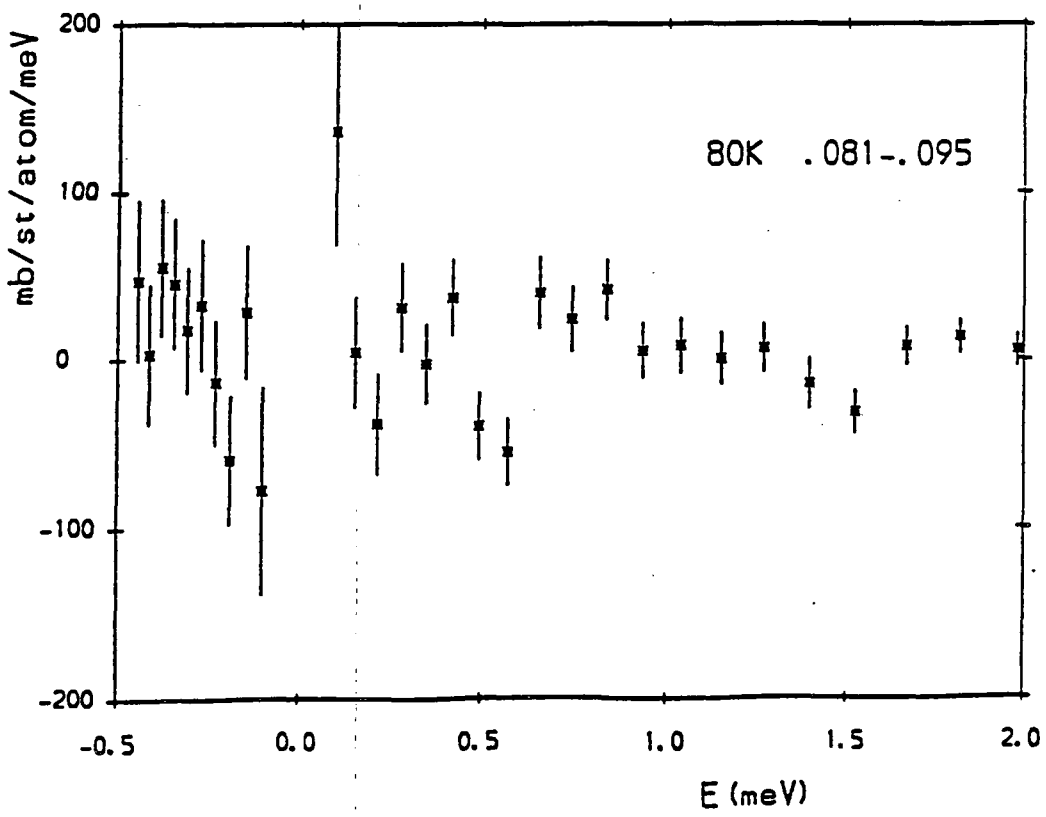
80K .081-.095
mb/st/atom/meV
200
100
0
-100
-200
-0.5
0.0
0.5
1.0
1.5
2.0
E (meV)

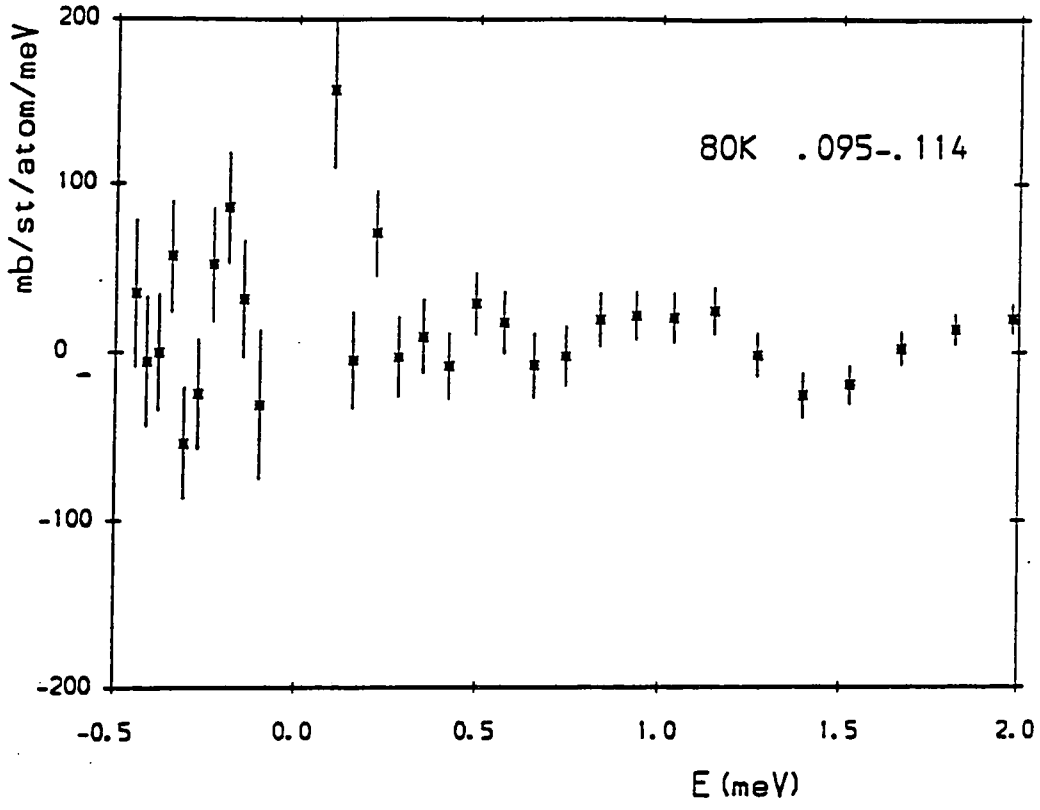
200
100
0
-100
-200
mb/st/atom/meV
80K .095-.114
-0.5
0.0
0.5
1.0
1.5
2.0
E (meV)

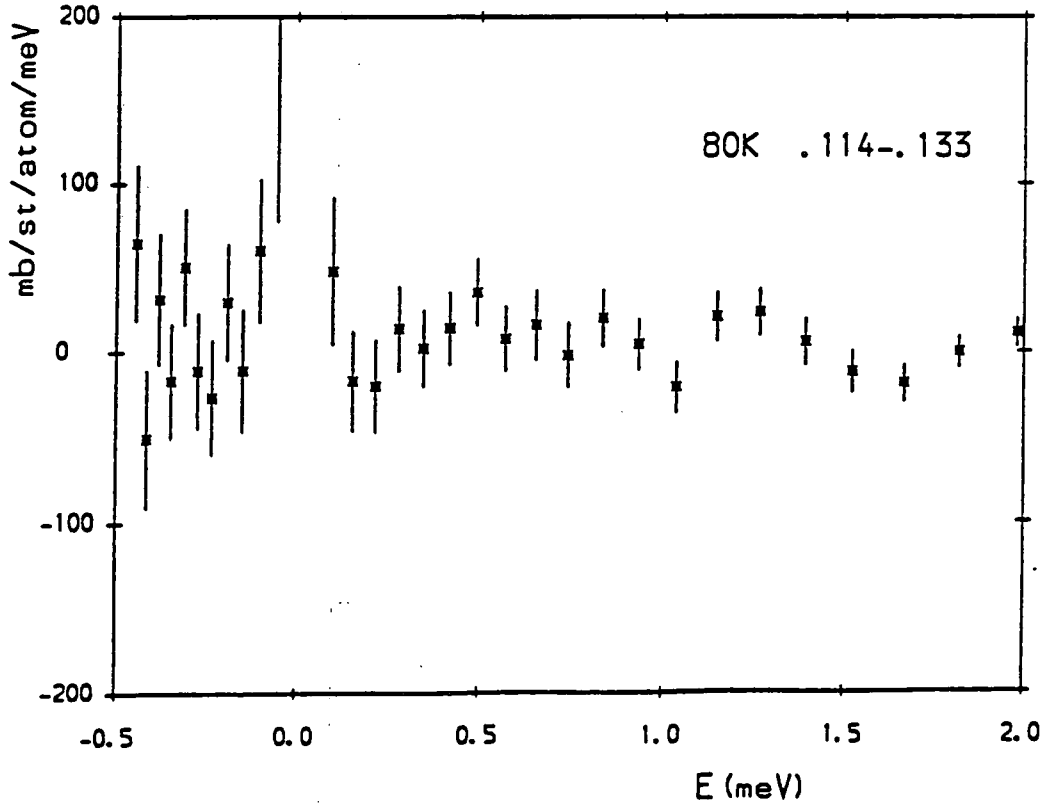
200
100
0
-100
-200
mb/st/atom/meV
80K .114-.133
-0.5
0.0
0.5
1.0
1.5
2.0
E (meV)

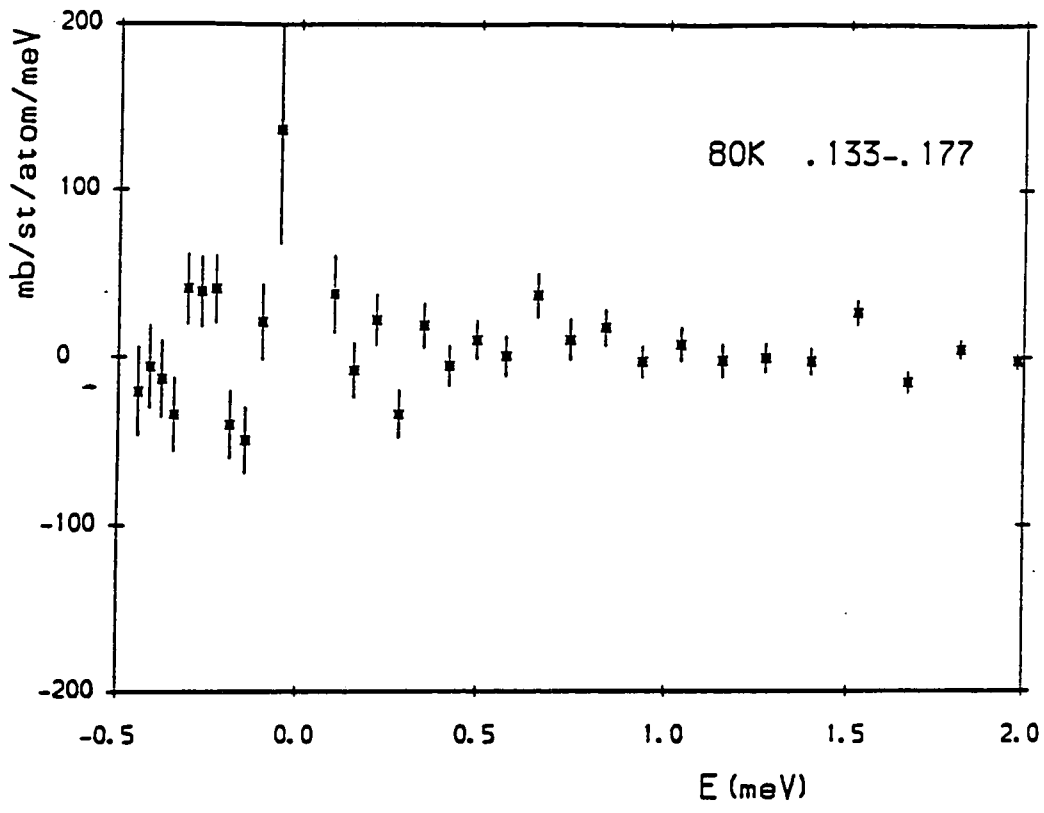
200
100
0
-100
-200
mb/st/atom/meV
80K .133-.177
-0.5
0.0
0.5
1.0
1.5
2.0
E (meV)

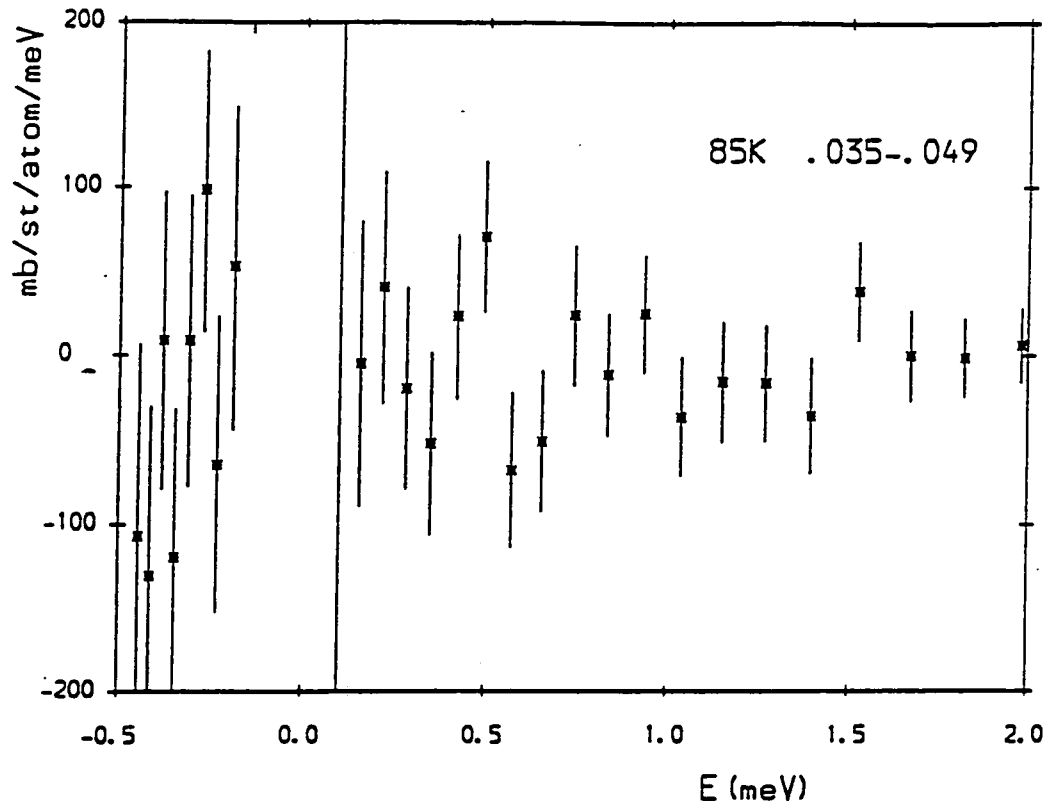
200
100
0
-100
-200
mb/st/atom/meV
85K .035-.049
-0.5
0.0
0.5
1.0
1.5
2.0
E (meV)

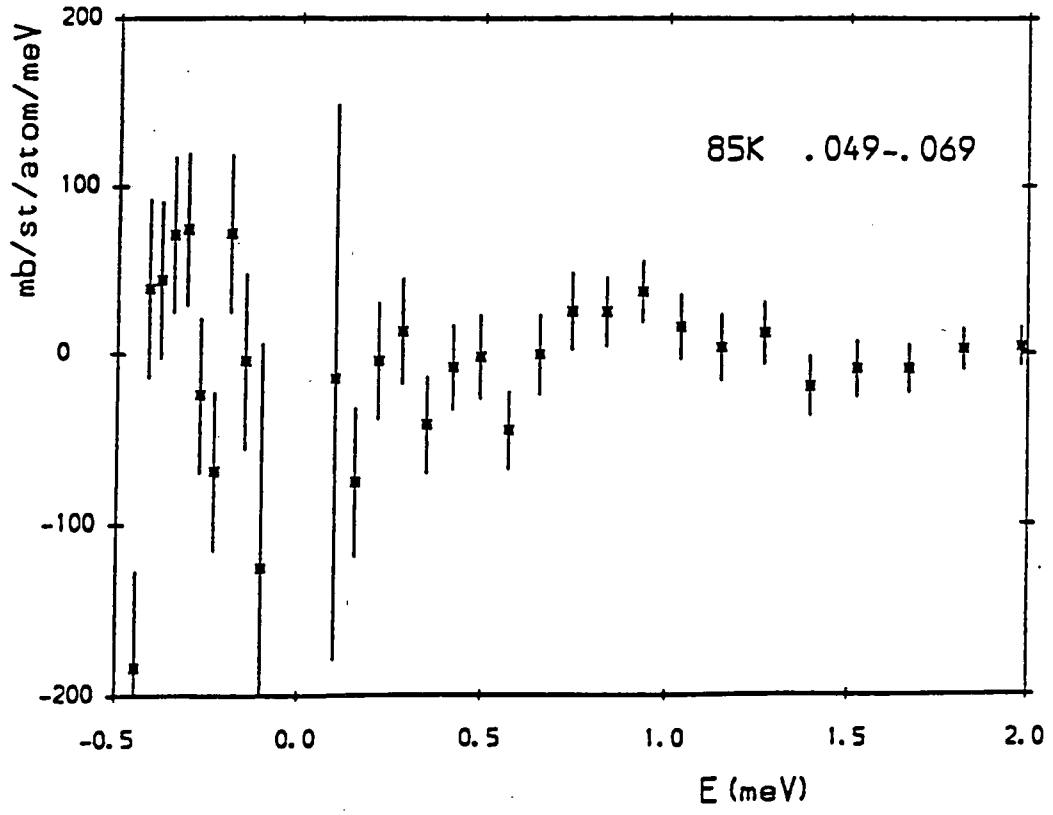
200
100
0
-100
-200
mb/st/atom/meV
85K .049-.069
-0.5
0.0
0.5
1.0
1.5
2.0
E (meV)

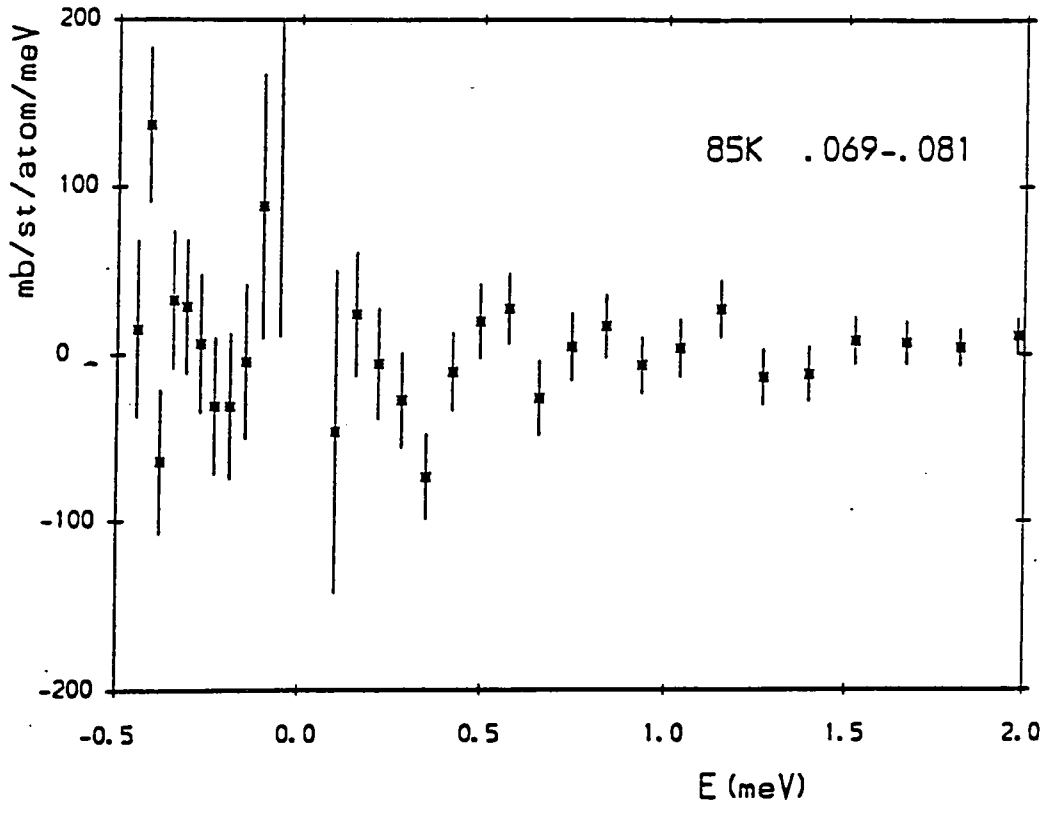
200
100
0
-100
-200
mb/st/atom/meV
85K .069-.081
-0.5
0.0
0.5
1.0
1.5
2.0
E (meV)

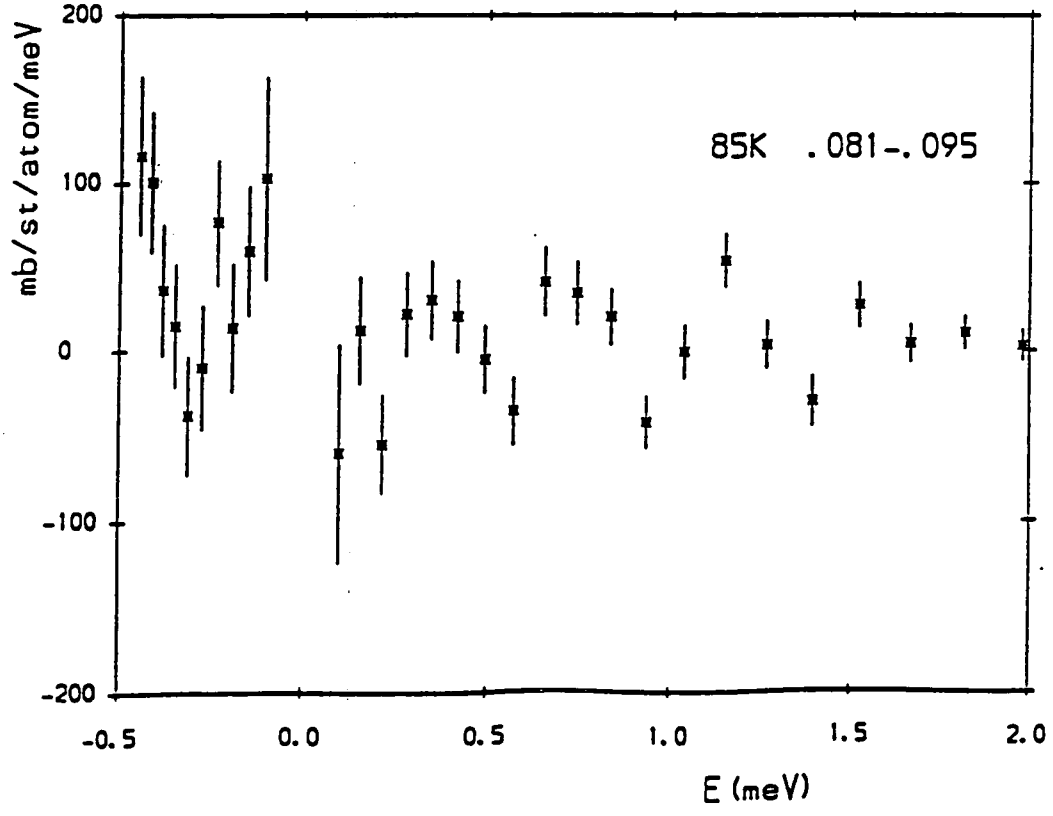
200
100
0
-100
-200
mb/st/atom/meV
85K .081-.095
-0.5
0.0
0.5
1.0
1.5
2.0
E (meV)

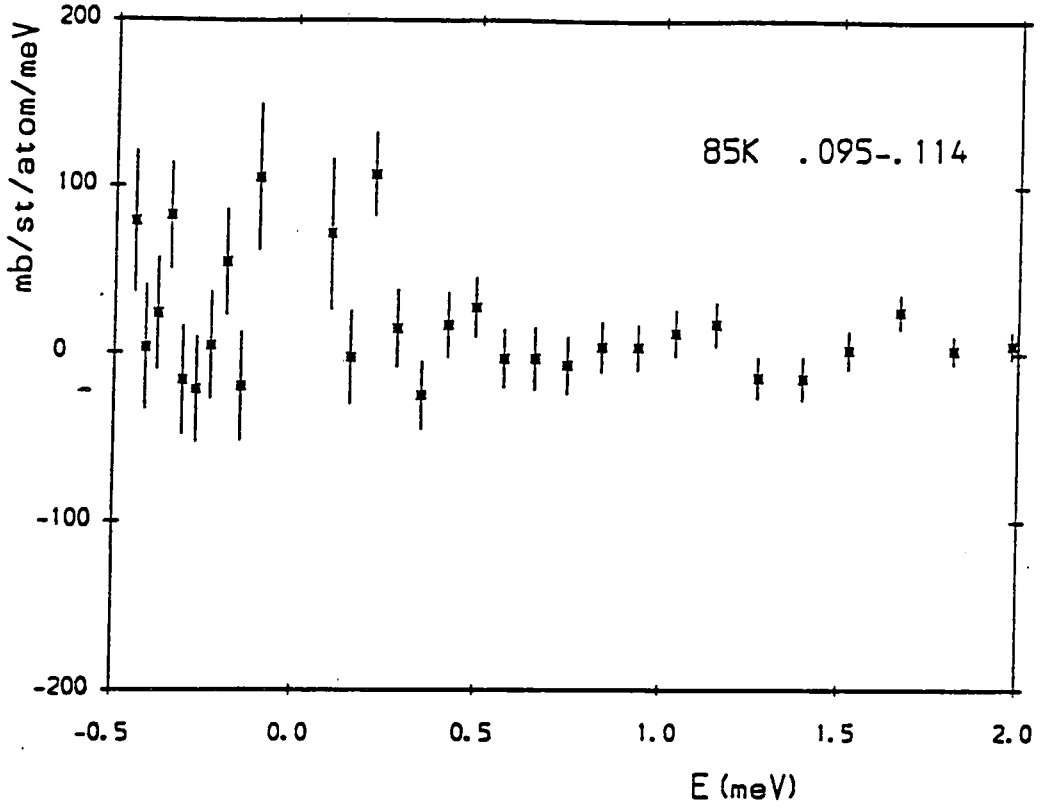
200
100
0
-100
-200
mb/st/atom/meV
85K .095-.114
-0.5
0.0
0.5
1.0
1.5
2.0
E (meV)

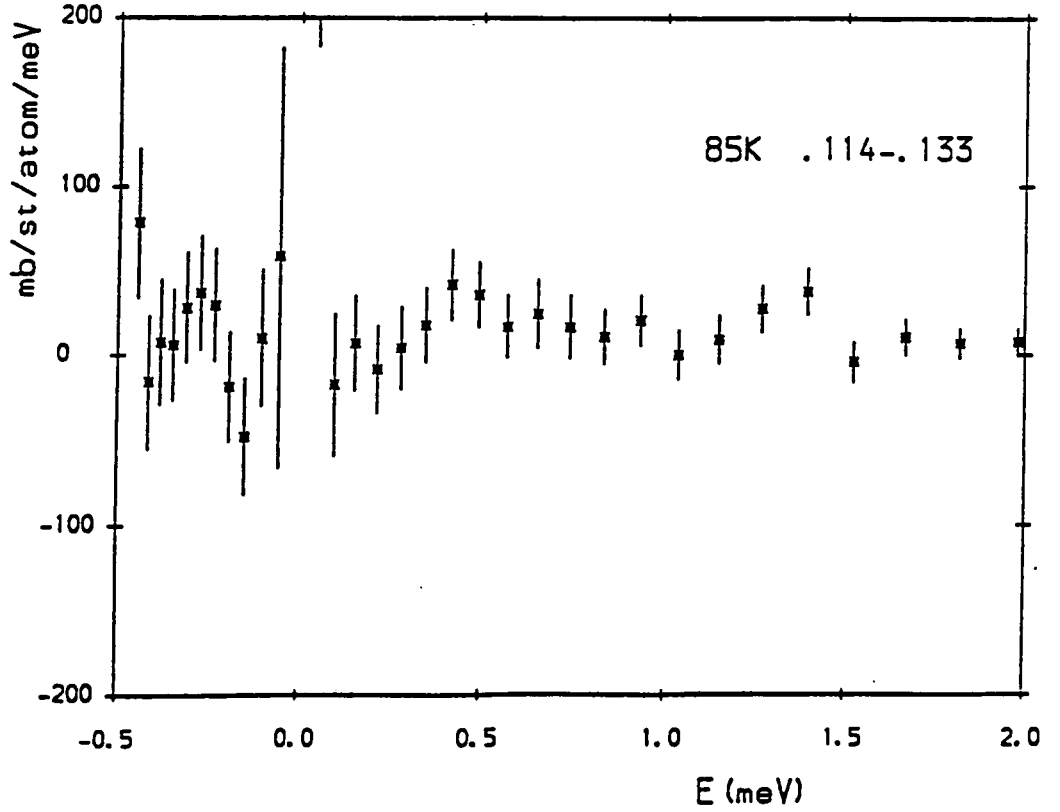
200
100
0
-100
-200
mb/st/atom/meV
85K .114-.133
-0.5
0.0
0.5
1.0
1.5
2.0
E (meV)

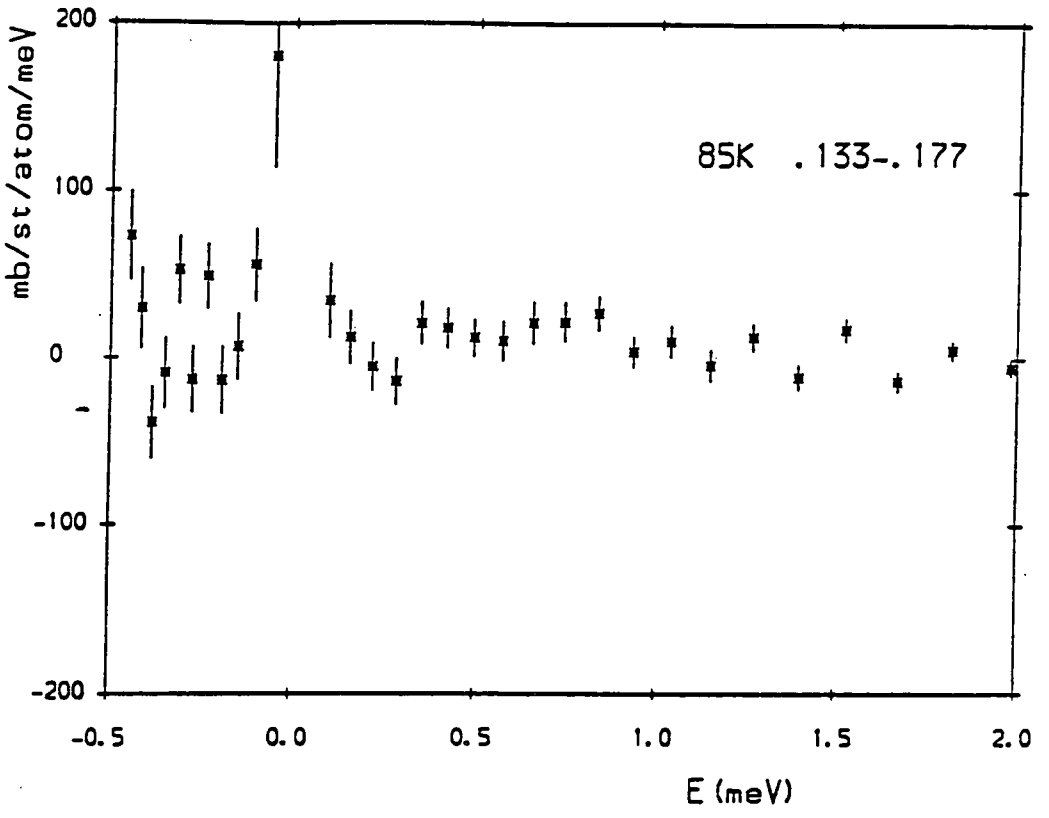
85K .133-.177
mb/st/atom/meV
200
100
0
-100
-200
-0.5
0.0
0.5
1.0
1.5
2.0
E (meV)

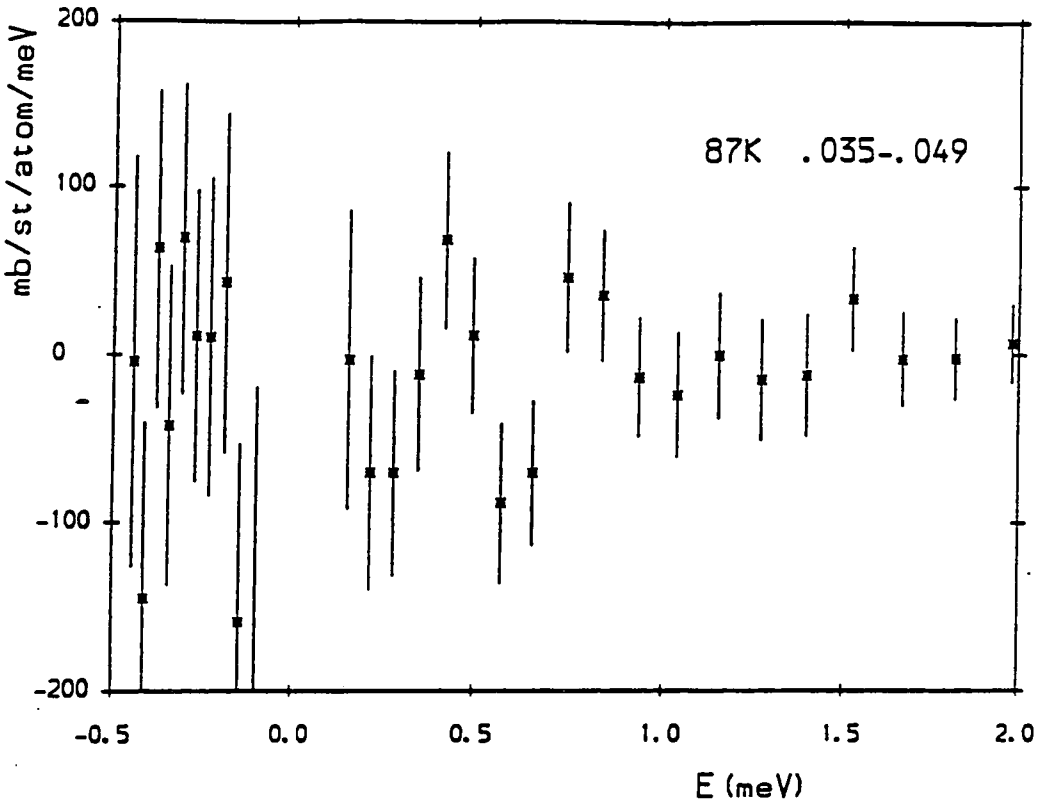
87K .035-.049
mb/st/atom/meV
200
100
0
-100
-200
-0.5
0.0
0.5
1.0
1.5
2.0
E (meV)

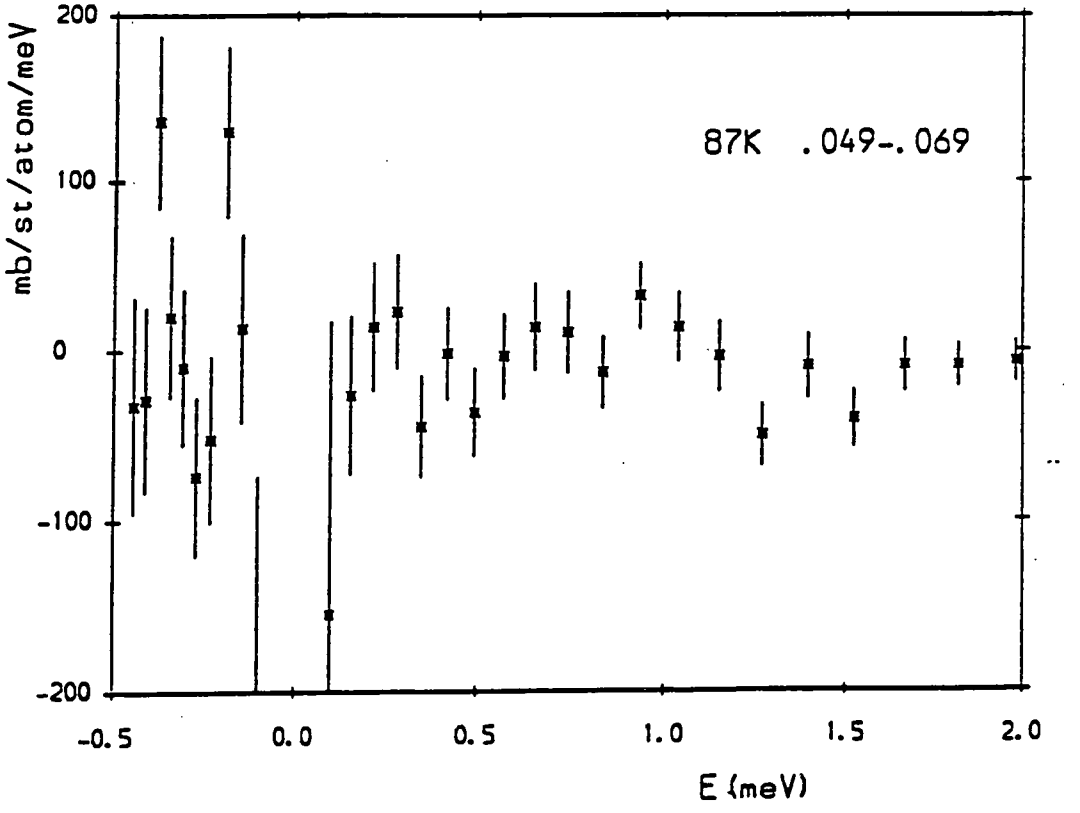
87K .049-.069
mb/st/atom/meV
200
100
0
-100
-200
-0.5
0.0
0.5
1.0
1.5
2.0
E (meV)

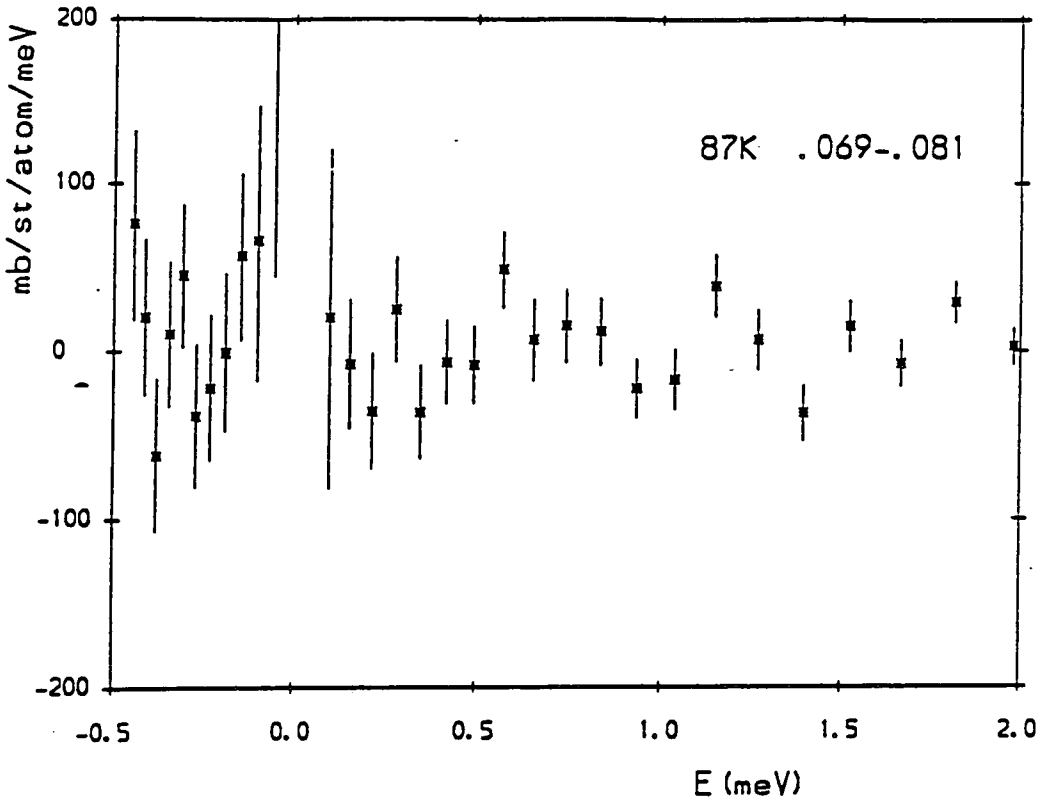
87K .069-.081
mb/st/atom/meV
E (meV)
200
100
0
-100
-200
-0.5
0.0
0.5
1.0
1.5
2.0

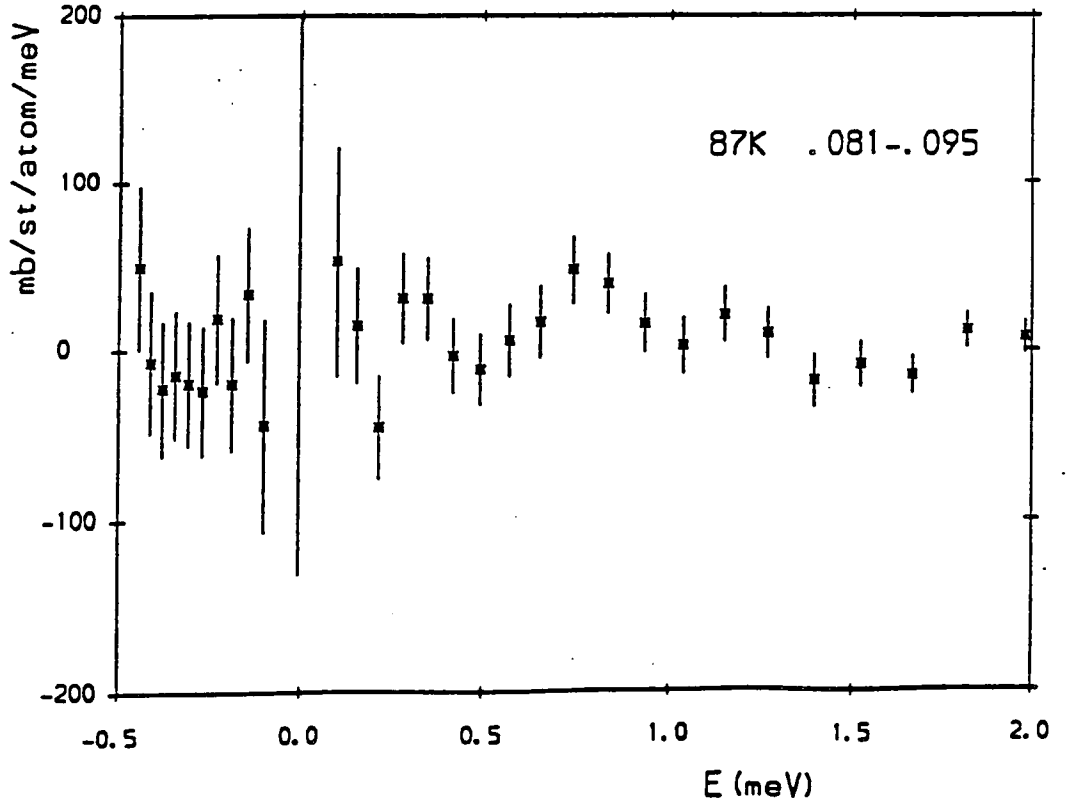
87K .081-.095
mb/st/atom/meV
E (meV)
200
100
0
-100
-200
-0.5
0.0
0.5
1.0
1.5
2.0

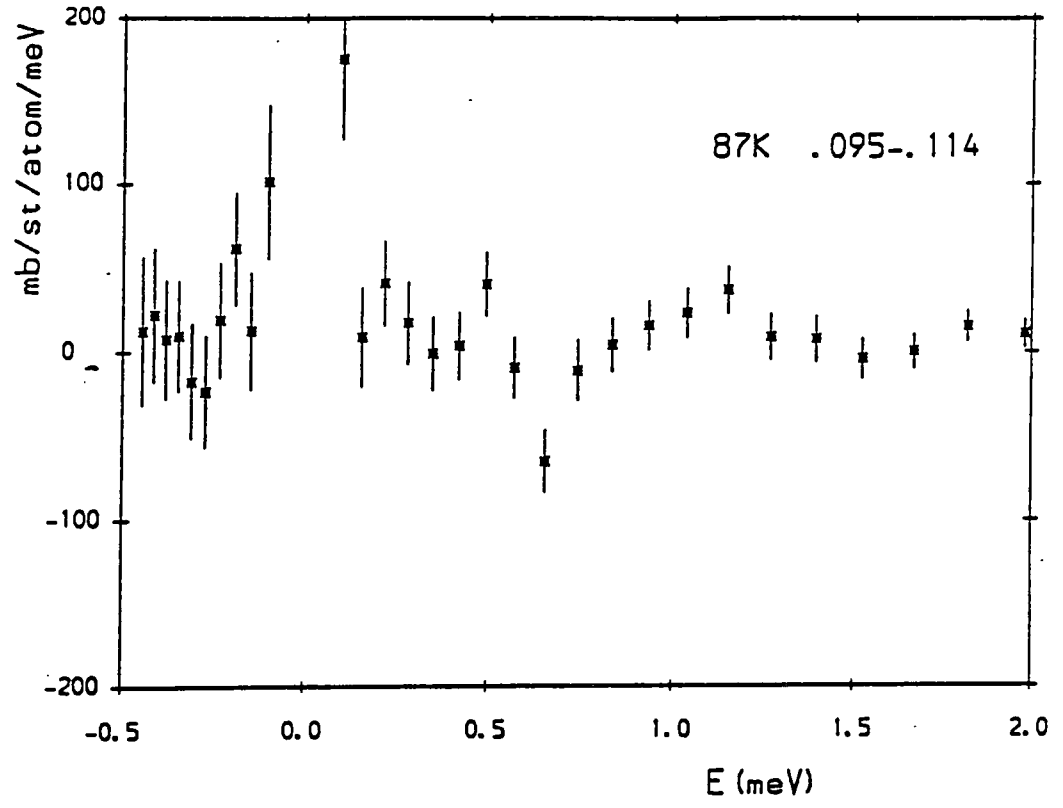
87K .095-.114
mb/st/atom/meV
200
100
0
-100
-200
-0.5
0.0
0.5
1.0
1.5
2.0
E (meV)

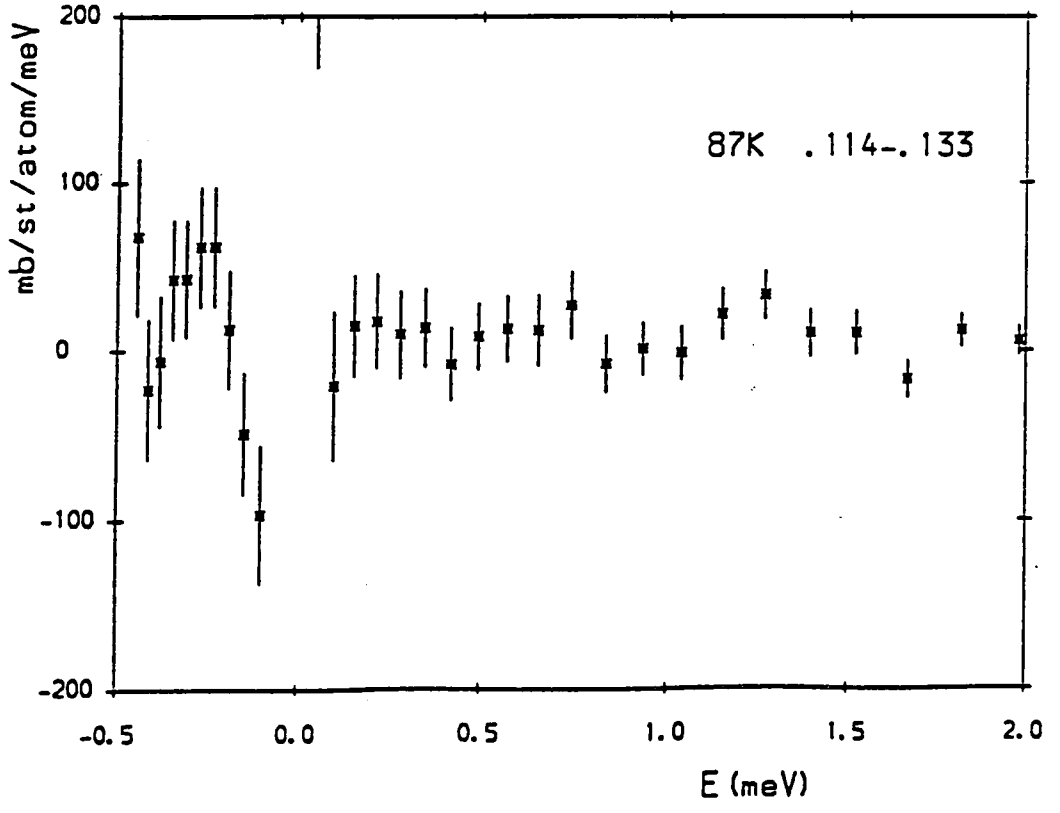
87K .114-.133
mb/st/atom/meV
200
100
0
-100
-200
-0.5
0.0
0.5
1.0
1.5
2.0
E (meV)

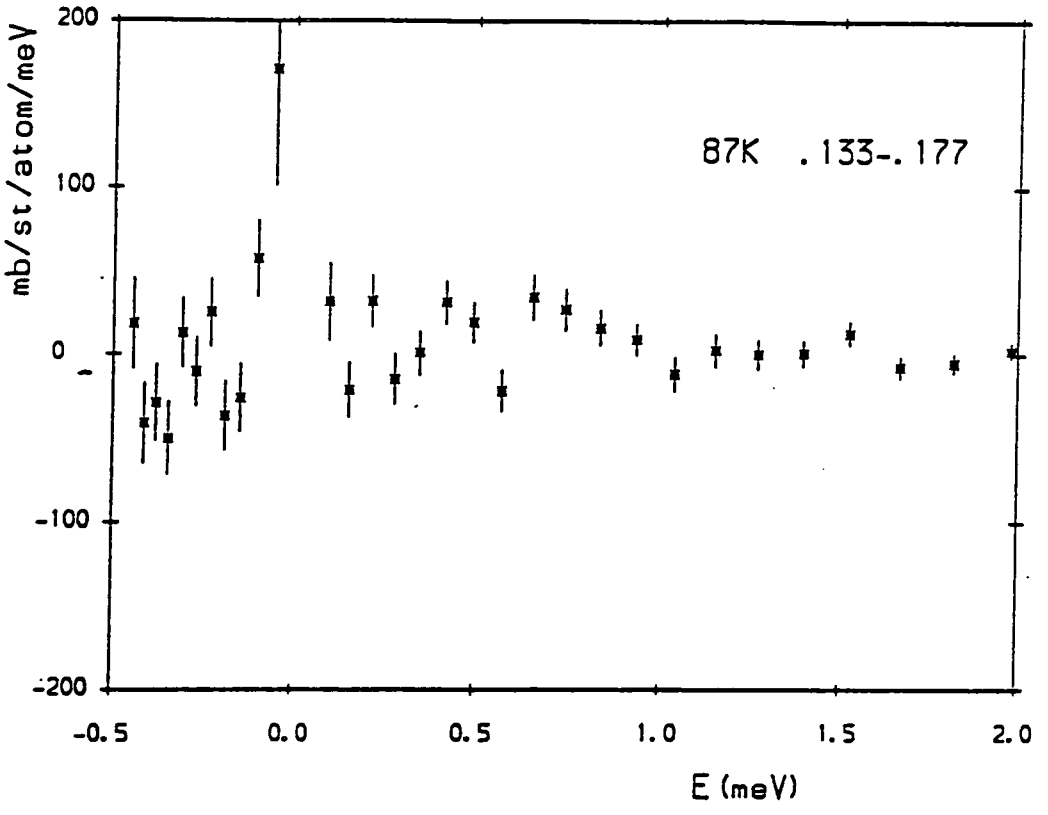
200
100
0
-100
-200
mb/st/atom/meV
87K .133-.177
-0.5
0.0
0.5
1.0
1.5
2.0
E (meV)

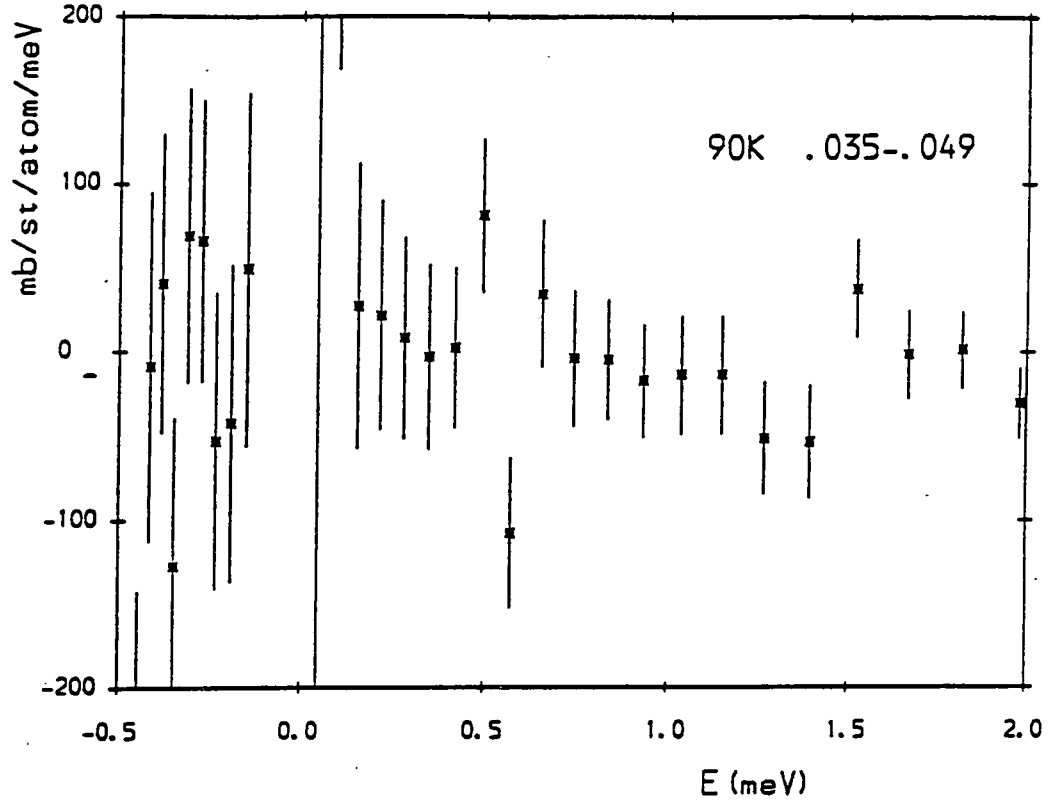
90K .035-.049
mb/st/atom/meV
200
100
0
-100
-200
-0.5
0.0
0.5
1.0
1.5
2.0
E (meV)

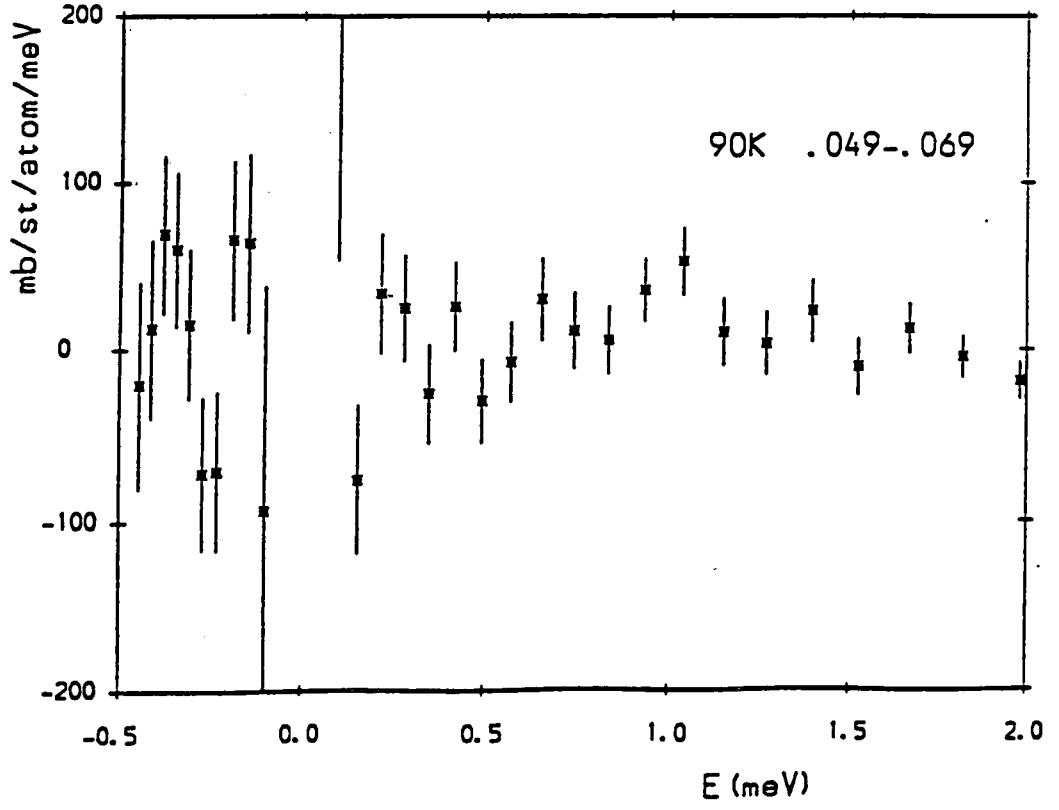
90K .049-.069
mb/st/atom/meV
200
100
0
-100
-200
-0.5
0.0
0.5
1.0
1.5
2.0
E (meV)

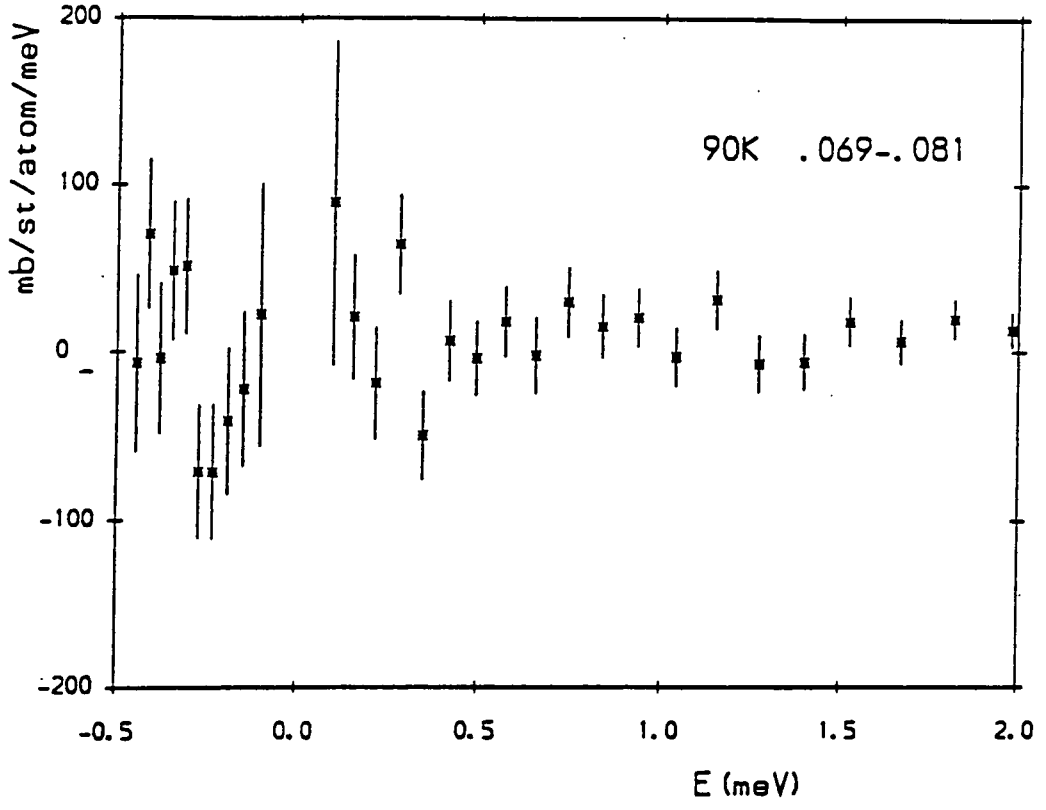
90K .069-.081
mb/st/atom/meV
200
100
0
-100
-200
-0.5
0.0
0.5
1.0
1.5
2.0
E (meV)

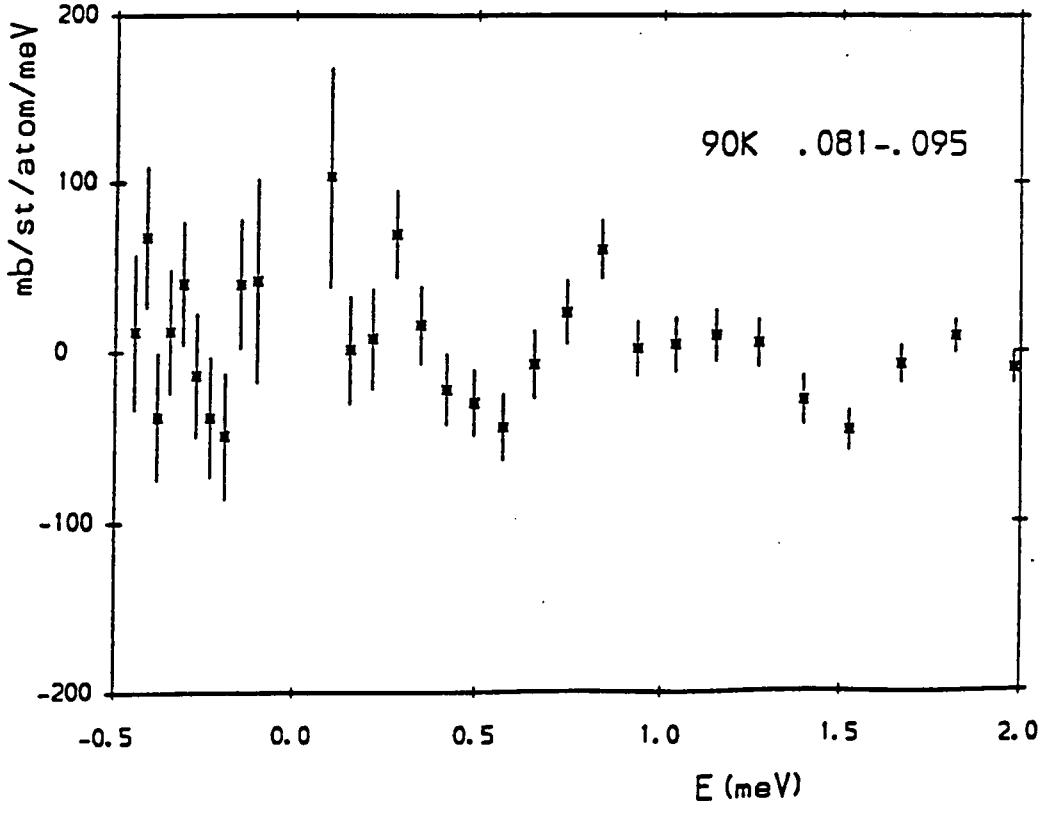
90K .081-.095
mb/st/atom/meV
200
100
0
-100
-200
-0.5
0.0
0.5
1.0
1.5
2.0
E (meV)

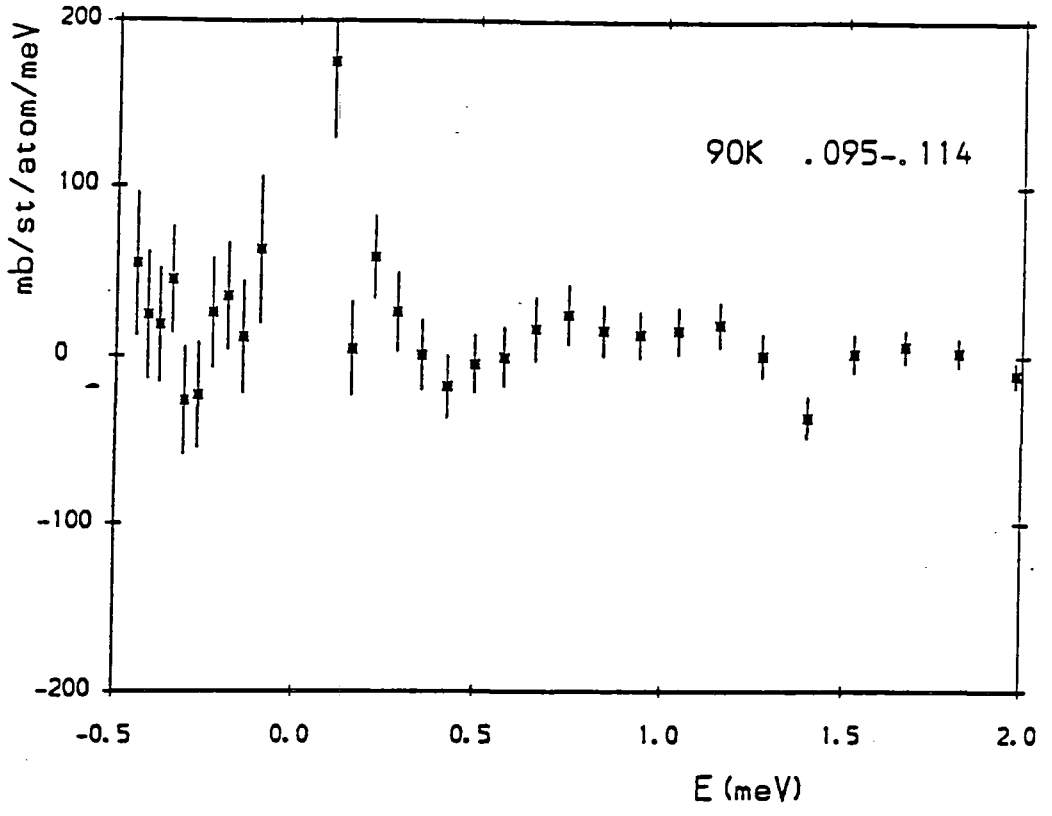
90K .095-.114
mb/st/atom/meV
E (meV)
200
100
0
-100
-200
-0.5
0.0
0.5
1.0
1.5
2.0

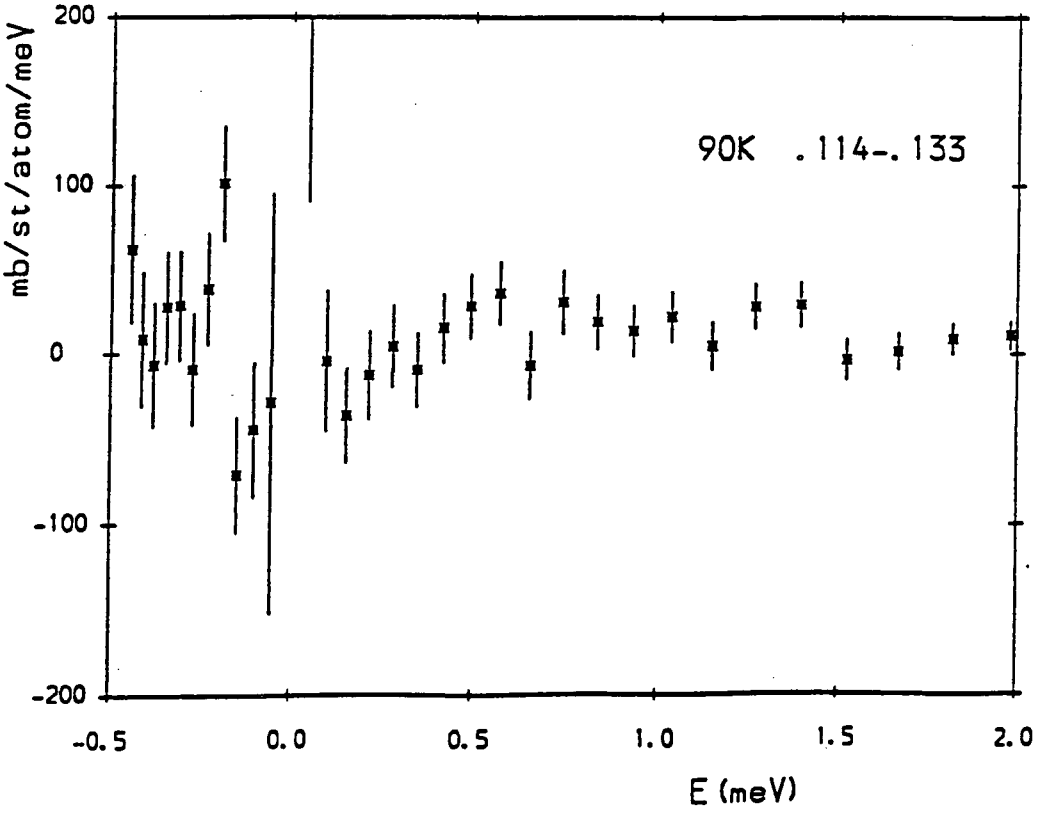
90K .114-.133
mb/st/atom/meV
E (meV)
200
100
0
-100
-200
-0.5
0.0
0.5
1.0
1.5
2.0

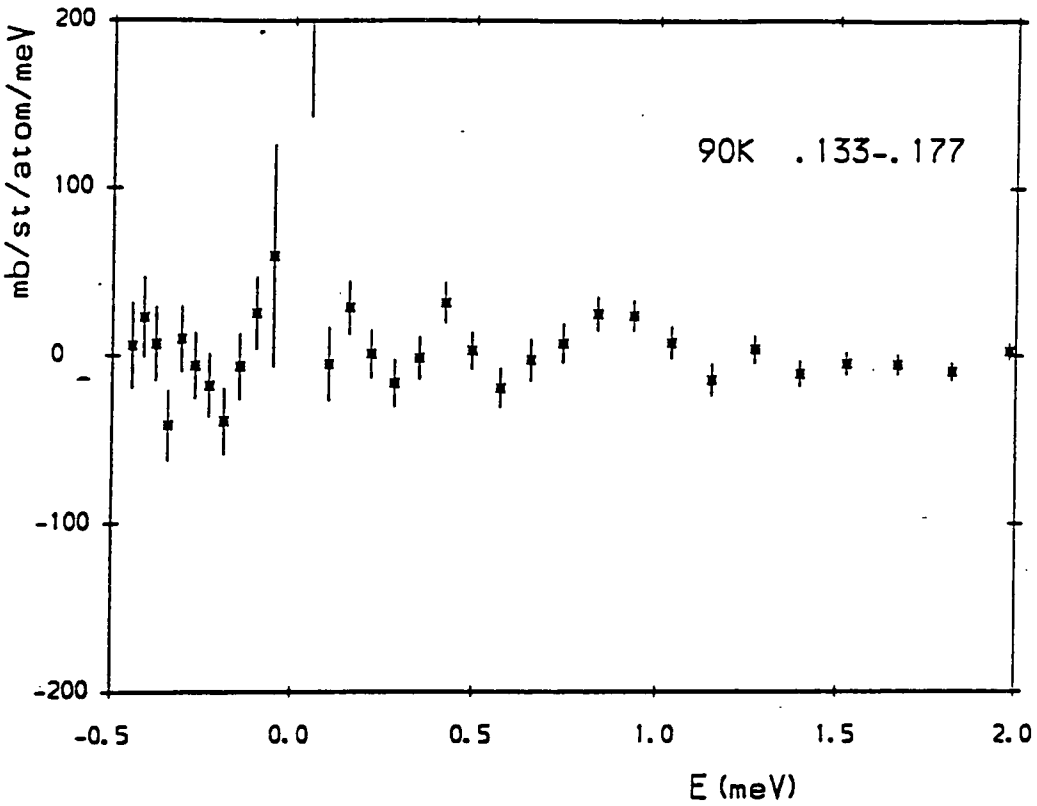
200
100
0
-100
-200
mb/st/atom/meV
90K .133-.177
-0.5
0.0
0.5
1.0
1.5
2.0
E (meV)

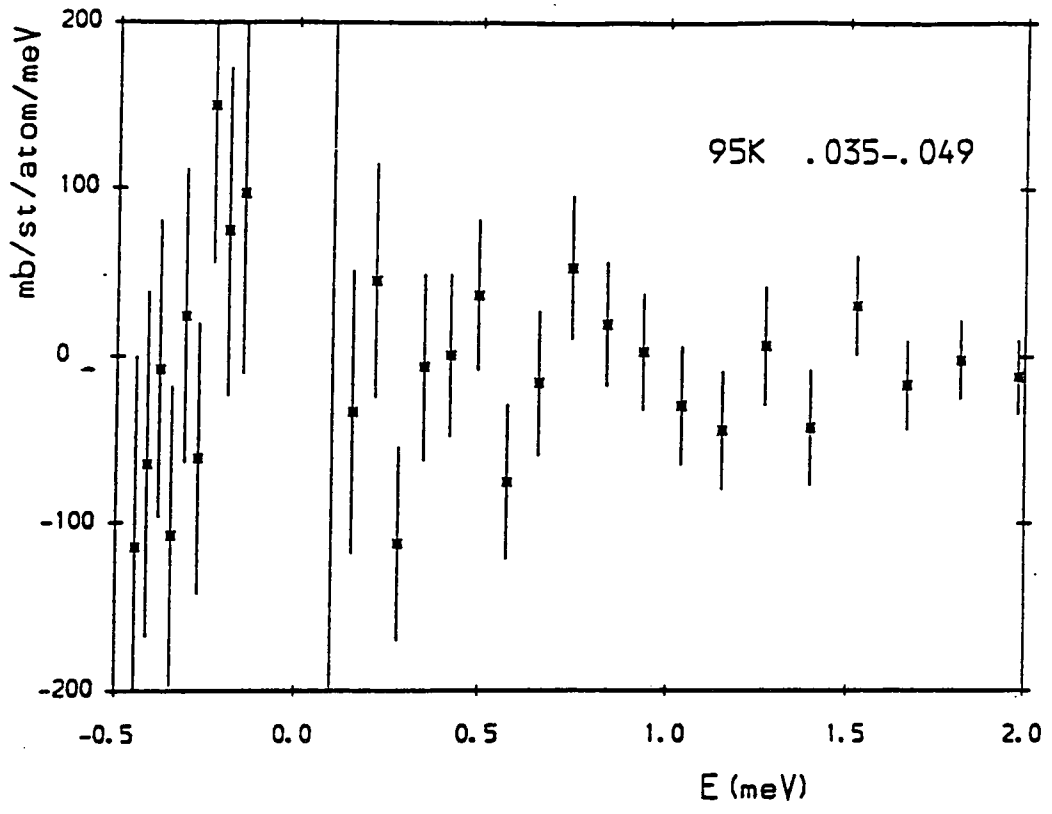
95K .035-.049
mb/st/atom/meV
200
100
0
-100
-200
-0.5
0.0
0.5
1.0
1.5
2.0
E (meV)

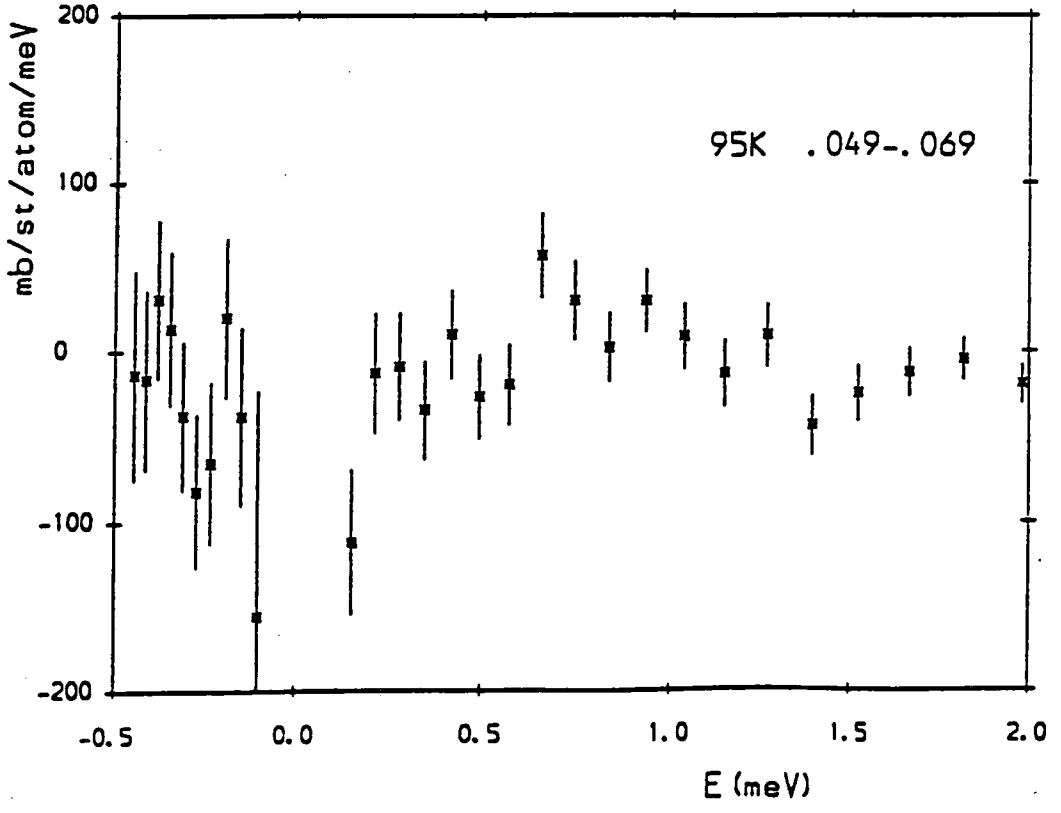
95K .049-.069
mb/st/atom/meV
200
100
0
-100
-200
-0.5
0.0
0.5
1.0
1.5
2.0
E (meV)

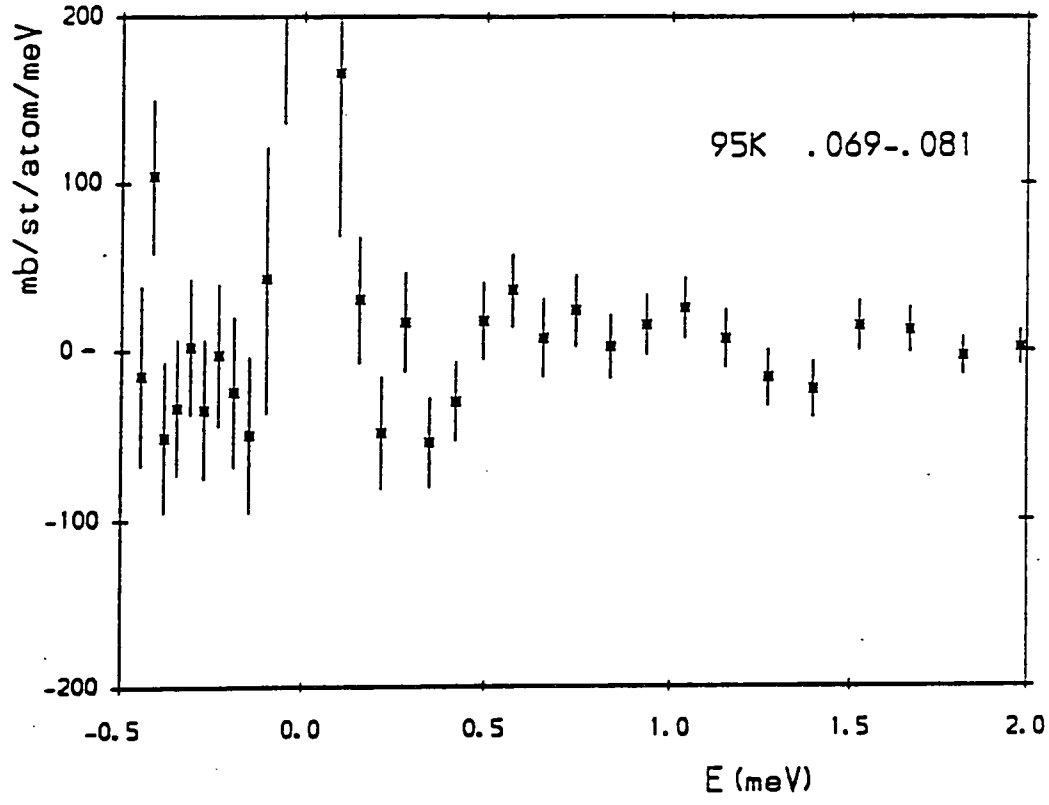
95K .069-.081
mb/st/atom/meV
200
100
0
-100
-200
-0.5
0.0
0.5
1.0
1.5
2.0
E (meV)

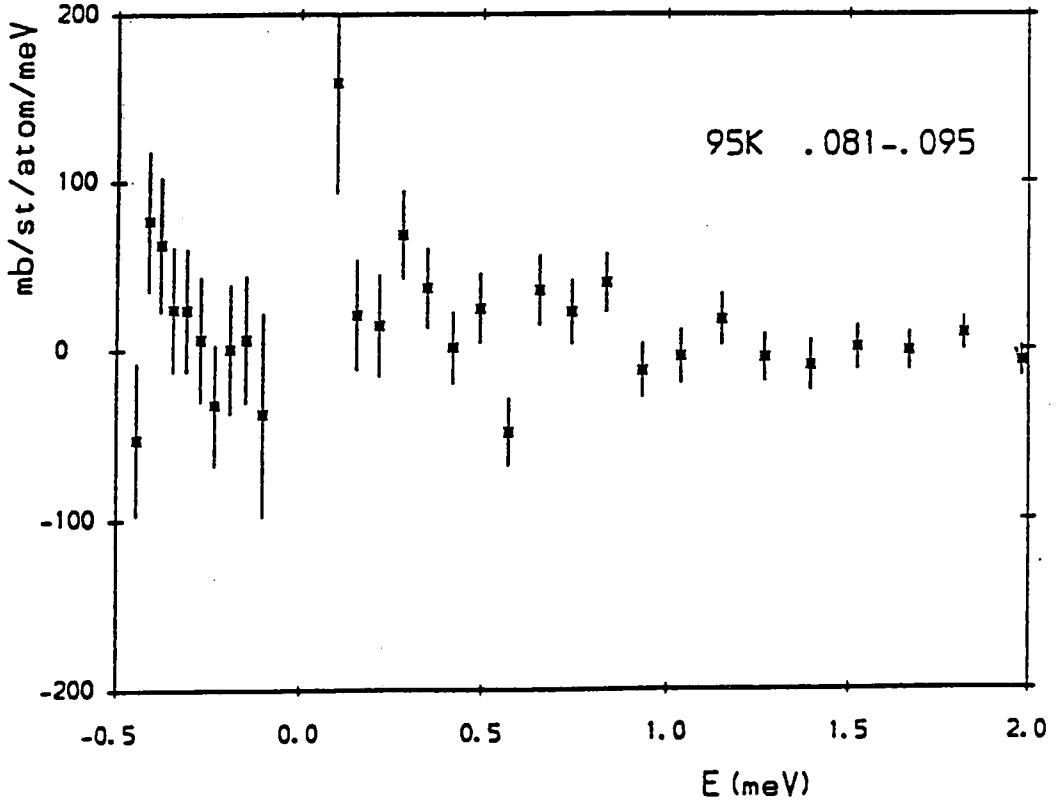
95K .081-.095
mb/st/atom/meV
200
100
0
-100
-200
-0.5
0.0
0.5
1.0
1.5
2.0
E (meV)

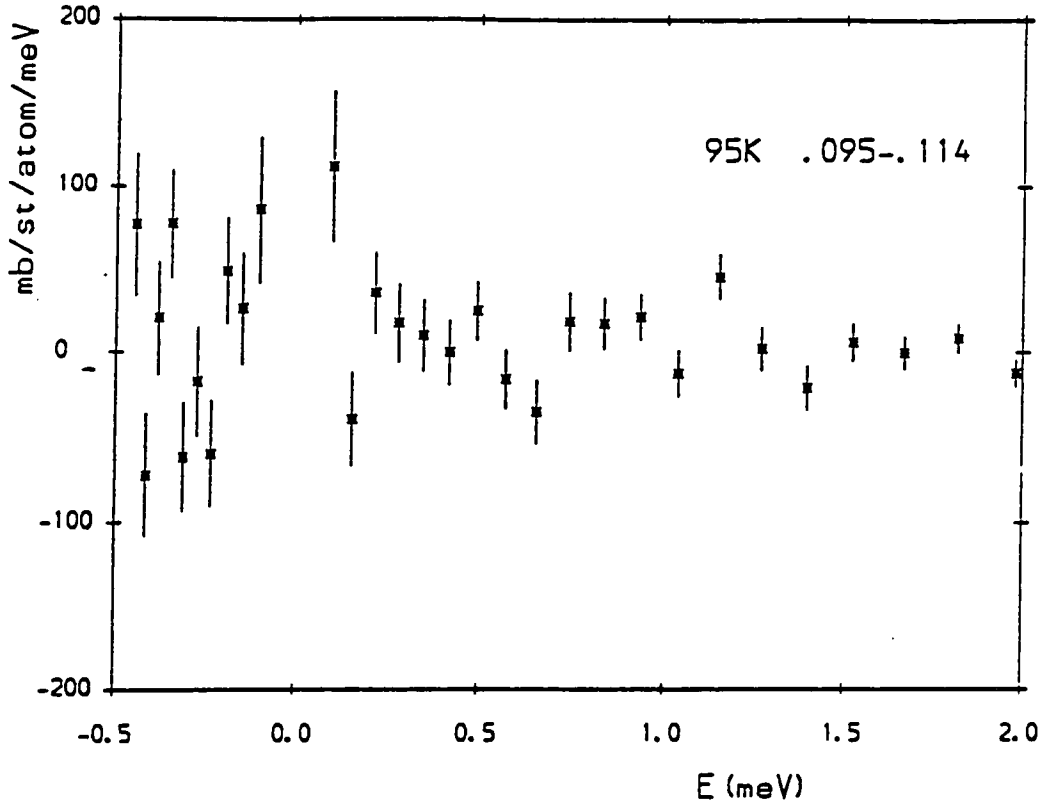
95K .095-.114
mb/st/atom/meV
200
100
0
-100
-200
-0.5
0.0
0.5
1.0
1.5
2.0
E (meV)

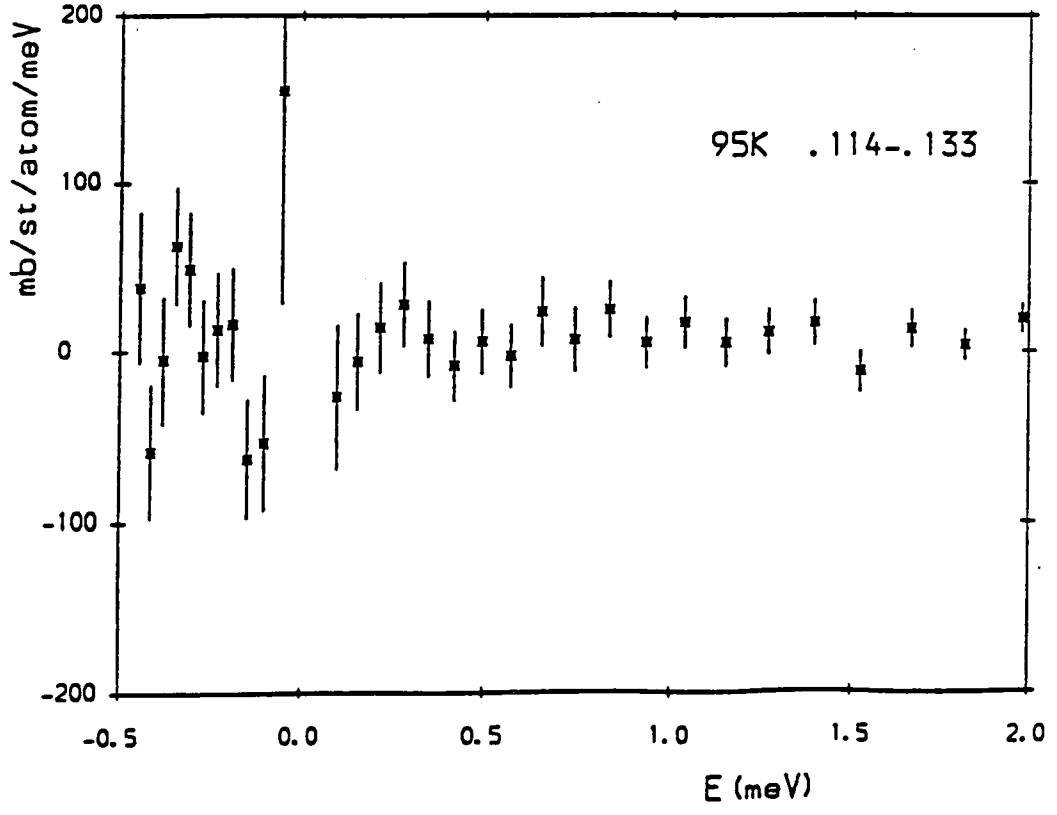
95K .114-.133
mb/st/atom/meV
200
100
0
-100
-200
-0.5
0.0
0.5
1.0
1.5
2.0
E (meV)

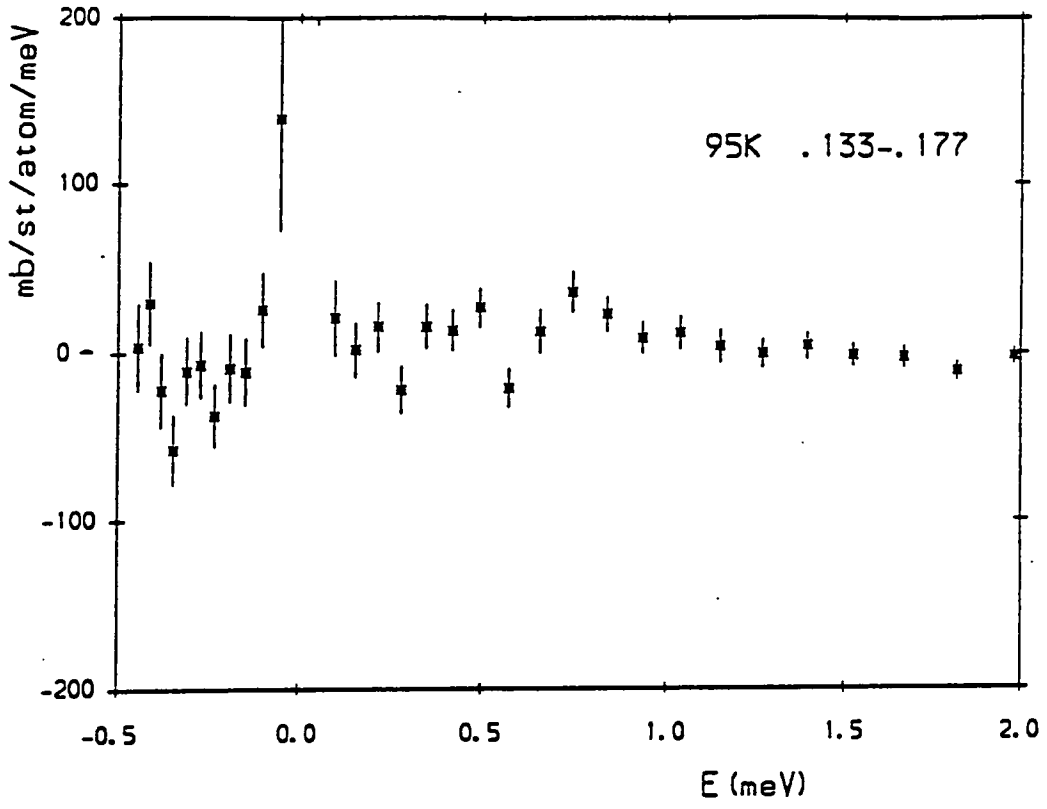
95K .133-.177
mb/st/atom/meV
200
100
0
-100
-200
-0.5
0.0
0.5
1.0
1.5
2.0
E (meV)

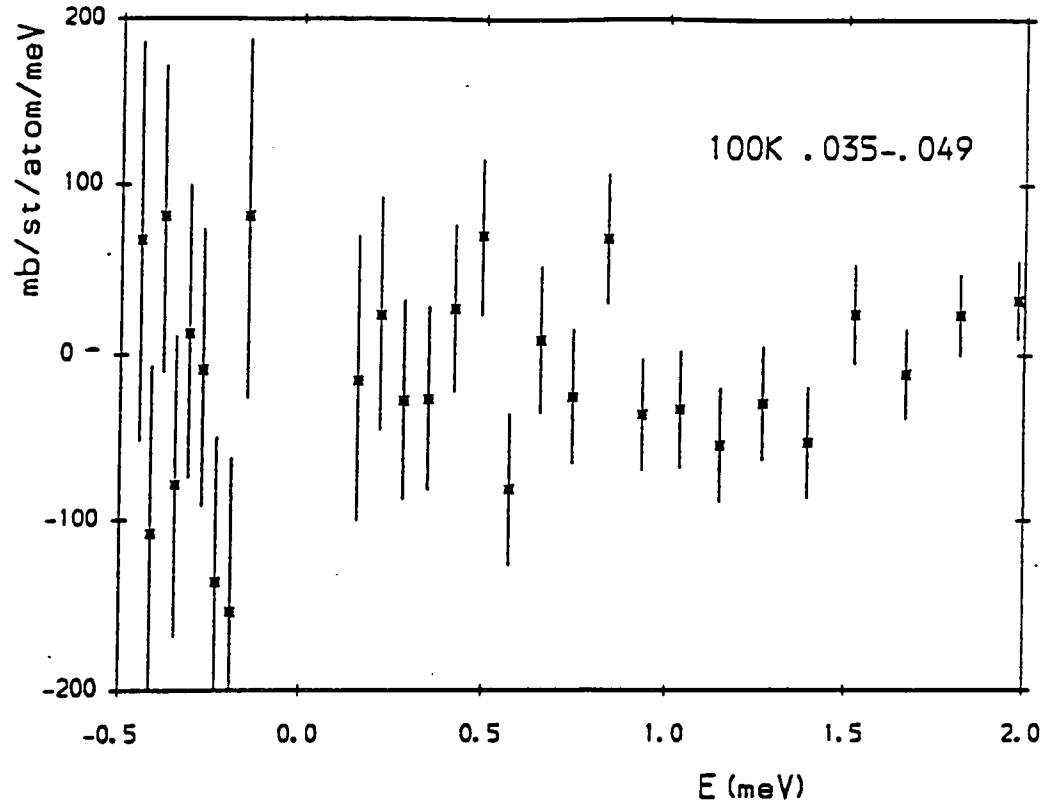
100K .035-.049
mb/st/atom/meV
200
100
0
-100
-200
-0.5
0.0
0.5
1.0
1.5
2.0
E (meV)

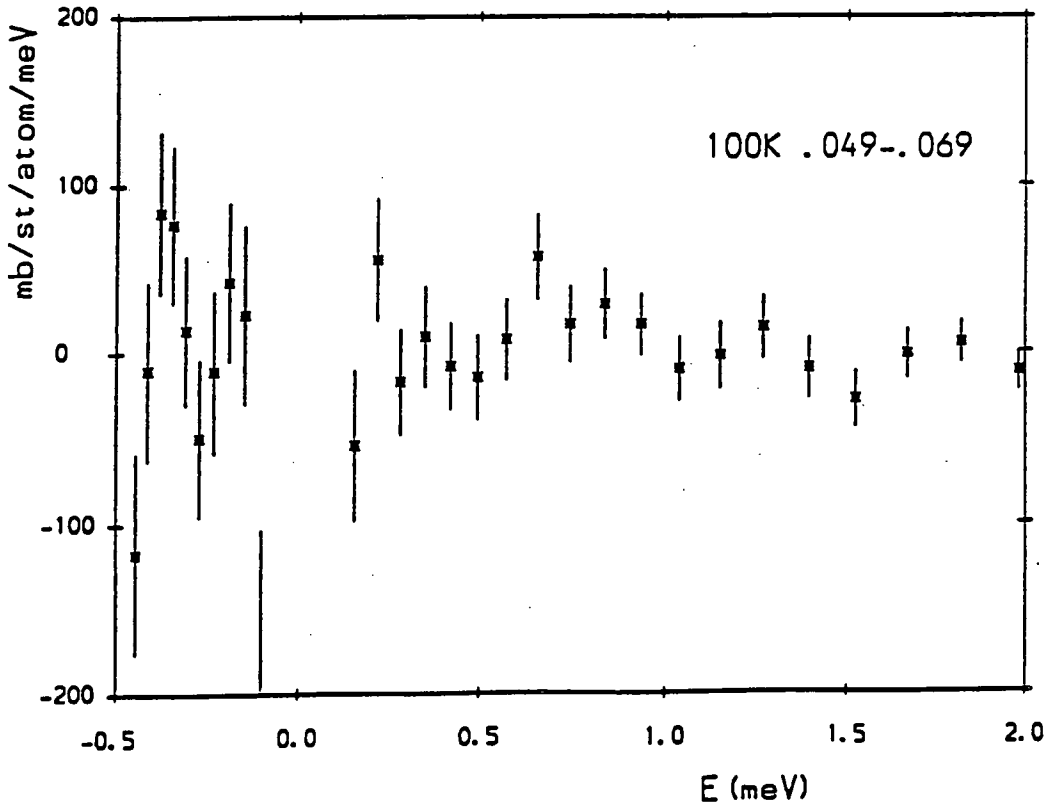
100K .049-.069
mb/st/atom/meV
200
100
0
-100
-200
-0.5
0.0
0.5
1.0
1.5
2.0
E (meV)

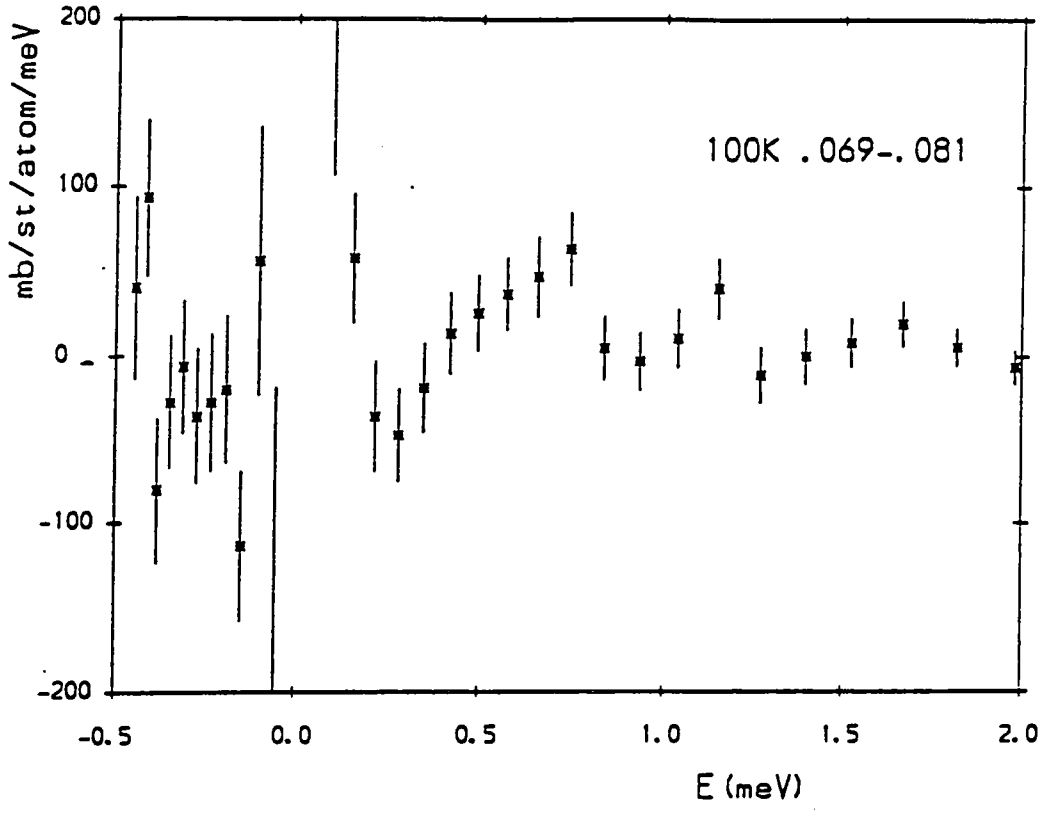
200
100
0
-100
-200
mb/st/atom/meV
100K .069-.081
-0.5
0.0
0.5
1.0
1.5
2.0
E (meV)

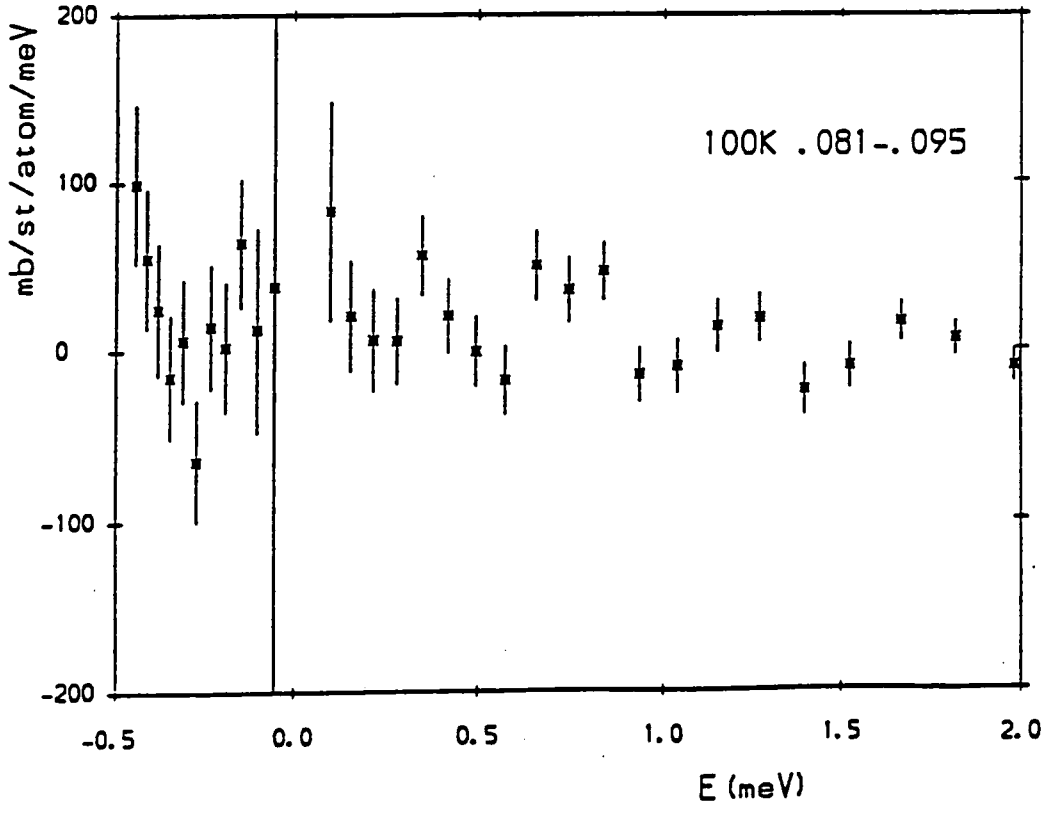
200
100
0
-100
-200
mb/st/atom/meV
100K .081-.095
-0.5
0.0
0.5
1.0
1.5
2.0
E (meV)

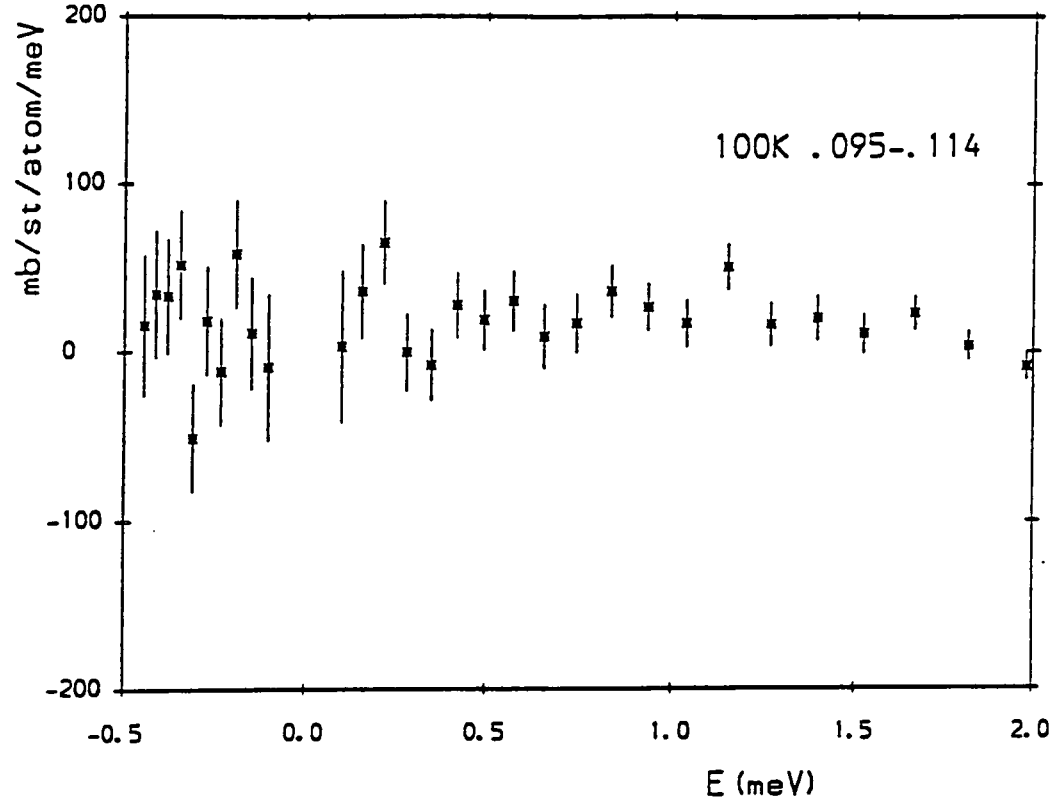
100K .095-.114
mb/st/atom/meV
200
100
0
-100
-200
-0.5
0.0
0.5
1.0
1.5
2.0
E (meV)

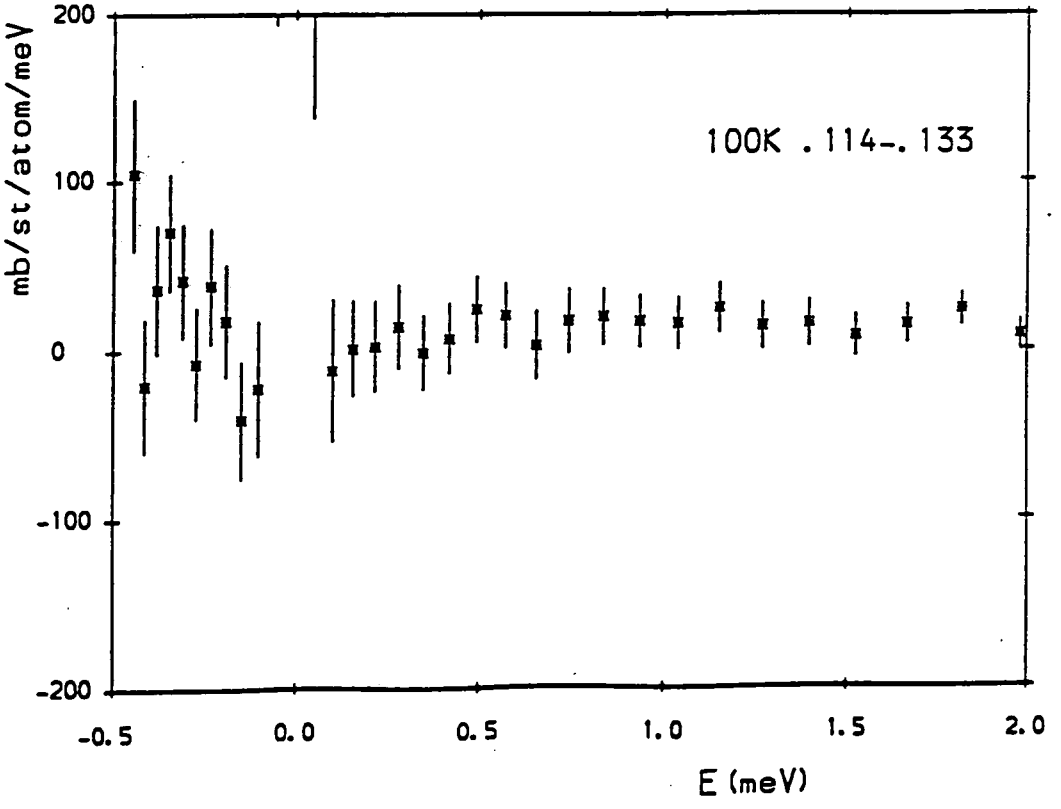
100K .114-.133
mb/st/atom/meV
200
100
0
-100
-200
-0.5
0.0
0.5
1.0
1.5
2.0
E (meV)

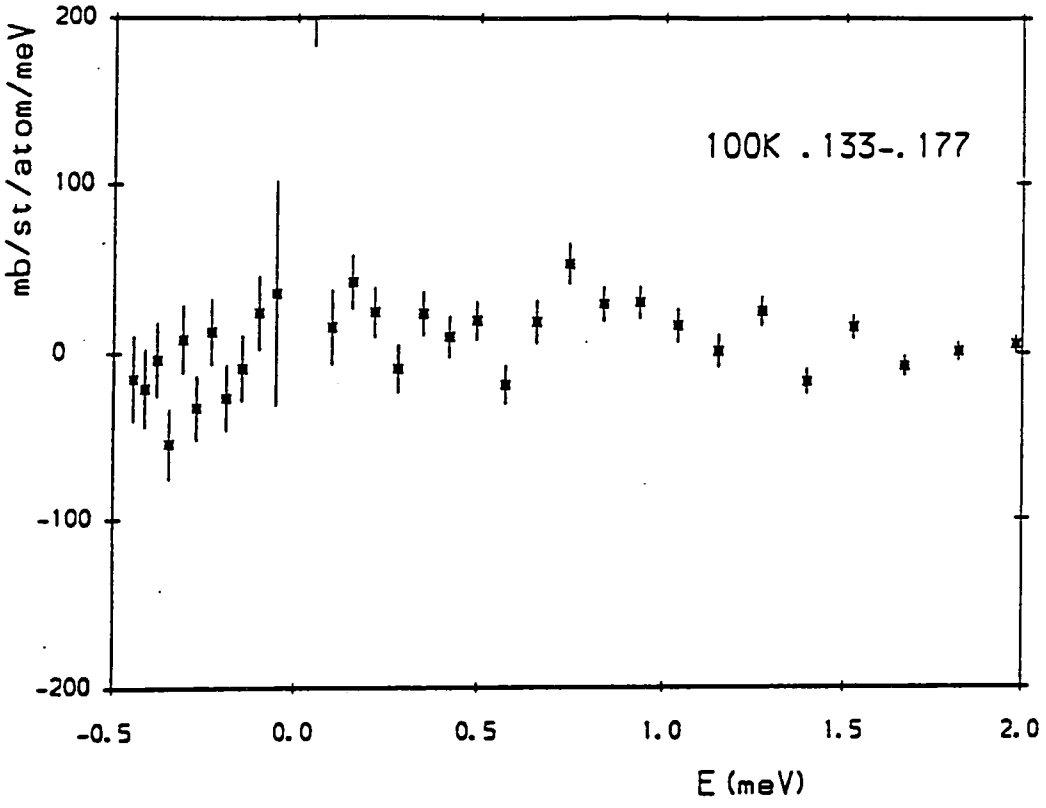
100K .133-.177
mb/st/atom/meV
200
100
0
-100
-200
-0.5
0.0
0.5
1.0
1.5
2.0
E (meV)

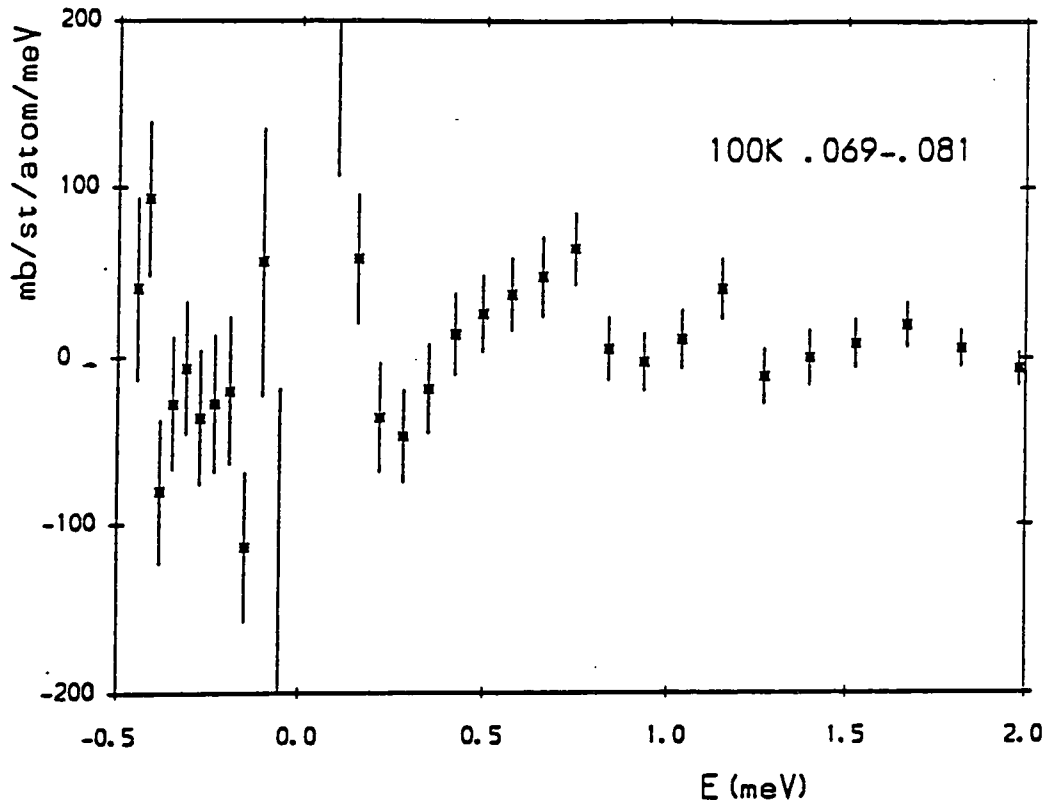
200
100
0
-100
-200
mb/st/atom/meV
100K .069-.081
-0.5
0.0
0.5
1.0
1.5
2.0
E (meV)

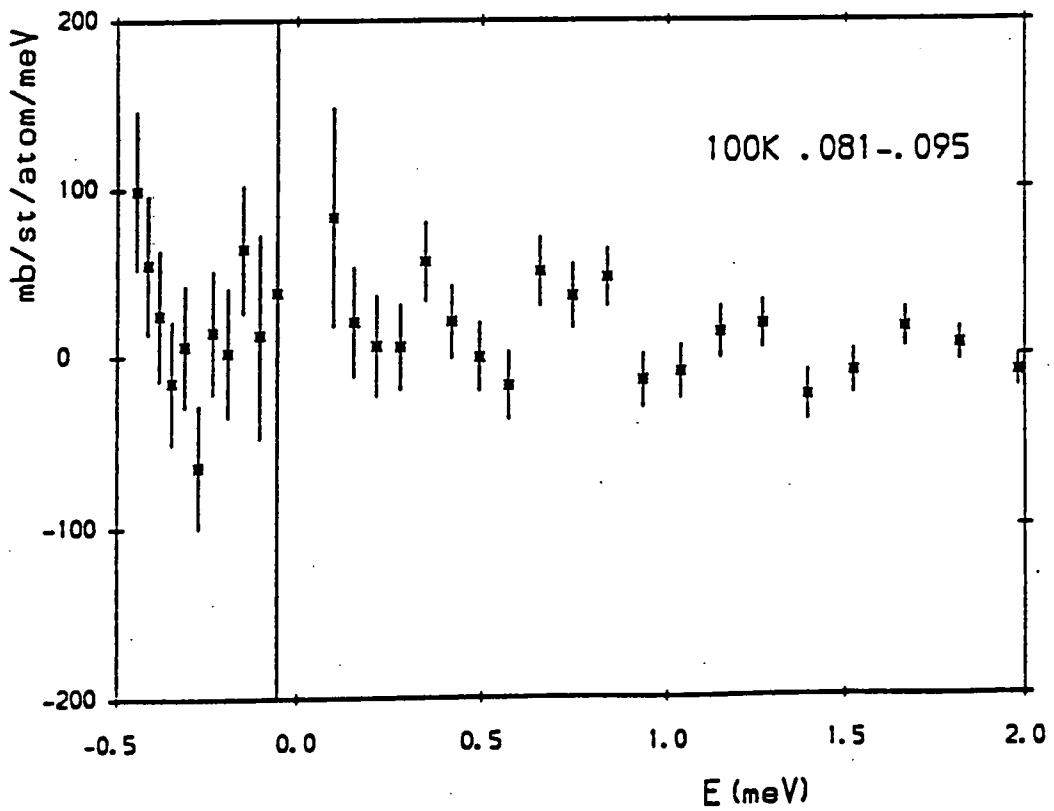
200
100
0
-100
-200
mb/st/atom/meV
100K .081-.095
-0.5
0.0
0.5
1.0
1.5
2.0
E (meV)

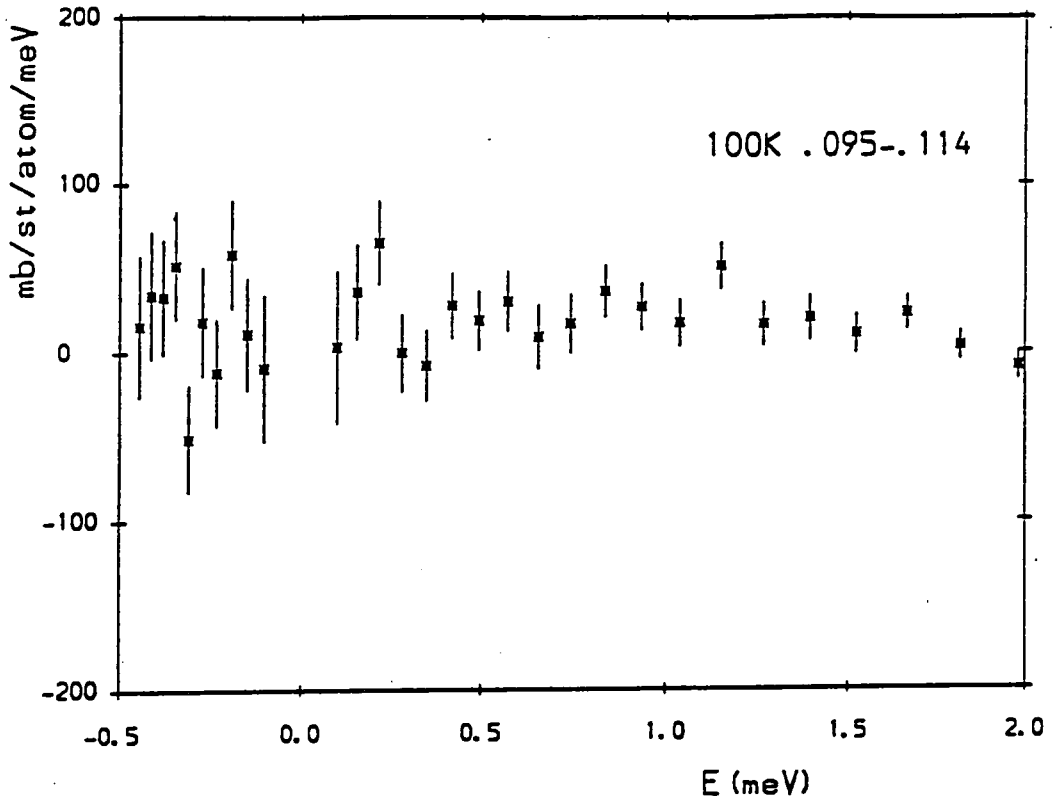
100K .095-.114
mb/st/atom/meV
200
100
0
-100
-200
-0.5
0.0
0.5
1.0
1.5
2.0
E (meV)

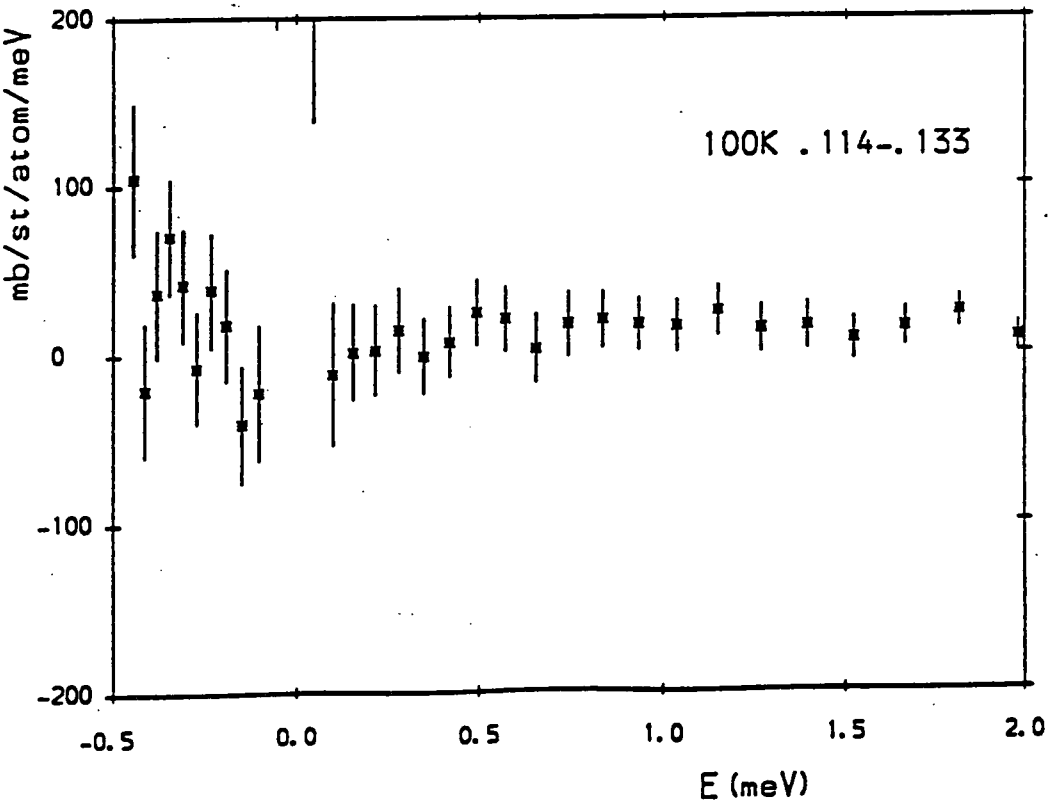
100K .114-.133
mb/st/atom/meV
200
100
0
-100
-200
-0.5
0.0
0.5
1.0
1.5
2.0
E (meV)

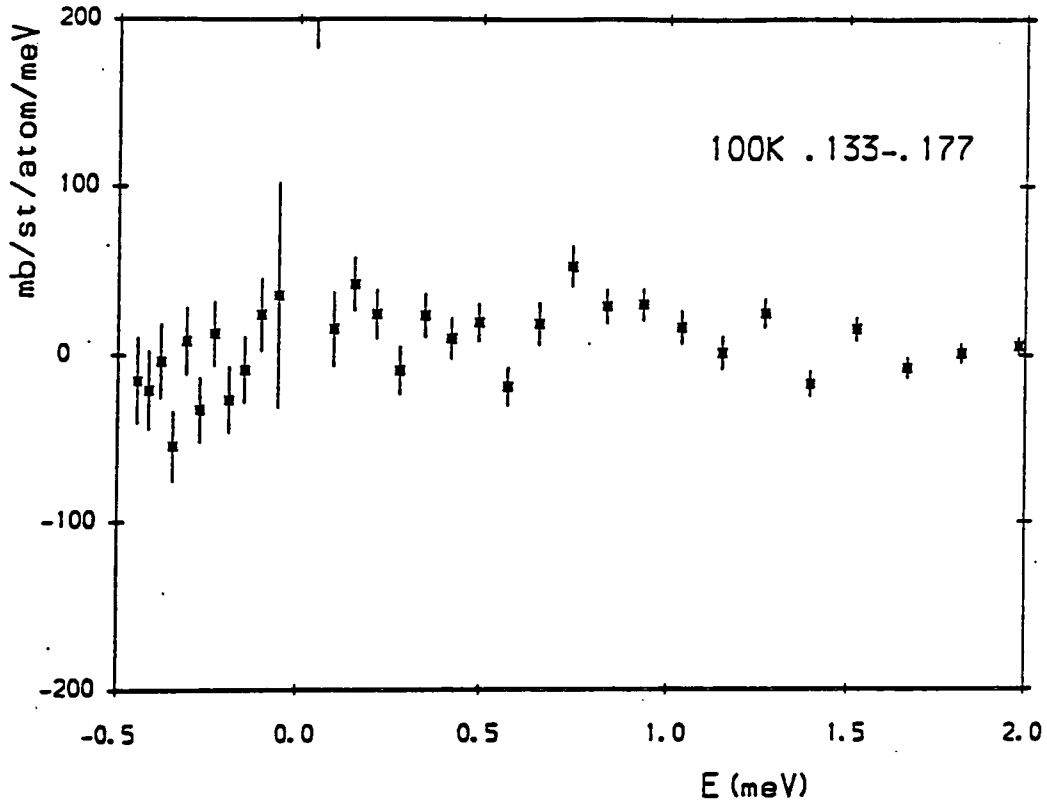
200
100
0
-100
-200
mb/st/atom/meV
100K .133-.177
-0.5
0.0
0.5
1.0
1.5
2.0
E (meV)